



Technische Universität München
Fakultät für Maschinenwesen
Lehrstuhl für Flugsystemdynamik

GNSS-denied navigation of fixed-wing aircraft using low-cost sensors and aerodynamic motion models

Dipl.-Ing. Univ. Lorenz Johannes Moritz Görcke

Vollständiger Abdruck der von der Fakultät für Maschinenwesen der Technischen Universität München zur Erlangung des akademischen Grades eines Doktor-Ingenieurs (Dr.-Ing.) genehmigten Dissertation.

Vorsitzender: Prof. Dr.-Ing. Volker Gümmer

Prüfer der Dissertation:

1. Prof. Dr.-Ing. Florian Holzapfel
2. Prof. Dr.-Ing. Gert F. Trommer

Die Dissertation wurde am 27.09.2017 bei der Technischen Universität München eingereicht und durch die Fakultät für Maschinenwesen am 21.06.2018 angenommen.

Abstract

This work is concerned with the application of high-quality flight dynamics models to GNSS-denied navigation of airplanes with low-cost sensors. Embedded in a 12-DOF aerodynamic motion simulation, the flight dynamics model offers valuable information on true airplane motion. Because only pilot control inputs must be measured, this potential extension to a classical navigation system comes at low hardware cost. Accurate models of aerodynamic flight are not cheap, because a large number of flight test hours is usually required to gather the data needed for system identification. However, because such models are also needed for pilot training simulators, finding an extra use of already available flight dynamics models might be attractive to save cost.

The aerodynamic navigation approach is specifically applied to small conventional airplanes. This choice of platform promises good navigation performance but also presents some severe obstacles. Most notably, flight is affected by instationary and non-uniform motion of air mass and other non-standard atmosphere conditions with potentially extreme phases. The limitations of accurately and reliably modeling these processes and the related uncertainties demand for a solution with minimized dependency on such models. On the other hand, the flight characteristics of conventional airplanes offer the potential to propagate the horizontal airplane position estimate in time with superior linear error growth compared to polynomial error growth of low-cost inertial navigation.

A detailed study of system theory points to advantageous characteristics of aided low-cost inertial navigation and airplane aerodynamic motion propagation in GNSS-denied flight but also reveals significant drawbacks of each model operating alone. This motivates the combination of both propagation methods and first, optimal state estimation techniques with equality constraints are applied to fuse models. The effort to develop a robust optimal model fusion method is hindered by the sensitivity to unreliable atmosphere models and loss of robustness in strong turbulence. Although a tuned model fusion method is developed which is robust in all simulations, dependence on modeling assumptions still persists because now the simulation environment used for tuning and testing must be verified.

This work therefore proposes a covariance-free integration of low-cost inertial navigation and high-quality airplane aerodynamics model. Inertial navigation is implemented in a modified form and integrated with barometric altitude and 3-D magnetometer for best orientation and vertical motion performance. The aerodynamic motion model is corrected using inertial navigation reference information by application of a set of aerodynamically desensitized constraints. The validity of this covariance-free integration is thoroughly justified. It is based on the observed drawbacks of optimal model fusion and the specifics of the tuned model fusion method for airplane aerodynamic navigation. If required, add-on covariance information can be provided using best available statistical models of aerodynamic flight uncertainties. It will however not affect navigation data processing.

A high-fidelity simulation tool is used for method development and testing throughout. A new approach to realistically account for flight dynamics model errors is proposed. Assuming state-of-art dynamic atmosphere models, statistical evaluation of performance is conducted using Monte Carlo simulation. The new covariance-free method is applied to real flight data in navigation postprocessing demonstrating the maturity of the new method.

Kurzfassung

Diese Arbeit untersucht die Anwendung hochgenauer Modelle der Flugdynamik in Kombination mit günstigen Sensoren zur Navigation bei Ausfall der GNSS-Stützung. Ein solches flugdynamisches Modell kann genutzt werden, um die aerodynamische Bewegung des Flugzeuges in 12 Freiheitsgraden zu simulieren und somit die wahre Flugzeugbewegung zu approximieren. Es bietet also eine zusätzliche Information zur Erweiterung eines klassischen Navigationssystems zur Bestimmung der Flugzeugposition, -Geschwindigkeit und -Orientierung. Da zusätzlich nur die Steuereingaben des Piloten gemessen werden müssen, ist diese Erweiterung mit geringen Hardware-Kosten verbunden. Die Erstellung hochgenauer flugdynamischer Modelle ist aufgrund der gewöhnlich großen Anzahl der zur Systemidentifikation benötigten Flugteststunden sehr aufwendig. Da solche Modelle aber außerdem für Flugtrainingssimulatoren benötigt werden, ist die doppelte Verwendung dieser Modelle wirtschaftlich sinnvoll.

Es wird gezeigt, dass die Flugeigenschaften kleiner, konventioneller Flugzeuge die Entwicklung einer aerodynamischen Methode zur Positionspropagation ermöglichen, die durch Nutzung des flugdynamischen Modells ein horizontales Positionsfehlerwachstum erster Ordnung in der Zeit ermöglicht. Dies bedeutet eine deutliche Verbesserung zur polynomialen Fehlerdrift, die für konventionelle Inertialnavigation bei Nutzung günstiger Sensoren charakteristisch ist. Allerdings wird der reale aerodynamische Flug stark von Atmosphäreneffekten beeinflusst, die aufgrund der Komplexität der zugrunde liegenden atmosphärischen Prozesse nur sehr begrenzt modelliert und somit berücksichtigt werden können. In einer einfachen Simulation des aerodynamischen Fluges kann eine falsche oder fehlende Modellierung z.B. der instationären und ungleichförmigen Luftmassenbewegung und anderer Atmosphäreneffekte in der Umgebung des Flugzeuges unter extremen Bedingungen zu großen Abweichungen führen. Somit ist es notwendig, dass eine neue aerodynamische Navigationsmethode die Abhängigkeit von Atmosphärenmodellen minimiert.

In einer Untersuchung der Systemeigenschaften von Inertialnavigation mit günstigen Sensoren und aerodynamischer Positionspropagation werden in der vorliegenden Arbeit die charakteristischen Vorteile herausgearbeitet, wie auch die Einschränkungen, wenn beide Methoden einzeln eingesetzt werden. Die Ergebnisse sind die Grundlage für die Entwicklung einer kombinierten Methode, wobei zunächst optimale Datenfusionsmethoden mit Zwangsbedingungen zur Fusion der inertialen und aerodynamischen Propagationsmodelle angewendet werden. Hier zeigt sich in Simulationen mit turbulenter Atmosphäre, dass die Abhängigkeit von unzuverlässigen Modellen der Atmosphäreneffekte eine deutliche Einschränkung der Robustheit der Methode bedeutet. Es ist zwar möglich, die Parameter der Methode so zu adaptieren, dass sie auch in Simulationen mit turbulenter Atmosphäre gut funktioniert, allerdings bleibt damit eine Abhängigkeit von der gewählten Atmosphärenmodellierung, die nun als Teil der Simulationsumgebung verifiziert werden muss.

Mit diesem Ergebnis wird ein alternativer Lösungsansatz begründet, der die Kovarianz-freie Integration von Inertialnavigation mit günstigen Sensoren und hochgenauem flugdynamischen Modell vorschlägt. Die Inertialnavigation kann hinsichtlich vertikaler Positionierung und Orientierungsbestimmung optimiert werden, was mit der Integration einer modifizierten Implementierung des inertialen Propagationsmodells mit 3-D Magnetometer

und barometrischen Höhenmessungen erreicht wird. Es werden aerodynamisch unempfindliche Zwangsbedingungen entwickelt, die es erlauben, das flugdynamische Modell mit den inertialen Referenzinformationen zu korrigieren. Dieser Kovarianz-freie Integrationsansatz ist unabhängig von der Modellierung der Unsicherheit der beiden Prozesse, kann aber mit einem separaten Kovarianzmodell für die Ausgabe ergänzt werden.

In dieser Arbeit wird eine detaillierte Simulationsumgebung entwickelt und durchgehend zur Untersuchung der entwickelten Methoden eingesetzt. Dabei kommt ein neuer Ansatz zur Berücksichtigung der Fehler in der flugdynamischen Modellierung zum Einsatz. Mit in der Literatur gängigen Modellen der dynamischen Atmosphäre wird eine Monte Carlo Evaluation der Navigationsleistung durchgeführt. Zudem wird die Funktion der neuen Kovarianz-freien Navigationsmethode anhand realer Sensoraufzeichnungen aus einem Flugtest bewiesen.

Table of contents

1	INTRODUCTION.....	1
1.1	PROBLEM SPECIFICATION AND STATE OF THE ART	1
1.2	FIELD OF RESEARCH.....	2
1.2.1	<i>History of dynamic model aided navigation</i>	3
1.3	CONTRIBUTION	4
1.4	OUTLINE.....	6
2	METHODS FOR GNSS-DENIED FLIGHT NAVIGATION.....	7
2.1	TOTAL STATE PROPAGATION.....	7
2.1.1	<i>Heading and airspeed dead reckoning</i>	8
2.1.2	<i>Inertial navigation</i>	12
2.1.3	<i>Aerodynamic motion model</i>	17
2.1.4	<i>Relevant aspects</i>	26
2.2	ERROR STATE PROPAGATION.....	28
2.2.1	<i>Heading and airspeed dead reckoning</i>	28
2.2.2	<i>Inertial navigation</i>	31
2.2.3	<i>Aerodynamic motion model</i>	46
2.2.4	<i>Method comparison</i>	54
2.3	MOTION MODEL AIDING	56
2.3.1	<i>Heading and airspeed dead reckoning</i>	57
2.3.2	<i>Inertial navigation</i>	58
2.3.3	<i>Aerodynamic motion model</i>	65
2.3.4	<i>Method comparison</i>	69
2.4	CONCLUSION.....	71
3	ARCHITECTURES FOR INTEGRATING INERTIAL AND AERODYNAMIC MOTION MODELS.....	72
3.1	OPTIMAL STATE ESTIMATION (CLASSICAL DATA FUSION)	73
3.1.1	<i>Signal-level model fusion</i>	74
3.1.2	<i>State-level model fusion</i>	77
3.1.3	<i>Modeling uncertainties of aerodynamic flight</i>	80
3.1.4	<i>Tuned model fusion filter</i>	81
3.1.5	<i>Shortcomings of state estimation techniques</i>	83
3.2	COVARIANCE-FREE INTEGRATION	84
3.2.1	<i>Aerodynamically desensitized model constraints</i>	86
3.2.2	<i>Integration with the modified inertial motion model</i>	92
3.2.3	<i>Add on covariance model</i>	93
3.2.4	<i>Wind information, aiding measurements and operational integration</i>	96
3.3	CONCLUSION.....	97
4	SYSTEM SIMULATION AND REAL DATA POST PROCESSING.....	99
4.1	SIMULATION FRAMEWORK.....	100
4.1.1	<i>Evaluation of preliminary flight navigation methods</i>	100
4.1.2	<i>Trajectory generation</i>	102
4.1.3	<i>Dynamic atmosphere models</i>	103
4.1.4	<i>Sensor error models</i>	105
4.1.5	<i>Aerodynamic model uncertainty</i>	107
4.2	METHOD EVALUATION IN MONTE CARLO SIMULATION.....	117
4.2.1	<i>Position drift</i>	118
4.2.2	<i>Velocity and attitude errors</i>	122

4.2.3	Robustness in rough atmosphere	124
4.2.4	Effect of IMU and aerodynamic model quality on method performance	128
4.3	POST PROCESSING OF REAL FLIGHT DATA	130
5	SYSTEM IMPROVEMENTS FOR FUTURE APPLICATIONS REQUIRING CERTIFICATION	133
5.1	IMPROVEMENT OF SYSTEM PERFORMANCE WITH WIND INFORMATION	134
5.2	WEATHER PREDICTION AND AIRCRAFT-TO-AIRCRAFT WEATHER INFORMATION	136
6	SUMMARY AND CONCLUSIONS.....	137
	REFERENCES	141
	APPENDIX A	147
A.1	MATH	147
A.2	TRANSLATIONAL MOTION OF A POINT MASS	155
A.3	SPECIFIC FORCE LEVER ARM	162
A.4	RIGID BODY EQUATIONS OF ROTATIONAL MOTION	164
A.5	ERROR STATE PROPAGATION MODEL FOR HEADING AND AIRSPEED DEAD RECKONING	166
A.6	PERTURBATION ERROR DIFFERENTIAL EQUATIONS.....	168
A.7	INTEGRATED INS/GNSS NAVIGATION	174
A.8	EXTENDED KALMAN FILTER WITH AUGMENTED AND CONSIDERED STATES	180
A.9	SPECIFIC FORCE LINEARIZATION	182

Figures

FIGURE 01:	GEOMETRY OF DEAD RECKONING FOR STRAIGHT AND LEVEL FLIGHT	9
FIGURE 02:	CONTROL DEFLECTIONS AND BODY-FIXED FRAME FOR A CONVENTIONAL AIRPLANE	22
FIGURE 03:	HORIZONTAL POSITION ERROR OF NAVIGATION GRADE INERTIAL NAVIGATION.....	38
FIGURE 04:	HORIZONTAL POSITION ERROR OF LOW TACTICAL GRADE INERTIAL NAVIGATION	39
FIGURE 05:	INITIAL POSITION ERROR GROWTH OF LOW TACTICAL GRADE INERTIAL NAVIGATION	40
FIGURE 06:	TRANSIENT ATTITUDE ERRORS IN COORDINATED TURNING FLIGHT WITH 30° BANK ANGLE.....	44
FIGURE 07:	TRANSIENT ATTITUDE ERRORS IN COORDINATED TURNING FLIGHT WITH 30° BANK ANGLE.....	44
FIGURE 08:	HORIZONTAL ERROR PROPAGATION AND DYNAMICS.....	54
FIGURE 09:	LATERALLY DIVERGENT AERODYNAMIC POSITION PROPAGATION WITH SPEED OVER GROUND AIDING	66
FIGURE 10:	AERODYNAMIC POSITION PROPAGATION WITH ORIENTATION ERROR AIDING.....	66
FIGURE 11:	DIVERGING COMPUTED AERODYNAMIC FLIGHT IN PRESENCE OF DYNAMIC WIND ERROR AND PILOT CONTROL..	67
FIGURE 12:	COMPARISON OF AIDED INS AND AIDED AERODYNAMIC MOTION MODEL (AIDED VDM).....	69
FIGURE 13:	SIGNAL-LEVEL MODEL FUSION	73
FIGURE 14:	STATE-LEVEL MODEL FUSION.....	77
FIGURE 15:	ERRORS IN AERODYNAMIC ORIENTATION ANGLES.....	87
FIGURE 16:	SIMPLIFIED AERODYNAMIC ORIENTATION ERRORS	88
FIGURE 17:	FLIGHT PATH A FOR MONTE CARLO EVALUATION (REALIZATION FOR SEED 1)	101
FIGURE 18:	WIND VELOCITY VECTOR AND WGS84 HEIGHT (REALIZATION FOR SEED 1)	101
FIGURE 19:	IDEAL POSITION ERROR DUE TO WIND DRIFT WITH EXACT INITIAL GUESS EXPONENTIALLY DECAYING.....	101
FIGURE 20:	FLIGHT PATHS GENERATED FOR KINEMATIC BANK ANGLE LIMITS OF 60° AND 30° (FROM [87]).....	102
FIGURE 21:	BAROMETRIC ALTITUDE MEASUREMENT MODEL	106
FIGURE 22:	AIRSPEED MEASUREMENT MODEL	106
FIGURE 23:	3-D MAGNETOMETER MEASUREMENT MODEL	106
FIGURE 24:	DYNAMIC FLIGHT PATH FOR SYSTEM ID SIMULATIONS (AVERAGE KINEMATIC VELOCITY OF 70m/s)	108
FIGURE 25:	WIND VELOCITY VECTOR	110

FIGURE 26: WGS84 HEIGHT AND AIRSPEED	110
FIGURE 27: ROLL ANGLE AND TURN RATE	110
FIGURE 28: DIRECT PITCH COMMAND INPUT AND PHUGOID RESPONSE (ONE OF THREE OCCURRENCES)	111
FIGURE 29: DIRECT ROLL AND YAW COMMAND INPUT AND RESPONSE (ONE OF THREE OCCURRENCES)	111
FIGURE 30: COMMANDED ANGLE OF SIDESLIP AND RESPONSE (ONE OF THREE OCCURRENCES)	111
FIGURE 31: ESTIMATION OF “ Δ -MODEL” COEFFICIENTS \mathbf{cv} (500 SAMPLE ESTIMATES AND $3\text{-}\sigma$)	115
FIGURE 32: FLIGHT PATH B FOR MONTE CARLO EVALUATION AND NAVIGATION TRAJECTORY FOR RUN 1	118
FIGURE 33: WIND VELOCITY AND WIND RATES VECTORS (REALIZATION FOR SEED 1)	118
FIGURE 34: WGS84 HEIGHT AND ROLL ANGLE (REALIZATION FOR SEED 1)	119
FIGURE 35: IDEAL POSITION ERROR DUE TO WIND DRIFT WITH EXACT INITIAL GUESS EXPONENTIALLY DECAYING	119
FIGURE 36: MODIFIED INERTIAL MODEL ATTITUDE ERRORS FOR RUN 1	120
FIGURE 37: MODIFIED INERTIAL MODEL VERTICAL ORIENTATION ERROR FOR RUN 1	120
FIGURE 38: AERODYNAMIC MODEL AIRSPEED ERROR FOR RUN 1	120
FIGURE 39: AERODYNAMIC MODEL AERODYNAMIC ANGLE OF ATTACK AND ANGLE OF SIDESLIP ERRORS FOR RUN 1	120
FIGURE 40: POSITION DRIFT STATISTICS FOR 500 RUNS	121
FIGURE 41: OUTLIER-PRONE EMPIRICAL CUMULATIVE DISTRIBUTION (ECDF) OF AIRSPEED ERRORS	122
FIGURE 42: OUTLIER-PRONE EMPIRICAL CUMULATIVE DISTRIBUTION (ECDF) OF ANGLE OF ATTACK ERRORS	123
FIGURE 43: OUTLIER-PRONE EMPIRICAL CUMULATIVE DISTRIBUTION (ECDF) OF ANGLE OF SIDESLIP ERRORS	123
FIGURE 44: FLIGHT PATH A FOR ROBUSTNESS EVALUATION (ONE OF THREE REALIZATIONS)	124
FIGURE 45: WGS84 HEIGHT	125
FIGURE 46: SAMPLE WIND VELOCITY VECTOR IN SEVERE TURBULENCE	125
FIGURE 47: SAMPLE WIND RATES VECTOR IN SEVERE TURBULENCE	125
FIGURE 48: HORIZONTAL POSITION ERROR IN FLIGHT PATH A ROBUSTNESS TEST	125
FIGURE 49: FLIGHT PATH B FOR ROBUSTNESS EVALUATION (MANUALLY PILOTED)	126
FIGURE 50: WGS84 HEIGHT	127
FIGURE 51: SAMPLE WIND VELOCITY VECTOR	127
FIGURE 52: SAMPLE WIND RATES VECTOR	127
FIGURE 53: HORIZONTAL POSITION ERROR IN MANUALLY PILOTED FLIGHT PATH ROBUSTNESS TEST	127
FIGURE 54: IMPROVEMENT OF POSITION DRIFT WITH IMU QUALITY, IDEAL WIND INFORMATION AVAILABLE	128
FIGURE 55: IMPROVEMENT OF POSITION DRIFT WITH IMU QUALITY, WIND INITIALLY ESTIMATED	128
FIGURE 56: IMPROVEMENT OF POSITION DRIFT WITH AERODYNAMIC MODEL QUALITY	129
FIGURE 57: FLIGHT PATH OF NAVIGATION METHOD AND REFERENCE DATA. GNSS-DENIED FROM 200s	130
FIGURE 58: MODIFIED INERTIAL MODEL ATTITUDE ERRORS (VERSUS REFERENCE)	131
FIGURE 59: AERODYNAMIC MODEL HORIZONTAL POSITION ERRORS	132
FIGURE 60: MODIFIED INERTIAL MODEL VERTICAL ORIENTATION ERROR (VERSUS REFERENCE)	132
FIGURE 61: AERODYNAMIC MODEL VERTICAL VELOCITY ERROR	132
FIGURE 62: AERODYNAMIC MODEL ANGLE OF ATTACK AND ANGLE OF SIDESLIP ERRORS (VERSUS KINEMATIC REFERENCE)	132
FIGURE 63: IMPROVEMENT OF POSITION DRIFT WITH WIND INFORMATION	134

Tables

TABLE 1: LATERAL ERROR DYNAMICS NATURAL FREQUENCY ω_0 AND RELATIVE DAMPING ζ (EXAMPLE) 52

TABLE 2: LATERAL ERROR DYNAMICS EIGENVECTORS (EXAMPLE) 52

TABLE 3: AIRPLANE AERODYNAMIC MOTION MODEL AIDED BY REFERENCE MEASUREMENT 66

TABLE 4: IMU QUALITIES. ALL VALUES EXCEPT NOISE ARE RMS OF FLICKER NOISE PROCESSES. SF PROCESSES ARE LOW PASS FILTERED AT 0.001Hz. * TOTAL OPERATIONAL IN RUN VARIABILITY 105

TABLE 5: POINT MASS UNCERTAINTIES (STANDARD DEVIATION) FOR ACCURATE AND NORMAL WEIGHT AND BALANCE UNCERTAINTY MODEL 112

Acronyms and abbreviations

2drms	Twice the RMS radial error
AOA	Aerodynamic angle of attack
AOSS	Aerodynamic angle of sideslip
CAD	Computer-aided design
CEP	Circular error probable
DOF	Degree of freedom
ECDF	Empirical cumulative distribution function
ECEF	Earth-centered earth-fixed coordinate frame
ECI	Earth-centered inertial coordinate frame
EGM	Earth gravitational model
EKF	Extended Kalman filter
FOG	Fiber-optic gyro
FTE	Flight technical error
GNSS	Global navigation satellite system
GPS	Global positioning system
HDG	Heading
IMU	Inertial measurement unit
INS	Inertial navigation system (inertial motion model)
MCE	Monte Carlo evaluation
MEMS	Micro-electro-mechanical systems
NCEP	U.S. National Centers for Environmental Prediction
NED	North-East-Down coordinate frame
R95	95% radial position accuracy
RAIM	Receiver autonomous integrity monitoring
RAP	Rapid Refresh numerical weather model
Ref	Reference true motion
RLG	Ring laser gyro
RMS	Root mean square
RNAV	Area navigation
RNP	Required navigation performance
RPM	Revolutions per minute
SF	Scale factor error
TRAJ	Flight path trajectory

TSE	Total system error
VDM	Vehicle dynamics model (aerodynamic motion model)
WGS84	World geodetic system 1984
WMM	World magnetic model

Coordinate frames and axes transformations

3-D vectors written in coordinates of one of the following Cartesian coordinate frames are denoted by a bold symbol with index denoting the frame, e.g. \mathbf{v}_n .

Axes of one coordinate frame can be aligned with those of another coordinate frame by consecutive rotations. In this work, the corresponding transformation angles are defined by rotations about the individual axes in order 3-2-1. The axes of the second and third rotation are given by the intermediate frame resulting from the preceding rotations.

Index	Name	Description	Axes transformations
i	ECI frame	Earth-centered, non-rotating. x_3 -axis aligned with Earth's rotation axis.	
e	ECEF frame	Earth-centered, earth-fixed. x_1 -axis points at Greenwich meridian, x_3 -axis aligned with Earth's rotation axis.	
n	NED frame	Centered in navigation reference point R , axes pointing North, East and down w.r.t. WGS84 ellipsoid	$e \rightarrow n: (0 \quad -\phi \quad -\pi/2 \quad \lambda)$
b	body-fixed frame	Centered in navigation reference point R , axes pointing forward, right and down with respect to vehicle geometry	$n \rightarrow b: (\Phi_{nb} \quad \Theta_{nb} \quad \Psi_{nb})$
a_l	level aerodynamic frame	Centered in navigation reference point R , axes by rotating NED frame to align x_1 -axis with aerodynamic velocity vector	$n \rightarrow a_l: (0 \quad \gamma_A \quad \chi_A)$ $a_l \rightarrow a: (\mu_A \quad 0 \quad 0)$
a	aerodynamic frame	Centered in navigation reference point R , axes by rotating body-fixed frame to align x_1 -axis with aerodynamic velocity vector	$a \rightarrow b: (0 \quad \alpha_A \quad -\beta_A)$

Symbols and notation

Aerodynamics

Aerodynamic motion variables may be denoted by $(\cdot)_A$ if necessary to distinguish them from kinematic $(\cdot)_K$ or wind motion $(\cdot)_W$ variables.

q	Dynamic pressure
S_{ref}	Wing reference area
l	Reference length
\bar{c}	Mean aerodynamic chord
b	Wing span
s	Semi-span
ρ	Air density
μ	Dynamic air viscosity
a	Speed of sound
Re	Reynolds number
M	Mach number
V	Airspeed
α	Aerodynamic angle of attack
β	Aerodynamic angle of sideslip
χ	Aerodynamic course angle
γ	Aerodynamic climb angle
μ	Aerodynamic bank angle

Airplane model

$(\cdot)_{Aero}$ refers to aerodynamic modeling, $(\cdot)_{Prop}$ refers to modeling of propulsion forces and moments.

\mathbf{F}	Force vector
m	Airplane mass
\mathbf{M}	Moment vector
\mathbf{I}_{bb}^G	Inertia matrix in body-fixed coordinates w.r.t. G
I_{xx}, I_{yy}, I_{zz}	Moments of inertia
I_{xy}, I_{xz}, I_{yz}	Products of inertia
\mathbf{u}_p	Control input vector
ξ	Roll control input
η	Pitch control input
ζ	Yaw control input
δ_T	Throttle setting
\mathbf{c}_v	Vehicle model coefficients

Earth models

\mathbf{g}	Gravitation vector
g	Gravitational acceleration
$\boldsymbol{\gamma}$	Gravity vector
R	Earth radius
GM	Earth's gravitational constant
ω_S	Schuler frequency

Error states

For a given erroneous variable, $\delta(\cdot)$ denotes the corresponding error. The given variable may be measured ($\widetilde{(\cdot)}$) or computed ($\widehat{(\cdot)}$). Because the perturbation form is chosen for error analysis throughout this work, the error $\delta(\cdot)$ will be equivalent to the additive correction of the given variable required to compute the true value. E.g. if the variable is a vector with true value \mathbf{v}_n and computed value $\widehat{\mathbf{v}}_n$, the correction is $\mathbf{v}_n = \widehat{\mathbf{v}}_n + \delta\mathbf{v}_n$.

Generally, for error perturbation of orientation variables a multiplicative definition of error is employed. For example $\check{\mathbf{q}}_{nb} \cdot \widehat{\mathbf{q}}_{nb}^{-1}$ and $\mathbf{R}_{nb} \widehat{\mathbf{R}}_{nb}^T$ describe the errors in computed orientation quaternion $\widehat{\mathbf{q}}_{nb}$ and rotation matrix $\widehat{\mathbf{R}}_{nb}$. The following two orientation error parametrizations are adopted in this work, which are equivalent in linear approximation:

$\boldsymbol{\phi}_n = [\phi_N \ \phi_E \ \phi_D]^T$	Phi angle orientation error in NED frame coordinates
$\boldsymbol{\Phi} = [\delta\phi_1 \ \delta\phi_2 \ \delta\phi_3]^T$	Vector of orientation error Euler angles

Estimation

The common notations of expectation value $E[\cdot]$, variance $Var[\cdot]$ and covariance $Cov[\cdot, \cdot]$ are used. Computed values before correction are denoted by $(\cdot)^-$, values after correction are denoted by $(\cdot)^+$.

\mathbf{z}	Total state vector
\mathbf{x}	Filter state vector (error state space)
$\delta\mathbf{s}$	Filter input vector
$\boldsymbol{\omega}$	Process noise
\mathbf{A}	Filter system matrix
\mathbf{B}	Filter input matrix
$\boldsymbol{\Phi}$	Discrete filter state model transition matrix
$\boldsymbol{\Gamma}$	Discrete filter state model input matrix
$\tilde{\mathbf{y}}$	Filter observation (error state space)
\mathbf{v}	Measurement noise
\mathbf{b}	Slowly-varying measurement error
\mathbf{n}	Noisy measurement error
\mathbf{H}	Observation matrix
\mathbf{G}_ω	Process noise measurement feedthrough matrix
\mathbf{K}	Filter gain matrix
\mathbf{P}	Filter state covariance matrix
\mathbf{R}	Measurement noise covariance matrix
\mathbf{Q}	Process noise covariance matrix

Vectors and matrices

$\mathbf{e}_1 = [1 \ 0 \ 0]^T$	First basis vector
$\mathbf{e}_2 = [0 \ 1 \ 0]^T$	Second basis vector
$\mathbf{e}_3 = [0 \ 0 \ 1]^T$	Third basis vector
$\mathbf{a}_n = [a_N \ a_E \ a_D]^T$	Vector \mathbf{a} in NED frame coordinates
$\mathbf{a}_b = [a_x \ a_y \ a_z]^T$	Vector \mathbf{a} in body-fixed frame coordinates
$skew(\mathbf{a})$	Matrix equivalent of vector cross product $\mathbf{a} \times$
$veck(\mathbf{M})$	Vector equivalent of skew-symmetric part of matrix \mathbf{M}
$\mathbf{a}_{\parallel b}$	Component of vector \mathbf{a} parallel to vector \mathbf{b}
$\mathbf{a}_{\perp b}$	Component of vector \mathbf{a} orthogonal to vector \mathbf{b}

Vehicle motion

Kinematic motion variables may be denoted by $(\cdot)_K$ if necessary to distinguish them from aerodynamic $(\cdot)_A$ or wind motion $(\cdot)_W$ variables. A vector denoted by $(\cdot)_H$ contains horizontal motion states in North and East direction only.

$(\cdot)^G$ denotes motion variables that refer to the vehicle center of gravity, $(\cdot)^R$ refers to the navigation reference point R . $(\cdot)^{RG}$ denotes a relative motion variable, e.g. $\mathbf{r}^{RG} = \mathbf{r}^G - \mathbf{r}^R$.

\mathbf{z}_n	Navigation state vector in NED frame parametrization
$\mathbf{z}_v = [\mathbf{z}_n^T \ \boldsymbol{\omega}_{ib}^T]^T$	Vehicle state vector (rigid body motion)
ϕ	WGS84 latitude
λ	WGS84 longitude
h	WGS84 height
$\boldsymbol{\Lambda} = [\phi \ \lambda \ h]^T$	Column vector of WGS84 position
\mathbf{r}	3-D position vector with respect to ECEF frame
\mathbf{v}	Velocity vector with respect to ECEF frame
V	Velocity vector magnitude
χ	Kinematic course angle
γ	Kinematic climb angle
$\tilde{\mathbf{q}}_{nb}$	Orientation quaternion
\mathbf{R}_{nb}	Direction cosine matrix
ϕ_{nb}	Roll angle
θ_{nb}	Pitch angle
ψ_{nb}	Heading angle
\mathbf{a}	Acceleration vector
\mathbf{f}	Specific force vector
$\boldsymbol{\omega}$	Angular rates vector
ω	Angular rates vector magnitude
p	Roll rate
q	Pitch rate
r	Yaw rate

1 INTRODUCTION

Integrated inertial and satellite navigation (INS/GNSS) is the future standard for low-cost aircraft navigation. GNSS alone provides sufficient accuracy and reliability for lateral navigation for enroute operations with state of the art receiver autonomous integrity monitoring. Future solutions for estimation of aircraft position, velocity and orientation in all segments of general aviation flight will largely rely and depend on the potential of GNSS technology and integration with low-cost INS.

One important limitation of this optimistic outlook is the fundamental lack of robustness of satellite signal transmission. While reliable detection of signal-related failure conditions is possible, elaborate jamming will always be a single point of failure of satellite navigation. Consequently, the possibility of losing the performance enhancement of GNSS for low-cost aircraft navigation must be considered.

1.1 PROBLEM SPECIFICATION AND STATE OF THE ART

This thesis addresses the need for a backup positioning function for small general aviation that allows safely continuing flight when GNSS aiding becomes unavailable. Given the visibility of typically 20 or more satellites from 4 different GNSSs at an elevation of 10° or higher in North America and Europe in 2017 [1], the reasons for unavailable GNSS aiding in flight are primarily user equipment faults and disturbance of signal reception. While the first case can be mitigated by redundant hardware, the latter condition is most likely spatially limited (e.g. jamming). It is arguable if in such a scenario similar good positioning accuracy as with GNSS aiding is required. Instead, the backup navigation function must be sufficient to allow safely leaving the area where GNSS reception is disturbed. This makes a slow degradation over time of positioning performance acceptable. At the same time, additional system cost, weight and power consumption for implementation of this backup function must be small because it is not used under normal conditions.

Classical ground-based navigation aids (i.e. radio navigation) currently undergo significant change: Both the Long-Range Navigation system (LORAN) and the Distance Measuring Equipment architecture (DME) are subject of current research aiming at enhancement of the (still) existing ground infrastructure (and the on-board equipment) to meet the requirements of a backup system to GNSS. eLoran [2] should meet meter-level positioning accuracy, but the number of stations has already critically reduced [3, 4]. eDME [5, 6] is enhanced by carrier phase tracking and other innovations that increase the capacity and accuracy of the system. Technically, both enhanced systems are designed to be a full backup system to GPS (alternative positioning, navigation and timing, APNT). While these systems do provide the required positioning function specified above, they require at least an extra receiver and antenna on-board and would be obsolete while GNSS is available. In addition, they might over-perform: As described above, if GNSS reception is disturbed, a reasonable contingency plan is to leave the denied area, e.g. fly to an alternate airport instead of continuing approach and landing. Finally, because these radio navigation

systems provide similar functionality as GNSS, they would very likely be subject to the same jamming or spoofing action that is targeting GNSS.

Consequently, a simple, on-board backup system with negligible additional system cost, weight and power consumption that specifically provides the navigation information required for safe contingency operation in the unlikely event of GNSS denial is needed. It is specifically not intended for use in flight segments with stringent performance requirements (e.g. landing), because here GNSS is assumed available (if need be, at the alternate airport).

A high-quality Inertial Navigation System (INS) can provide coarse (and drifting) position information with highest availability and resilience [7], but not at acceptable cost for application in small general aviation. Here, a low-cost INS/GNSS will be the core of future navigation systems for operation under normal conditions. Because low-cost INS/GNSS means low-cost inertial sensors with insufficient accuracy for unaided position propagation, the required backup navigation function cannot be implemented with this architecture by itself. In order to improve the accuracy of position (and other navigation information, such as velocity) during outages of GNSS, additional information must be integrated with INS. Sensor measurements are an obvious choice to allow for observation and estimation of navigation errors, for example air data and 3-D magnetometer.

An existing method for backup enroute (and oceanic) flight navigation is heading and airspeed dead reckoning. This method is for example implemented in the Garmin G1000 Cockpit for the Cessna Citation Mustang [8] where it continues to provide an estimate of aircraft position based on the last valid position fix obtained with GPS and a relative horizontal motion computed from airspeed and magnetic heading measurements.

These state of the art techniques inertial navigation, sensor measurement aiding of INS and heading and airspeed dead reckoning will be studied in this thesis considering the chosen application. The engineering problem specified above will additionally be addressed by application of dynamic model aided navigation, which is a promising field of research for low-cost GNSS-denied navigation for small general aviation airplanes.

1.2 FIELD OF RESEARCH

This thesis presents research on the integration of a software model of flight dynamics for backup navigation of small general aviation airplanes. Generally, dynamic model aided navigation offers an improvement in navigation performance by integration of additional knowledge on how the vehicle moves and reacts to control inputs. Compared to conventional navigation sensors, hardware cost of including this software model and measuring control inputs is low. In addition, it is insensitive to a large number of environmental conditions affecting air data and magnetic field measurements.

While these advantages have been highlighted before in the available literature, this thesis is the first to specifically address the characteristics of airplane flight dynamics. An aerodynamic navigation method that takes the specifics of conventional airplanes into account and exploits favorable properties should have superior performance. Small general aviation airplanes have especially benign flight characteristics and at the same time would

strongly benefit from low-cost backup navigation. This motivates research on aerodynamic navigation for airplanes.

Integration of a dynamics model of the vehicle is fundamentally different from conventional sensor measurement aiding of INS. The following gives a brief review of the history of dynamic model aided navigation by presenting the publications that are most relevant for the research in this thesis.

1.2.1 History of dynamic model aided navigation

The first application of aircraft vehicle dynamics to navigation is due to Koifman and Bar-Itzhack and was published in 1999 [9]. Navigation applications were preceded by earlier research on attitude and heading determination with aerodynamic models, e.g. [10].

The 1999 paper by Koifman and Bar-Itzhack considers inertial navigation and the dynamics model of an airplane as two navigation systems running in parallel. The authors propose the notion that “nature and behavior of the errors of the two systems differ from one another, therefore the EKF should distinguish between the two error groups and estimate them”. Errors are observed in the differences of the computed navigation states of the two models. This corresponds to constraining the extended Kalman filter to state estimates that are exactly equal for both models.

Consequently, the first publication on navigation with aerodynamic models already presents a complete mathematical framework for combination of the two propagation models using optimal state estimation techniques: The models are assumed to refer to exactly the same truth motion, which allows to observe differences of errors in differences of computed total states of both models.

Although apparently not known to the authors of [9], earlier theoretical research on optimal state estimation with multiple propagation models by Julier and Durrant-Whyte published in 1996 [11] provides a consistent mathematical foundation for model fusion. The authors prove that mathematical optimality, i.e. the best estimator based on the available information, is achieved with a combined system of multiple propagation model states and linear constraints relating equivalent states. This is termed “horizontal model fusion”. The question how exactly these constraints should be designed is not addressed, but equality constraints on e.g. equivalent position or velocity states in all models are proposed.

The next significant step in the field is due to Vasconcelos et al., who make a different choice for implementing the aerodynamic propagation model and equality constraints in the publications [12] (2006) and [13] (2010). Application to model-scale rotorcraft requires a reduction of computational cost, which is achieved by only including one state for the vehicle angular rate vector in the combined model with INS. Vehicle angular rates are constrained to be equal to measured inertial angular rates. Although the propagation of vehicle orientation, velocity and position states is omitted, the complete information on vehicle dynamics is still included in the estimation: A second equality constraint is implemented for accelerations computed by inertial navigation and the vehicle dynamics equations of motion. Thus, the information on both translational and rotational motion is fused.

In a 2013 publication [14], Crocoll and the author propose a “Unified model technique” for inertial and aerodynamic model fusion. This method matches the computational efficiency of the method of Vasconcelos but is mathematically equivalent to the optimal method of Koifman with equality constraints on velocity and orientation states. The authors explain restrictions in the selection of motion states for the definition of model fusion equality constraints.

1.3 CONTRIBUTION

This work deals with the development of a low-cost backup navigation function and in particular with a new approach to dynamic model aided navigation specifically for small general aviation airplanes.

First, it is noted that the lack of position fixing during outages of GNSS requires substantial use of propagation methods such as INS. In any case, a propagation method – or a combination of methods – will be the backbone of the desired navigation function. Therefore, the first part of the research presented here studies navigation propagation methods with respect to

- Their error characteristics in a low-cost implementation. What are sources of error, how does error propagate and accumulate in specific motion states?
- Available low-cost measures to effectively reduce error. How well can adverse error characteristics identified before be mitigated by including additional information?
- Their comparative qualities. Is there a potential for improvement by combination of the studied methods?

The study of low-cost navigation propagation methods provides the theoretical basis for the development of GNSS-denied navigation. The specific interest in a possible advantageous combination of propagation methods leads to results that motivate the focus on aerodynamic navigation in the remainder of this work. After answering the question, whether there is any potential improvement by combination, research on how to realize this improvement is the logical next step.

The integration of inertial navigation and aerodynamic model for the application in small general aviation airplanes presents new challenges. Robust operation must be guaranteed in a wide range of environmental conditions encountered in long operation times and travelled distances. This especially includes rough atmosphere conditions such as strong wind, gusts and turbulence. The enormous complexity of real atmosphere processes and the characteristic intermittency of rough atmosphere conditions lead to a modeling problem: These effects can neither be predicted accurately with on-board software models, nor can errors of simpler models be statistically accounted for with sufficient significance required for state of the art integration techniques. Consequently, the focus of this part of the thesis is to

- Study the application of optimal model fusion techniques to small general aviation airplanes in a realistic atmosphere environment. Provide a detailed understanding of the causes of low robustness encountered for these methods in the specific application
- Develop a new technique for integration of inertial and aerodynamic models. How to combine models without depending on unreliable or unavailable models? How to

exploit the characteristics of inertial navigation and airplane aerodynamic motion to that end?

The development of a new method for model integration aims to overcome significant obstacles of a real application of aerodynamic navigation for manned airplanes: Only if the method is robust per design even in extremely rough atmosphere it can be considered reliable for safety-of-life applications. The central part of this work is dedicated to find a solution to this problem by accounting for the specific and dissimilar qualities of inertial navigation and airplane aerodynamic motion.

Finally, a realistic assessment of method behavior, robustness and performance is required to allow for further development and use in real applications. Because a large number of tests and long total flight duration is necessary for meaningful evaluation, a simulation tool must be developed. This work presents a novel approach to account for aerodynamic model uncertainties in simulation. Automatic generation of input data for various flight scenarios and wind conditions allows studying aerodynamic navigation in a detailed Monte Carlo simulation:

- What behavior and performance can realistically be expected from the proposed method?
- How does modeling quality of aerodynamic motion affect the results?

In addition, application of the proposed aerodynamic navigation method to real flight data is necessary to prove its applicability under real world conditions and provide verification of theoretical results and simulations.

To summarize briefly, this thesis has three goals. The first is to provide a fundamental theoretical understanding of low-cost GNSS-denied navigation and identify potential improvements by combination of propagation methods. Second, integration of inertial navigation and airplane aerodynamic motion model must be realized in a way that is fully independent from unreliable or unknown knowledge of processes and statistics for best performance and robustness. To conclude this work, the new aerodynamic navigation method must be evaluated in simulation and real data tests to show its potential.

1.4 OUTLINE

This thesis is organized as follows: The first three chapters address the main goals defined previously. Each section of chapter 2 studies a different theoretical aspect of low-cost GNSS-denied flight navigation. After a presentation of available navigation propagation methods, their required computation models and inputs, they are discussed and compared with respect to sources and propagation of error (section 2). In section 3, their suitability for aiding with auxiliary on-board information is studied. The focus is on mitigation of the weaknesses specific to each method. Chapter 2 concludes by highlighting the potential performance gain by combination of inertial navigation and the aerodynamic motion model.

Chapter 3 explains how the problem of unreliable or unavailable models for aerodynamic flight in rough atmosphere is solved, which is the major difficulty in applying aerodynamic navigation to small general aviation airplanes. The text follows the actual course of research of the author's work. It first discusses the application of optimal state estimation techniques to combine inertial and aerodynamic models in a model fusion filter in section 1. The limitations of this approach when dealing with intermittent and unknown rough dynamic atmosphere processes are explained. The steps taken to adapt model fusion accordingly and the remaining shortcomings of the improved state estimation technique are described. The motivation for a fundamentally different approach and the development of a new covariance-free integration of inertial and aerodynamic models then follow in section 2.

The first section of chapter 4 presents the simulation framework developed for the evaluation of navigation with an airplane aerodynamic motion model. This comprises generation of realistic reference data with an automatic trajectory generation tool, modeling of dynamic atmosphere effects, measurement errors and a new technique of modeling aerodynamic model uncertainty. Section 2 then conducts a rigorous assessment of the proposed aerodynamic navigation method in Monte Carlo simulation. Accuracy, robustness in rough atmosphere and the sensitivity to two central system quality parameters are evaluated. Section 3 concludes chapter 4 with the application of the proposed method to *30min* of real flight data in postprocessing.

Chapter 5 completes the research on a new method for aerodynamic navigation of small general aviation airplanes with a study of a potential future use case. This includes a discussion of applicable flight navigation certification aspects. From this, necessary system improvements are identified and the next step of development and extensions of the future navigation system are proposed.

2 METHODS FOR GNSS-DENIED FLIGHT NAVIGATION

For applications where position information is critical, position-fixing must be supplemented by a backup function for computation of position estimate in case of primary function failure. Without any absolute horizontal position information available, this backup function provides an estimate of change in position since the last available position fix. Referring to its most important application scenario, this backup function will be termed GNSS-denied flight navigation in this work. For highest reliability, only information available on-board and independent of external infrastructure, weather and visibility is used. In addition, this thesis aims at developing a method providing a backup navigation function based on the systems already available on standard general aviation aircraft, not requiring additional expensive equipment.

The aim of this chapter is to analyze and compare three methods for aircraft position estimate propagation and understand how their respective qualities are favorable and might be combined for a low-cost application. First, the underlying computation schemes are presented, which differ in the underlying motion models describing state propagation, including position, and their inputs that need to be available from measurements or knowledge.

The second section in this chapter then takes a detailed look at these methods with respect to how errors in initial state or inputs propagate to and accumulate in position and other motion model states. This is essential in order to judge how accurately position can be propagated using any of the motion models for a longer time open loop. On the other hand, identified short term error dynamics will be essential for the performance of aided position propagation.

In some cases, unfavorable error propagation and dynamics can be contained if additional information is available, e.g. by integration of an extra on-board measurement. The third section therefore presents improvements to unaided motion model propagation by means of low-cost aiding.

Finally, a number of aided position propagation methods with well-understood advantages and weaknesses presents the basis for further research of GNSS-denied flight navigation. If complementary qualities of any two of these methods can be found, these could be implemented in parallel in an attempt to improve performance. Based on the findings of this chapter, research on how to optimally combine these methods will follow in chapter 3.

2.1 TOTAL STATE PROPAGATION

Propagation of position state requires determination and time integration of velocity. Consequently, the kinematic equations are at the core of any of the methods presented in the following. Differences arise depending on whether velocity is available as measurement, or integrated from acceleration. Acceleration again may be available as measurement or computed from equations of motion and models of forces and moments acting on the vehicle. Because in the latter case there is no measurement of motion involved, this can be

considered a simulation approach to determine vehicle motion using a dynamics model. In contrast, the first two alternatives which use measured velocity or acceleration as input to the kinematic equations may be considered a measurement approach to determine vehicle motion with a kinematics model only.

Three different motion models for position propagation can be distinguished. The first, which integrates a measurement of velocity in order to obtain position change relative to initial condition, is known as dead reckoning. This is a very general classification independent of the actual type of velocity measurement used. The most common low-cost type of dead reckoning methods for aircraft using measurements of heading and airspeed will be studied in the following subsection.

Inertial navigation allows the computation of motion from measured acceleration, and is presented in the second subsection. Although the same kinematic equation for time integration of velocity to obtain position is used, the term dead reckoning will not be used for inertial navigation. The reason for this differentiation lies in the strongly dissimilar error propagation characteristics, as will be discussed in section 2.2. The term dead reckoning will exclusively be used for methods that integrate position from a measurement of velocity and exhibit the typical error drift of such a motion model.

If acceleration can be computed with some model, vehicle motion may be determined without any actual measurement of motion. This constitutes the third type of motion model, a vehicle dynamics model (VDM). For aircraft, this can be realized using models of aerodynamic and propulsion forces and moments, models of weight and balance and translational and rotational equations of motion. Instead of velocity or acceleration, the inputs to the aerodynamics and propulsion model must be available as measurement or from some additional model. In this work, the term aerodynamic motion model will be used for the vehicle dynamics model of an aircraft.

The diversity of these three motion models for position propagation justifies a detailed study of their respective qualities for low-cost GNSS-denied flight navigation.

2.1.1 Heading and airspeed dead reckoning

The dead reckoning method is the simplest way to predict the change of vehicle position and is applied to horizontal motion only for most types of vehicles. Measurements of speed and direction of motion are combined in a two-dimensional velocity vector which is integrated in time starting from the last known position [7]. While manual dead reckoning will compute a new position estimate only once it is needed using averaged speed and direction of motion, this work is concerned with computer methods where high rate computation is the standard.

Figure 1 shows the geometry of heading and airspeed dead reckoning for straight and level flight. The measured quantities, vehicle heading Ψ_{nb} and magnitude of the aerodynamic velocity vector $V_A = \|\mathbf{v}_A\|_2$, are used to compute an approximation of the North and East components of aerodynamic velocity vector \mathbf{v}_{An} . Here it is assumed that the aerodynamic velocity vector is aligned with the aircraft centerline \mathbf{e}_x . Adding an estimate of wind velocity vector then yields an approximation of North and East components of true kinematic velocity vector \mathbf{v}_n which are integrated in time in order to propagate position estimate. The

procedure is similar for ships, where a measurement of speed through water is used and combined with heading and an estimate of water drift velocity.

Generally, three sources of error can be identified for heading and airspeed dead reckoning. First, measurements of aircraft heading and airspeed are distorted by measurement error. Second, the assumption that aerodynamic velocity vector is aligned with the aircraft centerline is not correct in presence of aerodynamic angle of sideslip β_A . Finally, true wind velocity vector \mathbf{v}_{Wn} may differ significantly from the available estimate which further increases dead reckoning error. The last two error effects contribute to the kinematic angle of sideslip β_K which is the difference of vehicle heading and true course angle χ_K in straight and level flight. Again, dead reckoning for ships using heading, speed through water and an estimate of water drift velocity shows equivalent error sources.

In this work, only aircraft applications are of interest and a basic dead reckoning method for aircraft will be described in the following. Error propagation of heading and airspeed dead reckoning is discussed in more detail in section 2.2.1.

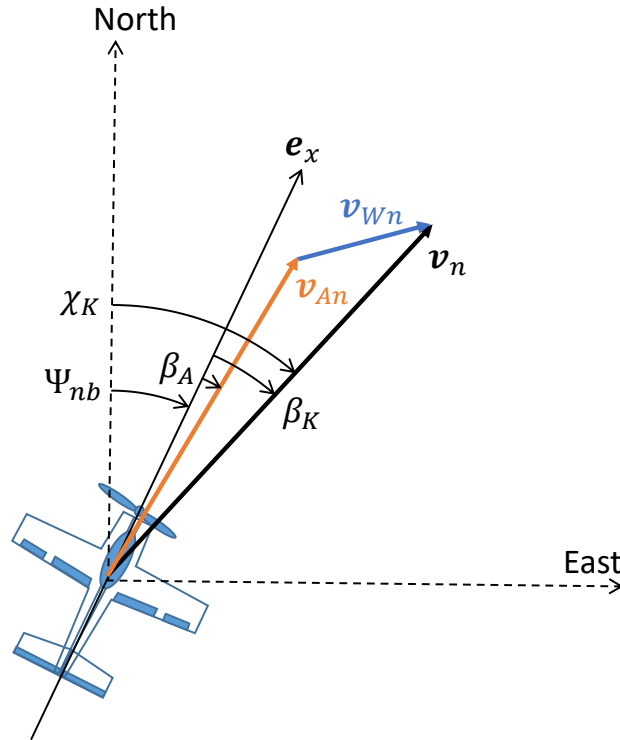


Figure 1: Geometry of dead reckoning for straight and level flight

2.1.1.1 System equations

Given airspeed V_A , heading angle Ψ_{nb} and horizontal wind velocity vector at aircraft location \mathbf{v}_{HWn} (North and East components of air mass velocity), the horizontal kinematic velocity vector can be computed approximately as

$$\mathbf{v}_{Hn} \approx \mathbf{v}_{HWn} + \begin{bmatrix} \cos(\Psi_{nb}) \\ \sin(\Psi_{nb}) \end{bmatrix} V_A \quad (2-1)$$

This assumes $\Psi_{nb} \approx \chi_A$ and $\cos(\gamma_A) \approx 1$, which holds for small aerodynamic angle of sideslip in straight and level flight.

The dead reckoning method uses the approximation of horizontal kinematic velocity vector in equation (2-1) to continuously compute the desired position information. Horizontal position of navigation reference point R is parametrized as vector $\mathbf{\Lambda}_H$ of geodetic latitude and longitude (see e.g. [15–17]) with respect to the WGS84 ellipsoid [18]

$$\mathbf{\Lambda}_H = \begin{bmatrix} \phi_{WGS84}^R \\ \lambda_{WGS84}^R \end{bmatrix} \begin{array}{l} \dots \text{geodetic latitude} \\ \dots \text{geodetic longitude} \end{array}$$

Starting from initial estimate $\mathbf{\Lambda}_{H,0}$, e.g. the last available GNSS position, the horizontal WGS84 position vector $\mathbf{\Lambda}_H$ can be propagated in time by integration of the differential equation (see appendix A.2 for a derivation including the vertical)

$$\dot{\mathbf{\Lambda}}_H = \begin{bmatrix} \frac{1}{M(\phi_{WGS84,0}^R) + h_{WGS84}^R} & 0 \\ 0 & \frac{1}{(N(\phi_{WGS84,0}^R) + h_{WGS84}^R) \cos(\phi_{WGS84}^R)} \end{bmatrix} \mathbf{v}_{Hn} \quad (2-2)$$

For simplicity, normal and meridian curvature radii M and N (see [16] and appendix A.2) may be computed at initial latitude. This simplification introduces negligible error given the overall low accuracy of the dead reckoning method. A more detailed discussion will follow in the next section and in [19].

The cosine of latitude in equation (2-2) must be computed regularly at the propagated position since its value changes significantly at high latitudes for nonzero north velocity. A different choice of position parametrization for use in high latitude regions is strongly recommended (direction cosine matrices or quaternions, c.f. polar navigation and world-wide capability in [20, 21]).

If no information on height is available, using the last known $h_{WGS84,0}^R$ is acceptable for small general aviation airplanes with typically low service ceilings.

2.1.1.2 Algorithm inputs

The dead reckoning method assumes vehicle heading information is available as system input. Because heading cannot be simply measured on a moving and rotating platform, this input generally is generated by another system. This system could be a magnetic compass, AHRS or navigation system. In any case, system behavior has a strong effect on the generated heading information used by the dead reckoning method. Consequently, a characterization of this signal is rather complex and requires the heading system to be included in the analysis as a whole.

Information on airspeed is commonly available on all types of aircraft, because it is of fundamental importance for flight control. Depending on size, speed and complexity of the aircraft, the airspeed may be computed as indicated, calibrated or true airspeed (IAS/CAS/TAS). The first two only require measurement of impact pressure, i.e. the differential pressure between static and total air pressure, but neglect deviations of the properties of air

at aircraft location from sea level conditions. CAS is more exact and more complex because instrument and installation position errors have been corrected [22]. Furthermore, for flight Mach numbers above 0.3, compressible flow effects are accounted for assuming sea level conditions. Computation of TAS accounts for local air conditions but requires measurements of static air pressure and total air temperature (or outside air temperature) in addition to impact pressure. This means two more physical air measurements to be installed, calibrated and maintained.

Finally, horizontal wind vector at aircraft location is nearly impossible to determine when navigation precision is degraded (due to loss of GNSS) and without precise air data measurements. Instead, a long term wind vector average computed while in normal operation or a weather model predicted wind vector may be used. If available, weather radio information on wind vector may be an option, too.

2.1.2 Inertial navigation

Inertial navigation uses an accelerometer to determine the acceleration by which the trajectory of an object is perturbed from the freely-falling trajectory at its current position. An accelerometer can determine this acceleration by observing the inertial resistance of an accurately modeled mechanical probe against disturbance from moving by inertia.

For example, an ideal point-mass satellite would not experience any interference while it follows a freely-falling trajectory in the gravitational field of earth, moon, sun and all other large celestial objects. Consequently, an ideal accelerometer installed on board would produce zero output (see [23] for a similar thought experiment). If the satellite has finite size, it will experience solar radiation and atmospheric drag (for low perigee). This prevents the satellite and the mechanical probe inside the accelerometer from moving with inertia. Both will resist this disturbance, and the observed effect on the mechanical state of the accelerometer's probe allows to compute the experienced acceleration by application of the laws of motion. For a slowly moving object in a weak and stationary gravitational field, Newton's equations of motion are applicable [24]. For an introductory discussion of inertia and gravitation, the reader is referred to [25, 26].

For the simplest mechanical probe that could be used in an accelerometer – a point mass attached to a spring – the inertial resistance is observed as a force acting on and stretching or compressing the spring. The measured acceleration is spring force divided by mass of the probe. Therefore, the accelerometer output is generally referred to as specific force.

For practical use, the object's motion should be described in some fixed reference system, such as the earth-centered inertial (ECI) frame. This requires the apparent relative acceleration of the ECI frame (i.e. freely-falling center of gravity of the earth) and the current freely-falling frame at object position to be added to the measured acceleration. Resolved in an inertial frame (e.g. at the center of gravity of the solar system), this relative acceleration is the difference in gravitational acceleration experienced by the center of gravity of the earth and the object.

For terrestrial inertial navigation, i.e. in close proximity of the earth, this choice of reference frame avoids the complexity of computing gravitation due to all (close) celestial bodies. Because earth itself is affected by gravitation of the same bodies, only earth's gravitation and the differential gravitational accelerations remain. Referring to their effect on the large water masses on earth, the latter are referred to as tidal accelerations. Due to their differential nature, they are small close to the earth. The largest tidal acceleration is caused by the gravitational attraction and coupled motion of earth and moon and has a maximum value on earth's surface of $\sim 0.115\mu g$ at the point closest to the moon (c.f. [27]). The tidal acceleration of the sun is smaller by approximately 55% [27]. For all but highest accuracy terrestrial inertial navigation, these tidal accelerations can be neglected and only earth's gravitational acceleration remains in the equation.

Because the accelerometer's measurement is resolved in direction of a defined input axis of its mechanical probe, computing position and velocity of the object in reference frame coordinates requires a triad of accelerometers aligned with the reference frame axes. If it is not possible to keep the triad constantly aligned with the reference frame axes, the relative orientation must be known and used for projection of the individual measurements in the direction of velocity integration. Technical designs that aim to keep the accelerometer triad

of input axes aligned with the ECI (or other) reference frame axes are called gimballed (or platform) inertial navigation systems. Similar to the measurement principle of accelerometers, gimballed inertial systems rely on the inertial resistance of mechanical gyroscopes against rotation around their input axes to keep the platform carrying the accelerometer triad aligned. The mechanical complexity and resulting cost of these designs is their most important drawback [28]. The modern alternative is called strapdown inertial navigation [21, 29] and uses a navigation computer for the transformation of measurements of the accelerometer triad which is rigidly installed on the object and defines the body-fixed coordinate frame in this work. This requires high rate propagation of the triad orientation with respect to the reference frame, accomplished by integrating inertial angle increments of a triad of gyroscopes. A brief account on the historical development and best practice recommendation of processing (rotation) inertial data in strapdown systems can be found in [29].

The reader is referred to [21, 23, 28, 30] for more information on inertial navigation technology.

2.1.2.1 System equations

The navigation state vector with reference point R is parametrized with position in geodetic latitude, geodetic longitude and height with respect to the WGS84 ellipsoid [15–18], velocity relative to ECEF frame written in NED coordinates and the orientation quaternion from NED frame to body-fixed frame (see appendix A.1):

$$\mathbf{z}_n = \begin{bmatrix} \phi_{WGS84}^R \\ \lambda_{WGS84}^R \\ h_{WGS84}^R \\ \mathbf{v}_n^R \\ \tilde{\mathbf{q}}_{nb} \end{bmatrix} \begin{array}{l} \dots \text{geodetic latitude} \\ \dots \text{geodetic longitude} \\ \dots \text{height above WGS84 ellipsoid} \\ \dots \text{ECEF velocity in NED coordinates} \\ \dots \text{NED to body-fixed frame orientation quaternion} \end{array}$$

Both indications for WGS84 coordinates and navigation reference point R are omitted in the following and throughout this thesis for brevity anywhere possible. Instead, alternative position reference frames or state vector reference points will be noted. The vector of WGS84 position is defined as $\mathbf{\Lambda} = [\phi, \lambda, h]^T$.

The set of ordinary differential equations (2-3) (see [31, 32] and appendix A.2) describes the motion of a point mass in presence of specific forces along the orthogonal axes of the body-fixed frame $\mathbf{f}_b = \mathbf{f}_{b\parallel e_x} + \mathbf{f}_{b\parallel e_y} + \mathbf{f}_{b\parallel e_z}$ and gravity of the earth $\boldsymbol{\gamma}_n$. The rotation of body-fixed frame b ($\mathbf{e}_{b,x}, \mathbf{e}_{b,y}, \mathbf{e}_{b,z}$) with respect to inertial frame is described by the inertial angular rates vector $\boldsymbol{\omega}_{ib}$:

$$\begin{aligned} \dot{\phi} &= \frac{v_N}{M(\phi) + h} \\ \dot{\lambda} &= \frac{v_E}{(N(\phi) + h) \cos(\phi)} \\ \dot{h} &= -v_D \end{aligned} \tag{2-3}$$

$$\dot{\mathbf{v}}_n = \mathbf{R}_{nb}(\tilde{\mathbf{q}}_{nb})\mathbf{f}_b + \boldsymbol{\gamma}_n(\phi, h) - (2\mathbf{R}_{en}^T(\phi, \lambda)\boldsymbol{\omega}_{ie} + \boldsymbol{\omega}_{en}(\phi, h, v_N, v_E)) \times \mathbf{v}_n$$

$$\ddot{\tilde{\mathbf{q}}}_{nb} = \frac{1}{2}(\tilde{\mathbf{q}}_{nb} \cdot \ddot{\boldsymbol{\omega}}_{ib} - \ddot{\boldsymbol{\omega}}_{in}(\phi, \lambda, h, v_N, v_E) \cdot \tilde{\mathbf{q}}_{nb})$$

Note that the differential equations for WGS84 position in the horizontal are the same as for heading and airspeed dead reckoning (2-2) but with normal and meridian curvature radii M and N computed at current latitude ϕ . \mathbf{R}_{nb} and \mathbf{R}_{en} are direction cosine matrices defined by NED to body-fixed frame orientation quaternion and WGS84 latitude and longitude respectively. They are computed using (see appendix A.1)

$$\mathbf{R}(\tilde{\mathbf{q}}) = \begin{bmatrix} q_0^2 + q_1^2 - q_2^2 - q_3^2 & 2(q_1q_2 - q_0q_3) & 2(q_1q_3 + q_0q_2) \\ 2(q_1q_2 + q_0q_3) & q_0^2 - q_1^2 + q_2^2 - q_3^2 & 2(q_2q_3 - q_0q_1) \\ 2(q_1q_3 - q_0q_2) & 2(q_2q_3 + q_0q_1) & q_0^2 - q_1^2 - q_2^2 + q_3^2 \end{bmatrix}$$

and

$$\mathbf{R}_{en} = \begin{bmatrix} -\sin(\phi) \cos(\lambda) & -\sin(\lambda) & -\cos(\phi) \cos(\lambda) \\ -\sin(\phi) \sin(\lambda) & \cos(\lambda) & -\cos(\phi) \sin(\lambda) \\ \cos(\phi) & 0 & -\sin(\phi) \end{bmatrix}$$

The transport rate $\boldsymbol{\omega}_{en}$ appears in the differential equations for ECEF velocity in NED coordinates \mathbf{v}_n and for NED to body-fixed frame orientation quaternion with

$$\boldsymbol{\omega}_{in} = \boldsymbol{\omega}_{en} + \mathbf{R}_{en}^T \boldsymbol{\omega}_{ie}$$

While earth rotation rate vector $\boldsymbol{\omega}_{ie}$ is constant to sufficient accuracy for inertial navigation applications with $\omega_{ie} = \|\boldsymbol{\omega}_{ie}\|_2 = 7292115 \cdot 10^{-11} \text{rad/s}$ [18], transport rate must be computed using

$$\boldsymbol{\omega}_{en} = \begin{bmatrix} \frac{v_E}{N(\phi) + h} \\ \frac{v_N}{M(\phi) + h} \\ -\frac{\tan(\phi) v_E}{N(\phi) + h} \end{bmatrix}$$

The so-called strapdown equations in NED frame (2-3) will be abbreviated in the remainder of this work as function $\mathbf{s}(\mathbf{z}_n, \mathbf{f}_b, \boldsymbol{\omega}_{ib})$.

An inertial navigation system (INS) computes \mathbf{z}_{nINS} over time according to above strapdown equations (2-3), given an initial value and specific force and inertial angular rates measured by IMU, denoted as $\tilde{\mathbf{f}}_b$ and $\tilde{\boldsymbol{\omega}}_{ib}$.

Although equations (2-3) can be numerically integrated using any time integration scheme, such as classical 4th order Runge-Kutta [33], accuracy in applications with large rotational movements is much higher using the exact quaternion update for orientation propagation, which is derived in appendix A.1. In the following, a simple strapdown navigation algorithm suitable for the navigation studies presented in this work is summarized.

Defining a time-averaged angular rates vector $\boldsymbol{\omega}_{ib}$ in time interval $[t, t + \Delta t]$, and with equation (A-41), the orientation of body-fixed frame b is propagated in time as follows

$$\tilde{\mathbf{q}}_{ib_{t+\Delta t}} = \tilde{\mathbf{q}}_{ib_t} \cdot (\cos(\Delta t \|\boldsymbol{\omega}_{ib}\|/2) + \sin(\Delta t \|\boldsymbol{\omega}_{ib}\|/2) \tilde{\mathbf{n}}_b)$$

With $\tilde{\mathbf{n}}_b$ the quaternion counterpart of normalized angular rates vector $\mathbf{n}_b = \boldsymbol{\omega}_{ib} / \|\boldsymbol{\omega}_{ib}\|$.

In this work, $\check{\mathbf{q}}_{nb}$ is chosen to parametrize body-fixed frame orientation and the initial quaternion $\check{\mathbf{q}}_{ib_t}$ is computed using the position and NED to body-fixed frame orientation quaternion at time t

$$\check{\mathbf{q}}_{ib_t} = \check{\mathbf{q}}_{eb_t} = \check{\mathbf{q}}_{en}(\phi_t, \lambda_t) \cdot \check{\mathbf{q}}_{nb_t}$$

For simplicity, alignment of inertial frame i and ECEF frame e can be assumed at time t , i.e. $\check{\mathbf{q}}_{ie_t} = 1$. $\check{\mathbf{q}}_{en}(\phi_t, \lambda_t)$ is computed by solving equation (A-66) for the coefficients of the quaternion according to equation (A-32).

Now the earth rotation in time interval $[t, t + \Delta t]$ can be accounted for

$$\check{\mathbf{q}}_{ie_{t+\Delta t}} = \check{\mathbf{q}}_{ie_t} \cdot (\cos(\Delta t \|\boldsymbol{\omega}_{ie}\|/2) + \sin(\Delta t \|\boldsymbol{\omega}_{ie}\|/2) \check{\mathbf{n}}_e)$$

With $\check{\mathbf{n}}_e$ the quaternion counterpart of normalized earth rate vector $\mathbf{n}_e = \boldsymbol{\omega}_{ie}/\|\boldsymbol{\omega}_{ie}\|$.

The propagated ECEF to body-fixed frame quaternion at time $t + \Delta t$ is

$$\check{\mathbf{q}}_{eb_{t+\Delta t}} = \check{\mathbf{q}}_{ie_{t+\Delta t}}^{-1} \cdot \check{\mathbf{q}}_{ib_{t+\Delta t}}$$

With the propagated position at time $t + \Delta t$ and with $\check{\mathbf{q}}_{ie_t} = 1$, the propagated NED to body-fixed frame quaternion at time $t + \Delta t$ is

$$\begin{aligned} \check{\mathbf{q}}_{nb_{t+\Delta t}} &= \check{\mathbf{q}}_{en}^{-1}(\phi_{t+\Delta t}, \lambda_{t+\Delta t}) \cdot \check{\mathbf{q}}_{eb_{t+\Delta t}} \\ &= \check{\mathbf{q}}_{en}^{-1}(\phi_{t+\Delta t}, \lambda_{t+\Delta t}) \cdot (\cos(\Delta t \|\boldsymbol{\omega}_{ie}\|/2) - \sin(\Delta t \|\boldsymbol{\omega}_{ie}\|/2) \check{\mathbf{n}}_e) \cdot \check{\mathbf{q}}_{en}(\phi_t, \lambda_t) \cdot \check{\mathbf{q}}_{nb_t} \\ &\quad \cdot (\cos(\Delta t \|\boldsymbol{\omega}_{ib}\|/2) + \sin(\Delta t \|\boldsymbol{\omega}_{ib}\|/2) \check{\mathbf{n}}_b) \end{aligned} \quad (2-4)$$

Note that approximation of the change of body rotation axis in the output time interval is possible e.g. as proposed in [34]. Also refer to [29] for recommended steps to account for effects due to high frequency motion.

For integration of position and velocity states in INS, a 2nd order Runge-Kutta time integration scheme without intermediate step is used in this work (the explicit trapezoidal method [33] also known as improved Euler method [35]). It can be combined with above orientation quaternion update (2-4), abbreviated as function \mathbf{p} in the following. Defining a subset $\mathbf{s}_{trans}(\mathbf{z}_{n_{trans}}, \mathbf{f}_n)$ of the ordinary differential equations (2-3) for translational state vector $\mathbf{z}_{n_{trans}} = [\phi, \lambda, h, \mathbf{v}_n^T]^T$ only, a concise description of the time integration method is possible.

The improved Euler method consists of a forward Euler prediction step

$$\begin{aligned} \mathbf{z}_{n_{trans}^*_{t+\Delta t}} &= \mathbf{z}_{n_{trans}_t} + \Delta t \mathbf{s}_{trans}(\mathbf{z}_{n_{trans}_t}, \mathbf{f}_{n_t}) \\ \check{\mathbf{q}}_{nb_{t+\Delta t}^*} &= \mathbf{p}(\check{\mathbf{q}}_{nb_t}, \phi_t, \lambda_t, \phi_{t+\Delta t}^*, \lambda_{t+\Delta t}^*, \boldsymbol{\omega}_{ib_t}, \Delta t) \end{aligned} \quad (2-5)$$

With $\mathbf{f}_{n_t} = \mathbf{R}(\check{\mathbf{q}}_{nb_t})\mathbf{f}_{b_t}$. The preliminary results denoted by a * are improved in a successive trapezoidal rule correction step yielding the final propagated navigation state $\mathbf{z}_{n_{trans}_{t+\Delta t}}$ and $\check{\mathbf{q}}_{nb_{t+\Delta t}}$

$$\begin{aligned} \mathbf{z}_{n_{trans}_{t+\Delta t}} &= \mathbf{z}_{n_{trans}_t} + \frac{\Delta t}{2} \left(\mathbf{s}_{trans}(\mathbf{z}_{n_{trans}_t}, \mathbf{f}_{n_t}) + \mathbf{s}_{trans}(\mathbf{z}_{n_{trans}^*_{t+\Delta t}}, \mathbf{f}_{n_{t+\Delta t}^*}) \right) \\ \check{\mathbf{q}}_{nb_{t+\Delta t}} &= \mathbf{p} \left(\check{\mathbf{q}}_{nb_t}, \phi_t, \lambda_t, \phi_{t+\Delta t}, \lambda_{t+\Delta t}, \frac{1}{2} \boldsymbol{\omega}_{ib_t} + \frac{1}{2} \boldsymbol{\omega}_{ib_{t+\Delta t}}, \Delta t \right) \end{aligned} \quad (2-6)$$

With $\mathbf{f}_{n_{t+\Delta t}}^* = \mathbf{R}(\tilde{\mathbf{q}}_{nb_{t+\Delta t}}^*)\mathbf{f}_{b_{t+\Delta t}}$. Note that transport rate integration is not included in the orientation propagation step but solely represented by position propagation.

The presented strapdown navigation algorithm (2-4), (2-5) and (2-6) for time propagation of navigation state vector \mathbf{z}_n is a simplification of more evolved schemes found in the literature, e.g. [34, 36]. Similar to all available algorithms, it introduces time discretization errors due to truncation of terms of (in this case) 3rd and higher order in Δt in equations (2-5) and (2-6) and due to the assumption of a specific behavior of specific force and inertial angular rates vectors in interval $[t, t + \Delta t]$. Here constant directions of these vectors in $[t, t + \Delta t]$ are assumed. This simplification is acceptable for the navigation studies presented in this work where high-rate inertial data is available and the effects of high-frequency motion are negligible compared to other error effects.

2.1.2.2 Algorithm inputs

For inertial navigation using the strapdown algorithm described above, three input signals are required. First, measurements of specific force vector and inertial angular rates vector must be provided at sufficiently high rate. Because no other information on vehicle motion is used in inertial navigation, these measurements must contain full bandwidth motion information. If true motion is not fully resolved by time discrete inertial measurements, discretization errors may be rectified in the integration of motion.

Because inertial angular rates measurements should describe rotational motion of the accelerometer sensor triad, the gyroscopes are always closely integrated mechanically with the accelerometers in an inertial measurement unit (IMU). Thus the IMU produces vector measurements of specific force and inertial angular rate, usually at equal rates.

Various measurement technologies have been developed over the last decades and used in IMUs for inertial navigation. Classical mechanical designs have been mostly replaced by quartz and MEMS (micro-electro-mechanical systems) designs for accelerometers and MEMS, FOG (fiber-optic gyro) and RLG (ring laser gyro) designs for gyroscopes (c.f. [30]).

The third required input for inertial navigation is the gravity vector $\boldsymbol{\gamma}_n$. Because this gravity vector includes the effects of earth gravitation and centripetal acceleration in a frame fixed to rotate with the earth (such as ECEF which is used to define velocity \mathbf{v}_n), it can also be computed given gravitation vector and earth rotation rate using

$$\boldsymbol{\gamma}_n = \mathbf{R}_{en}^T(\mathbf{g}_e - \boldsymbol{\omega}_{ie} \times (\boldsymbol{\omega}_{ie} \times \mathbf{r}_e)) \quad (2-7)$$

In any case, accurate computation models exist for terrestrial navigation: Normal gravity (the best approximation of earth's gravity assuming an ellipsoidal shape and rotation) can be computed with the formula of Somigliana valid at the surface of the WGS84 reference ellipsoid and a Taylor series expansion for small positive heights (see appendix A.2, [18] and [37]). Alternatively, gravitation vector for use with equation (2-7) can be computed as gradient of a series expression approximating actual earth gravitational potential (e.g. EGM96 [18] or EGM2008 [38]).

2.1.3 Aerodynamic motion model

The previous methods for position propagation presented in this section both use measurements of the actual motion. With fundamental kinematic equations to integrate these measurements, the type of object to be navigated is irrelevant. These methods may even be applied to objects that cannot move at all. Now, the possibility of navigation of a vehicle with well-understood system dynamics shall be considered. In this case, measurement of motion may be replaced by simulation of motion using models of vehicle dynamics (a vehicle dynamics model, VDM).

The ultimate goal of development of a vehicle is to realize the desired system behavior in the final product. Consequently, understanding of its dynamics is present for any professionally developed vehicle. Due to the potentially catastrophic consequences when the final products (or prototypes) behavior in flight is not stable, this is especially true for aircraft. In two ways: First, considerable effort is made to understand and define a desired system behavior, which would guarantee safe flight. Second, throughout the development process and intensively already before first flight of a prototype, achievement of desired behavior is constantly verified by design reviews. This process should result in converging qualities of defined and verified system behavior. The preferable form to define desired or identify actual (preliminary) system behavior is a dynamics model. A dynamics model allows for software simulation of a part or the whole of the systems behavior in a given application scenario. In this work, a vehicle dynamics model (VDM) shall be defined as a model that allows for simulation of translational and rotational motion of a coordinate frame fixed to the vehicle (body-fixed frame), given control and environmental inputs. Flight control or control and stability augmentation systems shall not be part of the VDM, and control inputs are as applied on the actuators and engines.

Airplanes with conventional design have distinctive flight dynamics that are also present in the vehicle dynamics model. This makes airplane VDM especially suited for use a position propagation method as will be detailed in later sections.

It is assumed that other means of navigation are always available during taxi and takeoff or mission is aborted. The aerodynamic motion model for position propagation will only be usable in flight. Because it is considered for use in a backup navigation function, landing is not considered an issue: For landing, visual reference or accurate means of navigation must be available.

As explained above, the high-quality aerodynamic motion model is expected to be available from airplane development. This work is not concerned with high-fidelity models for airplane flight – typically comprising aerodynamics, propulsion system, fuel flow, weight and balance models among others. The following focuses on the aspects that are relevant for this research: A characterization of the information available from a high-fidelity aerodynamic motion model that is usable for low-cost integrated navigation. The available information is related to the navigation states and the dependencies of the model are identified. Some simplifications are permissible at this point, because only the significant influences need to be accounted for an acceptable characterization of the behavior and uncertainty of a general aviation airplane model.

2.1.3.1 System equations

The model of airplane aerodynamic forces and moments is complemented by models of propulsion forces and moments, fuel consumption, loading and weight and balance. Altogether, the vehicle dynamics model (VDM) can be used to simulate flight of a rigid body airplane given a correct initial condition and control inputs over time:

$$\dot{\mathbf{z}}_v = \frac{d}{dt} \begin{bmatrix} \mathbf{z}_n \\ \boldsymbol{\omega}_{ib} \end{bmatrix} = \begin{bmatrix} \mathbf{s}(\mathbf{z}_n, \mathbf{f}_b^R, \boldsymbol{\omega}_{ib}) \\ \mathbf{I}_{bb}^G^{-1} (\mathbf{M}_b^G - \boldsymbol{\omega}_{ib} \times (\mathbf{I}_{bb}^G \boldsymbol{\omega}_{ib})) \end{bmatrix} \quad (2-8)$$

The 12-DOF vehicle state vector \mathbf{z}_v is composed of position, kinematic velocity and orientation that are parametrized in the same way as in a common inertial navigation mechanization (\mathbf{z}_n) plus inertial angular rates in body-fixed frame $\boldsymbol{\omega}_{ib}$. Therefore, strapdown navigation differential equations \mathbf{s} appear in the first row of the right hand side of equation (2-8).

The specific force vector that determines point mass motion corresponds to the holding forces acting on the actual IMU accelerometer triad (which defines the navigation reference point R), divided by its mass. Because the vehicle is assumed perfectly rigid here, this is equal to the sum of external forces computed from the models and acting on the vehicle plus inner forces at point R , divided by aircraft mass m . Inner forces are due to rotation and angular acceleration of the vehicle and lever arm between R and vehicle center of gravity G (with $\dot{\mathbf{r}}_b^{RG} = \mathbf{0}$ and all geometry assumed to be rigid, c.f. appendix A.3)

$$\mathbf{f}_b^R = \frac{\mathbf{F}_b^R}{m} = \sum_{Aero, Prop} \frac{\mathbf{F}_{bi}^G}{m} - \boldsymbol{\omega}_{ib} \times \mathbf{r}_b^{RG} - \boldsymbol{\omega}_{ib} \times (\boldsymbol{\omega}_{ib} \times \mathbf{r}_b^{RG}) \quad (2-9)$$

The second row of equation (2-8) consists of the Euler equation of rotational motion for a rigid body with time invariant mass distribution (a restriction that can be relaxed considering time scales for mass change to be much larger than for rotational motion). See appendix A.4 and [39] for a detailed derivation.

The effective moment acting in center of gravity G is the sum of external moments only:

$$\mathbf{M}_b^G = \sum_{Aero, Prop} \mathbf{M}_{bi}^G$$

Aerodynamic and propulsion forces in the center of gravity $\mathbf{F}_{b\ Aero}^G$ and $\mathbf{F}_{b\ Prop}^G$ are surface integrals of air pressure and friction forces acting on airplane wings, fuselage, propeller etc. A physically exact model would therefore be of infinite order. Modeling fidelity and complexity is significantly reduced by directly modeling forces and moment vector pairs used in the equations above, localized at a defined model reference point instead of computing actual surface integrals, e.g.

$$\begin{aligned} \mathbf{F}_{b\ Aero}^G &= \mathbf{F}_{b\ Aero}^A(\mathbf{z}_v, \dot{\mathbf{z}}_v, \mathbf{v}_{Wn}, \boldsymbol{\omega}_{Wb}, \mathbf{u}_p, \mathbf{c}_v) \\ \mathbf{M}_{b\ Aero}^G &= \mathbf{M}_{b\ Aero}^A(\mathbf{z}_v, \dot{\mathbf{z}}_v, \mathbf{v}_{Wn}, \boldsymbol{\omega}_{Wb}, \mathbf{u}_p, \mathbf{c}_v) - \mathbf{r}_b^{AG} \times \mathbf{F}_{b\ Aero}^A(\mathbf{z}_v, \dot{\mathbf{z}}_v, \mathbf{v}_{Wn}, \boldsymbol{\omega}_{Wb}, \mathbf{u}_p, \mathbf{c}_v) \end{aligned}$$

This aerodynamic model computes a force and moment vector pair acting in the corresponding model reference point A . \mathbf{u}_p is the vector of direct pilot control inputs or actuated controls and \mathbf{c}_v is the vector of model coefficients. Note that this aerodynamic

model does not introduce any additional states and, in combination with the equations of motion (2-8) that give $\dot{\mathbf{z}}_v$, presents a direct algebraic scheme to compute aerodynamic forces and moments. The propulsion model takes a similar form. Although high fidelity propulsion system models might include states for shaft speed and other, this is not considered here.

Computation of the specific force vector in the navigation reference point R using equation (2-9) requires both the vehicles inertial angular rates in body-fixed frame $\boldsymbol{\omega}_{ib}$ and corresponding time derivative $\dot{\boldsymbol{\omega}}_{ib}$ to account for relative acceleration effects due to the lever arm between navigation reference point and time variable center of gravity location \mathbf{r}^{RG} . The inertial angular rates time derivative is obtained from the Euler equation of rotational motion, the second row in equation (2-8).

The presented equations of motion (2-8), (2-9) are valid for a rigid body, i.e. under the assumption that mass distribution over the vehicle geometry is time invariant. Although this is not strictly the case for a conventional small general aviation airplane with a reciprocating or turboprop engine, the rate of change of total mass due to consumption of fuel in fuselage or wing tanks is small. Consequently, the loss of accuracy due to truncation of terms accounting for time variant mass distribution in the equations of motion is negligible compared the inevitable modeling errors in aerodynamic and propulsion forces and moments. Still, mass m , inertia matrix \mathbf{I}_{bb}^G and center of gravity location G change significantly over the duration of a long flight and must be continuously computed from models that take fuel consumption and mass distribution into account.

Note that unlike for inertial navigation, common time-integration schemes may be used to integrate above system of differential equations. A good choice of method offers numerical robustness and accuracy at reasonable computational cost. The classical 4th order Runge-Kutta method [33] is typically applied for fixed airplane simulation [22, 40, 41] and is therefore selected here. With input data valid at equidistant time points $t, t + \frac{1}{2}\Delta t$ and $t + \Delta t$, the vehicle state vector $\mathbf{z}_v = [\mathbf{z}_n^T \boldsymbol{\omega}_{ib}^T]^T$ is propagated in time as

$$\mathbf{z}_{v_{t+\Delta t}} = \mathbf{z}_{v_t} + \frac{\Delta t}{6} \left(\dot{\mathbf{z}}_{v_t} + 2\dot{\mathbf{z}}_{v_{t+1/2\Delta t}}^* + 2\dot{\mathbf{z}}_{v_{t+1/2\Delta t}}^\diamond + \dot{\mathbf{z}}_{v_{t+\Delta t}}^* \right)$$

For this single propagation step of state vector \mathbf{z}_v from time t to time $t + \Delta t$, the right hand side of equation (2-8) must be evaluated 4 times:

1. At the initial state \mathbf{z}_{v_t} and using input data valid at time t , which gives $\dot{\mathbf{z}}_{v_t}$. This is used to compute the predicted state (denoted by a *) at intermediate time $t + \frac{1}{2}\Delta t$

$$\mathbf{z}_{v_{t+1/2\Delta t}}^* = \mathbf{z}_{v_t} + \frac{1}{2}\Delta t \dot{\mathbf{z}}_{v_t}$$

2. At predicted intermediate state $\mathbf{z}_{v_{t+1/2\Delta t}}^*$ and using input data valid at time $t + \frac{1}{2}\Delta t$, which gives $\dot{\mathbf{z}}_{v_{t+1/2\Delta t}}^*$. This is used to compute the corrected state (denoted by a \diamond) at intermediate time $t + \frac{1}{2}\Delta t$

$$\mathbf{z}_{v_{t+1/2\Delta t}}^\diamond = \mathbf{z}_{v_t} + \frac{1}{2}\Delta t \dot{\mathbf{z}}_{v_{t+1/2\Delta t}}^*$$

3. At corrected intermediate state $\mathbf{z}_{v_{t+1/2\Delta t}}^\diamond$ and using input data valid at time $t + \frac{1}{2}\Delta t$, which gives $\dot{\mathbf{z}}_{v_{t+1/2\Delta t}}^\diamond$. This is used to compute the predicted state at time $t + \Delta t$

$$\mathbf{z}_{v_{t+\Delta t}}^* = \mathbf{z}_{v_t} + \Delta t \dot{\mathbf{z}}_{v_{t+1/2\Delta t}}^\circ$$

4. Finally at predicted state $\mathbf{z}_{v_{t+\Delta t}}^*$ and using input data valid at time $t + \Delta t$, which gives $\dot{\mathbf{z}}_{v_{t+\Delta t}}^*$

For a given rate of input data, vehicle state vector is computed at only half that rate. If this is for some reason undesirable (e.g. because input data rate is already low), a 2nd order Runge-Kutta scheme with equal rates of input and propagated state vector data can be used (improved Euler or explicit trapezoidal method [33, 35]). Because both precision and stability of vehicle motion propagation is affected, time integration should be tested thoroughly in simulation.

2.1.3.2 Algorithm inputs

For evaluation of equations (2-8) and (2-9), the sums of external forces and moments in some defined reference point of the aerodynamic model, aircraft mass and inertia matrix must be available. Furthermore, center of gravity position is required to compute forces and moments in center of gravity.

Aircraft mass m , inertia I_{bb}^G and center of gravity position \mathbf{r}_b^{RG} are computed with a weight and balance model. Such a model could be based on CAD data of geometry and mass distribution of the empty aircraft in combination with a fuel load and inertia model (for reciprocating or turboprop engines) and models for passenger and luggage load and inertia. Fuel consumption must be provided by the engine model to account for the slow change in weight and balance properties in flight. While measuring initial weight and balance on ground and using a model for change due to fuel burn only would certainly be more accurate, this is a considerable operational burden and not always possible.

Dimensional analysis of aerodynamics (see [42, 43]) shows that resulting aerodynamic forces and moments acting on a body of a specific shape and a specific orientation with respect to free stream air motion relative to the body can be formulated as dimensionless coefficients

$$\begin{aligned} C_L &= \frac{1}{\frac{1}{2}\rho V_A^2 S_{ref}} F_{Aero,Lift} \\ C_Y &= \frac{1}{\frac{1}{2}\rho V_A^2 S_{ref}} F_{Aero,Sideforce} \\ C_D &= \frac{1}{\frac{1}{2}\rho V_A^2 S_{ref}} F_{Aero,Drag} \\ C_l &= \frac{1}{\frac{1}{2}\rho V_A^2 S_{ref} l_x} M_{Aero,x} \\ C_m &= \frac{1}{\frac{1}{2}\rho V_A^2 S_{ref} l_y} M_{Aero,y} \\ C_n &= \frac{1}{\frac{1}{2}\rho V_A^2 S_{ref} l_z} M_{Aero,z} \end{aligned} \tag{2-10}$$

The components of aerodynamic moment are written in body-fixed frame coordinates. For airplanes, lift is defined as force perpendicular to free stream motion relative to the airplane, lying in the plane of \mathbf{e}_x and \mathbf{e}_z body-fixed axes (the plane of symmetry of a conventional airplane). The scalar product of the vector of aerodynamic force and the body-fixed $-\mathbf{e}_z$ vector determines the sign of lift. Drag is the force acting in direction of free stream motion (for positive values). Aerodynamic sideforce is perpendicular to both, positive in the right-wing hemisphere.

S_{ref} and l_x, l_y, l_z are reference area and lengths. For airplanes, they are chosen as wing reference area and $l_x = l_z = b$, $l_y = \bar{c}$ with wing span b and mean aerodynamic chord \bar{c} (see [22]).

With ambient air density ρ , dynamic pressure, which appears in all of above definitions, is

$$q := \frac{1}{2} \rho V_A^2$$

Dimensional analysis finds that for any given body geometry and body orientation with respect to free stream motion relative to the body, the aerodynamic coefficients (2-10) are functions of two dimensionless parameters among others

$$Re = \frac{\rho V_A l_{Re}}{\mu} \dots \text{Reynolds number}$$

$$M = \frac{V_A}{a} \dots \text{Mach number}$$

with a reference length l_{Re} (e.g. mean aerodynamic chord \bar{c}), dynamic viscosity μ and speed of sound a . Despite the importance of vehicle weight in the context of stability and trim, there is only a weak and indirect influence of gravity on aerodynamics due to vertical gradients in the atmospheric conditions.

The free stream motion of air relative to the body is described by the aerodynamic velocity vector, which is the vector difference of body kinematic velocity and velocity of the ambient air mass at the point of interest, typically the reference point of the aerodynamic model. In NED coordinates, this is (c.f. Figure 1)

$$\mathbf{v}_{An} = \mathbf{v}_n - \mathbf{v}_{Wn} \quad (2-11)$$

In equation (2-11), wind velocity vector \mathbf{v}_{Wn} is defined as having an equivalent, but opposite in sign, effect on aerodynamic forces and moments compared to the kinematic velocity vector \mathbf{v}_n , when all other properties of air and vehicle states are unchanged. This can be exemplified by the equivalency of aerodynamics in wind tunnel testing at zero kinematic velocity and in real flight. Wind velocity vector \mathbf{v}_{Wn} corresponds to the average undisturbed air mass velocity relative to ECEF frame in a volume where it affects airplane aerodynamics.

In flight, airplane geometry will vary with control surface deflections, flaps and gear position. In addition, angle of attack and angle of sideslip with respect to aerodynamic velocity vector change dynamically due to body rotation or wind. For real time capable computation of aerodynamic forces and moments, which is required here, algebraic models are used. Various possible forms used for modeling aerodynamics of airplanes can be found in the literature [22, 41, 44]. One suitable possibility for airplanes valid over large portions of

the allowed values for angle of attack is a linear model of all aerodynamic coefficients except drag, which is better modeled with a quadratic model

$$\begin{aligned}
 C_L &= C_{L0} + C_{L\alpha}\alpha_A \\
 C_Y &= C_{Y0} + C_{Y\beta}\beta_A \\
 C_D &= C_{D0} + k(C_L - C_{L0})^2 \\
 C_l &= C_{l0} + C_{l\beta}\beta_A + C_{lp}p^* + C_{lr}r^* + C_{l\xi}\xi \\
 C_m &= C_{m0} + C_{m\alpha}\alpha_A + C_{mq}q^* + C_{m\eta}\eta \\
 C_n &= C_{n0} + C_{n\beta}\beta_A + C_{np}p^* + C_{nr}r^* + C_{n\zeta}\zeta
 \end{aligned}
 \tag{2-12}$$

With aerodynamic angles of attack and sideslip, α_A and β_A , nondimensional aerodynamic rates p^* , q^* and r^* and control inputs for roll, pitch and yaw ξ, η and ζ (see Figure 2).

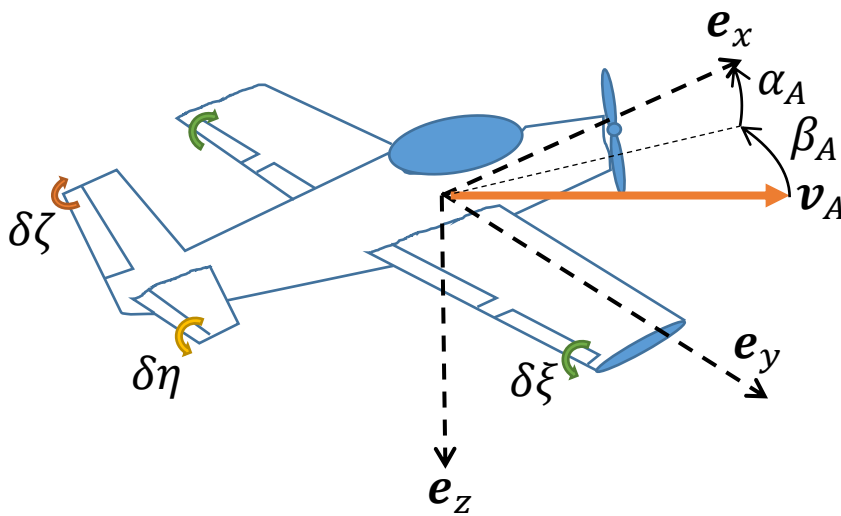


Figure 2: Control deflections and body-fixed frame for a conventional airplane

For a higher fidelity of the model, more terms and derivatives may be used. All of above derivatives and the coefficient of induced drag k are functions of Reynolds number Re , Mach number M and changes in geometry such as flaps and gear position. In addition, bilinear and higher order (nonlinear) effects of control surface deflections, aerodynamic angle of attack and aerodynamic angle of sideslip may be represented by varying aerodynamic derivatives. As mentioned above, the goal here is not to present a high-fidelity model but to study the predominant model characteristics instead. A linear model (2-12) with constant derivatives is sufficient to model the relevant aerodynamics of a conventional general aviation airplane in proximity of a regular reference flight condition, where changes in Re and M are small and nonlinear effects are small (e.g. no high aerodynamic angle of attack).

In equation (2-12), the influence of airplane orientation with respect to aerodynamic velocity vector is accounted for by aerodynamic angles of attack and sideslip, α_A and β_A . In case of rotation of the airplane with a kinematic angular rate, there is an additional effect on aerodynamics due to gradual change of relative free stream orientation over the geometry of the airplane. Instationary effects may be present because changes in the aerodynamics, e.g. of the wings, will affect the aerodynamics at airplane tail with some delay. Similarly, air

mass motion could be inhomogeneous in space or change in time at the aircraft location, leading to equivalent effects on aerodynamics. Both is accounted for by the aerodynamic rates which appear in above equation in nondimensionalized form:

$$\begin{aligned} p^* &= \frac{\omega_{Ax}b}{2V_A} \\ q^* &= \frac{\omega_{Ay}\bar{c}}{2V_A} \\ r^* &= \frac{\omega_{Az}b}{2V_A} \end{aligned} \quad (2-13)$$

The vector of aerodynamic rates is defined as linear combination of kinematic and air mass motion with equivalent effect (but with opposite sign) on aerodynamics:

$$\boldsymbol{\omega}_{Ab} = \boldsymbol{\omega}_{ib} - \boldsymbol{\omega}_{Wb} \quad (2-14)$$

This quantity describes the gradual change in relative motion of undisturbed air and local vehicle surface over the whole vehicle geometry. Changes of the unperturbed air flow parallel to air velocity vector are negligible for all sizes of real airplanes.

The wind angular rates vector $\boldsymbol{\omega}_{Wb}$ is a simplified representation of time and spatial changes in the air mass velocity vector field $\mathbf{v}_{air}(\mathbf{r}, t)$. It can be considered as the sum of all equivalent effects due to air mass velocity vector gradients $\partial\mathbf{v}_{air}/\partial t$ and $\partial\mathbf{v}_{air}/\partial\mathbf{r}^T$ in combination with movement of the vehicle, with negative sign.

The parameters in the functions of aerodynamic coefficients (2-12) as well as dynamic pressure needed to compute dimensional aerodynamic forces and moments using equation (2-10) could all be measured using a total pressure tube, airflow vanes for α and β and a gyroscope for inertial rates in (2-14) while neglecting wind angular rates $\boldsymbol{\omega}_{Wb}$. Together with weight and balance information and propulsion forces and moments, this would allow to compute virtual specific force measurements at IMU position using equation (2-9) and time derivatives of inertial angular rates using the Euler equation of rotational motion for a rigid body in the second row of equation (2-8). That way, the measurements of a real IMU for strapdown inertial navigation could be replaced by a virtual measurement based on vehicle models and measurements such as aerodynamic angle of attack. Because for example an acceleration accuracy of $1mg$ would require aircraft mass to be known in flight within 0.1% error, it is obvious that even low-cost IMU measurements, once calibrated, would be superior and the approach to measure inputs for equations (2-10) and (2-12) is dismissed.

Instead, it is preferable to compute the parameters using the known navigation state vector \mathbf{z}_n . This implements a feedback of navigation errors to the aerodynamic model with a favorable effect on error dynamics, as will be shown in the next section. Equation (2-11) is used to compute aerodynamic velocity vector which, in combination with vehicle orientation, defines aerodynamic angles of attack and sideslip α and β . For this, wind velocity vector \mathbf{v}_{Wn} must be known, which will prove to be a drawback of this approach.

Using an atmosphere model, air density can be computed as a function of height (e.g. with the standard atmosphere [45], which is representative for middle latitudes in the northern hemisphere [46]) and can be used together with aerodynamic velocity magnitude to calculate dynamic pressure. This is an alternative to computing air density from measured static pressure and outside air temperature, which does not require an outside air temperature sensor. In this work, the variability of air density at sea level and as function of

the vertical is not addressed or studied in the method evaluation. While computing air density from static pressure and temperature measurements will consistently account for real atmosphere conditions, computing air density from an atmosphere model requires model calibration for non-standard conditions.

For the nondimensional aerodynamic rates (2-13), the aerodynamic angular rates vector $\boldsymbol{\omega}_{Ab}$ is computed using (2-14). The inertial angular rates $\boldsymbol{\omega}_{ib}$ are contained in the vehicle state vector \mathbf{z}_v , the wind angular rates $\boldsymbol{\omega}_{Wb}$ must be known.

With exception of gyroscopic moments due to internal rotating masses, the propulsion system forces and moments are largely independent of kinematic velocity and inertial angular rates of the vehicle too. Instead, aerodynamic velocity \mathbf{v}_{Ab} and aerodynamic angular rates $\boldsymbol{\omega}_{Ab}$ are influential model parameters. Dependence of aerodynamic and propulsion models on vehicle state time derivative will not be considered in the rest of this work. Therefore, with influential parameters only, the models for aerodynamic and propulsion forces and moments can be written as

$$\begin{aligned}
 & \mathbf{F}_{b\ Aero}^A(h, \mathbf{v}_{Ab}, \boldsymbol{\omega}_{Ab}, \mathbf{u}_p, \mathbf{c}_v) \\
 & \mathbf{M}_{b\ Aero}^A(h, \mathbf{v}_{Ab}, \boldsymbol{\omega}_{Ab}, \mathbf{u}_p, \mathbf{c}_v) \\
 & \mathbf{F}_{b\ Prop}^P(h, \mathbf{v}_{Ab}, \boldsymbol{\omega}_{Ab}, \mathbf{u}_p, \mathbf{c}_v) \\
 & \mathbf{M}_{b\ Prop}^P(h, \mathbf{v}_{Ab}, \boldsymbol{\omega}_{Ab}, \mathbf{u}_p, \mathbf{c}_v)
 \end{aligned} \tag{2-15}$$

For the problem at hand, it will not be possible to predict the values of \mathbf{v}_{Wb} and $\boldsymbol{\omega}_{Wb}$ or model their change in time as the vehicle flies along a specific trajectory. Similarly to heading and airspeed dead reckoning, a long term wind vector average, weather model predicted wind vector or weather radio information on wind vector may be used. Since the wind angular rates vector $\boldsymbol{\omega}_{Wb}$ represents changes in air mass velocity vector field, it can be expected to be more variable than actual wind velocity vector and there is no way to provide this information to the aerodynamic propagation method. Consequently, it must be assumed zero.

The required input of pilot or autopilot controls \mathbf{u}_p , including ξ, η and ζ as well as all other controls for engines, gear, etc. can accurately be provided by measurements of control surface and mechanical control system deflections. Depending on whether axial or angular displacement is measured, laser distance and magnetic angle measurements are options for sensor types to be used. In a digital fly-by-wire flight control system, actuator position and digital control signals are available in addition.

Finally, the coefficients of aerodynamic and propulsion models \mathbf{c}_v are needed. More generally, accurate models of aerodynamics and propulsion systems must be available for the specific airplane the desired navigation function is developed for.

Airplane flight simulators for use in pilot training need to be validated against a number of requirements in order to be qualified for training purposes (c.f. [47]). Beside aspects of flight operation, realistic cockpit simulation, visualization, motion cueing and simulator control, the simulated flying qualities are thoroughly compared against true airplane qualities. This includes flight stability and performance, e.g. tolerances on airspeed, climb, attitude and dynamics for a number of typical and emergency flight segments. Consequently, the software models of flight simulators with high flight model fidelity levels V and VII [47] with strict tolerances on airplane-specific flight dynamics are well suited for use as position

propagation motion model as intended in this work. Simulators with flight model fidelity level III have reduced tolerances (i.e. representative models). But they are still strictly required to correctly model the flight dynamics qualitatively – i.e. in terms of principal stability of flight dynamics. The usability of airplane models of such lower quality for backup navigation will be assessed later in this work.

The cost of development and certification of such an airplane specific simulation software is high due to the large number of flight test hours required both for identification of the model using system identification techniques (e.g. [48]) and following validation of the created model against independent flight data according (see e.g. [49] for an example of highest qualification level flight simulator aerodynamic identification and validation).

2.1.4 Relevant aspects

This section has discussed the characteristics of three different motion models for position propagation that can be used for GNSS-denied flight navigation. Given the criticality of position information for the applications of interest, high reliability of the backup position estimation function is desired. This strongly depends on the number and type of physical measurements required, and specifically on their integrity and robustness.

It is found that all of the three motion models take inputs that must be measured on-board: Heading and airspeed for dead reckoning, specific forces and inertial angular rates for inertial navigation and control inputs for the aerodynamic motion model. The low-cost design usually mandates a simplex sensor suite. In this case, the integrity of input data is to large extent determined by the probability of an out-of-tolerance measurement, because detection of such an event is generally difficult without sensor redundancy or high overall accuracy. Only for some sensors the occurrence of out-of-tolerance measurements might be related to typical sensor faults that are relatively easy to detect with a priori measures (e.g. frozen digital output). For other sensors, faults might be much more complex in their appearance and harder to detect. This is especially the case for airspeed and control deflection measurements, being exposed to open air or soiling and partly mechanical. Both MEMS inertial sensors and solid-state magnetic compass are closed box sensors well protected from pollution that could impair their measurement function. For the magnetic compass, disturbances of the environmental magnetic field due to a large number of conditions (e.g. driving electrical actuators) may corrupt sensor output. For control inputs, a redundant measurement (or availability of digitalized control input) appears possible even in a low-cost design. This increases integrity of control input information over integrity of simplex measurements in the scope of this analysis. In terms of availability, sensors with interior on-board measurements such as solid state magnetic compass and inertial measurements are preferable. Only hardware fault might interrupt operation, while for airspeed, interruptions due to icing or blockage seem much more probable assuming unfavorable weather conditions. For control inputs, the larger number of sensors can be considered a limitation of availability because probability of single hardware fault is approximately multiplied by the number of individual sensors.

Besides measured inputs, all three of the described motion models need further input information for the propagation of position estimate. Inertial navigation and the aerodynamic motion model need a value for gravity at current position. At least in the accuracy required for low-cost applications, this information is reliably available for world-wide operation using EGM2008 gravitation or Somigliana gravity models (see [38] and [18] respectively). Heading and airspeed dead reckoning as well as the aerodynamic motion model need information on wind velocity vector at aircraft position. As has been noted before, provision of accurate and reliable wind vector information proves very difficult.

Finally, simplifications and model imperfections must be considered in this comparison. Given exact gravity input, inertial navigation is an exact motion model. No simplifications are necessary in an actual implementation of this method, except for discrete time integration. Time discretization errors can be reduced to be orders of magnitude smaller than errors due to measurement and gravity imperfections by design using state-of-the-art strapdown algorithms that match the application [29, 34, 36, 50]. Using classical 4th order Runge-Kutta time integration and low-pass filtering of measured input data if needed, time discretization

errors are negligible for dead reckoning and the aerodynamic motion model. These methods more significantly suffer from simplifications necessary for implementation. Heading and airspeed dead reckoning assumes a simplified geometry where aerodynamic velocity is always horizontally aligned with body longitudinal axis. For a number of dynamic flight conditions, this causes error in the approximated velocity used in position time integration. While geometry and kinematics are exact in the aerodynamic motion model, this method uses approximate models of aerodynamic and propulsion forces and moments, weight and balance and vehicle geometry.

As result of this study of required measurements, model inputs and simplifications for implementation, inertial navigation offers some advantages compared to the other models if only a single motion model is used. Regarding the input data, it is the most reliable option and, in addition, it is the only motion model that describes true motion without simplifications or imperfections. Compared to heading and airspeed dead reckoning, the aerodynamic motion model uses more reliable measurements of control inputs. Still, both require wind velocity vector at aircraft position that is hardly available. Because dead reckoning computes an approximation of horizontal velocity and the aerodynamic motion model relies on a simplified model of true flight physics, inertial navigation is the choice for a single motion model with maximum validity for a wide range of operational and environmental conditions.

One important aspect that distinguishes the aerodynamic motion model from dead reckoning or inertial navigation is that the implementation of this method is very specific to the navigation platform (i.e. vehicle). In contrast, inertial navigation is perfectly indifferent to the platform carrying the navigation system. For heading and airspeed dead reckoning the type of vehicle only affects the validity of assuming alignment of aerodynamic velocity and longitudinal axis. Aerodynamic motion propagation will require different software and measured inputs for any different vehicle. Consider for example the difference for two similar airplanes, one with retractable landing gear, the other with fixed landing gear. The first will need an additional measurement of gear position to be included in the motion model input vector. In addition, aerodynamic properties are affected by gear position and this must be accounted for in the software model used to compute aerodynamic and propulsion forces and moments.

2.2 ERROR STATE PROPAGATION

Without absolute position information, the change in position starting from the last known or accurately measured point must be predicted using one of the methods introduced in the previous section. Errors, once introduced in initial values, measured inputs or inputs computed from models, will remain in the computation. The way how these navigation errors propagate and accumulate, especially in estimates of position and velocity, is of great interest for assessment of propagation method usability.

The following analysis will allow to quantitatively predict method performance if used open loop, i.e. without updates or corrections to the motion model states. A performance study is based on statistical models of initial value and input errors, and uses either the error covariance model, which can be derived from linear(ized) error dynamics, or Monte Carlo simulation of the error dynamics to yield statistical measures of performance. If a position prediction method is designed to meet a specific open loop performance, e.g. position accuracy over time (drift), this error propagation analysis and specifically the long term error dynamics are the basis for deriving required input and sensor accuracy. While historically limited computational capabilities required simulation of linear(ized) error dynamics (or analytical discussion where possible), Monte Carlo simulation of the whole navigation system software is possible today. This has the advantage of greatest possible correspondence of operational method and analysis, and will be the preferred approach to performance assessment and design in this work.

Observability analysis of system errors, as will follow in the next section, is yet another reason for error propagation analysis. The short term error dynamics of system states in combination with system-specific observations determine the closed loop behavior with an estimation filter, such as the extended Kalman filter (EKF). Implementation of the EKF requires a covariance model of system error dynamics.

If filter estimates of motion model errors are used to update or correct the model, the open loop performance will be only of importance for short time intervals between filter updates. At least for model errors that are observable and will be corrected by the filter, short term error dynamics are of greater interest than the long term dynamics in closed loop.

2.2.1 Heading and airspeed dead reckoning

The dead reckoning method is the simplest algorithm to compute change in position over time, requiring only a single time integration. This simplicity represents an advantage, because the number of error sources is very limited. As will be shown in the following subsection, integration of position from speed and direction measurements results in linear position error growth. This first order error influence and resulting steady position drift constitutes the distinctive characteristic of the dead reckoning method and makes it suitable for use with low-cost equipment over long time intervals.

2.2.1.1 Position drift

The position error of dead reckoning is described by the following differential equation found by perturbation analysis of equation (2-2) and subsequent linearization. Input errors, elevation angle θ_{nb} , aerodynamic angles of attack and sideslip and errors error in computed roll and pitch are assumed small (see appendix A.5).

$$\delta \dot{\Lambda}_H = \begin{bmatrix} 1 & 0 \\ \frac{1}{M(\phi_{WGS84,0}^R) + h_{WGS84}^R} & 1 \\ 0 & \frac{1}{(N(\phi_{WGS84,0}^R) + h_{WGS84}^R) \cos(\phi_{WGS84}^R)} \end{bmatrix} \cdot \left(\delta \mathbf{v}_{HWn} + \begin{bmatrix} \cos(\Psi_{nb}) \\ \sin(\Psi_{nb}) \end{bmatrix} \delta V_A + \begin{bmatrix} -\sin(\Psi_{nb}) \\ \cos(\Psi_{nb}) \end{bmatrix} (\delta \Psi_{nb} + \cos(\Phi_{nb}) \beta_A - \sin(\Phi_{nb}) \alpha_A) V_A \right) \quad (2-16)$$

Again, $\Psi_{nb} \approx \chi_A$ and $\cos(\gamma_A) \approx 1$ is assumed, which holds for small angles of aerodynamic sideslip in straight and level flight and thus for the greatest part of the flight.

Errors in the computation of normal and meridian radii have been neglected in this analysis because they correspond to scale factor errors on the order of $1ppm$ for distances travelled in north direction of $\sim 100km$ (and radii computed at initial position). Similarly, errors in height of up to $5500m$ (approximately $18000ft$) will cause a scale factor error in position propagation of less than $1000ppm$ which is still negligibly small. Notice that integration of longitude becomes very sensitive to latitude errors at high latitudes. $10km$ north position error introduce a scale factor error in longitude propagation of $15000ppm$ at 85° latitude and $2600ppm$ at 60° latitude respectively. For the applications considered here, this effect may be dismissed from analysis as well.

Equation (2-16) describes three different error sources in aircraft dead reckoning: First, there is a wind drift directly related to the integration of error in horizontal wind velocity vector $\delta \mathbf{v}_{HWn}$ used for position propagation. Second, the airspeed measurement error δV_A will cause along-track error. Finally, heading error and deviations from to assumed zero-sideslip straight and level flight condition introduce across-track error or misalignment error.

All of these errors are accumulated in position estimate by integration over time. For zero velocity and with above simplifications

$$\delta \Lambda_H(t) \approx \begin{bmatrix} 1 & 0 \\ \frac{1}{M(\phi_{WGS84,0}^R) + h_{WGS84}^R} & 1 \\ 0 & \frac{1}{(N(\phi_{WGS84,0}^R) + h_{WGS84}^R) \cos(\phi_{WGS84}^R)} \end{bmatrix} \cdot \left(\int_{t_0}^t \delta \mathbf{v}_{HWn} dt + \int_{t_0}^t \begin{bmatrix} \cos(\Psi_{nb}) \\ \sin(\Psi_{nb}) \end{bmatrix} \delta V_A dt + \int_{t_0}^t \begin{bmatrix} -\sin(\Psi_{nb}) \\ \cos(\Psi_{nb}) \end{bmatrix} (\delta \Psi_{nb} + \cos(\Phi_{nb}) \beta_A - \sin(\Phi_{nb}) \alpha_A) V_A dt \right) + \delta \Lambda_H(t_0) \quad (2-17)$$

All error terms are first order in elapsed time $\Delta t = t - t_0$. Partial cancellation of integrated position error due to constant input error in airspeed or heading may occur if direction of

motion changes. Similarly, time variant input errors in airspeed or heading may be rectified by changes in direction of motion. Still, for any motion trajectory, errors of heading and airspeed dead reckoning scale linearly with time. This is a very favorable error characteristic for low-cost applications where input errors can be large. It effectively weights temporary errors with the time duration of occurrence. Consequently, large input errors due to low cost instrumentation are permissible and have little effect on position accuracy as long as they exist for short times only.

2.2.2 Inertial navigation

Because the inertial motion model by itself is accurate without approximation, system dynamics are independent of actual navigation state vector parametrization. Consequently, the error dynamics are the same for e.g. a local-level, ECEF or ECI strapdown inertial navigation mechanization using the same initial and input values (i.e. inertial measurements and gravity or gravitation).

For terrestrial navigation systems, inertial navigation error dynamics are commonly analyzed in a local-level mechanization, such as NED or wander frame. As has been noted above, equivalence for different mechanization holds – but a local-level parametrization of errors is preferable because it isolates characteristic error behavior in vertical and horizontal channels. This offers greater insight in system error behavior. Although system implementation and characteristics of input errors are significantly different, inertial navigation error analysis is largely equivalent for gimballed platform and strapdown (i.e. analytic platform) systems. This is the reason why the results of early inertial navigation error propagation analysis still hold for modern systems, while consideration of input error faces new problems due to new technologies (see e.g. suggestions in [29]).

The error analysis of terrestrial inertial navigation with a local-level mechanization can be classified in two different approaches. They differ in the definition of error of the computed local-level velocity: Comparing the computed velocity vector against the true velocity vector written in coordinates of the local-level frame at true position – or comparing the computed velocity vector against the true velocity vector written in coordinates of the local-level frame at computed position.

The first is known as perturbation error approach [51]. The perturbation velocity error motivates definition of orientation error as misalignment of the true local-level frame and the (analytic) platform frame, where accelerometer measurements are integrated. This is the phi formulation of orientation error [20, 52], the corresponding rotation vector is referred to as phi angle orientation error. The alternative velocity error, defined in the computed local-level frame [20], is usually combined with orientation error defined as misalignment of the computed local-level frame and the (analytic) platform frame, known as psi formulation [20, 52–54] and defining the psi angle orientation error.

Both approaches have been shown to be equivalent for small errors [52], but differ in implementation when used for integrated navigation [20]. If suitable for the given navigation task, other combinations of velocity error and orientation error definitions are possible.

Even more diversity in inertial navigation error models found in the literature is due to different choices of position error definition. The misalignment between the true local-level frame and the computed local-level frame, commonly referred to as delta theta vector, is a parametrization of horizontal position error. For small errors, this misalignment vector is the difference of phi and psi orientation errors. The vertical component of theta corresponds to an additional degree of freedom of heading error definition (c.f. [55]). Depending on the type of local-level mechanization (e.g. NED or wander frame), several choices are possible to fix (e.g. set to zero or constant) one of the linearly dependent errors in vertical direction [20], thus determining all by estimating just one. When using the misalignment parametrization of position error, an additional height error state must be included.

In this work, position error is defined as additive error of WGS84 position, velocity error is defined using the perturbation approach (which will also be applied for all vector error definitions in this work) and phi formulation is adopted for orientation error parametrization. Error propagation analysis is applied to the strapdown inertial navigation algorithm presented in the previous section. Since this is a NED frame mechanization, there is no error due to computed wander angle, and the vertical component of position misalignment vector is a function of latitude error only (c.f. [56]). Thus the 9-DOF representation of strapdown inertial navigation errors derived in the following is complete.

2.2.2.1 Perturbation error analysis of terrestrial inertial navigation

The computed navigation states are corresponding to section 2.1.2.1

$$\hat{\mathbf{z}}_n = \begin{bmatrix} \hat{\phi} \\ \hat{\lambda} \\ \hat{h} \\ \hat{\mathbf{v}}_n \\ \hat{\mathbf{q}}_{nb} \end{bmatrix} \begin{array}{l} \dots \text{geodetic latitude} \\ \dots \text{geodetic longitude} \\ \dots \text{height above WGS84 ellipsoid} \\ \dots \text{ECEF velocity in NED coordinates} \\ \dots \text{NED to body-fixed frame orientation quaternion} \end{array}$$

The computed navigation states denoted by a hat are propagated using the strapdown inertial navigation algorithm described in section 2.1.2.1 and possibly corrected by estimates of navigation state error if available (as in an integrated navigation system). In addition to initial errors and errors in the navigation state corrections, errors in the strapdown propagation of navigation state contribute to the total error of computed navigation states. The propagation errors are mostly due to input errors in the IMU measurements of specific force and inertial angular rates, $\tilde{\mathbf{f}}_b$ and $\tilde{\boldsymbol{\omega}}_{ib}$. The input error in computed gravity vector is neglected in this work because it is very small compared to accelerometer measurement error for the applications of interest. In the following, the navigation state errors will be defined.

For the perturbation error model, velocity error is simply the difference of the true NED velocity vector and the computed velocity vector:

$$\delta \mathbf{v}_n = \mathbf{v}_n - \hat{\mathbf{v}}_n$$

The error of the vector of WGS84 position is

$$\delta \boldsymbol{\Lambda} = \begin{bmatrix} \delta \phi \\ \delta \lambda \\ \delta h \end{bmatrix} = \begin{bmatrix} \phi - \hat{\phi} \\ \lambda - \hat{\lambda} \\ h - \hat{h} \end{bmatrix}$$

The computed NED to body-fixed frame orientation quaternion $\hat{\mathbf{q}}_{nb}$ is used in the strapdown algorithm (2-3) to transform body-fixed accelerometer measurements to an approximation of the NED frame, referred to as platform frame. The misalignment of this approximation with respect to the NED frame can be described by the product of true and inverse of computed NED to body-fixed frame orientation quaternions. With the relationship of an orientation quaternion and a rotation vector (A-41), a corresponding orientation error rotation vector $\boldsymbol{\phi}_n$ with magnitude ϕ and unit vector \mathbf{n}_ϕ can be defined:

$$\check{\mathbf{q}}_{nb} \cdot \widehat{\mathbf{q}}_{nb}^{-1} = \begin{bmatrix} \cos\left(\frac{\phi}{2}\right) \\ \sin\left(\frac{\phi}{2}\right) \mathbf{n}_\phi \end{bmatrix} \quad (2-18)$$

The rotation vector $\boldsymbol{\phi}_n$ is the phi angle orientation error in NED frame coordinates

$$\boldsymbol{\phi}_n = \begin{bmatrix} \phi_N \\ \phi_E \\ \phi_D \end{bmatrix}$$

It is sometimes referred to as (equivalent) tilt in literature [57, 58].

Equation (2-18) can be linearized as

$$\check{\mathbf{q}}_{nb} \cdot \widehat{\mathbf{q}}_{nb}^{-1} \doteq \begin{bmatrix} 1 \\ \frac{1}{2} \boldsymbol{\phi}_n \end{bmatrix}$$

With equation (A-20) the relationship of true and computed NED to body-fixed frame rotation matrix and phi angle orientation error is

$$\mathbf{R}_{nb} \widehat{\mathbf{R}}_{nb}^T = \mathbf{I} + \sin(\phi) \text{skew}(\mathbf{n}_\phi) + (1 - \cos(\phi)) \text{skew}(\mathbf{n}_\phi)^2 \quad (2-19)$$

with the computed NED to body-fixed frame rotation matrix $\widehat{\mathbf{R}}_{nb}^T$. The corresponding linearized relationship is

$$\mathbf{R}_{nb} \widehat{\mathbf{R}}_{nb}^T \doteq \mathbf{I} + \text{skew}(\boldsymbol{\phi}_n)$$

Defining a vector of orientation error Euler angles

$$\boldsymbol{\Phi} = \begin{bmatrix} \delta\phi_1 \\ \delta\phi_2 \\ \delta\phi_3 \end{bmatrix}$$

the misalignment of platform frame with respect to true NED frame can be described as a Euler angle rotation sequence:

$$\check{\mathbf{q}}_{nb} \cdot \widehat{\mathbf{q}}_{nb}^{-1} = \begin{bmatrix} \cos\left(\frac{\delta\phi_3}{2}\right) \\ 0 \\ 0 \\ \sin\left(\frac{\delta\phi_3}{2}\right) \end{bmatrix} \cdot \begin{bmatrix} \cos\left(\frac{\delta\phi_2}{2}\right) \\ 0 \\ \sin\left(\frac{\delta\phi_2}{2}\right) \\ 0 \end{bmatrix} \cdot \begin{bmatrix} \cos\left(\frac{\delta\phi_1}{2}\right) \\ \sin\left(\frac{\delta\phi_1}{2}\right) \\ 0 \\ 0 \end{bmatrix} \quad (2-20)$$

Linearization of equation (2-20) gives

$$\check{\mathbf{q}}_{nb} \cdot \widehat{\mathbf{q}}_{nb}^{-1} \doteq \begin{bmatrix} 1 \\ \frac{1}{2} \boldsymbol{\Phi} \end{bmatrix}$$

Consequently, the Euler angle parametrization of orientation error $\boldsymbol{\Phi}$ and the phi angle orientation error $\boldsymbol{\phi}_n$ are equivalent in linear approximation. Because only linear perturbation error analysis will be conducted in this work the two definitions of orientation error can be used interchangeably since the derived linearized differential equations are the same:

$$\dot{\boldsymbol{\phi}}_n \Big|_{\boldsymbol{\phi}_n=0} \doteq \dot{\boldsymbol{\Phi}} \Big|_{\boldsymbol{\Phi}=0}$$

The orientation error Euler angles $\boldsymbol{\phi}$ are related to the error in computed NED to body-fixed frame rotation matrix $\hat{\mathbf{R}}_{nb}^T$ as follows:

$$\boldsymbol{\phi} = \begin{bmatrix} \text{atan2}(R_{32}, R_{33}) \\ \text{asin}(-R_{31}) \\ \text{atan2}(R_{21}, R_{11}) \end{bmatrix} \text{ with } \mathbf{R}_{nb} \hat{\mathbf{R}}_{nb}^T = \begin{bmatrix} R_{11} & R_{12} & R_{13} \\ R_{21} & R_{22} & R_{23} \\ R_{31} & R_{32} & R_{33} \end{bmatrix} \quad (2-21)$$

With above error definitions, the vector of navigation state errors for perturbation error analysis of inertial navigation in this work is defined as

$$\delta \mathbf{z}_n := \begin{bmatrix} \delta \phi \\ \delta \lambda \\ \delta h \\ \delta \mathbf{v}_n \\ \boldsymbol{\phi}_n \end{bmatrix}$$

The linearized system of ordinary differential equations for inertial navigation error dynamics from perturbation analysis is

$$\delta \dot{\mathbf{z}}_n = \mathbf{A} \delta \mathbf{z}_n + \mathbf{B} \delta \mathbf{s} \quad (2-22)$$

Neglecting gravity model errors in the analysis of low-cost methods, $\delta \mathbf{s} = [\delta \mathbf{f}_{b_{IMU}}^T, \delta \boldsymbol{\omega}_{ib_{IMU}}^T]^T$ is the vector of IMU measurement errors defined as

$$\begin{aligned} \delta \mathbf{f}_{b_{IMU}} &= \mathbf{f}_{b_{IMU}} - \tilde{\mathbf{f}}_b \\ \delta \boldsymbol{\omega}_{ib_{IMU}} &= \boldsymbol{\omega}_{ib_{IMU}} - \tilde{\boldsymbol{\omega}}_{ib} \end{aligned}$$

The system and input matrices in (2-22) are summarized in the following (derivations found in appendix A.6, in [39] and in [32], where it is related to the error model in [59]. A similar error model with position error defined in local level coordinates is found in [60]).

$$\begin{aligned} \mathbf{A}_{\delta \Lambda, \delta \Lambda} &= \begin{bmatrix} 0 & 0 & -\frac{\hat{v}_N}{(M(\hat{\phi}) + \hat{h})^2} \\ \frac{\tan(\hat{\phi}) \hat{v}_E}{(N(\hat{\phi}) + \hat{h}) \cos(\hat{\phi})} & 0 & -\frac{\hat{v}_E}{(N(\hat{\phi}) + \hat{h})^2 \cdot \cos(\hat{\phi})} \\ 0 & 0 & 0 \end{bmatrix} \\ \mathbf{A}_{\delta \Lambda, \delta \mathbf{v}_n} &= \begin{bmatrix} \frac{1}{M(\hat{\phi}) + \hat{h}} & 0 & 0 \\ 0 & \frac{1}{(N(\hat{\phi}) + \hat{h}) \cdot \cos(\hat{\phi})} & 0 \\ 0 & 0 & -1 \end{bmatrix} \\ \mathbf{A}_{\delta \Lambda, \boldsymbol{\phi}_n} &= \mathbf{0} \end{aligned}$$

$$\mathbf{A}_{\delta v_n, \delta \Lambda} = \begin{bmatrix} -2\omega_{ie} \cos(\hat{\phi}) \hat{v}_E - \frac{\hat{v}_E^2}{(N(\hat{\phi}) + \hat{h}) \cos^2(\hat{\phi})} & 0 & \frac{\tan(\hat{\phi}) \hat{v}_E^2}{(N(\hat{\phi}) + \hat{h})^2} - \frac{\hat{v}_N \hat{v}_D}{(M(\hat{\phi}) + \hat{h})^2} \\ 2\omega_{ie} (\cos(\hat{\phi}) \hat{v}_N - \sin(\hat{\phi}) \hat{v}_D) + \frac{\hat{v}_N \hat{v}_E}{(N(\hat{\phi}) + \hat{h}) \cos^2(\hat{\phi})} & 0 & -\frac{\tan(\hat{\phi}) \hat{v}_N \hat{v}_E + \hat{v}_E \hat{v}_D}{(N(\hat{\phi}) + \hat{h})^2} \\ \left. \frac{d\gamma_D}{d\phi} \right|_{\hat{\phi}, \hat{h}} + 2\omega_{ie} \sin(\hat{\phi}) \hat{v}_E & 0 & \left. \frac{d\gamma_D}{dh} \right|_{\hat{\phi}, \hat{h}} + \frac{\hat{v}_E^2}{(N(\hat{\phi}) + \hat{h})^2} + \frac{\hat{v}_N^2}{(M(\hat{\phi}) + \hat{h})^2} \end{bmatrix}$$

Where the partial derivatives of gravity in down direction with respect to height and latitude must be derived from the gravity model used or a simplified spherical model.

$$\mathbf{A}_{\delta v_n, \delta v_n} = \begin{bmatrix} \frac{\hat{v}_D}{M(\hat{\phi}) + \hat{h}} & -2\omega_{ie} \sin(\hat{\phi}) - \frac{2 \tan(\hat{\phi}) \hat{v}_E}{N(\hat{\phi}) + \hat{h}} & \frac{\hat{v}_N}{M(\hat{\phi}) + \hat{h}} \\ 2\omega_{ie} \sin(\hat{\phi}) + \frac{\tan(\hat{\phi}) \hat{v}_E}{N(\hat{\phi}) + \hat{h}} & \frac{\tan(\hat{\phi}) \hat{v}_N + \hat{v}_D}{N(\hat{\phi}) + \hat{h}} & 2\omega_{ie} \cos(\hat{\phi}) + \frac{\hat{v}_E}{N(\hat{\phi}) + \hat{h}} \\ -\frac{2\hat{v}_N}{M(\hat{\phi}) + \hat{h}} & -2\omega_{ie} \cos(\hat{\phi}) - \frac{2\hat{v}_E}{N(\hat{\phi}) + \hat{h}} & 0 \end{bmatrix}$$

$$\mathbf{A}_{\delta v_n, \phi_n} = -\text{skew}(\hat{\mathbf{R}}_n \hat{\mathbf{f}}_b)$$

$$\mathbf{A}_{\phi_n, \delta \Lambda} = \begin{bmatrix} \omega_{ie} \sin(\hat{\phi}) & 0 & \frac{\hat{v}_E}{(N(\hat{\phi}) + \hat{h})^2} \\ 0 & 0 & -\frac{\hat{v}_N}{(M(\hat{\phi}) + \hat{h})^2} \\ \omega_{ie} \cos(\hat{\phi}) + \frac{\hat{v}_E}{(N(\hat{\phi}) + \hat{h}) \cos^2(\hat{\phi})} & 0 & -\frac{\tan(\hat{\phi}) \hat{v}_E}{(N(\hat{\phi}) + \hat{h})^2} \end{bmatrix}$$

$$\mathbf{A}_{\phi_n, \delta v_n} = \begin{bmatrix} 0 & -\frac{1}{N(\hat{\phi}) + \hat{h}} & 0 \\ \frac{1}{M(\hat{\phi}) + \hat{h}} & 0 & 0 \\ 0 & \frac{\tan(\hat{\phi})}{N(\hat{\phi}) + \hat{h}} & 0 \end{bmatrix}$$

$$\mathbf{A}_{\phi_n, \phi_n} = \begin{bmatrix} 0 & -\omega_{ie} \sin(\hat{\phi}) - \frac{\tan(\hat{\phi}) \hat{v}_E}{N(\hat{\phi}) + \hat{h}} & \frac{\hat{v}_N}{M(\hat{\phi}) + \hat{h}} \\ \omega_{ie} \sin(\hat{\phi}) + \frac{\tan(\hat{\phi}) \hat{v}_E}{N(\hat{\phi}) + \hat{h}} & 0 & \omega_{ie} \cos(\hat{\phi}) + \frac{\hat{v}_E}{N(\hat{\phi}) + \hat{h}} \\ -\frac{\hat{v}_N}{M(\hat{\phi}) + \hat{h}} & -\omega_{ie} \cos(\hat{\phi}) - \frac{\hat{v}_E}{N(\hat{\phi}) + \hat{h}} & 0 \end{bmatrix}$$

While precise motion propagation with the strapdown inertial navigation equation requires calculation of curvature radii and gravity of an oblate ellipsoidal earth, simplifications assuming a spherical model are permissible for error propagation analysis.

The effect of input errors on inertial navigation error dynamics is given by

$$\begin{aligned} \mathbf{B}_{\delta v_n, \delta f_b} &= \hat{\mathbf{R}}_{nb} \\ \mathbf{B}_{\phi_n, \delta \omega_{ib}} &= \hat{\mathbf{R}}_{nb} \end{aligned} \quad (2-23)$$

Because measured specific force in NED coordinates $\hat{\mathbf{R}}_{nb} \tilde{\mathbf{f}}_b$ directly appears in the $\mathbf{A}_{\delta v_n, \phi_n}$ block matrix of the system matrix in (2-22), use of advanced methods for integrated navigation filter design may be advantageous to avoid problems due to measurement noise [56].

2.2.2.2 Error dynamics and stability

The errors of NED frame strapdown inertial navigation are studied with respect to their dynamics in short time intervals and in long time intervals.

The integration of inertial angular rates and specific force measurements corresponds to propagation of IMU measurement errors to orientation error and velocity error respectively, according to (2-23). Orientation errors are in turn propagated to velocity error, due to integration of imperfectly rotated specific force vector, represented by the block matrix $\mathbf{A}_{\delta v_n, \phi_n}$. Finally, velocity error is directly propagated to position error in the position time integration, see $\mathbf{A}_{\delta \Lambda, \delta v_n}$. Consequently, IMU measurement errors are propagated as follows to position error (neglecting error feedback loops)

$$\delta \Lambda(t) \sim \iint \mathbf{A}_{\delta \Lambda, \delta v_n} \left(\mathbf{B}_{\delta v_n, \delta f_b} \delta \mathbf{f}_{b_{IMU}} + \mathbf{A}_{\delta v_n, \phi_n} \int \mathbf{B}_{\phi_n, \delta \omega_{ib}} \delta \omega_{ib_{IMU}} dt \right) dt^2 \quad (2-24)$$

By inspection of $\mathbf{A}_{\delta v_n, \phi_n}$, the third order error propagation due to inertial angular rates error is restricted to directions perpendicular to $\hat{\mathbf{R}}_{nb} \tilde{\mathbf{f}}_b$. For sustained flight, external force cancels weight and thus third order error propagation is present in the horizontal. Note that it would not be an issue in free fall since specific force would vanish. Additionally, specific force measurement error causes second order position error growth in all dimensions.

A mathematically more rigorous analysis is possible for simplified versions of the system of error differential equations (2-22). The direct propagation of input error to position error according to equation (2-24) will be shaped into a particular solution of the differential equations, given a specific time history of input errors (c.f. [30]). It is instructive to study the homogenous solution, i.e. the Eigendynamics of the error system, to understand how the system will dynamically react given initial error. Based on a study of Eigendynamics, some fundamental statements of how the system will shape input error are made. A special case of input signal shaping by an undamped oscillatory system is amplification, or resonance, for periodical inputs close to one of the systems Eigenfrequencies. Alternatively, particular solutions of a simplified error system and basic input functions may be discussed (see [30]).

Studying the dynamics of the coupled system of error differential equations (2-22) reveals large time constants, as will be shown in the following. Consequently, the polynomial position error growth discussed above will be observed in short term, and will be dominated by the coupled system dynamics of (2-22) in the long term.

Neglecting the specialties of the chosen position parametrization in latitude and longitude, it appears that error dynamics would be the same everywhere on a spherical non-rotating

earth. Studying the available sensor accuracies for the given low-cost applications, simplifications by assuming spherical earth geometry and gravitation are admissible. Earth rate is negligibly small compared to IMU measurement error, and flight times are short compared to the period of earth rotation. In addition, velocities are sufficiently low to neglect errors in Coriolis effect. Thus, using an isotropic local-level parametrization by choosing latitude $\hat{\phi} = 0$, a strongly simplified system of error differential equations is attained. Height appears in equation (2-22) only in sums with earth radii and as a parameter of gravity gradient. Therefore, $\hat{h} = 0$ is a good approximation here. Furthermore, in the analysis of long-term error propagation, horizontal accelerations are neglected.

For a spherical non-rotating earth model with mean radius $R_1 = 6371008.7714\text{m}$ [18, 61], neglecting transport rate effects and at latitude $\hat{\phi} = 0$ and height $\hat{h} = 0$, equation (2-22) can be simplified to

$$\mathbf{A}_{\delta v_n, \delta v_n} = \mathbf{A}_{\phi_n, \delta \Lambda} = \mathbf{A}_{\phi_n, \phi_n} = \mathbf{0}$$

$$\mathbf{A}_{\delta \Lambda, \delta v_n} = \begin{bmatrix} \frac{1}{R_1} & 0 & 0 \\ 0 & \frac{1}{R_1} & 0 \\ 0 & 0 & -1 \end{bmatrix}$$

$$\mathbf{A}_{\delta v_n, \delta \Lambda} = \begin{bmatrix} 0 & 0 & 0 \\ 0 & 0 & 0 \\ 0 & 0 & -2\omega_S^2 \end{bmatrix}$$

With the definition of Schuler frequency

$$\omega_S = \sqrt{\frac{g}{R_1}} \quad (2-25)$$

With the gravitational acceleration of a spherical earth at its surface $g = \frac{GM}{R_1^2} \approx 9.8\text{m/s}^2$ (for earth's gravitational constant GM see e.g. [18]). With definition (2-25), $-2\omega_S^2$ corresponds to the vertical gravitation gradient of a spherical earth in $\mathbf{A}_{\delta v_n, \delta \Lambda}$.

Now, assuming alignment with local-level axes, i.e. $\hat{\mathbf{R}}_{nb} = \mathbf{I}$, and neglecting long-term horizontal accelerations

$$\mathbf{A}_{\delta v_n, \phi_n} = \begin{bmatrix} 0 & -g & 0 \\ g & 0 & 0 \\ 0 & 0 & 0 \end{bmatrix}$$

And finally

$$\mathbf{A}_{\phi_n, \delta v_n} = \begin{bmatrix} 0 & -\frac{1}{R_1} & 0 \\ \frac{1}{R_1} & 0 & 0 \\ 0 & 0 & 0 \end{bmatrix}$$

This gives a set of homogeneous differential equations for horizontal error dynamics

$$\delta\ddot{\phi} \approx \frac{d^2}{dt^2} \left(\frac{1}{R_1} \delta v_N \right) \approx \frac{1}{R_1} \frac{d}{dt} (-g\phi_E) \approx -\frac{\omega_S^2}{R_1} \delta v_N$$

$$\delta\ddot{\lambda} \approx \frac{d^2}{dt^2} \left(\frac{1}{R_1} \delta v_E \right) \approx \frac{1}{R_1} \frac{d}{dt} (g\phi_N) \approx -\frac{\omega_S^2}{R_1} \delta v_E$$

And for vertical error

$$\delta\ddot{h} \approx \frac{d}{dt} (-\delta v_D) \approx 2\omega_S^2 \delta h \quad (2-26)$$

As noted above, these are slow error dynamics with a period of $T_S = \frac{2\pi}{\omega_S} \approx 84(60)s$ for the stable undamped oscillatory horizontal error dynamics (known as Schuler dynamics) and a time-to-double of $T_{2,\delta h} = \frac{\ln(2)}{\sqrt{2}\omega_S} \approx 400s$ for the exponentially unstable vertical error dynamics.

It follows that while polynomial measurement error propagation according to equation (2-24) dominates in the short term, error growth in the horizontal will be restrained by the stable Schuler dynamics for propagation times exceeding a significant portion of the Schuler period (e.g. $\frac{T_S}{4} \approx 21(60)s$), while vertical error growth will even be aggravated by the instable dynamics (2-26) in the long term or if initial height error is large.

The problem of vertical error instability is often directly addressed in the mechanization algorithm. For aviation applications, barometric altitude is used for vertical channel damping by means of higher order feedback loops [62] or a vertical channel Kalman filter [63]. The combination Baro-INS is the state of art, as it is a very robust solution to the vertical problem and independent of GNSS availability (c.f. [7, 15, 20]).

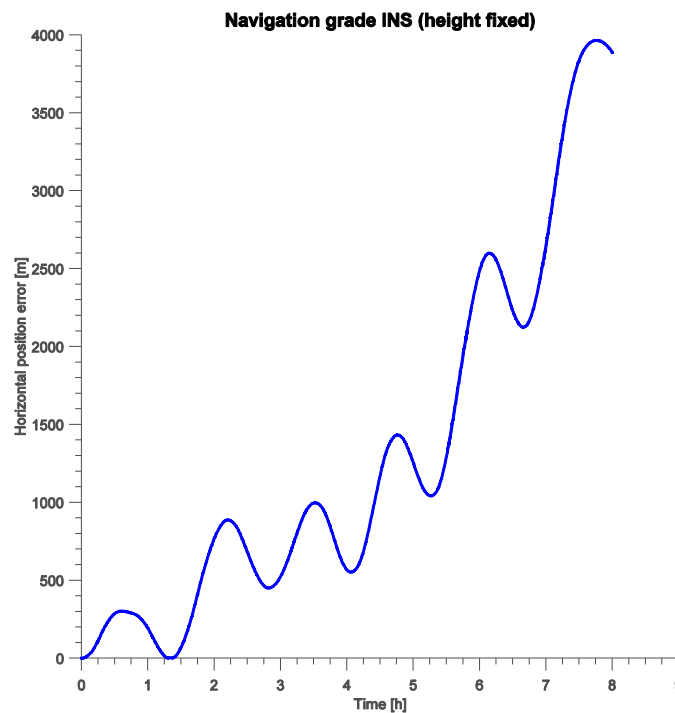


Figure 3: Horizontal position error of navigation grade inertial navigation (stationary laboratory test)

For constant error of specific force input in the horizontal $\delta \mathbf{f}_{HIMU}$ (i.e. due to y-axis accelerometer bias in level flight), the horizontal error dynamics will be the same as for an initial error in attitude (i.e. leveling error): The computed platform will accelerate horizontally (and rotate with transport rate) until the sum of specific force misalignment error and accelerometer bias is zero:

$$g \frac{\delta \mathbf{x}_{H,avg}}{R_1} \approx \delta \mathbf{f}_{HIMU}$$

This will stimulate Schuler oscillation, centered at a position offset by $\delta \mathbf{x}_{H,avg} \approx \delta \mathbf{f}_{HIMU} / \omega_S^2$ (see the definition of Schuler frequency (2-25)) and with a stable bound of total horizontal position error of approximately $2\delta \mathbf{f}_{HIMU} / \omega_S^2$ [30]. Although this equivalent effect of initial misalignment and horizontal accelerometer on horizontal error can be effectively eliminated with leveling of the computed platform at navigation system initialization, accelerometer bias is not constant in low-cost sensors. With perfect gyros and zero initial error, constant $1mg$ of accelerometer bias causes approximately $3.44NM$ (or $6371m$) average position error and stable Schuler oscillations with an amplitude of the same value.

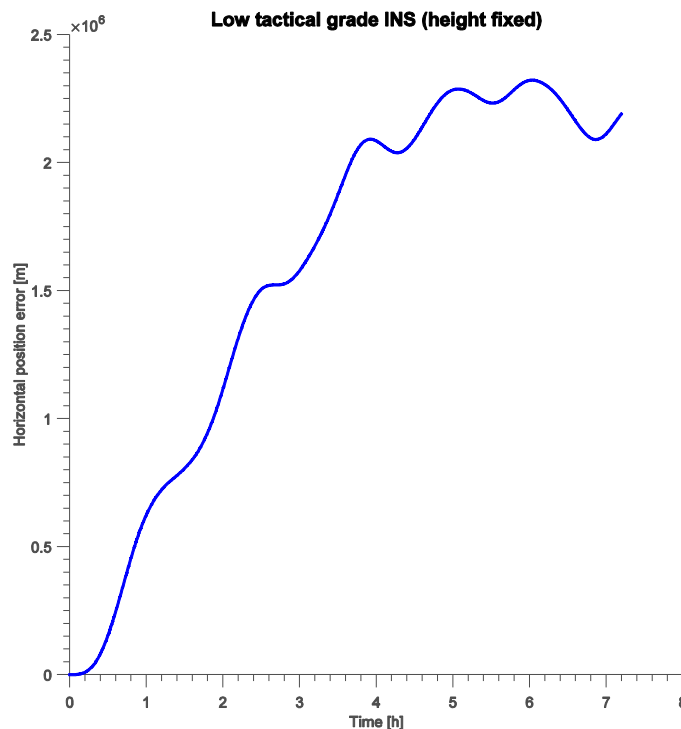


Figure 4: Horizontal position error of low tactical grade inertial navigation (stationary laboratory test)

A constant horizontal inertial angular rates error $\delta \boldsymbol{\omega}_{HIMU}$ will accumulate to linear growth of attitude error (hence the term gyro drift), superposed by Schuler oscillations. Given the equivalence of horizontal accelerometer bias and misalignment discussed above, this results in linear growth of average position error:

$$\frac{d}{dt} \delta \mathbf{x}_{H,avg} \approx R_1 \delta \boldsymbol{\omega}_{HIMU}$$

This explains how the stable Schuler dynamics, driven by IMU measurement errors of specific force and inertial angular rates, allow for accurate free inertial horizontal terrestrial navigation using high end sensors with linear growth of average horizontal position error and drift rates below $2NM/h$ (see Figure 3 for an example of navigation grade INS performance). For example, with above approximation, a constant $0.01^\circ/h$ gyro bias correspond to $0.6NM/h$ horizontal position drift. Note that this simple math does not account for the effect of other sensor errors stimulated in strapdown systems.

As has been noted above, periodical input error with frequency close to the Schuler frequency will be amplified in the open-loop inertial error dynamics [30]. While ideal white noise input error of both accelerometer and gyro will too lead to a long term growth of average position error, it scales with square of propagation time. Due to relatively low noise specifications of inertial sensors, the random walk caused by high frequency noise errors is negligible for long term horizontal position propagation with the inertial model.

For low-cost inertial navigation, any reasonable bound on horizontal position or velocity error will be exceeded before Schuler dynamics become relevant for long propagation times, see Figure 4 and Figure 5.

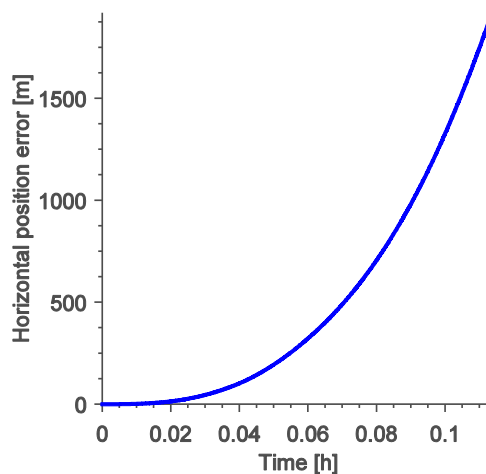


Figure 5: Initial position error growth of low tactical grade inertial navigation (stationary laboratory test)

Heading error is also affected by Schuler dynamics via transport rate, but is mostly characterized by unbounded error growth due to gyro drift. Large heading error will adversely affect horizontal velocity and attitude accuracy in presence of horizontal accelerations and must be corrected.

2.2.2.3 Modified inertial motion model error dynamics

For accurate determination of attitude with low-cost inertial sensors, a modification of the strapdown equations (2-3) can improve performance if horizontal accelerations occur only temporarily.

For ideal stationary translational motion, external forces acting on the vehicle exactly cancel weight. With constant $\boldsymbol{\omega}_{ib} = \mathbf{0}$, the gravity vector and the true value of IMU specific force measurement are related as

$$\mathbf{f}_{b_{stationary}} = -\mathbf{R}_{nb}^T \boldsymbol{\gamma}_n \quad (2-27)$$

The NED frame velocity vector changes due to rotation of NED frame with earth and transport rate

$$\dot{\mathbf{v}}_{n_{stationary}} = -\left(2\mathbf{R}_{en}^T(\phi, \lambda)\boldsymbol{\omega}_{ie} + \boldsymbol{\omega}_{en}(\phi, h, v_N, v_E)\right) \times \mathbf{v}_n$$

Neglecting deflections of the vertical, the NED frame gravity vector is

$$\boldsymbol{\gamma}_n \approx \begin{bmatrix} 0 \\ 0 \\ \gamma_D \end{bmatrix}$$

Consequently, under the assumption of stationary horizontal motion (2-27), scaling the IMU specific force measurement according to

$$\frac{\omega^2}{\omega_S^2} \mathbf{f}_b$$

does not affect the horizontal translational motion computed with equations (2-3). A modified NED frame kinematic velocity differential equation can be defined

$$\dot{\mathbf{v}}_{n_{mod}} = \mathbf{R}_{nb} \frac{\omega^2}{\omega_S^2} \mathbf{f}_b + \boldsymbol{\gamma}_n(\phi_{ref}, h) - (2\boldsymbol{\omega}_{ie}^n + \boldsymbol{\omega}_{en}) \times \mathbf{v}_n - 2\zeta\omega(\mathbf{v}_n - \mathbf{v}_{n_{ref}}) \quad (2-28)$$

Under the condition of stationary translational motion, constant $\boldsymbol{\omega}_{ib} = \mathbf{0}$ and with accurate reference position and velocity $\mathbf{v}_{n_{ref}}$, this modification is consistent with true horizontal motion:

$$\dot{v}_{N_{mod}} = \dot{v}_{N_{stationary}}$$

$$\dot{v}_{E_{mod}} = \dot{v}_{E_{stationary}}$$

For accurate vertical inertial motion, the vertical velocity differential equation should be implemented independently using the reference values for horizontal motion

$$\dot{v}_D = f_D + \gamma_D(\phi_{ref}, h) - \omega_N v_{E_{ref}} + \omega_E v_{N_{ref}} \quad (2-29)$$

With

$$\boldsymbol{\omega}_n = \begin{bmatrix} \omega_N \\ \omega_E \\ \omega_D \end{bmatrix} = 2\mathbf{R}_{en}^T(\phi_{ref}, \lambda_{ref})\boldsymbol{\omega}_{ie} + \boldsymbol{\omega}_{en}(\phi_{ref}, h, v_{N_{ref}}, v_{E_{ref}})$$

Similar to original inertial navigation, barometric altitude should be used for damping of vertical errors in a Baro-inertial vertical channel.

The effect of error in the assumption of stationary horizontal motion (2-27) and the homogeneous errors dynamics of the modified inertial model will be discussed in the following. Accounting for errors in the computation

$$\hat{\mathbf{v}}_{n_{\text{mod}}} = \hat{\mathbf{R}}_{nb} \frac{\omega^2}{\omega_S^2} (\mathbf{f}_b - \delta \mathbf{f}_{b_{IMU}}) + \boldsymbol{\gamma}_n - \frac{d\boldsymbol{\gamma}_n}{d\delta\boldsymbol{\Lambda}^T} \delta\boldsymbol{\Lambda} - (2\boldsymbol{\omega}_{ie}^n + \boldsymbol{\omega}_{en} - 2\delta\boldsymbol{\omega}_{ie}^n - \delta\boldsymbol{\omega}_{en}) \times (\mathbf{v}_n - \delta\mathbf{v}_n) - 2\zeta\boldsymbol{\omega} (\mathbf{v}_n - \delta\mathbf{v}_n - \mathbf{v}_{n_{ref}})$$

The linearized error differential equation corresponding to equation (2-28) is, assuming an ideal reference kinematic velocity $\mathbf{v}_{n_{ref}} = \mathbf{v}_n$

$$\delta\dot{\mathbf{v}}_n \doteq \left(1 - \frac{\omega^2}{\omega_S^2}\right) \mathbf{f}_n + \frac{\omega^2}{\omega_S^2} \mathbf{R}_{nb} \delta \mathbf{f}_{b_{IMU}} - \frac{\omega^2}{\omega_S^2} \mathbf{f}_n \times \boldsymbol{\phi}_n + \frac{d\boldsymbol{\gamma}_n}{d\delta\boldsymbol{\Lambda}^T} \delta\boldsymbol{\Lambda} - (2\delta\boldsymbol{\omega}_{ie}^n + \delta\boldsymbol{\omega}_{en}) \times \mathbf{v}_n - (2\boldsymbol{\omega}_{ie}^n + \boldsymbol{\omega}_{en}) \times \delta\mathbf{v}_n - 2\zeta\boldsymbol{\omega} \delta\mathbf{v}_n$$

The assumption (2-27) is violated due to accelerations of the vehicle and relative acceleration of navigation reference point R and vehicle center of gravity G for nonzero inertial rates and angular accelerations. Neglecting vertical disturbances, the specific force vector is

$$\mathbf{f}_n \approx \begin{bmatrix} f_N \\ f_E \\ -g \end{bmatrix}$$

For this study, the effect of NED frame north alignment and earth rate will be neglected. Therefore approximately

$$2\boldsymbol{\omega}_{ie}^n + \boldsymbol{\omega}_{en} \approx \begin{bmatrix} \omega_N \\ \omega_E \\ 0 \end{bmatrix}$$

And vertical orientation error can be set to zero

$$\boldsymbol{\phi} = \begin{bmatrix} \phi_N \\ \phi_E \\ 0 \end{bmatrix}$$

Neglecting transport rate rotation of vertical velocity error, gravity gradient and accelerometer measurement error, the horizontal velocity error components evolve as

$$\delta\dot{v}_N \approx \left(1 - \frac{\omega^2}{\omega_S^2}\right) f_N - \frac{\omega^2}{\omega_S^2} g \phi_E - \delta\omega_E v_D - 2\zeta\omega \delta v_N$$

$$\delta\dot{v}_E \approx \left(1 - \frac{\omega^2}{\omega_S^2}\right) f_E + \frac{\omega^2}{\omega_S^2} g \phi_N + \delta\omega_N v_D - 2\zeta\omega \delta v_E$$

Neglecting the terms in vertical velocity v_D , and with the simplified error dynamics of horizontal orientation error at latitude $\hat{\phi} = 0$ and height $\hat{h} = 0$ and the definition of Schuler frequency (2-25)

$$\begin{aligned}\ddot{\phi}_N &\approx -\frac{\delta\dot{v}_E}{R_1} \approx -\omega^2\phi_N - 2\zeta\omega\dot{\phi}_N + \omega^2 \underbrace{\left(1 - \frac{\omega_S^2}{\omega^2}\right)}_{f_{\phi_N}} \frac{f_E}{g} \\ \ddot{\phi}_E &\approx \frac{\delta\dot{v}_N}{R_1} \approx -\omega^2\phi_E - 2\zeta\omega\dot{\phi}_E + \omega^2 \underbrace{\left(\frac{\omega_S^2}{\omega^2} - 1\right)}_{f_{\phi_E}} \frac{f_N}{g}\end{aligned}\quad (2-30)$$

The homogeneous error dynamics of horizontal velocity and orientation errors have a natural frequency ω that corresponds to the scaling of specific force input. Choosing $\zeta = 1/\sqrt{2}$ and $\omega < \omega_S$ will implement non-resonating damped error dynamics with good values for both rise and settling time ($T_{5\%} \approx 3/\zeta\omega \approx 0.68T_\omega$ [64]). This significantly improves accuracy of horizontal orientation in unaccelerated motion with $f_N = f_E = 0$.

In sustained turning flight with kinematic velocity V_K and turning rate $\dot{\chi}_K$, the periodical horizontal accelerations

$$\begin{aligned}f_N &\approx -V_K\dot{\chi}_K\sin(\dot{\chi}_K t + \chi_0) \\ f_E &\approx V_K\dot{\chi}_K\cos(\dot{\chi}_K t + \chi_0)\end{aligned}\quad (2-31)$$

will drive above orientation error differential equations (2-30). For $\dot{\chi}_K \gg \omega$, the error response amplitude is strongly reduced by approximately $40dB/\lg(\dot{\chi}_K/\omega)$ [64]. For sustained turning flight of fixed-wing small general aviation aircraft typically

$$\begin{aligned}\dot{\chi} &\geq 3^\circ/s \\ \sqrt{f_N^2 + f_E^2} &\leq g \tan(30^\circ)\end{aligned}$$

The combination of lowest turning rate and largest horizontal acceleration corresponds to a kinematic velocity of approximately $108m/s$ identified as worst case.

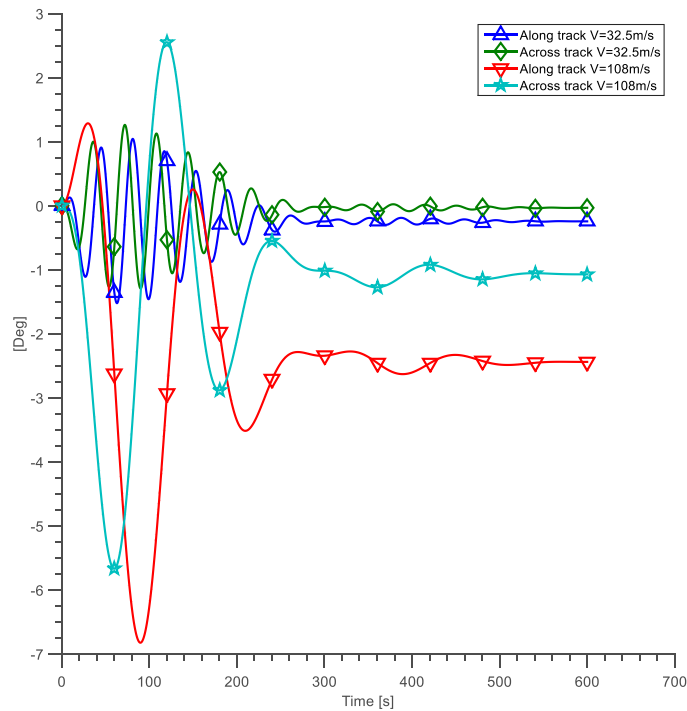


Figure 6: Transient attitude errors in coordinated turning flight with 30° bank angle. $\zeta = 1/\sqrt{2}$, $\omega = 2\pi/7(60)s$

For a choice of $\omega = 2\pi/7(60)s$, the worst-case of forcing functions f_{ϕ_N} and f_{ϕ_E} in sustained turning flight would induce periodical errors ϕ_N and ϕ_E with an amplitude of approximately 3° after transients have settled (or a constant orientation error of the same magnitude in a turning coordinate frame).

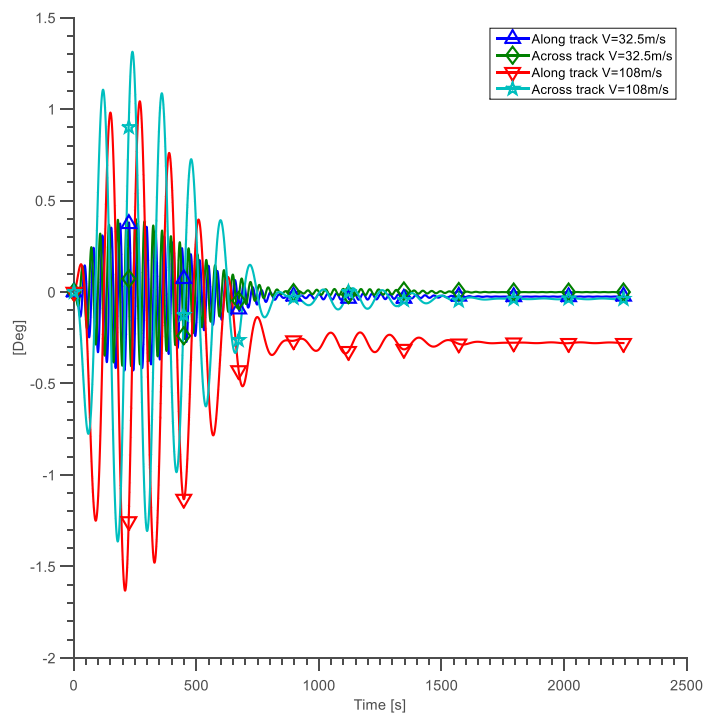


Figure 7: Transient attitude errors in coordinated turning flight with 30° bank angle. $\zeta = 1/\sqrt{2}$, $\omega = 2\pi/21(60)s$

Because airplane maneuvers usually only consist of turns of a fraction of full circle, the transient response of error equations (2-30) is of greater interest. Figure 6 shows along-track and across-track orientation error in sustained turns with lateral acceleration of $g \tan(30^\circ)$ and velocities of $32.5m/s$ and $108m/s$ for $\omega = 2\pi/7(60)s$. Figure 7 shows the same results for $\omega = 2\pi/21(60)s$

If rate of turn $\dot{\chi}_K$ can be determined accurately, the lateral acceleration in turning flight can be corrected according to equations (2-31). Note that this requires accurate attitude and heading information. Alternatively, thresholds on inertial rates and violation of equation (2-27) can be implemented to automatically set $\omega = \omega_s$ in accelerated flight.

2.2.3 Aerodynamic motion model

The error dynamics of 12-DOF vehicle dynamics model simulation are more complex than in case of inertial navigation. Since point mass motion is assumed for the VDM center of gravity, inertial error dynamics are contained in the full 12-DOF error dynamics as well, but they are covered in the more significant error dynamics of aerodynamic flight. These strongly depend on the type of aircraft, and will be discussed for conventional small general aviation airplanes.

The airplanes considered here are designed and verified to exhibit benign flight dynamics minimizing the stress and required skill for the pilot (see e.g. §23.181(b) in [65, 66]). Unlike airplanes flown by extensively trained pilots (such as fighter airplanes and competition-level sailplanes), small general aviation airplanes will react to small disturbances from the current flight condition in a dynamically stable way. A software model of flight dynamics that has been qualified in accordance to high fidelity flight model certification specifications [47] or verified in a similar way, will accurately replicate the flight characteristics of the true airplane. Therefore, such a model will show similar dynamics after a disturbance from a defined reference flight condition. Given this similarity and the stability of both true and modeled flight dynamics, the dynamics of errors of flight simulation will exhibit the same benign characteristics as the true airplane flight dynamics: The dynamics of errors of aerodynamic position propagation and the tested and verified benign flight dynamics of the small general aviation airplane are similar.

In this section, a short and simplified perturbation error analysis of decoupled 12-DOF airplane motion will be conducted to show how the stability and damping qualities of the total state flight dynamics translate to the corresponding error dynamics of modeled flight. Assuming an ideal model and in linear approximation, the dynamics of perturbation of true flight from a reference flight condition and the dynamics of error of modeled flight compared to true flight are equivalent. A rigorous analysis of perturbed state flight dynamics assuming decoupled lateral and longitudinal airplane motion is found in many textbooks (e.g. [22, 41]) and not repeated here. The important conclusion is that using high-quality models, the error dynamics of the aerodynamic motion model will inherit the flight dynamics of the airplane.

To confirm the characteristics of aerodynamic model error dynamics for complex nonlinear models and flight conditions that do not agree with the simplifications of theoretical analysis, and to extend the analysis to model error and large input errors, an extensive simulation study is required. This may include that the airplane software model is tested in simulation similar to the flight test program conducted with the real airplane (e.g. according to [67]) and compared against flight test data over the whole operational envelope. Furthermore, it has to be verified that errors in the weight and balance model are limited so that they do not affect flight dynamics.

In this thesis, the reliability of error dynamics for conventional airplanes is confirmed by Monte Carlo simulation using one model for truth flight dynamics and a large number of approximate models.

2.2.3.1 Perturbation error analysis of aerodynamic flight

To demonstrate how flight dynamics stability and damping translate to the error dynamics of 12-DOF aerodynamic motion model simulation, a perturbation error analysis will be conducted in the following. This analysis is valid for small errors, i.e. computed state and measured input in vicinity of true state and input. Then the true aerodynamic forces and moments in center of gravity G can be approximated based on computed values and errors in a linear coefficient form, for example as follows:

$$\begin{aligned} C_L &= C_{L\alpha}\delta\alpha_A + \hat{C}_L \\ C_Y &= C_{Y\beta}\delta\beta_A + \hat{C}_Y \\ C_l^G &= C_{l\beta}\delta\beta_A + C_{lp}\delta p^* + C_{lr}\delta r^* + C_{l\xi}\delta\xi + C_{l\zeta}\delta\zeta + \hat{C}_l \\ C_m^G &= C_{m\alpha}\delta\alpha_A + C_{mq}\delta q^* + C_{m\eta}\delta\eta + \hat{C}_m \\ C_n^G &= C_{n\beta}\delta\beta_A + C_{np}\delta p^* + C_{nr}\delta r^* + C_{n\xi}\delta\xi + C_{n\zeta}\delta\zeta + \hat{C}_n \end{aligned}$$

Which are the formulas for coefficients of lift, sideforce, roll moment, pitch moment and yaw moment respectively, c.f. (2-10) with aerodynamic reference point at center of gravity location for simplicity. Wind vector will always be assumed zero for this analysis. $\delta\alpha_A$ and $\delta\beta_A$ denote the errors of computed aerodynamic angles of attack and sideslip (without indices in the following).

$\delta\xi$, $\delta\eta$ and $\delta\zeta$ are errors of control surface deflections (aileron, elevator and rudder) which are used as input to the model. These can be measured accurately and their errors will be neglected for this analysis. Assuming a high-quality aerodynamic motion model is used, errors in model coefficients as well as weight and balance errors are neglected as well.

The errors of computed aerodynamic rates vector $\boldsymbol{\omega}_{Ab}$ are represented here by the nondimensional (aerodynamic) rates in roll, pitch and yaw direction (in order p, q, r)

$$\begin{aligned} \delta p^* &= \frac{\delta\omega_{Ax}b}{2\hat{V}_A}, \delta r^* = \frac{\delta\omega_{Az}b}{2\hat{V}_A} \\ \delta q^* &= \frac{\delta\omega_{Ay}\bar{c}}{2\hat{V}_A} \end{aligned}$$

With the computed airspeed $\hat{V}_A = \|\hat{\boldsymbol{v}}_n - \hat{\boldsymbol{v}}_{Wn}\|_2$, wingspan b and mean aerodynamic chord \bar{c} .

The aerodynamic drag coefficient can for example be modeled with a quadratic formula (see (2-12)). Accounting for state errors and linearization gives to following perturbation formula

$$C_D = k \left((C_L - C_{L0})^2 - (\hat{C}_L - C_{L0})^2 \right) + \hat{C}_D \doteq 2k(\hat{C}_L - C_{L0})C_{L\alpha}\delta\alpha + \hat{C}_D$$

In flight simulation, the computed aerodynamic coefficients are used to determine external forces and moments. The true aerodynamic forces and moments differ from computed values in linear approximation as follows

$$\begin{aligned} \mathbf{F}_{b\ Aero}^G &= q S_{ref} \mathbf{R}_{ab}^T \begin{bmatrix} -C_D \\ C_Y \\ -C_L \end{bmatrix} \\ &\doteq \delta q \frac{\widehat{\mathbf{F}}_{b\ Aero}^G}{\widehat{q}} - \widehat{q} S_{ref} \widehat{\mathbf{R}}_{ab}^T \left(\boldsymbol{\Psi}_{a\bar{a}} \times \begin{bmatrix} -C_D \\ C_Y \\ -C_L \end{bmatrix} \right) \end{aligned} \quad (2-32)$$

$$\begin{aligned} &+ \widehat{q} S_{ref} \widehat{\mathbf{R}}_{ab}^T \begin{bmatrix} -2k(\widehat{C}_L - C_{L0}) C_{L\alpha} \delta\alpha_A \\ C_{Y\beta} \delta\beta_A \\ -C_{L\alpha} \delta\alpha_A \end{bmatrix} + \widehat{\mathbf{F}}_{b\ Aero}^G \\ \mathbf{M}_{b\ Aero}^G &= q S_{ref} \begin{bmatrix} b C_l^G \\ \bar{c} C_m^G \\ b C_n^G \end{bmatrix} \doteq \delta q \frac{\widehat{\mathbf{M}}_{b\ Aero}^G}{\widehat{q}} + \widehat{q} S_{ref} \begin{bmatrix} b(C_{l\beta} \delta\beta_A + C_{lp} \delta p^* + C_{lr} \delta r^*) \\ \bar{c}(C_{m\alpha} \delta\alpha_A + C_{mq} \delta q^*) \\ b(C_{n\beta} \delta\beta_A + C_{np} \delta p^* + C_{nr} \delta r^*) \end{bmatrix} + \widehat{\mathbf{M}}_{b\ Aero}^G \end{aligned} \quad (2-33)$$

With the dynamic pressure $q := \frac{1}{2} \rho V_A^2$, where ρ is the altitude-dependent air density, and reference wing area S_{ref} . The error of computed dynamic pressure can be linearized as

$$\delta q \doteq \frac{1}{2} \widehat{V}_A^2 \frac{\partial \rho}{\partial h} \delta h + \widehat{\rho} \widehat{V}_A \delta V_A$$

The vector $\boldsymbol{\Psi}_{a\bar{a}}$ is defined to model the misalignment of the computed aerodynamic frame in linear approximation: $\mathbf{R}_{ab} \widehat{\mathbf{R}}_{ab}^T \doteq \mathbf{I} + [\boldsymbol{\Psi}_{a\bar{a}} \times]$ (from linearization of equation (A-20)). $\boldsymbol{\Psi}_{a\bar{a}}$ can be interpreted as small angle rotation vector or vector of small Euler angles (c.f. discussion of $\boldsymbol{\phi}_n$ and $\boldsymbol{\Phi}$ in 2.2.2.1). Assuming small absolute values of aerodynamic angles of attack and sideslip allow to write

$$-\widehat{q} S_{ref} \widehat{\mathbf{R}}_{ab}^T \left(\boldsymbol{\Psi}_{a\bar{a}} \times \begin{bmatrix} -C_D \\ C_Y \\ -C_L \end{bmatrix} \right) \approx \widehat{\mathbf{F}}_{b\ Aero}^G \times \begin{bmatrix} 0 \\ \delta\alpha_A \\ -\delta\beta_A \end{bmatrix}$$

The influence of error in aerodynamic motion model state is much less for propulsion forces and moments and will be neglected for this analysis.

Above perturbation formulas, in combination with linearizations of equation (2-9) and the Euler equation of rotational motion (2-8), and the system of strapdown navigation error dynamics (2-22) constitute a simplified system of error dynamics for the aerodynamic motion model.

2.2.3.2 Error dynamics and stability

The basic mechanisms of 12-DOF aerodynamic motion model error dynamics can be identified by studying simplified equations of motion driven by the forces and moments (2-32) and (2-33).

Analysis is significantly simplified by assuming constant zero wind velocity vector, so that

$$\begin{aligned} \mathbf{v}_A &= \mathbf{v}_K \\ V &= V_A = V_K \\ \alpha &= \alpha_A = \alpha_K \\ \beta &= \beta_A = \beta_K \\ \gamma &= \gamma_A = \gamma_K \\ \boldsymbol{\omega}_A &= \boldsymbol{\omega}_K \end{aligned} \quad (2-34)$$

And similar equalities for all corresponding error quantities.

From the first error term in aerodynamic force (2-32)

$$\delta q \frac{\hat{\mathbf{F}}_{b\ Aero}^G}{\hat{q}} = \hat{\mathbf{F}}_{b\ Aero}^G \left(\frac{1}{\hat{\rho}} \frac{\partial \rho}{\partial h} \delta h + 2 \frac{\delta V_A}{\hat{V}_A} \right) \quad (2-35)$$

one can see that an error in computed air density or in airspeed will have significant effect in all flight conditions where aerodynamic force is large. From the principle of aerodynamic flight – aerodynamic lift cancels weight – it follows that this is most often the case. For all these flight conditions, and because air density reduces with increasing height, a positive error in aerodynamic motion model height will have a negative contribution to the error in aerodynamic lift.

With $\delta \dot{v}_D \approx \frac{1}{m} \frac{\partial F_z^G}{\partial h} \delta h + \frac{\partial \gamma_D}{\partial h} \delta h$, the simplified dynamics of aerodynamic motion model height error, isolated from the dynamics of airspeed error, can be derived as

$$\delta \ddot{h} = -\delta \dot{v}_D \approx \left(\gamma_D \frac{1}{\hat{\rho}} \frac{\partial \rho}{\partial h} - \frac{\partial \gamma_D}{\partial h} \right) \delta h$$

Although gravity gradient $\frac{\partial \gamma_D}{\partial h}$ is small in magnitude, it has negative sign and causes exponential error growth of vertical errors in inertial navigation. $\frac{\partial \gamma_D}{\partial h}$ is on the order of $-3 \cdot 10^{-6} \frac{1}{s^2}$ [30] and $\gamma_D \frac{1}{\hat{\rho}} \frac{\partial \rho}{\partial h}$ on the order of $-1 \cdot 10^{-3} \frac{1}{s^2}$ in troposphere and stratosphere regimes. Consequently, the isolated height error dynamics for an airplane in level flight are undamped but neutrally stable with a time period on the order of 200s.

The second term in parenthesis in equation (2-35) gives rise to another error mechanism for level flight conditions. The simplified dynamics of vertical velocity error in level flight are with $\delta \dot{v}_D \approx \frac{1}{m} \frac{\partial F_z^G}{\partial V} \delta V$, neglecting the effect of height error

$$\delta \dot{v}_D \approx -2\gamma_D \frac{\delta V}{\hat{V}}$$

Which can alternatively be represented by error in climb angle γ (not be be confused with vertical gravity γ_D) in linear approximation

$$\delta \dot{\gamma} \approx 2\gamma_D \frac{\delta V}{\hat{V}^2}$$

Due to its physical nature, aerodynamic lift is tilted in NED frame when climb angle changes, to remain perpendicular to velocity vector. In linear approximation for zero climb angle γ

$$\delta \dot{V} \approx -\gamma_D \delta \gamma$$

This gives the following error dynamics for magnitude of velocity

$$\delta \dot{V} \approx -2\gamma_D^2 \frac{\delta V}{\hat{V}^2}$$

which directly corresponds to the (1-DOF) phugoid Eigenmode of airplane dynamics, with a well-known formula for the (approximate) Eigenfrequency $\omega_{0,Ph} \approx \sqrt{2}\gamma_D/\hat{V}$.

Note that this 1-DOF analysis is overly simplified since it neglects simultaneous changes in any other parameter that determines aerodynamic lift. Especially angle of attack (or the error thereof) is not constant. For a more rigorous 2-DOF analysis of coupled phugoid and short period airplane dynamics, see [22]. The results also apply to aerodynamic motion model error dynamics.

The low-frequency phugoid Eigenmode is present in flight dynamics of the true airplane, the 12-DOF aerodynamic motion model and in the corresponding error dynamics. According to the certification specifications for small airplanes [65, 66], for periods greater 15s even instability of the phugoid mode of flight dynamics is admissible, with doubling times greater 55s. For instable phugoid dynamics of the true airplane, the corresponding error dynamics of the aerodynamic motion model need to be damped. This is not addressed further in this work because the airplane model used exhibits sufficiently damped phugoid dynamics.

Rotational motion is barely affected by error in dynamic pressure. In equation (2-33), the error term for aerodynamic moments in center of gravity $\delta q \frac{\hat{M}_{b,Aero}^G}{\hat{q}}$ is negligible for stationary flight conditions where $\hat{M}_{b,Aero}^G \approx \mathbf{0}$. More notable are the dynamics of errors of lateral rotational motion due to their influence on aerodynamic moments, which will be discussed later in this section.

Errors of aerodynamic angle of attack strongly influence lift vector, since for conventional airplanes $C_{L\alpha}$ is somewhere near the theoretical value of 2π found with thin airfoil theory [42]. For analysis of angle of attack error dynamics for zero wind vector, a simplified equation of rotational motion based on the second row of equation (2-8) is used with equation (2-33)

$$\delta \dot{q}^* \approx \underbrace{\frac{\bar{c}}{2\hat{V}}}_{\text{nondimensionalization}} \underbrace{\frac{1}{I_{yy}}}_{\text{moment of inertia}} \underbrace{\frac{\hat{q}S_{ref}\bar{c}(C_{m\alpha}\delta\alpha + C_{mq}\delta q^*)}{\text{aerodynamic moment}}}_{\text{aerodynamic moment}} \quad (2-36)$$

assuming zero products of inertia and neglecting inertia cross coupling of rotational motion.

With approximately zero computed and true angle of sideslip, the error of angle of attack changes as

$$\delta \dot{\alpha} \approx \frac{2\hat{V}}{\bar{c}} \delta q^* \quad (2-37)$$

Above equation assumes that angle of attack dynamics settle much faster than point mass motion will be affected by changing aerodynamic force. This is verified by the high frequency for this error Eigenmode. Taking the time derivative of (2-36) and inserting (2-37) gives

$$\delta \ddot{q}^* \approx \frac{\bar{c}}{2\hat{V}} \frac{\hat{q}S_{ref}\bar{c}C_{mq}}{I_{yy}} \delta \dot{q}^* + \underbrace{\frac{\hat{q}S_{ref}\bar{c}C_{m\alpha}}{I_{yy}}}_{-\omega_{0,SP}^2} \delta q^*$$

The natural frequency $\omega_{0,SP}$ is on the order of $(2\pi)Hz$ for small general aviation airplanes. For these aircraft, this damped, high-frequency mode is always stable. Again, this error mode has its total state equivalent in the short period mode of flight dynamics.

To gain an understanding of the error dynamics of lateral motion, a corresponding set of simplified equations of motion is derived. Euler angles of roll Φ_{nb} and azimuth Ψ_{nb} are chosen

as lateral orientation state parametrization and for true and computed values of roll and azimuth approximately zero and small pitch angle θ_{nb} (omitting indices)

$$\delta\Phi \approx \frac{2\hat{V}}{b} \delta p^* \quad (2-38)$$

$$\delta\Psi \approx \frac{2\hat{V}}{b} \delta r^* \quad (2-39)$$

The error dynamics of rotational motion are approximated based on the second row of equation (2-8) and equation (2-33) as

$$\delta\dot{p}^* \approx \frac{b}{2\hat{V}} \frac{1}{I_{xx}} \hat{q} S_{ref} b (C_{l\beta} \delta\beta + C_{lp} \delta p^* + C_{lr} \delta r^*) \quad (2-40)$$

$$\delta\dot{r}^* \approx \frac{b}{2\hat{V}} \frac{1}{I_{zz}} \hat{q} S_{ref} b (C_{n\beta} \delta\beta + C_{np} \delta p^* + C_{nr} \delta r^*) \quad (2-41)$$

Again the products of inertia are assumed zero and inertia cross coupling is neglected.

There is a lateral error in velocity mainly due to rotation of aerodynamic lift to remain in the plane of symmetry of the airplane. For level flight conditions with aerodynamic lift equal to weight and with equation (2-32)

$$\delta\dot{v}_y \approx \gamma_D \delta\Phi + \frac{\hat{q} S_{ref}}{m} (C_{Y\beta} - \hat{C}_D) \delta\beta \quad (2-42)$$

Perturbation analysis of NED frame velocity vector yields the following linearization for $\mathbf{R}_{nb} = \mathbf{R}_{ba} = I$ (i.e. assuming zero Azimuth, roll angle and angle of sideslip and negligible pitch angle and angle of attack)

$$\delta\mathbf{v}_n = \delta \left(\mathbf{R}_{nb} \mathbf{R}_{ba} \begin{bmatrix} V \\ 0 \\ 0 \end{bmatrix} \right) \doteq \begin{bmatrix} \delta\Phi \\ \delta\Theta \\ \delta\Psi \end{bmatrix} \times \begin{bmatrix} \hat{V} \\ 0 \\ 0 \end{bmatrix} - \begin{bmatrix} 0 \\ \delta\alpha \\ -\delta\beta \end{bmatrix} \times \begin{bmatrix} \hat{V} \\ 0 \\ 0 \end{bmatrix} + \begin{bmatrix} \delta V \\ 0 \\ 0 \end{bmatrix}$$

This gives for the lateral component with $\delta v_y = \delta v_E$

$$\delta\beta \approx -\delta\Psi + \frac{1}{\hat{V}} \delta v_y \quad (2-43)$$

The time derivative is

$$\delta\dot{\beta} \approx -\delta\dot{\Psi} + \frac{1}{\hat{V}} \delta\dot{v}_y$$

Inserting equations (2-39) and (2-42) gives

$$\delta\dot{\beta} \approx -\frac{2\hat{V}}{b} \delta\dot{r}^* + \frac{1}{\hat{V}} \left(\gamma_D \delta\Phi + \frac{\hat{q} S_{ref}}{m} (C_{Y\beta} - \hat{C}_D) \delta\beta \right) \quad (2-44)$$

Equations (2-38), (2-40), (2-41) and (2-44) can be combined as a 4-DOF system of error dynamics

$$\frac{d}{dt} \begin{bmatrix} \delta\Phi \\ \delta\beta \\ \delta p^* \\ \delta r^* \end{bmatrix} \approx \begin{bmatrix} 0 & 0 & \frac{2\hat{V}}{b} & 0 \\ \frac{1}{\hat{V}}\gamma_D & \frac{1}{\hat{V}}\frac{\hat{q}S_{ref}}{m}(C_{Y\beta} - \hat{C}_D) & 0 & -\frac{2\hat{V}}{b} \\ 0 & \frac{b}{2\hat{V}}\frac{1}{I_{xx}}\hat{q}S_{ref}bC_{l\beta} & \frac{b}{2\hat{V}}\frac{1}{I_{xx}}\hat{q}S_{ref}bC_{lp} & \frac{b}{2\hat{V}}\frac{1}{I_{xx}}\hat{q}S_{ref}bC_{lr} \\ 0 & \frac{b}{2\hat{V}}\frac{1}{I_{zz}}\hat{q}S_{ref}bC_{n\beta} & \frac{b}{2\hat{V}}\frac{1}{I_{zz}}\hat{q}S_{ref}bC_{np} & \frac{b}{2\hat{V}}\frac{1}{I_{zz}}\hat{q}S_{ref}bC_{nr} \end{bmatrix} \begin{bmatrix} \delta\Phi \\ \delta\beta \\ \delta p^* \\ \delta r^* \end{bmatrix}$$

This model is equivalent to the corresponding 4-DOF models of decoupled lateral airplane dynamics found in the literature on flight dynamics and stability. With typical values for small general aviation airplane flight

$$\hat{C}_D = 0.05, \hat{V} = 80m/s, \hat{q} = 3920Pa, \gamma_D = 9.80665m/s^2, b = 10.2m, S_{ref} = 17.1m^2$$

and vehicle dynamics model coefficients and weight and balance parameters taken from [44] (data for the NAVION general aviation airplane)

$$C_{Y\beta} = -0.564$$

$$C_{l\beta} = -0.074, C_{lp} = -0.41, C_{lr} = 0.107$$

$$C_{n\beta} = 0.071, C_{np} = -0.0575, C_{nr} = -0.125$$

$$m = 1250kg$$

$$I_{xx} = 1420kgm^2$$

$$I_{zz} = 4800kgm^2$$

it is possible to numerically determine exemplary Eigenvectors and Eigenvalues of the linear dynamical system above. One can identify three error modes that correspond to the flight dynamic modes for spiral, Dutch-roll and roll typical for fixed-wing aircraft. The natural frequencies and relative damping coefficients are

	Spiral error	Dutch-Roll error	Roll error
Natural frequency ω_0 [$\frac{rad}{s}$]	0.0057	3.5263	12.5985
Relative damping ζ [-]	1	0.2166	1

Table 1: Lateral error dynamics natural frequency ω_0 and relative damping ζ (Example)

The Eigenvectors for these lateral error dynamics of aerodynamic motion model 12-DOF simulation are (magnitude and phase angles for each participating error state)

	Spiral error		Dutch-Roll error		Roll error	
$\delta\Phi$	0.9999	0°	0.6248	$\pm 78.9484^\circ$	0.7787	180°
$\delta\beta$	0.0128	0°	0.7510	$\pm 0^\circ$	0.0415	0°
δp^*	0.0004	180°	0.1404	$\mp 178.5417^\circ$	0.6254	0°
δr^*	0.0075	0°	0.1610	$\mp 83.6528^\circ$	0.0262	0°

Table 2: Lateral error dynamics Eigenvectors (Example)

As expected, these results are again equivalent to those of linearized airplane flight dynamics analysis for decoupled lateral motion.

The oscillatory error mode (second column in above tables) involves error dynamics of roll rate and roll angle as well as yaw rate and angle of sideslip, each two separated by a phase angle of about 90° . Its total state counterpart, the Dutch-Roll mode of airplane flight dynamics, receives special attention in the design of airplanes in order to meet strict handling qualities requirements (see e.g. §23.181 (b) in [65, 66]). Thanks to strong damping of this mode for both the real airplane and the used aerodynamic motion model, which is verified not only with linear analysis for level flight but extensively in flight testing, the corresponding dynamic error mode can generally considered uncritical for the application of an aerodynamic motion model in navigation.

The third error mode identified with above analysis shows that errors in roll rate are quickly damped to zero without oscillation. Nevertheless, sustained roll rate error will occur for example due to errors in measured control inputs or aerodynamic motion model coefficients. The same is true for the first error mode found for lateral flight dynamics, which is considered to be the most critical for navigation use of 12-DOF airplane aerodynamic motion model simulation. Unlike the roll error mode, the non-oscillatory spiral error mode has a large time constant $T_s \approx 1100s$ for the example airplane, and thus makes 12-DOF simulation of airplanes similar to the one studied above very susceptible to input errors affecting roll orientation.

Although Ψ and v_y have been eliminated in the simple analysis above, the approximate lateral acceleration in horizontal flight equation (2-42)

$$\delta \dot{v}_y \approx \gamma_D \delta \Phi + \frac{\hat{q} S_{ref}}{m} (C_{Y\beta} - \hat{C}_D) \delta \beta$$

shows that the spiral error mode will strongly affect across-track positioning and course over ground accuracy. Additionally, with angle of sideslip error $\delta \beta$ remaining small, error of azimuth $\delta \Psi$ will grow quickly. Note that, according to small airplane certification specifications [65, 66], the corresponding total state dynamics spiral mode may often be “neutrally stable or even mildly divergent in roll and yaw”. Due to the noted equivalency of flight total state and error dynamics, the problem of lateral error divergence is severe.

Even with stable spiral error mode, small and temporary input errors will lead to a heading difference after flight dynamics of true airplane and aerodynamic motion model have recovered the initial flight condition. Large or constant input error affecting lateral motion will cause lateral divergence of true and simulated motion due to the spiral error mode. Consequently, means to make aerodynamic motion model simulation robust with respect to lateral divergence are required.

The reliability of the aerodynamic motion model, including a mechanism for heading error damping, must be studied in simulation to account for a vast number of combinations of reference flight condition, atmosphere dynamics and pilot reactions.

2.2.4 Method comparison

The analysis conducted in this section allows evaluating how well each of the three presented motion models is suited for unaided position propagation. For each motion model, the growth of individual errors has been studied and, if applicable, different characteristics for short or long time intervals of open-loop propagation have been identified. Generally, for the desired application, the long term error propagation characteristics of the motion model must be suitable for use in an unaided method. If that is not the case (at least for selected error states), the possible improvement with low-cost aiding will be addressed in the following section.

Because dead reckoning navigation is based on integration of position from a velocity measurement, position error is simply initial error plus a time integral of velocity measurement error. Consequently, large measurement errors will affect position accuracy only scaled by the duration of their occurrence. For low-cost sensors with complex error characteristics, this means a significant increase in method reliability. For example, the performance of heading and airspeed dead reckoning is hardly affected by gusts or temporary disturbances in airspeed or magnetic heading measurements (e.g. in dynamic flight), as long as the total duration is short compared to full mission time. Furthermore, linear position error growth increases method reliability because its characteristic strictly remains the same for full duration of flight and is independent of initial error. Consequently, judging by its error propagation characteristics, heading and airspeed dead reckoning is a good choice for use in low-cost applications.

	Dead reckoning	Inertial navigation	Aerodynamic position propagation
Short term and small errors	LINEAR VELOCITY ERROR PROPAGATION (1)	QUADRATIC + CUBIC IMU ERROR PROPAGATION (2)	LATERAL DIVERGENCE (4)
			LINEAR (HDG ALIGNED) (5)
Long term and large errors		LINEAR SCHULER DYNAMICS (3)	LINEAR FLIGHT ERROR PROPAGATION (6)

Figure 8: Horizontal error propagation and dynamics

Unlike dead reckoning, both inertial and aerodynamic motion models exhibit unfavorable higher order error propagation, see Figure 8. For inertial navigation, the error propagation analysis in this section revealed polynomial position error growth due to IMU measurement errors which will dominate the short term performance of the inertial motion model (see (2) in Figure 8). This error characteristic is especially critical, because it is directly and exclusively

related to the quality of sensors used. Sensor quality of low-cost systems nowadays still is far away from what would be termed navigation grade quality (i.e. gyro drift better $0.01^\circ/h$ and comparable level of other errors). Although polynomial error growth is suppressed for large errors, and oscillatory Schuler errors with long term linear growth of average error dominate (see (3) in Figure 8), the performance of low cost systems would be on the order of thousands of kilometers of error per hour. In contrast, for very short term motion propagation (e.g. only seconds with low-cost sensors) and starting from an accurate initial state, polynomial error growth corresponds to errors much smaller than possible with dead reckoning.

For aerodynamic position propagation, the case is even more complex. It has been found that the aerodynamic motion model is indifferent to heading, and heading error will accumulate due to temporary or continuous disturbances of lateral motion due to input or model error. A linear growth of the difference between true and simulated direction of flight would cause growth of lateral position error with second order in time for small errors (see (4) in Figure 8). Because, ultimately, heading error is limited and position error can only grow as fast as true and simulated airplane fly away from each other at opposite directions, aerodynamic position propagation is strictly limited to linear position error growth in the long term and for large errors (see (6) in Figure 8). But more importantly, and unlike for inertial navigation, the divergent lateral error propagation can be prevented by simple countermeasures: Position propagation with the aerodynamic motion model requires some means of heading alignment of simulated and true motion. If this is provided for, the aerodynamic motion model allows for accurate position propagation with first order error growth.

2.3 MOTION MODEL AIDING

In the previous sections of this chapter, three algorithms for propagation of position estimate have been studied. Because all of them exhibit increasing position error over time, they would typically be combined with accurate position information at regular time intervals, if available (e.g. with GPS). Integration of inertial navigation and GNSS is a very successful example of this strategy and subject of many textbooks [15, 20, 29]. An introductory derivation is found in appendix A.7.

With no absolute information on position available, a steady increase in position error has to be accepted. The previous section on error propagation showed that all of the three motion models exhibit favorable first order position error growth under certain circumstances. In fact, heading and airspeed dead reckoning was found to be always first order, while inertial navigation only adopts first order behavior in long term average drift, superposed by oscillating errors that scale with sensor quality. For short propagation times, a polynomial propagation of measurement error to position error renders the open-loop inertial motion model useless for low-cost applications. Consequently, ways to reset this polynomial error growth at short time intervals using auxiliary information on velocity or attitude are studied in this section in order to allow use of inertial navigation for low-cost position propagation.

The aerodynamic motion model is first order in position error growth for long times and large errors (because errors are the difference of true and simulated flight). But initially, the divergence in lateral motion due to spiral error mode will represent higher order position error propagation in time. Because of this, the aerodynamic motion model must be kept aligned with the true flight direction.

In the following, possibilities to improve the performance of above algorithms using measurements that are independent of external infrastructure, weather, time of day and visibility and furthermore low-cost are presented. The information on state vector error contained in the sensor measurement will be studied. In presence of suitable total state dynamics, observability of all motion model error states may be enhanced. This is assessed in an application-oriented observability analysis that uses an analytical approach to anticipate (a priori) and explain (a posteriori) observability in certain maneuvers in combination with extensive Monte Carlo simulation for realistic evaluation. This combined approach proved very efficient for observability analysis of systems with complex total state trajectories and uncertain dynamics.

The extended Kalman filter will be used as state estimation method of choice for correction of observed navigation errors using the available measurements. A brief description of the nomenclature used can be found in appendix A.8.

The extended Kalman filter method is superior to nonlinear methods of data fusion for problems where nonlinearities in process model and observations as well as estimation errors are small, and observations carry unimodal information. For integrated navigation based on inertial navigation, the gain from more precisely dealing with nonlinearities is negligible if orientation errors are small, and the much higher computational cost of nonlinear methods not justified. Nonlinearities of 3-D magnetometer and true airspeed measurements are manageable for accurate orientation and if the velocity error is small compared to true airspeed. Furthermore, no observation ambiguities are present. While use of the aerodynamic model requires linearization at higher rates, computational cost is still

acceptable and the extended Kalman is used throughout this work. For details on this method, see [68–70].

2.3.1 Heading and airspeed dead reckoning

The dead reckoning method offers little opportunity for state estimation, because only position is integrated and position aiding usually unavailable when this method is used. If additional information was available, e.g. from redundant velocity and heading sensors, the integrated measurements would rather be improved on signal level.

2.3.2 Inertial navigation

The inertial motion model requires closed-loop high-rate error correction in order to restrain 2nd order accelerometer error propagation in all directions and 3rd order gyro error propagation to position in directions perpendicular to measured specific force. In practical applications, accurately measuring both translational and rotational motion states in three dimensions is rarely possible. It is necessary to find a combination of available measurements that each offer observability of several motion error states. This is studied for low-cost GNSS-denied inertial navigation in this section. While Monte Carlo simulation of aided inertial navigation along a number of selected dynamical motion trajectories is the most straight forward way to assess effectiveness of low-cost aiding for a given application, a more theoretical approach based on covariance propagation will be chosen in the following.

2.3.2.1 Observability of inertial navigation errors

Assume the inertial motion model is used for propagation of state vector \mathbf{z}_n along a specific trajectory in a Monte Carlo experiment with a large number of repetitions. Initial errors and input errors are drawn from zero-mean normal distributions. As result, the computed motion model states z_i at the end are scattered randomly around an average value $\mu_i = E[z_i]$ with a certain variance $Var[z_i] = E[(z_i - \mu_i)^2]$.

Because the possibility to reduce errors in motion propagation using a deterministic computation scheme to be applied in every single Monte Carlo run is of interest, this is studied in the following. In the described Monte Carlo experiment, this would mean that the variance of a selected motion state z_i can be reduced by applying an additive correction term $\delta\hat{z}_i$:

$$Var[z_i + \delta\hat{z}_i] = Var[z_i] + Var[\delta\hat{z}_i] + 2Cov[z_i, \delta\hat{z}_i] < Var[z_i]$$

Consequently, the correction must be constructed so that

$$Var[\delta\hat{z}_i] + 2Cov[z_i, \delta\hat{z}_i] < 0$$

Assume a measurement \tilde{z}_j of some other motion state z_j is available, perturbed by zero mean error v_j with variance $Var[v_j] = R_j$

$$\tilde{z}_j = z_j + v_j$$

With a linear correction function

$$\delta\hat{z}_i = c \cdot \tilde{z}_j = c(z_j + v_j)$$

the condition for reduced variance of corrected state estimate $z_i + \delta\hat{z}_i$ becomes

$$Var[\delta\hat{z}_i] + 2Cov[z_i, \delta\hat{z}_i] = c^2 \cdot (Var[z_j] + R_j) + 2c \cdot Cov[z_i, z_j] < 0$$

With the obvious choice

$$c = -\frac{Cov[z_i, z_j]}{Var[z_j] + R_j} \quad (2-45)$$

the condition above is satisfied if and only if

$$Cov[z_i, z_j] \neq 0$$

Consequently, if the covariance of two selected states is nonzero and one of the two is measured, the other can be estimated as well. The effectiveness of correction (2-45) can be evaluated by studying the ratio of variance of corrected and uncorrected motion model state

$$\frac{Var[z_i + \delta \hat{z}_i]}{Var[z_i]} = 1 - \frac{1}{1 + \frac{R_j}{Var[z_j]}} \left(\frac{Cov[z_i, z_j]}{\sqrt{Var[z_i]Var[z_j]}} \right)^2$$

And with measurement uncertainty small compared to the uncertainty of measured state z_j , the decisive quantity for effective correction of state z_i is the magnitude of correlation coefficient [71]

$$\rho_{ij} = \frac{Cov[z_i, z_j]}{\sqrt{Var[z_i]Var[z_j]}}$$

Note that, with appropriate definitions, this concepts also holds for the observability of combinations and vectors of error states, which usually is the case.

The resemblance of above correction function (2-45) with the Kalman filter update step is obvious. This observability analysis addresses the question if and how well errors could be estimated in an optimal framework with exact system models. The correlation coefficient for a given trajectory can be evaluated by analytical or numerical covariance propagation, see below. For a more realistic study of estimation effectiveness in cases with noticeable modelling imperfections and complex measurement error, Monte Carlo simulation of state estimation must be used.

As has been mentioned above, the required update intervals for low-cost systems are so short that all error dynamics identified in the previous section, including vertical instability with a doubling time of 400s, can safely be neglected. Consequently, it is sufficient to evaluate the correlation of inertial motion model state errors due to propagation of errors. Because flight velocity is low, errors in transport rate are small compared to gyro errors and can be neglected for short flight segments. Similarly, earth rate will not have an influence for the quality of inertial sensors in low-cost systems. For short time intervals and small vertical errors, vertical gravity gradient can be neglected. This significantly reduces complexity and allows for an intuitive evaluation of observability. Orientation error $\boldsymbol{\phi}$, velocity error $\delta \mathbf{v}_n$ and cartesian position error $\delta \mathbf{x}_n$ are studied.

Several typical motion trajectories may be considered to discuss error observability. For low-cost systems it is sufficient to evaluate the propagation and correlation of errors for flight along a short trajectory consisting of unaccelerated segment followed by a 90° banked turn.

At the end of the first flight segment $t_1 = t_0 + \Delta t$, with $\hat{\mathbf{R}}_{nb} = \mathbf{I}$ and $\hat{\mathbf{R}}_{nb} \tilde{\mathbf{f}}_b = -g\mathbf{e}_3$

$$\boldsymbol{\phi}(t_1) \approx \boldsymbol{\phi}(t_0) + \Delta t \delta \boldsymbol{\omega}_{ibIMU}$$

$$\delta \mathbf{v}_n(t_1) \approx \delta \mathbf{v}_n(t_0) + \Delta t \delta \mathbf{f}_{bIMU} + g\mathbf{e}_3 \times \left(\Delta t \boldsymbol{\phi}(t_0) + \frac{1}{2} \Delta t^2 \delta \boldsymbol{\omega}_{ibIMU} \right)$$

$$\delta \mathbf{x}_n(t_1) \approx \delta \mathbf{x}_n(t_0) + \Delta t \delta \mathbf{v}_n(t_0) + \frac{1}{2} \Delta t^2 \delta \mathbf{f}_{bIMU} + g \mathbf{e}_3 \times \left(\frac{1}{2} \Delta t^2 \boldsymbol{\phi}(t_0) + \frac{1}{6} \Delta t^3 \delta \boldsymbol{\omega}_{ibIMU} \right)$$

At the end of the first segment, with zero initial covariance of errors

$$\begin{aligned} Var[\delta \mathbf{x}_n(t_1)] &= Var[\delta \mathbf{x}_n(t_0)] + \Delta t^2 Var[\mathbf{v}_n(t_0)] + \frac{1}{4} \Delta t^4 Var[\delta \mathbf{f}_{bIMU}] \\ &\quad + skew(g \mathbf{e}_3) \left(\frac{1}{4} \Delta t^4 Var[\boldsymbol{\phi}(t_0)] + \frac{1}{36} \Delta t^6 Var[\delta \boldsymbol{\omega}_{ibIMU}] \right) skew(g \mathbf{e}_3)^T \end{aligned}$$

$$\begin{aligned} Var[\delta \mathbf{v}_n(t_1)] &= Var[\delta \mathbf{v}_n(t_0)] + \Delta t^2 Var[\delta \mathbf{f}_{bIMU}] \\ &\quad + skew(g \mathbf{e}_3) \left(\Delta t^2 Var[\boldsymbol{\phi}(t_0)] + \frac{1}{4} \Delta t^4 Var[\delta \boldsymbol{\omega}_{ibIMU}] \right) skew(g \mathbf{e}_3)^T \end{aligned}$$

$$Var[\boldsymbol{\phi}(t_1)] = Var[\boldsymbol{\phi}(t_0)] + \Delta t^2 Var[\delta \boldsymbol{\omega}_{ibIMU}]$$

And the correlation of errors

$$\begin{aligned} Cov[\delta \mathbf{x}_n(t_1), \delta \mathbf{v}_n(t_1)] &= \Delta t Var[\mathbf{v}_n(t_0)] + \frac{1}{2} \Delta t^3 Var[\delta \mathbf{f}_{bIMU}] \\ &\quad + skew(g \mathbf{e}_3) \left(\frac{1}{2} \Delta t^3 Var[\boldsymbol{\phi}(t_0)] + \frac{1}{12} \Delta t^5 Var[\delta \boldsymbol{\omega}_{ibIMU}] \right) skew(g \mathbf{e}_3)^T \end{aligned}$$

$$Cov[\delta \mathbf{v}_n(t_1), \boldsymbol{\phi}(t_1)] = skew(g \mathbf{e}_3) \left(\Delta t Var[\boldsymbol{\phi}(t_0)] + \frac{1}{2} \Delta t^3 Var[\delta \boldsymbol{\omega}_{ibIMU}] \right)$$

With

$$skew(g \mathbf{e}_3) = \begin{bmatrix} 0 & -g & 0 \\ g & 0 & 0 \\ 0 & 0 & 0 \end{bmatrix}$$

It can be seen that only horizontal velocity errors become correlated with horizontal orientation errors and gyro measurement errors in unaccelerated flight. Because $Var[\boldsymbol{\phi}(t_0)]$ and $Var[\delta \boldsymbol{\omega}_{ibIMU}]$ are diagonal matrices, along-track velocity error is only correlated with across-track orientation error and vice versa. The correlation coefficient can be computed for zero initial motion model state covariance matrices

$$\rho_{\delta \mathbf{v}_n \boldsymbol{\phi}} = \begin{bmatrix} 0 & -\frac{1}{\sqrt{\frac{Var[\delta f_{xIMU}]}{\frac{1}{4} \Delta t^2 g^2 Var[\delta \omega_{yIMU}] + 1}} + 1} & 0 \\ \frac{1}{\sqrt{\frac{Var[\delta f_{yIMU}]}{\frac{1}{4} \Delta t^2 g^2 Var[\delta \omega_{xIMU}] + 1}}} & 0 & 0 \\ 0 & 0 & 0 \end{bmatrix}$$

As expected, the higher integration order of gyro input error dominates and causes full correlation of horizontal velocity and orientation errors in the medium term. This also applies to the correlation of horizontal position and orientation errors in unaccelerated flight. By inspection, the correlation coefficients of equal directions of position and velocity error tend

to one quickly as initial state covariance becomes negligible compared to integrated input error.

For the second flight segment $t \in [t_1, t_2]$, choosing $\dot{\chi} > 0$ with no loss of generality

$$\hat{\mathbf{R}}_{nb} = \begin{bmatrix} \cos(\dot{\chi}t) & -\sin(\dot{\chi}t) & 0 \\ \sin(\dot{\chi}t) & \cos(\dot{\chi}t) & 0 \\ 0 & 0 & 1 \end{bmatrix} \begin{bmatrix} 1 & 0 & 0 \\ 0 & \cos\left(\frac{\pi}{2}\right) & -\sin\left(\frac{\pi}{2}\right) \\ 0 & \sin\left(\frac{\pi}{2}\right) & \cos\left(\frac{\pi}{2}\right) \end{bmatrix} = \begin{bmatrix} \cos(\dot{\chi}t) & 0 & \sin(\dot{\chi}t) \\ \sin(\dot{\chi}t) & 0 & -\cos(\dot{\chi}t) \\ 0 & 1 & 0 \end{bmatrix}$$

and

$$\hat{\mathbf{R}}_{nb}\tilde{\mathbf{f}}_b = -g\mathbf{e}_3 + \hat{\mathbf{R}}_{nb} \begin{bmatrix} 0 \\ 0 \\ -V\dot{\chi} \end{bmatrix} = -g\mathbf{e}_3 + V\dot{\chi}(\cos(\dot{\chi}\Delta t)\mathbf{e}_2 - \sin(\dot{\chi}\Delta t)\mathbf{e}_1)$$

For simplicity, analytical evaluation will be restricted to errors in orientation and velocity. Because the coefficients of the position error differential equation are constant, observability is not affected by motion trajectory dynamics.

Again accounting for direct error propagation only in the short time interval $[t_1, t_2]$

$$\begin{aligned} \boldsymbol{\phi}(t_2) &\approx \boldsymbol{\phi}(t_1) + \int_{t_1}^{t_2} \hat{\mathbf{R}}_{nb} dt \delta\boldsymbol{\omega}_{ibIMU} \\ \delta\mathbf{v}_n(t_2) &\approx \delta\mathbf{v}_n(t_1) + \int_{t_1}^{t_2} \hat{\mathbf{R}}_{nb} dt \delta\mathbf{f}_{bIMU} - \int_{t_1}^{t_2} \text{skew}(\tilde{\mathbf{f}}_n) \left(\boldsymbol{\phi}(t_1) + \int_{t_1}^t \hat{\mathbf{R}}_{nb} dt \delta\boldsymbol{\omega}_{ibIMU} \right) dt \end{aligned}$$

The covariance becomes

$$\begin{aligned} \text{Cov}[\delta\mathbf{v}_n(t_2), \boldsymbol{\phi}(t_2)] &= \text{Cov}[\delta\mathbf{v}_n(t_1), \boldsymbol{\phi}(t_1)] + \text{Cov}[\delta\mathbf{v}_n(t_1), \delta\boldsymbol{\omega}_{ibIMU}] \int_{t_1}^{t_2} \hat{\mathbf{R}}_{nb}^T dt \\ &\quad - \int_{t_1}^{t_2} \text{skew}(\tilde{\mathbf{f}}_n) dt \text{Var}[\boldsymbol{\phi}(t_1)] - \int_{t_1}^{t_2} \text{skew}(\tilde{\mathbf{f}}_n) dt \text{Cov}[\boldsymbol{\phi}(t_1), \delta\boldsymbol{\omega}_{ibIMU}] \int_{t_1}^{t_2} \hat{\mathbf{R}}_{nb}^T dt \\ &\quad - \int_{t_1}^{t_2} \text{skew}(\tilde{\mathbf{f}}_n) \int_{t_1}^t \hat{\mathbf{R}}_{nb} dt dt \text{Cov}[\delta\boldsymbol{\omega}_{ibIMU}, \boldsymbol{\phi}(t_1)] \\ &\quad - \int_{t_1}^{t_2} \text{skew}(\tilde{\mathbf{f}}_n) \int_{t_1}^t \hat{\mathbf{R}}_{nb} dt dt \text{Var}[\delta\boldsymbol{\omega}_{ibIMU}] \int_{t_1}^{t_2} \hat{\mathbf{R}}_{nb}^T dt \end{aligned}$$

Neglecting correlation of motion model errors at t_1 and input error in $[t_1, t_2]$

$$\begin{aligned} \text{Cov}[\delta\mathbf{v}_n(t_2), \boldsymbol{\phi}(t_2)] &= \text{Cov}[\delta\mathbf{v}_n(t_1), \boldsymbol{\phi}(t_1)] - \int_{t_1}^{t_2} \text{skew}(\tilde{\mathbf{f}}_n) dt \text{Var}[\boldsymbol{\phi}(t_1)] \\ &\quad - \int_{t_1}^{t_2} \text{skew}(\tilde{\mathbf{f}}_n) \int_{t_1}^t \hat{\mathbf{R}}_{nb} dt dt \text{Var}[\delta\boldsymbol{\omega}_{ibIMU}] \int_{t_1}^{t_2} \hat{\mathbf{R}}_{nb}^T dt \end{aligned} \tag{2-46}$$

Flying a quarter cycle $\dot{\chi}\Delta t = \frac{\pi}{2}$, the matrices in above equation are

$$\int_{t_1}^{t_2} \text{skew}(\tilde{\mathbf{f}}_n) dt = \begin{bmatrix} 0 & \Delta tg & V \\ -\Delta tg & 0 & V \\ -V & -V & 0 \end{bmatrix}$$

$$\int_{t_1}^{t_2} skew(\tilde{\mathbf{f}}_n) \int_{t_1}^t \hat{\mathbf{R}}_{nb} dt dt = \begin{bmatrix} \left(\frac{\Delta t}{\pi}\right)^2 \cdot 4g \left(\frac{\pi}{2} - 1\right) & \frac{\Delta t}{\pi} \cdot 2V \left(\frac{\pi}{2} - 1\right) & -\left(\frac{\Delta t}{\pi}\right)^2 \cdot 4g \\ -\left(\frac{\Delta t}{\pi}\right)^2 \cdot 4g & \frac{\Delta t}{\pi} \cdot 2V & -\left(\frac{\Delta t}{\pi}\right)^2 \cdot 4g \left(\frac{\pi}{2} - 1\right) \\ -\frac{\Delta t}{\pi} \cdot 2V & 0 & \frac{\Delta t}{\pi} \cdot 2V \left(\frac{\pi}{2} - 1\right) \end{bmatrix}$$

$$\int_{t_1}^{t_2} \hat{\mathbf{R}}_{nb}^T dt = \frac{\Delta t}{\pi} \begin{bmatrix} 2 & 2 & 0 \\ 0 & 0 & \pi \\ 2 & -2 & 0 \end{bmatrix}$$

Both the second and last term in equation (2-46) introduce covariance of vertical velocity error and horizontal orientation errors and vice versa, assuming diagonal matrices $Var[\boldsymbol{\phi}(t_1)]$ and $Var[\delta\boldsymbol{\omega}_{ib_{IMU}}]$. This corresponds to an extension of observability due to horizontal accelerations, and vanishes for $V = 0$ in above analysis.

2.3.2.2 Barometric altitude

Ways to integrate a barometric altitude measurement with the vertical channel computation of inertial navigation have been mentioned earlier in the first section of this chapter. Notable references are [62, 63].

Neglecting the details of computing barometric altitude from absolute air pressure measurements and complex barometer error behavior (c.f. [72, 73] for details on this topic), the observation equation is

$$\tilde{y}_x = \tilde{h} - \hat{h} = \delta h - \delta h_{baro} + v_{baro}$$

Height error δh and a state-independent barometer error δh_{baro} are observable in combination.

As has been discussed above, vertical velocity and vertical position errors are always strongly correlated. In addition, in the presence of horizontal accelerations, vertical translational error becomes correlated with horizontal orientation errors. Therefore, a barometric altitude measurement provides (slight) observability of horizontal errors in dynamic flight.

2.3.2.3 Airspeed

The possibility to further aid INS by air data measurements is widely recognized. Which errors can be estimated depends on whether aerodynamic angle of attack and aerodynamic angle of sideslip sensors are available. In this work, it is generally assumed that aerodynamic angle of attack or aerodynamic angle of sideslip is not measured, as such sensors are rarely installed on small general aviation airplanes. Instead, the aerodynamic model can be used to estimate the direction of aerodynamic velocity, as will be studied later in this work (c.f. [74, 75]).

The most general way to implement true airspeed aiding is a nonlinear scalar function and is linearized to yield the following observation equation

$$\tilde{y}_x = \tilde{V}_A - \|\hat{\mathbf{v}}_n - \hat{\mathbf{v}}_{Wn}\|_2 \doteq \frac{1}{V_A} \mathbf{v}_{An} \cdot (\delta \mathbf{v}_n - \delta \mathbf{v}_{Wn}) + v_{pres}$$

Consequently, errors of kinematic and wind velocity vector are observable in combination and in direction of aerodynamic velocity vector only. For unaccelerated flight, this direction is constant. In this case, the translational errors in orthogonal horizontal direction are unobservable. Therefore, the third order propagation of input errors in this direction will quickly lead to position error exceeding any reasonable bound for navigation.

Because above observation is in fact implemented using computed aerodynamic velocity vector $\hat{\mathbf{v}}_{An}$, errors of kinematic and wind velocity vector will be estimated in direction of $\hat{\mathbf{v}}_{An}$. For sustained flight with constant direction of aerodynamic velocity in NED frame, unobserved kinematic velocity errors $\delta \mathbf{v}_n|_{\perp v_A}$ will grow large. Only due to the approximation $\mathbf{v}_{An} \approx \hat{\mathbf{v}}_{An}$ necessary to implement the observation above, these errors will cause inconsistent observability, an effect that could be described as artificial aiding. Of course, this will only happen when errors $\delta \mathbf{v}_n|_{\perp v_A}$ have become large compared to V_A already. Thus, performance of airspeed aided INS still depends on inertial sensor quality for longer phases of flight with constant direction, and systems with low-cost IMU will perform badly.

A possible way to mitigate this is to assume the direction of true airspeed measurement is known, e.g. aligned with body-fixed x-axis (i.e. assuming $\alpha = \beta = 0$ and therefore $\mathbf{R}_{ab} = \mathbf{I}$):

$$\tilde{y}_x = \begin{bmatrix} \tilde{V}_A \\ 0 \\ 0 \end{bmatrix} - (\hat{\mathbf{v}}_b - \hat{\mathbf{v}}_{Wb}) \doteq \mathbf{R}_{nb}^T (\delta \mathbf{v}_n - \delta \mathbf{v}_{Wn}) + \mathbf{v} \quad (2-47)$$

Because this is an artificial vector observation with significant approximation error in direction, the orientation error term has been neglected in the right hand side linearization. Otherwise, orientation error would be directly observable with an airspeed measurement, which is not recommended. Direction approximation error and orientation error can be considered as correlated measurement error in the covariance update computations

$$\mathbf{v} = \begin{bmatrix} v_{pres} \\ 0 \\ 0 \end{bmatrix} - \begin{bmatrix} 0 \\ \delta\alpha \\ -\delta\beta \end{bmatrix} \times \begin{bmatrix} \tilde{V}_A \\ 0 \\ 0 \end{bmatrix} - \hat{\mathbf{R}}_{nb}^T (\boldsymbol{\phi} \times \hat{\mathbf{v}}_{An})$$

Note that although the direction of differential pressure probe is known, this device is designed to measure pressure difference in stagnation point and (largely) unperturbed flow. Although it will not do so perfectly, and the measurement will be altered by larger misalignment with the airflow, it truly is a scalar measurement, not a vector measurement. Therefore, the implementation of TAS-aiding using measurement equation (2-47) inconsistently assumes zero aerodynamic angle of attack and aerodynamic angle of sideslip.

2.3.2.4 3-D Magnetometer

If no other means to accurately estimate orientation are available, the magnetic field vector measurement $\tilde{\mathbf{B}}_b$ provided by a 3-D magnetometer is a valuable source of information. Provided the engineering challenges of shielding or removing magnetic disturbances from onboard sources (e.g. electrical actuators) and calibrating soft and hard iron effects in the

measurement have been mastered, it corresponds to the local environmental magnetic field at the position of the aircraft. With increasing altitude and thus distance from man-made or otherwise irregular contributions to environmental magnetic field, the measurement mostly represents the earth magnetic field, for which accurate models are available. Defining the observation equation

$$\tilde{\mathbf{y}}_x := \tilde{\mathbf{B}}_b - \hat{\mathbf{R}}_{nb}^T \hat{\mathbf{B}}_n$$

The corresponding linearized form is

$$\tilde{\mathbf{y}}_x \doteq -\hat{\mathbf{R}}_{nb}^T (\boldsymbol{\phi} \times \hat{\mathbf{B}}_n) + \hat{\mathbf{R}}_{nb}^T \delta \mathbf{B}_n + \mathbf{v}_{mag}$$

In this work, the error of modeled local environmental magnetic field vector $\delta \mathbf{B}_n$, which is correlated in time, space and with position error, will not be given special attention. Instead, it is partly eliminated by constraining the observation to errors in orientation

$$\tilde{\mathbf{y}}_x := \tilde{\mathbf{B}}_b - \hat{\mathbf{R}}_{nb}^T \hat{\mathbf{B}}_n \left(1 + \frac{(\hat{\mathbf{R}}_{nb}^T \hat{\mathbf{B}}_n) \cdot (\tilde{\mathbf{B}}_b - \hat{\mathbf{R}}_{nb}^T \hat{\mathbf{B}}_n)}{\|\hat{\mathbf{B}}_n\|_2} \right)$$

With the linearization

$$\tilde{\mathbf{y}}_x \doteq -\hat{\mathbf{R}}_{nb}^T (\boldsymbol{\phi} \times \hat{\mathbf{B}}_n) + \hat{\mathbf{R}}_{nb}^T \delta \mathbf{B}_n|_{\perp \hat{\mathbf{B}}_n} + \mathbf{v}_{mag}$$

While the parallel part of model error does not affect orientation error estimation the remaining orthogonal part $\hat{\mathbf{R}}_{nb}^T \delta \mathbf{B}_n|_{\perp \hat{\mathbf{B}}_n}$ must at least approximately be accounted for by increasing measurement noise \mathbf{v}_{mag} .

Note that although this vector observation allows to estimate east orientation error, which always is perpendicular to earth magnetic field vector, this is not recommended. Modeling error of dip angle (c.f. [76]) is strongly correlated in space and thus in time travelling along a specific trajectory. Due to its combined observation with east orientation error, this model error must either be modeled and estimated, or this part of observation must be removed altogether.

The environmental magnetic field vector approaches 90° dip angle for high northern and southern latitudes. This causes the observability of vertical orientation error due to the term $-\hat{\mathbf{R}}_{nb}^T (\boldsymbol{\phi} \times \hat{\mathbf{B}}_n)$ to vanish. Consequently, heading information from 3-D magnetometer aiding becomes inaccurate for high latitudes and unavailable in proximity of the poles.

2.3.3 Aerodynamic motion model

The primary objective of aiding the aerodynamic motion model is to prevent lateral divergence due to spiral error mode. This is a prerequisite for achieving first order position propagation accuracy. In the initial phase of spiral error mode, there is mostly a contribution in roll, as has been demonstrated with the exemplary linear analysis of decoupled lateral errors in the previous section. Because with increasing roll angle the dynamic system of errors of the aerodynamic model changes significantly thus complicating an analytical approach, a Monte Carlo simulation study is preferred to assess observability of spiral mode error using various aiding measurements. The results of this study are discussed in the following and are the basis for further decisions on method design.

2.3.3.1 Simulation study

In the following, aiding of the aerodynamic motion model with accurate (reference) measurements is studied in simulation in order to determine the most beneficial aiding information for use with the available airplane model.

It is assumed that no external information on dynamic atmosphere is available. In this simulation, wind velocity and model coefficient errors are implemented as consider states in the extended Kalman filter framework, c.f. appendix A.8. Using consider states, only the respective uncertainty is accounted for in computing the filter covariance, but the actual values are not estimated, and e.g. constant $\hat{\mathbf{v}}_{wn} = \mathbf{0}$ and $\hat{\boldsymbol{\omega}}_{wb} = \mathbf{0}$ are used for wind velocity and angular rates. This consider state approach for wind and model coefficients is chosen because on-board sensor quality and the accuracy of corresponding statistical models are insufficient to estimate wind or improve a high-quality aerodynamic model by estimating model coefficient errors.

Besides reference measurements of vehicle state errors such as errors in height δh , kinematic velocity magnitude δV_K , orientation $\delta \phi_N$, $\delta \phi_E$, $\delta \phi_D$ and inertial angular rates $\delta \boldsymbol{\omega}_{ib}$, a measurement of error of specific force in navigation reference point R , $\delta \mathbf{f}_b^R$, is studied. The results of aided aerodynamic motion propagation in presence of realistic measurement and model errors and atmosphere dynamics are presented in Table 3. All Kalman filter updates are computed at a rate of 1Hz and the uncertainties and errors of the aiding measurements correspond to the accuracy of a tactical grade INS/GNSS navigation system. For more information about the simulation framework used for evaluation of preliminary methods, refer to section 4.1.1.

Aiding of attitude, heading or inertial rates errors is found to effectively mitigate the lateral divergent error mode of aerodynamic motion propagation. The Monte Carlo simulation study indicates that with any one of these aiding measurements, aerodynamic motion can be the basis of a position propagation method. Because the roll angle error is a major component of the spiral error mode, a measurement of horizontal orientation errors and thus errors of roll and pitch very effectively prevents lateral divergence of the airplane aerodynamic model. Heading error offers good observability of spiral error mode because it is strongly correlated with roll error in horizontal flight where the deflected lift vector causes lateral acceleration error. In addition, similar to aiding error in course over ground, heading

error aiding effectively improves the position propagation performance of the aerodynamic model by reducing first order error.

Aiding information	Position propagation performance in 1h
δh	Lateral divergence
δV_K and δh	Lateral divergence (see Figure 9)
$\delta\phi_N, \delta\phi_E$ and δh	$\sim 10\text{NM}/h$ (CEP) in first 600s, 14NM (CEP) max
$\delta\phi_N, \delta\phi_E, \delta\phi_D$ and δh	$\sim 5.4\text{NM}/h$ (CEP) in 1h (see Figure 10)
$\delta\phi_D$ and δh	$\sim 5.5\text{NM}/h$ (CEP) in 1h
$\delta\omega_{ib}$ and δh	$\sim 9\text{NM}/h$ (CEP) in first 600s, 26NM (CEP) max
δf_b^R and δh	Lateral divergence

Table 3: Airplane aerodynamic motion model aided by reference measurement

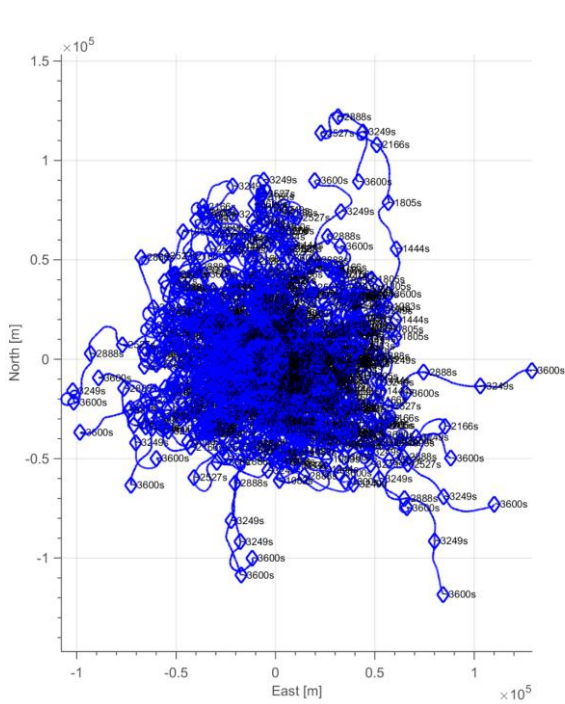


Figure 9: Laterally divergent aerodynamic position propagation with speed over ground aiding (100 runs)

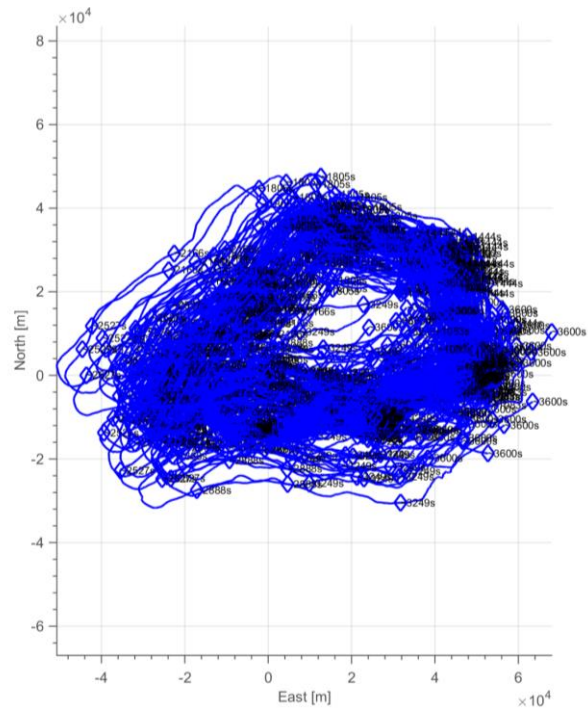


Figure 10: Aerodynamic position propagation with orientation error aiding (100 runs)

The simulation study shows that insufficient aiding such as measurements of height error, speed over ground error or specific force error will not prevent arbitrary lateral motion. See Figure 9 for the Monte Carlo results of aerodynamic motion propagation with aiding of speed over ground error only.

The quantitative results of the Monte Carlo simulation in Table 3 indicate that aiding of the vertical orientation error ϕ_D of aerodynamic motion is essential for accurate position propagation. With this aiding information, good results were achieved with a position error that very closely matches wind drift for the given set of flight trajectories (c.f. 4.1.1).

2.3.3.2 Restrictions of aiding the aerodynamic motion model

In addition to first results for positioning performance, the simulation study revealed a significant restriction of aiding the aerodynamic motion model. State estimation with the aerodynamic motion model is found to be not reliably robust in realistic dynamic atmosphere conditions if kinematic reference information is used. Navigation filter failure has been observed when aiding the aerodynamic motion model with a measurement of kinematic velocity vector error and keeping the wind state estimates constant.

Generally, GNSS-denied state estimation with the aerodynamic motion model and low cost on-board sensors cannot estimate dynamic wind well. Due to insufficient observability without GNSS aiding and dedicated measurement equipment, a suboptimal consider-state approach is applied in this simulation study, and wind state estimates are fixed to an uncertain constant value. Alternatively, estimation of long-term wind vector might be attempted, assuming a long correlation in time to account for the major contribution to position drift.

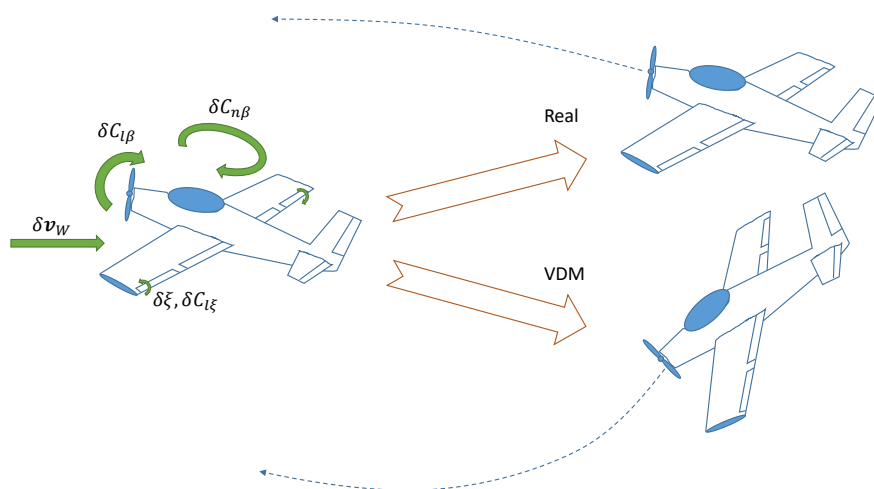


Figure 11: Diverging computed aerodynamic flight in presence of dynamic wind error and pilot control

With such a suboptimal approach for wind estimation, the correction of observed errors in kinematic velocity results in an equivalent change in aerodynamic velocity vector (see the discussion of equation (2-11) in 2.1.3.2). In body-fixed frame coordinates, the aerodynamic velocity vector corresponds to airspeed, aerodynamic angle of attack and aerodynamic angle of sideslip that have significant effect on the aerodynamic forces and moments (see 2.1.3.2). Consequently, a correction of these aerodynamic states has a strong effect especially on rotational aerodynamic motion, which can lead to divergence of computed and true airplane motion and significant linearization error in the extended Kalman filter.

Under realistic atmosphere conditions, dynamic wind estimation error is inevitable. In turbulent atmosphere, the pilot or autopilot will counteract the disturbances of the true airplane flight with dynamic control inputs, which are measured and used as input to compute aerodynamic motion. This, in combination with large dynamic errors in the aerodynamic motion model wind input, can result in fast divergence of true and computed aerodynamic motion. Because the pilot inputs are intended to cancel the disturbances of aerodynamic flight due to true dynamic atmosphere, they adversely affect computed flight, as illustrated in Figure 11. The estimated wind input for the aerodynamic motion model will at best account for the low-frequency content of dynamic wind.

If the resulting errors in the computed kinematic velocity vector are corrected suboptimally, e.g. assuming constant wind velocity as discussed above, the dynamic response of the aerodynamic motion model to the inconsistent correction of aerodynamic state can further aggravate the divergence. This will eventually result in a failure of the navigation filter when an extended Kalman filter is applied for state estimation. This is an important finding for aiding of the aerodynamic motion model that must be considered in the development of integration architectures in chapter 3.

Optimal, i.e. fully consistent, corrections of the aerodynamic model using kinematic reference information require simultaneous estimation of kinematic motion states, model coefficients, dynamic wind velocity vector and even wind rates. Flight dynamics trim errors, e.g. a constant error in airspeed, must be calibrated by an equilibrium correction of model coefficients and motion states. In addition, dynamic estimation of wind is required for consistent estimation of both kinematic and aerodynamic motion in dynamic atmosphere conditions. Unfortunately, on-line calibration of the high-quality model coefficients is not an option for the given application where on-board sensor quality and observability in GNSS-denied flight are insufficient. For wind estimation, a long-term average would be beneficial for reducing position drift in GNSS-denied navigation but suboptimal with respect to dynamic wind estimation. Nevertheless, a short-term wind vector estimation might be attempted to increase the robustness of state estimation with an aerodynamic motion model in turbulent atmosphere. This will be discussed further in chapter 3.

2.3.4 Method comparison

Both the inertial and the aerodynamic motion model need specific additional aiding information to remedy disadvantageous error propagation characteristics identified in the previous section. In case of the inertial propagation model, the problem consists of polynomial propagation of inertial measurement error to all directions of position error in 2nd order and perpendicular to specific force in 3rd order. The measurements available for aiding in GNSS-denied flight were shown to not reliably offer full observability of error in conventional flight conditions. While maneuvering flight enhances observability with a barometric altitude measurement to include horizontal position errors, and measurement of airspeed offers observability in direction of turning aerodynamic velocity vector, unaccelerated flight with negligible body rotation still suffers from unobserved polynomial error propagation.

For the aerodynamic propagation model, the improvement by integrating specific on-board measurements is significant. It has been shown that aiding of angular rates errors, attitude errors or heading error all prevent lateral divergence. This allows exploiting the first order position error characteristic of the integrated aerodynamic motion model.

Nevertheless, state estimation with the aerodynamic motion model proves to be difficult. Several differences of the inertial and aerodynamic motion models influence the characteristics of aided INS and aided aerodynamic motion model (aided VDM).

	Aided INS	Aided VDM	
Model dynamics	“Integration model”	Strong dynamic response	<i>Model perturbations (non-equilibrium changes) such as input errors or suboptimal corrections stimulate dynamic response</i>
Model errors	IMU calibration error	Coefficient errors Wind error	<i>Coefficient errors affect trim, stability and control</i> <i>Wind error introduces a mismatch of kinematic and aerodynamic motion</i>
Failure sources	IMU	Turbulent atmosphere	<i>Intermittent turbulence introduces dynamic wind error in combination with strong pilot control</i>

Figure 12: Comparison of aided INS and aided aerodynamic motion model (aided VDM)

The fundamental restrictions of aiding the aerodynamic motion model compared to aided INS are listed in Figure 12. First, changes of individual motion states can significantly affect computed aerodynamic forces and moments and thus stimulate a dynamic response of the motion model. This happens for example in an unbalanced correction of kinematic motion states and wind states, resulting in a change of the aerodynamic states, such as airspeed,

aerodynamic angle of attack and aerodynamic angle of sideslip. When estimated errors in the kinematic states are corrected, this dynamic response is undesired because it introduces additional (dynamic) error. For aided INS on the other hand, the dynamic response of the motion model to kinematic state error corrections is negligible given the very low frequency of Schuler and other error dynamics.

The airplanes and corresponding aerodynamic motion models discussed in this work exhibit stable “trim” flight conditions. Errors in the model coefficients result in errors in the aerodynamic states of these flight conditions. A correction of these errors will be reverted due to the stability – in addition to a possibly significant transient response as noted above. For aerodynamic course and bank angles, this effect is small. However, aerodynamic degrees of freedom with strong dynamic or static stability – such as airspeed, aerodynamic angles of attack and sideslip, aerodynamic climb angle – can only be corrected in combination with a correction of model coefficients preserving the equilibrium of forces and moments. If such a correction of model coefficients is not possible because a high-quality aerodynamic motion model is used that cannot reliably be calibrated with on-board means, the aerodynamic states should remain unchanged as well. An exception is possible for the states that are subject to weak (or no) stability. This will be addressed in chapter 3.

Aerodynamic velocity and aerodynamic angular rates, which strongly affect the aerodynamic forces and moments, differ from corresponding kinematic states (kinematic velocity and inertial angular rates) due to wind velocity and wind rates, see 2.1.3.2. Given measurements of kinematic motion, these aerodynamic motion states can consequently only be observed in combination with dynamic wind estimates. Large wind estimation error can result in inconsistent estimation of aerodynamic states from measurements of kinematic motion.

Finally, for the long flight durations and distances travelled that are typical for the addressed application, atmospheric turbulence is to be expected. As has been discussed in the previous subsection 2.3.3.2, this environmental condition is likely to cause divergence of computed and true airplane motion. Unlike for aided INS, where input errors can be overbounded reliably, a sudden and possibly extreme increase in aerodynamic motion model state error must be handled. Given the limitations of state estimation with the aerodynamic motion model discussed above, this constitutes a significant problem to be discussed in the next chapter.

Thanks to much weaker error state dynamics and reliable online calibration of IMU measurement biases, the inertial motion model does not suffer from such restrictions for aiding with filter updates. In addition to the accurate computation of attitude that is essential for heading error estimation with a 3-D magnetometer measurement, the inertial motion model represents the optimal platform for integration of auxiliary sensors such as barometer and magnetometer.

2.4 CONCLUSION

Judging by the required inputs and modeling assumptions, inertial navigation is the most robust of the three motion models presented in this chapter. It is an exact model that can be applied to any platform and is valid for any type of motion. In addition to gravity vector, only IMU measurements are used as inputs that are only affected by environmental disturbances at the location of installation, such as vibrations and temperature change. Furthermore, inertial navigation offers excellent observability of errors in a combination of straight and turning flight with 3-D position or velocity measurements. This makes it the perfect choice for integration with GNSS aiding, if available.

For GNSS-denied flight navigation, the inertial propagation model suffers from polynomial position error growth that only is observable for a continued succession of large changes in direction of flight. Except for high-quality and high-cost systems, these errors quickly exceed any acceptable limit. Here, the simple heading and airspeed dead reckoning method proved to offer a good alternative. Its position error is only due to integrated velocity measurement error and always grows first order in time. It is a simplified model of motion but temporary modeling and input errors, for example in turns or presence of magnetic disturbance, will only affect position accuracy scaled by their duration of occurrence. This exemplifies the advantageous characteristics that come with first order error propagation and are well suited for low-cost applications with simplex input measurements.

For conventional fixed-wing aircraft, the aerodynamic position propagation method, if integrated with some aiding measurement on lateral motion such as vehicle heading, was found to exhibit first order position error growth as well. If an accurate software model of flight dynamics, e.g. qualified for use in a flight training device, is available, simulated flight offers a precise model for longitudinal motion. Similarly to dead reckoning, wind input error is integrated in time and any information of wind velocity will improve position propagation accuracy. Moreover, the effect of wind and heading errors on position is negligible for short durations of occurrence. Nevertheless, the lack of accurate on-board models for predicting wind velocity and wind angular rates reduces method robustness.

Because the inertial model can provide very accurate information on attitude if aided with the horizontal motion provided by the aerodynamic propagation method, it constitutes the ideal platform for computation of magnetic heading using a 3-D magnetometer measurement. Heading (and attitude) in turn is the essential aiding information needed to make the airplane motion model an accurate first order position propagation method. Consequently, a combination of these two motion models promises a GNSS-denied flight navigation with the benefit of accurate attitude information and first order position error growth.

3 ARCHITECTURES FOR INTEGRATING INERTIAL AND AERODYNAMIC MOTION MODELS

Using both inertial and aerodynamic motion models in parallel is possible even in a low-cost application. Inertial sensors are either already installed on the aircraft (with an interface to the data available) or can be integrated as low-cost, small size and weight and power MEMS-based system. Except for measurement of pilot controls, the aerodynamic model requires additional real-time software only. Although the identification of a high-quality aerodynamic model is expensive, it may already be available from flight training simulators. The previous chapter showed that the inertial model is desirable for its high robustness and accurate measurement of angular motion. The aerodynamic model proved to be a first order accurate position propagation method that could outperform classical heading and airspeed dead reckoning. Now, the best way to combine the two motion models for GNSS-denied navigation of airplanes must be found.

Two approaches are discussed in this chapter: State estimation techniques that assume that all errors in modeling underlying processes can be described with satisfying statistical significance, and a new technique for airplanes that is insensitive to imperfections of the statistical models for aerodynamic flight and dynamic atmosphere.

First, assuming strict equivalence of motion described by inertial navigation and vehicle dynamics model (such as the aerodynamic motion model), the fusion of the two motion models is studied. Optimality of state estimation given multiple process models with equivalent states (i.e. related to an identical truth process) is discussed in [11]. Optimal model fusion has first been applied to airplane navigation in [9]. More efficient variants of optimal model fusion have later been proposed and studied in applications to rotorcraft [12, 13, 77, 78], airplanes [14, 79] and underwater vehicles [80]. This variety of vehicles addressed evidences the generic nature of this approach. Because the respective improvement of fused models depends on their relative uncertainty, sensitivity to the accuracy of statistical error models is high for optimal model fusion.

Studying method performance in rough atmosphere with turbulence and strong gusts reveals that state estimation techniques require careful tuning especially of aerodynamic and dynamic atmosphere uncertainty processes. Both robustness and accuracy of the method are affected. Although a specific setting of tuning parameters can be determined in Monte Carlo simulation in order to achieve robustness in rough atmosphere and good accuracy, it is desired to find a desensitized method for higher reliability and independence from simulation fidelity.

The second section of this chapter therefore proposes a new method for airplane aerodynamic model navigation. For this approach, the best combination of low-cost inertial and high-quality airplane aerodynamic models is not determined by fusion of equivalent information with known error statistics as in [11]. Instead, the valuable information content of each of the two motion models is identified in inertial rotational motion and aerodynamic translational motion.

In a robust solution to the given problem of GNSS-denied airplane flight navigation, models should therefore be combined in a complementary integration architecture, leaving their

individual characteristics intact. From this understanding results a simpler method of model combination with the benefit of independence from unreliable or unknown information on system statistics that is needed for determining relative information content in state estimation techniques.

The complementary integration architecture for inertial and aerodynamic models developed in this chapter presents a solution to the model combination problem if the uncertainty of aerodynamic flight cannot be modeled reliably. State estimation techniques are not applicable to model combination with unknown statistics. The new approach exploits the complementary characteristics of the two models studied in chapter 2 for a best possible solution without need for unreliable or unavailable covariance models of dynamic atmosphere processes.

3.1 OPTIMAL STATE ESTIMATION (CLASSICAL DATA FUSION)

Previous work on navigation using an aerodynamic motion model proposed the fusion of aerodynamic propagation and inertial navigation based on the notion that errors in motion states of the two models are statistically dissimilar and will be reduced by combination [9]. Although development of the proposed method will take a different way later in this chapter, two basic ways to fuse aerodynamic and inertial motion using an optimal filter will be assessed first.

If one compares the aerodynamic motion model (2-8) and (2-9) with strapdown inertial navigation (2-3), only two parts of it provide new information on vehicle motion:

- (1) Equation (2-9) replaces measured specific force as input to the strapdown equation with a computed quantity
- (2) Assuming a rigid vehicle body, the Euler equation of rotational motion and the models for external moments provide a differential equation for the otherwise measured inertial angular rates vector

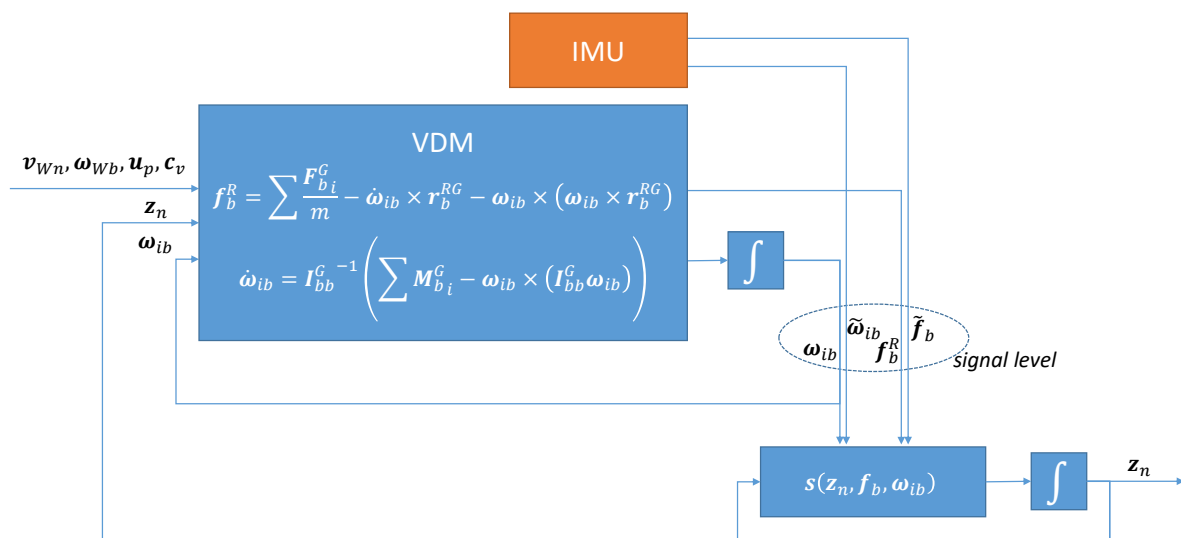


Figure 13: Signal-level model fusion

3.1.1 Signal-level model fusion

In each case above it is possible to compare the computed and measured specific force or inertial angular rates by value in order to determine IMU measurement errors and errors in the inputs and coefficients of the models. In an optimal filter, the computed specific force vector and inertial angular rates vector are fused with IMU measurements on "signal-level" in order to improve accuracy of the inputs for the strapdown equation used to propagate navigation state vector \mathbf{z}_n in time, see Figure 13.

The architecture depicted in Figure 13 can be implemented in two ways: One continuously using the aerodynamic motion model for integration of navigation state vector \mathbf{z}_n (c.f. [77, 81, 82]), and the other using the IMU measurements as inputs to the strapdown algorithm, which gives a conventional inertial motion model (c.f. [13]). In both cases, IMU measurements, vehicle rotational dynamics and the model for specific force are used for estimation of errors in \mathbf{z}_n , angular rates and inertial measurements. This will be described in detail in the following.

For the "signal-level" fusion architecture shown in Figure 13, the redundant signals are related mathematically

$$\begin{aligned}\boldsymbol{\omega}_{ib} &= \tilde{\boldsymbol{\omega}}_{ib} + \delta\boldsymbol{\omega}_{ib_{IMU}} \\ \mathbf{f}_b^R &= \tilde{\mathbf{f}}_b + \delta\mathbf{f}_{b_{IMU}}\end{aligned}$$

That is, the IMU measurements of inertial angular rates and specific force corrected by exact measurement error are stated to be identical to exact values of modeled inertial angular rates and specific force in navigation reference point R . Note that this differs from the definition of IMU measurements and errors, stating that their sum is exactly equal to rotation and acceleration of the real IMU. The assumed equivalence of inertial and aerodynamic model truth motion is the basis of the ideal model fusion techniques discussed in this section.

To integrate the stated relationship of IMU measurements and aerodynamic motion in the framework of an extended Kalman filter, an error state observation can be defined

$$\tilde{\mathbf{y}}_x := \begin{bmatrix} \tilde{\boldsymbol{\omega}}_{ib} - \hat{\boldsymbol{\omega}}_{ib} \\ \tilde{\mathbf{f}}_b - \hat{\mathbf{f}}_b^R \end{bmatrix} = \begin{bmatrix} \delta\boldsymbol{\omega}_{ib} - \delta\boldsymbol{\omega}_{ib_{IMU}} \\ \delta\mathbf{f}_b^R - \delta\mathbf{f}_{b_{IMU}} \end{bmatrix} \quad (3-1)$$

For estimation of IMU measurement errors, a slowly varying part \mathbf{b} and a complementary part \mathbf{n} are distinguished for both gyroscope and accelerometer errors. The intention is to estimate the first, while accounting for fluctuating and noisy disturbances due to the second only:

$$\begin{aligned}\delta\boldsymbol{\omega}_{ib_{IMU}} &= \mathbf{b}_{Gyro} + \mathbf{n}_{Gyro} \\ \delta\mathbf{f}_{b_{IMU}} &= \mathbf{b}_{Acc} + \mathbf{n}_{Acc}\end{aligned}$$

Refer to appendix A.8 and [83] for more information on extended Kalman filter augmentation and implementation accounting for complex input and measurement errors.

The error in modeled specific force vector in equation (3-1) is not a (filter) state and must be linearized with respect to rigid body errors and augmented filter states. Inserting the differential equation for inertial angular rates in the second row of (2-8) into equation (2-9), specific force can be computed as

$$\mathbf{f}_b^R = \sum \frac{\mathbf{F}_{bi}^G(\mathbf{z}_v, \mathbf{v}_{Wn}, \boldsymbol{\omega}_{Wb}, \mathbf{u}_p, \mathbf{c}_v)}{m} - \left(\mathbf{I}_{bb}^G{}^{-1} \left(\sum \mathbf{M}_{bi}^G(\mathbf{z}_v, \mathbf{v}_{Wn}, \boldsymbol{\omega}_{Wb}, \mathbf{u}_p, \mathbf{c}_v, \mathbf{r}_b^{RG}) - \boldsymbol{\omega}_{ib} \times (\mathbf{I}_{bb}^G \boldsymbol{\omega}_{ib}) \right) \right) \times \mathbf{r}_b^{RG} - \boldsymbol{\omega}_{ib} \times (\boldsymbol{\omega}_{ib} \times \mathbf{r}_b^{RG}) \quad (3-2)$$

The function of sum of external moments in center of gravity $\sum \mathbf{M}_{bi}^G$ takes the center of gravity position \mathbf{r}_b^{RG} as additional input parameter.

With navigation error states $\delta \mathbf{z}_n$ defined as in classical inertial navigation perturbation error analysis (see 2.2.2.1) and the vector of errors of moments and products of inertia defined as

$$\delta \mathbf{I}_{bb}^G := [\delta I_{xx}, \delta I_{yy}, \delta I_{zz}, \delta I_{xy}, \delta I_{xz}, \delta I_{yz}]^T$$

the error in modeled specific force vector can be linearized as

$$\delta \mathbf{f}_b^R \doteq \frac{\partial \mathbf{f}_b^R}{\partial \delta \mathbf{z}_n^T} \delta \mathbf{z}_n + \frac{\partial \mathbf{f}_b^R}{\partial \boldsymbol{\omega}_{ib}^T} \delta \boldsymbol{\omega}_{ib} + \frac{\partial \mathbf{f}_b^R}{\partial \mathbf{v}_{Wn}^T} \delta \mathbf{v}_{Wn} + \frac{\partial \mathbf{f}_b^R}{\partial \boldsymbol{\omega}_{Wb}^T} \delta \boldsymbol{\omega}_{Wb} + \frac{\partial \mathbf{f}_b^R}{\partial \mathbf{u}_p^T} \delta \mathbf{u}_p + \frac{\partial \mathbf{f}_b^R}{\partial \mathbf{c}_v^T} \delta \mathbf{c}_v + \frac{\partial \mathbf{f}_b^R}{\partial m} \delta m + \frac{\partial \mathbf{f}_b^R}{\partial \delta \mathbf{I}_{bb}^G{}^T} \delta \mathbf{I}_{bb}^G + \frac{\partial \mathbf{f}_b^R}{\partial \mathbf{r}_b^{RG}{}^T} \delta \mathbf{r}_b^{RG}$$

The individual linearizations of modeled specific force with respect to the various parameters can be found in appendix A.9. Note that the relative acceleration terms in equation (3-2) explicitly depend on inertial angular rates vector $\boldsymbol{\omega}_{ib}$. Navigation state and wind velocity vector on the other hand only appear as input parameters of the functions of external forces and moments (2-15). Referring to the discussion of aerodynamic motion model input parameters in 2.1.3.2, the linearization of modeled specific force vector can be written as

$$\delta \mathbf{f}_b^R \doteq \frac{\partial \mathbf{f}_b^R}{\partial h} \delta h + \frac{\partial \mathbf{f}_b^R}{\partial \mathbf{v}_{Ab}^T} \delta \mathbf{v}_{Ab} + \frac{\partial \mathbf{f}_b^R}{\partial \boldsymbol{\omega}_{ib}^T} \delta \boldsymbol{\omega}_{ib} + \frac{\partial \mathbf{f}_b^R}{\partial \boldsymbol{\omega}_{Wb}^T} \delta \boldsymbol{\omega}_{Wb} + \frac{\partial \mathbf{f}_b^R}{\partial \mathbf{u}_p^T} \delta \mathbf{u}_p + \frac{\partial \mathbf{f}_b^R}{\partial \mathbf{c}_v^T} \delta \mathbf{c}_v + \frac{\partial \mathbf{f}_b^R}{\partial m} \delta m + \frac{\partial \mathbf{f}_b^R}{\partial \delta \mathbf{I}_{bb}^G{}^T} \delta \mathbf{I}_{bb}^G + \frac{\partial \mathbf{f}_b^R}{\partial \mathbf{r}_b^{RG}{}^T} \delta \mathbf{r}_b^{RG} \quad (3-3)$$

The errors in equation (3-3) corresponding to uncertainty of vehicle model coefficients and dynamic atmosphere must be considered for filter tuning, e.g. as an augmented filter state and noise. Depending on the choice for augmenting filter state vector, equation (3-3) can be reordered defining a measurement matrix \mathbf{H} , a process noise feedthrough matrix \mathbf{G}_ω and a vector of artificial measurement noise $\mathbf{v} = [\mathbf{v}_{\omega PM}^T, \mathbf{v}_{f PM}^T]^T$

$$\tilde{\mathbf{y}}_x = \mathbf{H} \mathbf{x} + \mathbf{G}_\omega \boldsymbol{\omega} + \mathbf{v} \quad (3-4)$$

where $\boldsymbol{\omega}$ is the vector of white process noise. Pilot control input or atmospheric noise for example has already influenced the error state in the current propagation step (or similarly IMU noise), and reappears in this equation as measurement noise.

To consistently account for the correlation of process noise and measurement noise, a new optimal gain \mathbf{K} must be derived, seeking to minimize trace of a posteriori covariance (c.f. [69]).

With the a posteriori Kalman filter estimate

$$\mathbf{x}_{k+1}^+ = \mathbf{K}(\tilde{\mathbf{y}}_{x_{k+1}} - \mathbf{H}\mathbf{x}_{k+1}^-) + \mathbf{x}_{k+1}^-$$

and the time discrete filter state model with process noise $\boldsymbol{\omega}_k$ averaged in time interval $[t_k, t_{k+1}]$

$$\mathbf{x}_{k+1} = \boldsymbol{\Phi}_k \mathbf{x}_k + \boldsymbol{\Gamma}_k \boldsymbol{\omega}_k$$

the measurement equation (3-4) can be rewritten and inserted into above filter estimate update equation

$$\tilde{\mathbf{y}}_{x_{k+1}} = \mathbf{H}\boldsymbol{\Phi}_k \mathbf{x}_k + \mathbf{H}\boldsymbol{\Gamma}_k \boldsymbol{\omega}_k + \mathbf{G}_\omega \boldsymbol{\omega}_k + \mathbf{v}_k$$

and

$$\mathbf{x}_{k+1}^+ = \mathbf{K}(\mathbf{H}\boldsymbol{\Phi}_k \mathbf{x}_k + (\mathbf{H}\boldsymbol{\Gamma}_k + \mathbf{G}_\omega)\boldsymbol{\omega}_k + \mathbf{v}_k - \mathbf{H}\boldsymbol{\Phi}_k \mathbf{x}_k^+) + \boldsymbol{\Phi}_k \mathbf{x}_k^+$$

Taking the influence of process noise on both state propagation and measurement into account, the covariance of a posteriori filter estimate \mathbf{x}_{k+1}^+ is

$$\begin{aligned} \mathbf{P}_{k+1}^+ &= E[(\mathbf{x}_{k+1}^+ - \mathbf{x}_{k+1})(\mathbf{x}_{k+1}^+ - \mathbf{x}_{k+1})^T] \\ &= E[(\mathbf{K}(\mathbf{H}\boldsymbol{\Phi}_k \mathbf{x}_k + (\mathbf{H}\boldsymbol{\Gamma}_k + \mathbf{G}_\omega)\boldsymbol{\omega}_k + \mathbf{v}_k - \mathbf{H}\boldsymbol{\Phi}_k \mathbf{x}_k^+) + \boldsymbol{\Phi}_k \mathbf{x}_k^+ - \boldsymbol{\Phi}_k \mathbf{x}_k - \boldsymbol{\Gamma}_k \boldsymbol{\omega}_k)(\dots)^T] \\ &= E[(\mathbf{K}(\mathbf{H}\boldsymbol{\Phi}_k (\mathbf{x}_k^+ - \mathbf{x}_k) - (\mathbf{H}\boldsymbol{\Gamma}_k + \mathbf{G}_\omega)\boldsymbol{\omega}_k + \mathbf{K}\mathbf{v}_k)(\dots)^T] \\ &= (\mathbf{I} - \mathbf{K}\mathbf{H})\mathbf{P}_{k+1}^-(\mathbf{I} - \mathbf{K}\mathbf{H})^T - (\mathbf{I} - \mathbf{K}\mathbf{H})\boldsymbol{\Gamma}_k \mathbf{Q} \mathbf{G}_\omega^T \mathbf{K}^T - \mathbf{K} \mathbf{G}_\omega \mathbf{Q} \boldsymbol{\Gamma}_k^T (\mathbf{I} - \mathbf{K}\mathbf{H})^T \\ &\quad + \mathbf{K}(\mathbf{R} + \mathbf{G}_\omega \mathbf{Q} \mathbf{G}_\omega^T) \mathbf{K}^T \end{aligned}$$

Minimal trace of this a posteriori covariance matrix is chosen as optimality criterion and can be represented by the linear problem

$$\begin{aligned} \frac{\partial \text{tr}(\mathbf{P}_{k+1}^+)}{\partial \mathbf{K}} &= -2(\mathbf{H}\mathbf{P}_{k+1}^-)^T + 2\mathbf{K}(\mathbf{R} + \mathbf{G}_\omega \mathbf{Q} \mathbf{G}_\omega^T + \mathbf{H}\mathbf{P}_{k+1}^- \mathbf{H}^T) - (\mathbf{I} - \mathbf{K}\mathbf{H})\boldsymbol{\Gamma}_k \mathbf{Q} \mathbf{G}_\omega^T \\ &\quad - (\mathbf{G}_\omega \mathbf{Q} \boldsymbol{\Gamma}_k^T (\mathbf{I} - \mathbf{K}\mathbf{H})^T)^T + (\mathbf{H}\boldsymbol{\Gamma}_k \mathbf{Q} \mathbf{G}_\omega^T \mathbf{K}^T)^T + \mathbf{K} \mathbf{G}_\omega \mathbf{Q} \boldsymbol{\Gamma}_k^T \mathbf{H}^T \\ &= -2(\mathbf{H}\mathbf{P}_{k+1}^-)^T + 2\mathbf{K}(\mathbf{R} + \mathbf{G}_\omega \mathbf{Q} \mathbf{G}_\omega^T + \mathbf{H}\mathbf{P}_{k+1}^- \mathbf{H}^T) - 2(\mathbf{G}_\omega \mathbf{Q} \boldsymbol{\Gamma}_k^T)^T + 2\mathbf{K}\mathbf{H}\boldsymbol{\Gamma}_k \mathbf{Q} \mathbf{G}_\omega^T \\ &\quad + 2\mathbf{K} \mathbf{G}_\omega \mathbf{Q} \boldsymbol{\Gamma}_k^T \mathbf{H}^T = \mathbf{0} \end{aligned}$$

From this condition the optimal gain matrix \mathbf{K} can be derived

$$\mathbf{K} = (\mathbf{P}_{k+1}^- \mathbf{H}^T + \boldsymbol{\Gamma}_k \mathbf{Q} \mathbf{G}_\omega^T)(\mathbf{R} + \mathbf{G}_\omega \mathbf{Q} \mathbf{G}_\omega^T + \mathbf{H}\mathbf{P}_{k+1}^- \mathbf{H}^T + \mathbf{H}\boldsymbol{\Gamma}_k \mathbf{Q} \mathbf{G}_\omega^T + \mathbf{G}_\omega \mathbf{Q} \boldsymbol{\Gamma}_k^T \mathbf{H}^T)^{-1} \quad (3-5)$$

For high noise and high update rate this special gain matrix must be used for consistent error estimation. This increases implementation complexity, because it differs from Kalman gain computation for a conventional measurement update. Furthermore, input propagation matrix $\boldsymbol{\Gamma}_k$ must be kept in memory or computed again. When the process noise appearing in measurement equation (3-4) is small, it can be neglected and the conventional Kalman gain matrix can be used instead.

3.1.2 State-level model fusion

In an alternative architecture, the aerodynamic motion model runs in parallel to INS. This provides a fully redundant, highly available “software” solution for navigation state vector \mathbf{z}_n which can be used for combination and comparison on “state-level”:

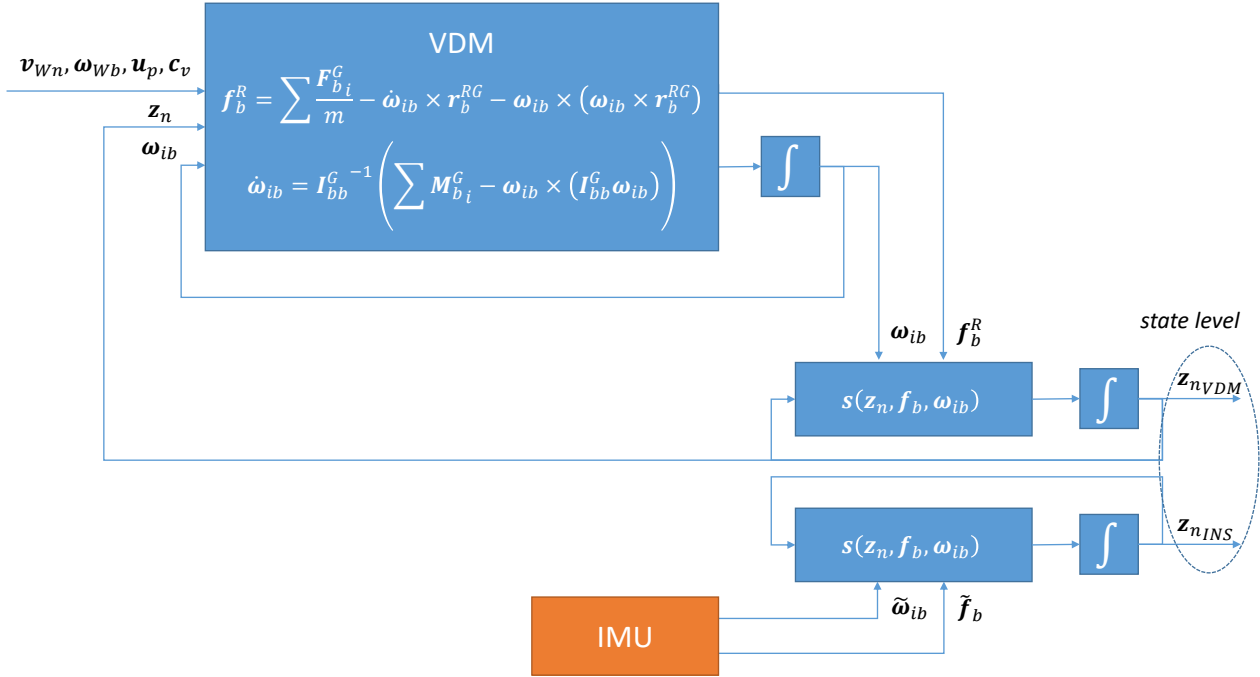


Figure 14: State-level model fusion

This approach to inertial and aerodynamic motion fusion, first proposed in similar form by Koifman [9], uses the following measurements, referred to as pseudo measurements in the following for lack of any real measured quantity (also called virtual or perfect measurements in the literature, c.f. [84]):

$$\tilde{\mathbf{y}}_{\delta v_n} := \hat{\mathbf{v}}_{nVDM} - \hat{\mathbf{v}}_{nINS}$$

In the extended Kalman filter framework, the following observation equation is used

$$\tilde{\mathbf{y}}_{\delta v_n} = \delta \mathbf{v}_{nINS} - \delta \mathbf{v}_{nVDM} + \mathbf{v}_{\delta v_n} \quad (3-6)$$

And similarly for orientation error the nonlinear measurement

$$\tilde{\mathbf{y}}_{\Phi} := \mathbf{f} \left(\hat{\mathbf{R}}_{nbINS} \hat{\mathbf{R}}_{nbVDM}^T \right) \quad (3-7)$$

The direction cosine matrices $\hat{\mathbf{R}}_{nbINS}$ and $\hat{\mathbf{R}}_{nbVDM}$ are computed from the NED-to-body-fixed frame orientation quaternions $\hat{\mathbf{q}}_{nbINS}$ and $\hat{\mathbf{q}}_{nbVDM}$ respectively. The function \mathbf{f} computes the vector of Euler angles corresponding to the direction cosine matrix $\hat{\mathbf{R}}_{nbINS} \hat{\mathbf{R}}_{nbVDM}^T$, c.f. equation (2-21).

Above pseudo measurement can be linearized to yield the corresponding Kalman filter observation equation [14]

$$\tilde{\mathbf{y}}_{\Phi} \doteq -\Phi_{INS} + \Phi_{VDM} + \mathbf{v}_{\Phi} \quad (3-8)$$

In both cases (3-6) and (3-8), virtual measurement noise $\mathbf{v}_{\delta v_n}$ and \mathbf{v}_{Φ} has been introduced. The pseudo measurement noise covariance matrices $\mathbf{R}_{v_n} = E[\mathbf{v}_{\delta v_n} \mathbf{v}_{\delta v_n}^T]$ and $\mathbf{R}_{\Phi} = E[\mathbf{v}_{\Phi} \mathbf{v}_{\Phi}^T]$ can be set to zero without numerical ramifications as discussed in [14]. This forces estimated states equal and implements the assumed equality of inertial and aerodynamic truth for translational and rotational motion. With zero measurement noise covariance, state-level motion fusion mathematically corresponds to methods studied or applied in [9, 14, 78, 79, 81, 85].

A similar measurement for redundant vehicle dynamics model reference point and INS position states could be defined

$$\tilde{\mathbf{y}}_{\delta \lambda} := \hat{\lambda}_{VDM} - \hat{\lambda}_{INS} = \delta \lambda_{VDM} - \delta \lambda_{INS} + \mathbf{v}_{\delta \lambda}$$

With the vector of WGS84 coordinates $\lambda = [\phi, \lambda, h]^T$. It has been shown in [14] that using pseudo measurements for position and velocity in parallel is superfluous and can cause numerical problems at high update rates.

For a physically more meaningful alternative to equation (3-6) with arbitrary location of navigation reference point R on the vehicle, inertial and aerodynamic translational motion can be constrained equal in the center of gravity

$$\mathbf{v}_{n_{INS}}^G = \mathbf{v}_{n_{VDM}}^G$$

With

$$\begin{aligned} \mathbf{v}_{n_{INS}}^G &= \mathbf{v}_{n_{INS}} + \mathbf{R}_{nb_{INS}} \left((\tilde{\omega}_{ib} + \delta \omega_{ib_{IMU}}) \times \mathbf{r}_b^{RG} \right) \\ \mathbf{v}_{n_{VDM}}^G &= \mathbf{v}_{n_{VDM}} + \mathbf{R}_{nb_{VDM}} (\omega_{ib} \times \mathbf{r}_b^{RG}) \end{aligned}$$

The following pseudo measurement is defined

$$\tilde{\mathbf{y}}_x := \hat{\mathbf{v}}_{n_{VDM}}^G - \hat{\mathbf{v}}_{n_{INS}}^G = \hat{\mathbf{v}}_{n_{VDM}} - \hat{\mathbf{v}}_{n_{INS}} + \hat{\mathbf{R}}_{nb_{VDM}} (\hat{\omega}_{ib} \times \hat{\mathbf{r}}_b^{RG}) - \hat{\mathbf{R}}_{nb_{INS}} (\tilde{\omega}_{ib} \times \hat{\mathbf{r}}_b^{RG}) \quad (3-9)$$

It is preferable to define the pseudo measurement in NED frame as above, because kinematic velocity vector errors will become observable independently of orientation errors in flight at zero angular rates. For a measurement defined in body-fixed frame, velocity and orientation errors would always be observable in combination only.

The pseudo measurement (3-9) can be linearized to yield the following filter observation equation (by adding $\mathbf{v}_{n_{INS}}^G - \mathbf{v}_{n_{VDM}}^G = \mathbf{0}$)

$$\begin{aligned} \tilde{\mathbf{y}}_x &\doteq \delta \mathbf{v}_{n_{INS}} - \delta \mathbf{v}_{n_{VDM}} - \text{skew}(\tilde{\omega}_{ib} \times \hat{\mathbf{r}}_b^{RG}) \Phi_{INS} + \text{skew}(\hat{\omega}_{ib} \times \hat{\mathbf{r}}_b^{RG}) \Phi_{VDM} \\ &\quad + \hat{\mathbf{R}}_{nb_{VDM}} \text{skew}(\hat{\mathbf{r}}_b^{RG}) \delta \omega_{ib} - \hat{\mathbf{R}}_{nb_{INS}} \text{skew}(\hat{\mathbf{r}}_b^{RG}) \mathbf{b}_{Gyro} \\ &\quad + \left(\hat{\mathbf{R}}_{nb_{INS}} \text{skew}(\tilde{\omega}_{ib}) - \hat{\mathbf{R}}_{nb_{VDM}} \text{skew}(\hat{\omega}_{ib}) \right) \delta \mathbf{r}_b^{RG} \\ &\quad - \hat{\mathbf{R}}_{nb_{INS}} \text{skew}(\hat{\mathbf{r}}_b^{RG}) \mathbf{n}_{Gyro} + \mathbf{v}_{\tilde{y}_x} \end{aligned} \quad (3-10)$$

With corresponding definitions of measurement matrix \mathbf{H} and process noise feedthrough matrix \mathbf{G}_ω , accounting for the gyro noise term $-\hat{\mathbf{R}}_{nbINS} skew(\hat{\mathbf{r}}_b^{RG}) \mathbf{n}_{Gyro}$, the observation equation can be written in the form

$$\tilde{\mathbf{y}}_x = \mathbf{H}\mathbf{x} + \mathbf{G}_\omega\boldsymbol{\omega} + \mathbf{v}$$

If this pseudo measurement is used at high rate with significant IMU inertial angular rates measurement noise, the adapted optimal filter gain matrix (3-5) should be used.

3.1.3 Modeling uncertainties of aerodynamic flight

The model fusion techniques compute a best estimate combination of inertial and vehicle motion models. To this end, accurate covariance information is required, as it determines the respective weighting of combined motion model information.

Ideal modeling of aerodynamic flight would include atmosphere process models accounting for an unsteady, non-uniform air mass velocity vector field traversed by the aircraft. This would allow to compute dynamic wind velocity vector and wind rates at aircraft location affecting aerodynamics and flight dynamics. In an application scenario for airplanes, where altitudes and travelled distances are large, such high-fidelity models of atmosphere processes are not available for on-board online use. Therefore, aerodynamic flight must instead be computed assuming steady and uniform wind (or wind changing according to some low frequency weather model). In addition to dynamic air mass motion, non-standard atmosphere conditions, such as air density at altitude, cause complex input and process error of the aerodynamic motion model.

Application of an optimal model fusion filter requires that any uncertainty in modeling aerodynamic flight is accounted for accurately by statistical models used for filter covariance propagation. Unfortunately, accurate high-fidelity statistical models are equally challenging to define and implement as the corresponding process models.

Consequently, optimal model fusion techniques suffer from a lack of reliability of dynamic atmosphere uncertainty models for aerodynamic flight in open-air. The intensity of aerodynamic disturbances encountered in flight can change unpredictably for the application of interest. Statistical models for smooth atmosphere dynamic wind vector and wind rates can abruptly become invalid on the onset of gale-force winds, gusts and turbulence. In this case, the inconsistent statistical information provided to the navigation filter can result in failure of the optimal filter.

Due to the large variety of atmospheric disturbances to be accounted for, an adaptive approach trying to identify rough atmosphere conditions using on-board measurements and switching filter covariance models accordingly is not considered robust. On the other hand, general overbounding of dynamic atmosphere uncertainty is not a solution either, because an optimal filter would mostly neglect aerodynamic motion model information for high magnitude and correlation time of wind and wind rates uncertainty.

The difficulty of implementing an optimal model fusion filter for inertial navigation and airplane aerodynamics is further increased by estimation of errors in aerodynamic model coefficients. Similarly to dynamic atmosphere processes, defining reliable statistical models for aerodynamic model uncertainty is challenging. Furthermore, uncertainty models for inertial navigation, dynamic atmosphere and aerodynamic motion must accurately compute covariance as well as respective correlation of errors. For the high accuracy aerodynamics models considered here, this constitutes a prohibitive risk of miscalibration of model coefficients due to statistics modeling error.

The ideal model fusion method is especially vulnerable to inconsistent statistical models as estimation error in wind velocity and aerodynamic model coefficients can significantly harm performance.

3.1.4 Tuned model fusion filter

In the preliminary effort of developing model fusion methods using optimal filters, an uncertainty model for wind velocity vector with small correlation time in combination with estimation of this high-frequency wind vector was key for good performance and robustness. This choice of wind uncertainty model is deliberately inconsistent with the dynamic atmosphere conditions in simulation where dynamic wind has a large correlation time coefficient. Although this result quantitatively still depends on the simulation environment and the atmospheric models, it indicates to the solution of the modeling problem of state estimation techniques.

First, note that this choice of tuning neglects the additional uncertainty in aerodynamic motion model velocity and position due to an unknown slowly varying or constant wind vector which would have to be considered in an ideal model fusion filter. Because this work is specifically concerned with the combination of low-cost inertial navigation and a high-quality aerodynamic model as discussed in chapter 2, the quantification of slowly-varying wind uncertainty is indeed expendable for model combination: For the desired mission times, translational uncertainty of the inertial model will nearly always exceed even extreme wind drift (c.f. the empirical atmosphere extremes in [86]). Therefore, neglecting the influence of long-term wind uncertainty in the fusion of low-cost inertial navigation and the aerodynamic motion model has little effect on model fusion position drift. This tuning further increases the confidence of the information on average kinematic velocity provided by the aerodynamic motion model compared to the inertial model.

Secondly, the increased uncertainty of aerodynamic moments and high-frequency wind vector reduces the weighting of rotational motion information of the aerodynamic motion model used by the model fusion filter. While this is consistent in rough atmosphere conditions, where the aerodynamic motion model orientation and angular rates can be significantly in error, it corresponds to a conservative overbounding of aerodynamic rotational motion uncertainty in normal, smooth atmosphere flight. With this choice of filter tuning, the model fusion filter will apply large corrections to both aerodynamic model orientation and wind velocity vector in rough atmosphere. For robustness of the aerodynamic navigation method, it is essential that the body-fixed frame aerodynamic velocity vector is not subjected to large changes by filter corrections. If the optimal model fusion method is applied, this can only be achieved by estimation of a high-frequency wind vector that compensates for discrepancies of kinematic and aerodynamic motion. At the same time, aerodynamic model attitude and heading are corrected thus improving position propagation accuracy.

The specialized tuning developed for model fusion methods implements a specific type of combination of low-cost inertial navigation and high-quality aerodynamic motion model. In contrast to the horizontal model fusion paradigm [11], which assumes homogeneous information in both (or multiple) models, this is a complementary combination of information from different motion degrees of freedom for each model. The best way to integrate the two models for the specific problem at hand is a vertical, or complementary, combination of inertial rotational motion (aided by 3-D magnetometer) and aerodynamic horizontal translational motion.

While choosing the better information from each of the two models to be combined, this complementary strategy also reduces the importance of statistical modeling by

conservatively overbounding insignificant information. In addition, the aerodynamic model coefficients are kept constant. This keeps the reliability of a certified high-quality model intact.

3.1.5 Shortcomings of state estimation techniques

Application of an optimal model fusion filter requires accurate statistical models of current atmospheric conditions, flight dynamics and inertial navigation uncertainty and error correlation. A specific tuning of the model fusion filter has been developed that avoids extensive modeling of uncertainties and exploits the complementary characteristics of the two motion models. That way, good position performance and method robustness is achieved in simulation.

The tuned model fusion filter approach is not directly applicable to a real-world airplane application. Quantitatively, the choice of tuning parameters depends on the simulation framework used for method optimization. In 2.3.3.2 the potential loss of method robustness due to inconsistent coupling of kinematic and aerodynamic motion has been discussed. The high-frequency dynamic wind vector uncertainty model has been found to be a robust countermeasure against filter failure in simulation but may not be sufficient in real rough atmosphere conditions to be encountered in operation for large altitudes, flight times and travelled distances.

The need of an accurate high-fidelity simulation tool to tune a navigation method to be robust results in a need for strict verification of this tool. Tuning of the high-frequency wind velocity vector estimation must guarantee for aerodynamic navigation method robustness even in extreme atmosphere conditions.

Consequently, it is desired to further reduce sensitivity of aerodynamic navigation method performance and robustness with respect to modeling and filter tuning. This will be the focus of the following section. Optimal model fusion is a formalized approach that can be applied to a wide range of problems but has been found to suffer from unreliable modeling. For the specific problem at hand, the complementary characteristics of inertial and airplane aerodynamic models will be exploited more extensively to improve aerodynamic navigation.

Note that this discussion is independent of the actual model fusion technique used. In ideal optimal estimation, state-level and signal-level are equivalent (exact constraints on translational and rotational kinematic motion). Differences arise due to finite filter update rates and for the tuned model fusion filter. In this case, the low-pass effect of orientation and c.g. velocity updates can be beneficial.

3.2 COVARIANCE-FREE INTEGRATION

The study of inertial and aerodynamic motion model characteristics, optimal model fusion and the results for tuning of model fusion indicate that a static, covariance-free integration can be implemented to combine the two models. The best tuning of a model fusion filter for good robustness in a variable and potentially rough dynamic atmosphere environment encountered in airplane applications largely neglects accurate atmosphere uncertainty modeling (because it is unavailable). Instead, it profits from a mostly invariable and complementary combination of inertial rotational and aerodynamic translational motion.

The distinctive qualities of low-cost inertial navigation aided by barometric altitude and 3-D magnetometer and the high-quality airplane aerodynamic model are perfectly suited for such a static complementary combination strategy. The potential performance gain in an ideal horizontal model fusion architecture [11], with bidirectional aiding of the models for all motion degrees of freedom, is small due to the significant inequality of information content. Furthermore, while realization of ideal model fusion ideally requires adaptive uncertainty models of atmosphere statistics, a new method can be defined that solely relies on safe assumptions on how to exclusively select complementary information from the two models. Such a method works without a model fusion filter depending on unreliable or unknown statistical models. Statistically weighted averaging of information is replaced by covariance-free exclusive selection in a fixed implementation of complementary model combination.

To that end, means to feed information from aerodynamic to inertial model and vice versa must be developed. The goal is to precisely define the lines between information used from one or the other model in complementary integration. A significant advantage of a covariance-free approach to inertial and aerodynamic motion model integration is the unrestricted freedom of designing a mechanism to couple the two models.

The main steps to improve the airplane aerodynamic motion model for accurate first order position propagation as studied in chapter 2 can be accomplished with a set of aerodynamically desensitized constraints presented in the following subsection. These constraints feed accurate reference information from the inertial motion model to the aerodynamic motion model while avoiding disturbances to the flight dynamics.

The modification of the inertial motion model presented in section 2.2.2.3 offers an advantageous form for this integration strategy: It is already modified for better attitude computation accuracy in vehicles with only temporary horizontal accelerations and its performance can directly be improved by provision of reference information on horizontal position and velocity. Because of the weak influence, the error statistics of reference information can be ignored in the reduced covariance model for rotational and vertical motion only used for integration of barometric altitude and 3-D magnetometer. Alternatively, error loops could be used for integration of these measurements.

No online improvement of the aerodynamic model is attempted due to the lack of sensor accuracy in GNSS-denied flight and in order to maintain the reliability of a certified high-quality model.

The covariance-free approach to complementary integration of inertial navigation and aerodynamic motion model is presented in the following subsections. First, the details of exchanging complementary information between the inertial and aerodynamic motion

models are discussed. Because covariance information might be required as navigation data output, an “add on” covariance model consistent with the proposed aerodynamic navigation method will be derived. This covariance model can use the best available statistical models for atmosphere uncertainty, but the computation of navigation state is not affected. Finally, the proposed method will be fit into the existing navigation framework and operational modes.

3.2.1 Aerodynamically desensitized model constraints

The aerodynamic motion model must be continuously corrected using reference information from the inertial motion model in order to achieve a number of goals. First, the divergent lateral error modes must be damped effectively without affecting longitudinal motion. Consequently, roll stabilization must be implemented in order to keep aerodynamic model lateral motion aligned.

In addition, simulation of the aerodynamic model must be robust in turbulent atmosphere with possibly intense measured pilot control input inconsistent with estimated wind. This leads to large dynamic distortions of aerodynamic model kinematic states. Correction of aerodynamic model attitude or orientation in general affects the fundamental degrees of freedom of airplane flight dynamics – the aerodynamic angles of attack and sideslip. The discussion in 2.3.3.2 revealed that due to the strong dynamics of aerodynamic flight and especially static stability, only equilibrium corrections should be made to aerodynamic states and aerodynamic model coefficients in order to preserve robustness in rough atmosphere. This is generally not possible for lack of accurate models. However, unlike in the tuned model fusion filter, where this problem is only evaded by a dynamical estimation of wind vector, which allows keeping aerodynamic states mostly unchanged in the correction of kinematic states, a more thorough solution is possible for the covariance-free method.

All corrections to the aerodynamic motion model must be implemented such that the fundamental degrees of freedom of airplane flight dynamics remain unchanged. This means that kinematic velocity and vehicle orientation may only be changed simultaneously while keeping aerodynamic angles of attack and sideslip, airspeed and aerodynamic climb angle constant. All of these quantities have a strong direct effect on aerodynamic forces and moments, or a direct effect on the longitudinal equilibrium of forces (as is the case for the aerodynamic climb angle). For given values of air density, aerodynamic bank angle, wind and control inputs, longitudinal stability and trim of the aerodynamic motion model prescribe certain equilibrium values of airspeed, aerodynamic angle of attack and aerodynamic climb angle (equivalently the longitudinal orientation of gravity vector). The aerodynamic angle of sideslip is governed by the equilibrium of body yaw moments.

On the other hand, the values of aerodynamic course angle χ_A and aerodynamic bank angle μ_A of the aerodynamic motion model may be corrected without concerns for robustness because the dynamic response of airplane flight dynamics is weak. This allows for aerodynamically desensitized corrections of aerodynamic motion model kinematic states.

Finally, translational propagation accuracy must be improved with error growth ideally close to ideal wind drift. To achieve this, the remaining sources of first order growth in position error must be addressed. Because no reference information on kinematic velocity vector or course over ground is available in the low-cost GNSS-denied application, vehicle heading constitutes the best available alternative. Again, correction of heading may perturb flight dynamics with potentially severe consequences for filter stability and an aerodynamically desensitized correction must be implemented.

Height h and horizontal position (if a reference value is available) can be corrected with negligible effect on flight dynamics, possibly with synchronous recalibration of the height model for air density. Continuous correction of height is important for robust aerodynamic

motion simulation in presence of large input or model errors that cause trim error in aerodynamic climb angle and a large deviation in altitude for stationary horizontal flight.

The corrections to height h , aerodynamic course angle χ_A and aerodynamic bank angle μ_A , while keeping γ_A , α_A , β_A and V_A unchanged, are sufficient to use the airplane aerodynamic motion model as accurate, first-order propagation method. These aerodynamically desensitized constraints will be described in detail in the following.

3.2.1.1 Aerodynamic orientation error

For the correction of aerodynamic course angle χ_A and aerodynamic bank angle μ_A , the errors of these quantities must be determined. Given a reference value of vehicle orientation of significantly better accuracy than the computed VDM orientation, errors in this reference value can be neglected and approximate orientation error Euler angles $\Phi = [\delta\phi_1, \delta\phi_2, \delta\phi_3]^T$ can be computed. As discussed in 2.2.2.1, these Euler angles describe the relative orientation of platform frame p with respect to the NED frame n and per definition of the platform frame are a parametrization of error of computed NED to body-fixed frame orientation.

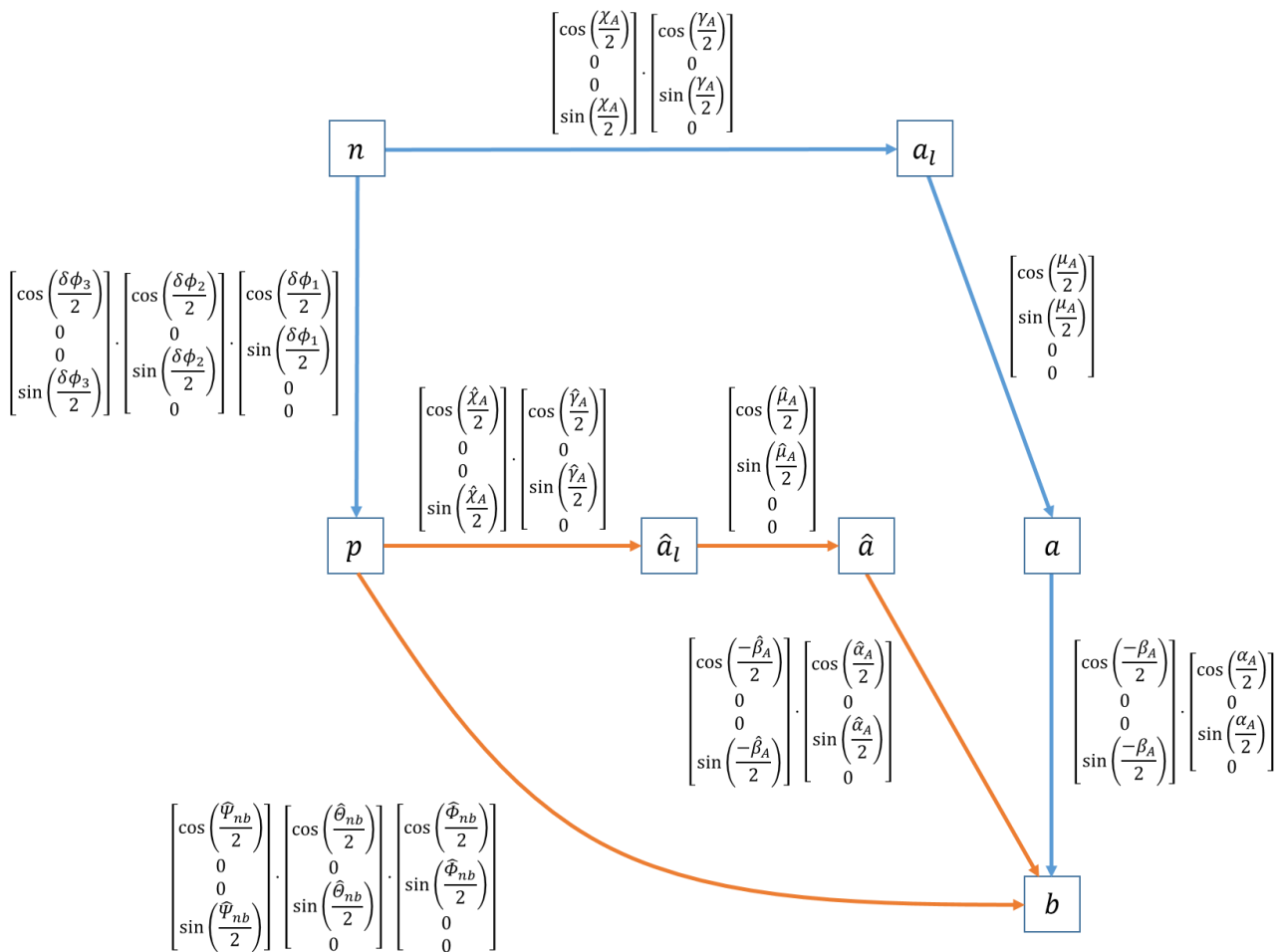


Figure 15: Errors in aerodynamic orientation angles

In addition to NED to body-fixed frame orientation quaternion, rotation matrix and Euler angles, the aerodynamic course, climb and bank angles χ_A, γ_A, μ_A in combination with aerodynamic angles of attack and sideslip α_A, β_A are a parametrization of vehicle orientation. Figure 15 shows the coordinate frame axis transformations between the body-fixed frame b and the NED, level aerodynamic and aerodynamic frames n, a_l, a as well as their computed counterparts p, \hat{a}_l, \hat{a} . The consecutive axis rotations that transform one frame into another are given by their equivalent orientation quaternion (c.f. appendix A.1).

Due to the equivalence of aerodynamic angle parametrization and e.g. the Euler orientation angles parametrization of NED to body-fixed frame orientation, the contained orientation errors are also equal. Consequently, corrections of the aerodynamic orientation angles can be derived from the orientation error Euler angles Φ .

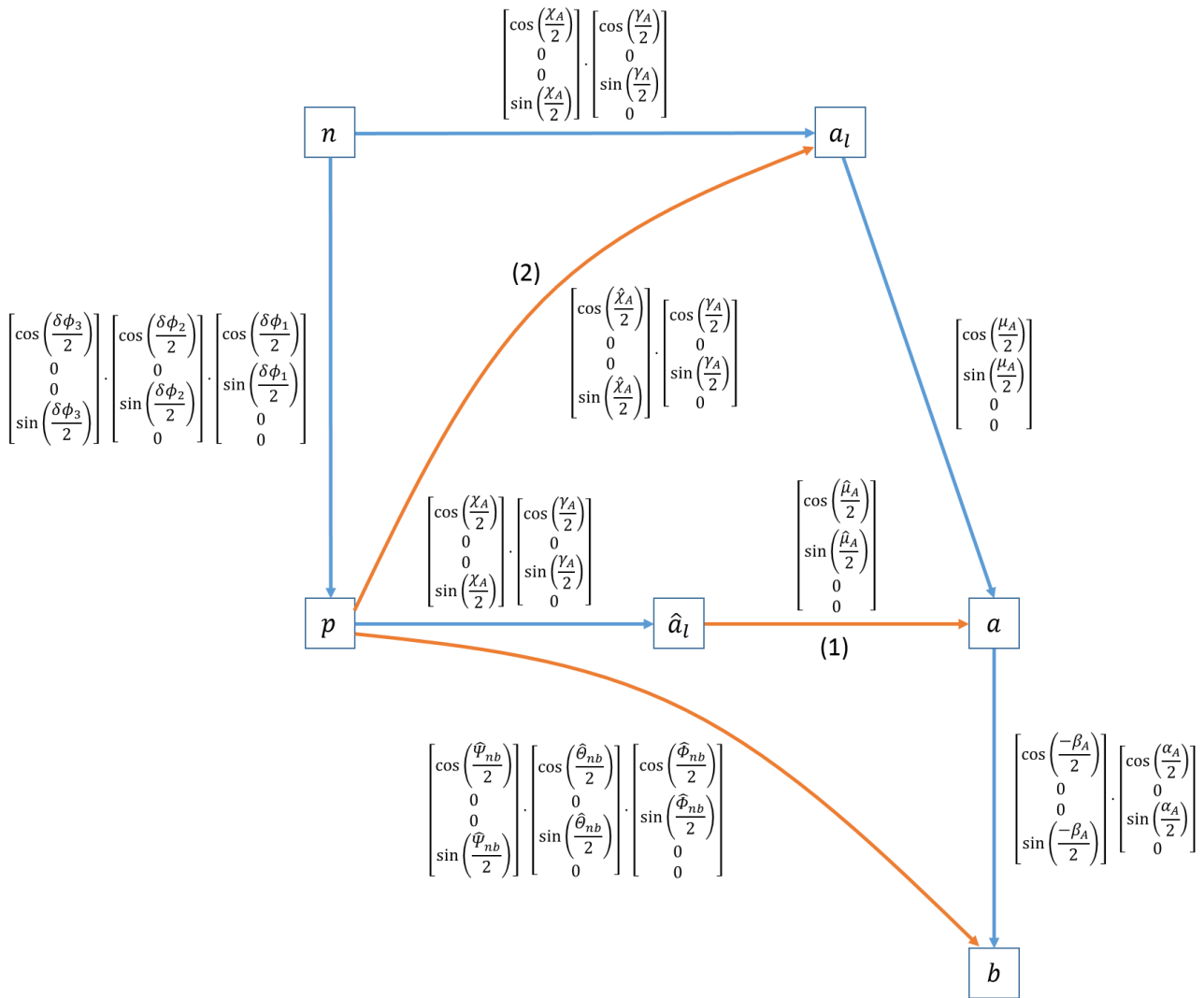


Figure 16: Simplified aerodynamic orientation errors

Determining the errors in the aerodynamic angles is significantly simplified by the assumption that the aerodynamic climb angle γ_A and the aerodynamic angles of attack and sideslip α_A, β_A are error free, as required for aerodynamically desensitized correction of VDM

orientation. With this, only the aerodynamic course angle χ_A and the aerodynamic bank angle μ_A contribute to the VDM orientation error. In addition, for flight condition with small aerodynamic climb angle γ_A , these two rotations are about orthogonal axes in good approximation. This allows studying the relationship of the orientation error Euler angles $\boldsymbol{\phi}$ and errors in computed aerodynamic course angle $\hat{\chi}_A$ and computed aerodynamic bank angle $\hat{\mu}_A$ separately. Figure 16 shows how errors in these two angles contribute to NED to platform frame misalignment if they are the only source of aerodynamic orientation error.

3.2.1.2 Correction of aerodynamic bank angle μ_A

By correcting the VDM aerodynamic bank angle μ_A the divergent lateral motion of the aerodynamic model can effectively be restrained. By inspection of case (1) shown in Figure 16, the error in computed aerodynamic bank angle can be determined as the misalignment of computed level aerodynamic frame \hat{a}_l with respect to the true level aerodynamic frame a_l . The NED to level aerodynamic frame orientation quaternion is considered known without error in the correction of aerodynamic bank angle:

$$\tilde{\mathbf{q}}_{na_l} = \begin{bmatrix} \cos\left(\frac{\chi_A}{2}\right) \\ 0 \\ 0 \\ \sin\left(\frac{\chi_A}{2}\right) \end{bmatrix} \cdot \begin{bmatrix} \cos\left(\frac{\gamma_A}{2}\right) \\ 0 \\ \sin\left(\frac{\gamma_A}{2}\right) \\ 0 \end{bmatrix}$$

The level aerodynamic frame is defined by rotation of the NED frame such that the x-axis is aligned with the aerodynamic velocity vector. The y-axis remains in the horizontal plane. The aerodynamic climb and course angles are

$$\gamma_A = \text{asin}\left(\frac{-(v_{DVDM} - v_{W,D})}{\|\mathbf{v}_{nVDM} - \mathbf{v}_W\|_2}\right)$$

$$\chi_A = \text{atan2}(v_{EVDM} - v_{W,E}, v_{NVDM} - v_{W,N})$$

Given a reference value of vehicle orientation $\tilde{\mathbf{q}}_{nb_{ref}}$, the error in computed aerodynamic bank angle $\delta\mu_A = \mu_A - \hat{\mu}_A$ can be extracted from the following orientation quaternion

$$\tilde{\mathbf{q}}_{a_l\hat{a}_l} = \tilde{\mathbf{q}}_{na_l}^{-1} \cdot \tilde{\mathbf{q}}_{nb_{ref}} \cdot \tilde{\mathbf{q}}_{nb_{VDM}}^{-1} \cdot \tilde{\mathbf{q}}_{na_l} = \begin{bmatrix} \cos\left(\frac{\delta\mu_A}{2}\right) \\ \sin\left(\frac{\delta\mu_A}{2}\right) \\ 0 \\ 0 \end{bmatrix}$$

Note that this quaternion product is equivalent to transformation of the phi angle orientation error $\boldsymbol{\phi}$ from NED frame to level aerodynamic frame coordinates $\boldsymbol{\phi}_{a_l} = \mathbf{R}_{na_l}^T \boldsymbol{\phi}_n$. Neglecting all other orientation errors, the error in computed aerodynamic bank angle is the projection of phi angle orientation error onto the direction of aerodynamic velocity:

$$\delta\mu_A = \mathbf{e}_1 \mathbf{R}_{na_l}^T \boldsymbol{\phi}_n = \frac{1}{V_A} \mathbf{v}_{An}^T \boldsymbol{\phi}_n$$

It is desired to rotate the aerodynamic model only in direction of aerodynamic velocity vector in order to leave \mathbf{v}_{AbVDM} unchanged. This corresponds to a change in aerodynamic bank angle μ_A of the aerodynamic motion model. Consequently, the aerodynamic model orientation quaternion is updated as follows

$$\check{\mathbf{q}}_{nbVDM} \rightarrow \check{\mathbf{q}}_{na_l} \cdot \check{\mathbf{q}}_{a_l\hat{a}_l} \cdot \check{\mathbf{q}}_{na_l}^{-1} \cdot \check{\mathbf{q}}_{nbVDM} \quad (3-11)$$

3.2.1.3 Correction of aerodynamic course angle χ_A

For correction of aerodynamic model heading, the aerodynamic model kinematic velocity vector in NED frame coordinates must be changed simultaneously in order to keep \mathbf{v}_{AbVDM} unchanged. This corresponds to a change of aerodynamic course angle χ_A . The heading correction is derived from the NED frame orientation error with respect to the reference $\check{\mathbf{q}}_{nbref}$

$$\check{\mathbf{q}}_{nbref} \check{\mathbf{q}}_{nbVDM}^{-1} = \begin{bmatrix} \cos\left(\frac{\delta\phi_3}{2}\right) \\ 0 \\ 0 \\ \sin\left(\frac{\delta\phi_3}{2}\right) \end{bmatrix} \cdot \begin{bmatrix} \cos\left(\frac{\delta\phi_2}{2}\right) \\ 0 \\ \sin\left(\frac{\delta\phi_2}{2}\right) \\ 0 \end{bmatrix} \cdot \begin{bmatrix} \cos\left(\frac{\delta\phi_1}{2}\right) \\ \sin\left(\frac{\delta\phi_1}{2}\right) \\ 0 \\ 0 \end{bmatrix}$$

As shown for case (2) in Figure 16 only an error in the aerodynamic course angle is assumed $\delta\chi_A = \chi_A - \hat{\chi}_A$. Neglecting the first two elements of the vector of orientation error Euler angles Φ , inspection of Figure 16 reveals that

$$\chi_A = \delta\phi_3 + \hat{\chi}_A$$

and consequently $\delta\phi_3 = \delta\chi_A$.

The VDM orientation and velocity vector are updated as follows

$$\check{\mathbf{q}}_{nbVDM} \rightarrow \begin{bmatrix} \cos\left(\frac{\delta\phi_3}{2}\right) \\ 0 \\ 0 \\ \sin\left(\frac{\delta\phi_3}{2}\right) \end{bmatrix} \cdot \check{\mathbf{q}}_{nbVDM} \quad (3-12)$$

$$\mathbf{v}_{nVDM} \rightarrow \mathbf{R}_D(\mathbf{v}_{nVDM} - \mathbf{v}_W) + \mathbf{v}_W$$

The rotation matrix \mathbf{R}_D that transforms the NED frame aerodynamic velocity vector can be computed from the heading correction with equation (A-20):

$$\mathbf{R}_D = \mathbf{I} + \sin(\delta\phi_3) \text{skew}(\mathbf{e}_3) + (1 - \cos(\delta\phi_3)) \text{skew}(\mathbf{e}_3)^2$$

The two correction schemes for lateral motion and heading do not affect aerodynamic model aerodynamic angles of attack and sideslip and can therefore be applied even if the reference orientation contains high frequency content inconsistent with the motion of simulated VDM. This approach increases robustness of the aerodynamic navigation method in all possible atmosphere conditions.

3.2.1.4 Correction of position

Finally, vertical translational motion can be updated in a straight-forward way. Vertical position is simply set to the reference value

$$h_{VDM} \rightarrow h_{ref} \quad (3-13)$$

If a reference value for 3-D position is available, a correction scheme equivalent to equation (3-13) can be used for updating all components of aerodynamic model position.

3.2.2 Integration with the modified inertial motion model

The reference values for vertical motion and orientation h_{ref} and $\tilde{\mathbf{q}}_{nb_{ref}}$ used for correction of the aerodynamic motion model as described in the previous subsection can be provided by the modified inertial motion model presented in 2.2.2.3. 3-D magnetometer aiding and barometric altitude damping of the vertical inertial channel are applied as discussed in 2.3.2. The reference values for horizontal position and velocity in the modified inertial motion model equation will be taken from the aerodynamic motion model.

The combined motion model can be summarized as follows. The aerodynamic motion model (2-8) and (2-9) is propagated using

$$\begin{aligned}\dot{\boldsymbol{\omega}}_{ib_{VDM}} &= \mathbf{I}_{bb}^G{}^{-1} \left(\mathbf{M}_b^G - \boldsymbol{\omega}_{ib_{VDM}} \times (\mathbf{I}_{bb}^G \boldsymbol{\omega}_{ib_{VDM}}) \right) \\ \dot{\mathbf{z}}_{n_{VDM}} &= \mathbf{s}(\mathbf{z}_{n_{VDM}}, \mathbf{f}_{b_{VDM}}, \boldsymbol{\omega}_{ib_{VDM}}) \\ \mathbf{f}_{b_{VDM}} &= \frac{\mathbf{F}_b^G}{m} - \dot{\boldsymbol{\omega}}_{ib_{VDM}} \times \mathbf{r}_b^{RG} - \boldsymbol{\omega}_{ib_{VDM}} \times (\boldsymbol{\omega}_{ib_{VDM}} \times \mathbf{r}_b^{RG})\end{aligned}$$

The external forces and moments in center of gravity G are computed using aerodynamic motion model states, NED frame wind velocity vector, control inputs, model coefficients and center of gravity position

$$\begin{aligned}\mathbf{M}_b^G &= \sum_{Aero, Prop} \mathbf{M}_{b_i}^G(h_{VDM}, \mathbf{R}_{nb_{VDM}}^T(\mathbf{v}_{n_{VDM}} - \mathbf{v}_{Wn}), \boldsymbol{\omega}_{ib_{VDM}}, \mathbf{u}_p, \mathbf{c}_v, \mathbf{r}_b^{RG}) \\ \mathbf{F}_b^G &= \sum_{Aero, Prop} \mathbf{F}_{b_i}^G(h_{VDM}, \mathbf{R}_{nb_{VDM}}^T(\mathbf{v}_{n_{VDM}} - \mathbf{v}_{Wn}), \boldsymbol{\omega}_{ib_{VDM}}, \mathbf{u}_p, \mathbf{c}_v)\end{aligned}$$

The modified inertial motion model is propagated with

$$\begin{aligned}\dot{\mathbf{v}}_{n_{INS}} &= \mathbf{R}_{nb_{INS}} \frac{\omega^2}{\omega_S^2} \mathbf{f}_{b_{IMU}} + \boldsymbol{\gamma}_n(\phi_{VDM}, h_{INS}) \\ &\quad - \left(2\mathbf{R}_{en}^T(\phi_{VDM}, \lambda_{VDM}) \boldsymbol{\omega}_{ie} + \boldsymbol{\omega}_{en}(\phi_{VDM}, h_{INS}, v_{N_{INS}}, v_{E_{INS}}) \right) \times \mathbf{v}_{n_{INS}} \\ &\quad - 2\zeta\omega(\mathbf{v}_{n_{INS}} - \mathbf{v}_{n_{VDM}}) \\ \dot{\tilde{\mathbf{q}}}_{nb_{INS}} &= \frac{1}{2} (\tilde{\mathbf{q}}_{nb_{INS}} \cdot \tilde{\boldsymbol{\omega}}_{ib_{IMU}} - \tilde{\boldsymbol{\omega}}_{in}(\phi_{VDM}, \lambda_{VDM}, h_{INS}, v_{N_{INS}}, v_{E_{INS}}) \cdot \tilde{\mathbf{q}}_{nb_{INS}})\end{aligned}$$

The vertical component of the velocity vector differential equation is replaced by

$$\begin{aligned}\dot{v}_{D_{INS}} &= f_{D_{INS}} + \gamma_D(\phi_{VDM}, h) - \omega_N v_{E_{VDM}} + \omega_E v_{N_{VDM}} \\ \boldsymbol{\omega}_n &= \begin{bmatrix} \omega_N \\ \omega_E \\ \omega_D \end{bmatrix} = 2\mathbf{R}_{en}^T(\phi_{VDM}, \lambda_{VDM}) \boldsymbol{\omega}_{ie} + \boldsymbol{\omega}_{en}(\phi_{VDM}, h_{INS}, v_{N_{VDM}}, v_{E_{VDM}}) \\ \dot{h}_{INS} &= -v_{D_{INS}}\end{aligned}$$

3.2.3 Add on covariance model

Although the model constraints presented in subsection 3.2.1 are independent of statistical models for vehicle model and dynamic atmosphere uncertainty, an auxiliary covariance model can be implemented if statistical models are available. The method behavior will remain unchanged, preserving its good reliability, but additional uncertainty information can be provided to the navigation data user.

Referring to the notation for extended Kalman filter states defined in appendix A.8, the model constraints can be written as error state updates in a linearized form

$$\mathbf{M}_{sel} \begin{bmatrix} \delta \mathbf{z}_{INS} \\ \delta \mathbf{z}_{VDM} \\ \mathbf{a} \end{bmatrix}^+ = \mathbf{T}^{-1} \mathbf{K}_1 \mathbf{T} \mathbf{M}_{sel} \begin{bmatrix} \delta \mathbf{z}_{INS} \\ \delta \mathbf{z}_{VDM} \\ \mathbf{a} \end{bmatrix}^- + \mathbf{T}^{-1} \mathbf{K}_2 \mathbf{M}_{ref} \begin{bmatrix} \delta \mathbf{z}_{INS} \\ \delta \mathbf{z}_{VDM} \\ \mathbf{a} \end{bmatrix}^- \quad (3-14)$$

The update matrices \mathbf{K}_1 and \mathbf{K}_2 depend on the specific correction scheme. The transformation matrix \mathbf{T} and its inverse will be defined accordingly. The rectangular binary matrices \mathbf{M}_{sel} and \mathbf{M}_{ref} have one entry of 1 in each row and full rank. \mathbf{M}_{sel} is defined to select the error states affecting aerodynamic motion from the augmented filter state vector. For the updates defined in subsection 3.2.1, \mathbf{M}_{sel} is defined such that

$$\mathbf{M}_{sel} \begin{bmatrix} \delta \mathbf{z}_{INS} \\ \delta \mathbf{z}_{VDM} \\ \mathbf{a} \end{bmatrix} = \begin{bmatrix} \delta \Lambda_{VDM} \\ \delta \mathbf{v}_{nVDM} \\ \boldsymbol{\phi}_{nVDM} \\ \delta \mathbf{v}_{Wn} \end{bmatrix}$$

\mathbf{M}_{ref} selects all other error states. Consequently with size n of augmented filter state vector and twelve VDM error states

$$\mathbf{M}_{sel} \mathbf{M}_{ref}^T = \mathbf{0}_{12 \times (n-12)}$$

$$\mathbf{M}_{ref} \mathbf{M}_{sel}^T = \mathbf{0}_{(n-12) \times 12}$$

And

$$\mathbf{M}_{ref}^T \mathbf{M}_{ref} + \mathbf{M}_{sel}^T \mathbf{M}_{sel} = \mathbf{I}$$

The update step for the complete filter state vector equivalent to equation (3-14) can be written as

$$\begin{bmatrix} \delta \mathbf{z}_{INS} \\ \delta \mathbf{z}_{VDM} \\ \mathbf{a} \end{bmatrix}^+ = (\mathbf{M}_{ref}^T \mathbf{M}_{ref} + \mathbf{M}_{sel}^T \mathbf{T}^{-1} \mathbf{K}_1 \mathbf{T} \mathbf{M}_{sel} + \mathbf{M}_{sel}^T \mathbf{T}^{-1} \mathbf{K}_2 \mathbf{M}_{ref}) \begin{bmatrix} \delta \mathbf{z}_{INS} \\ \delta \mathbf{z}_{VDM} \\ \mathbf{a} \end{bmatrix}^-$$

The augmented filter covariance matrix $\mathbf{P} = \text{Var}[[\delta \mathbf{z}_{INS}^T \quad \delta \mathbf{z}_{VDM}^T \quad \mathbf{a}^T]^T]$ can be updated with

$$\mathbf{M}_{sel} \mathbf{P}^+ \mathbf{M}_{sel}^T = \mathbf{T}^{-1} (\mathbf{K}_1 \mathbf{T} \mathbf{M}_{sel} \mathbf{P}^- \mathbf{M}_{sel}^T \mathbf{T}^T \mathbf{K}_1^T + \mathbf{K}_2 \mathbf{M}_{ref} \mathbf{P} \mathbf{M}_{ref}^T \mathbf{K}_2^T) \mathbf{T}^{-T} \quad (3-15)$$

$$\mathbf{M}_{sel} \mathbf{P}^+ \mathbf{M}_{ref}^T = \mathbf{T}^{-1} (\mathbf{K}_1 \mathbf{T} \mathbf{M}_{sel} \mathbf{P}^- \mathbf{M}_{ref}^T + \mathbf{K}_2 \mathbf{M}_{ref} \mathbf{P} \mathbf{M}_{ref}^T)$$

The covariance $\mathbf{M}_{ref} \mathbf{P} \mathbf{M}_{ref}^T$ remains unchanged.

With applicable values for the matrices \mathbf{K}_1 , \mathbf{K}_2 and \mathbf{T} , equation (3-15) can be used to consistently update the covariance matrix for aerodynamic navigation if one of the model constraints presented in 3.2.1 is applied.

For the lateral error correction (3-11), a transformation of error states facilitates the definition of a linearized error state update equation. Furthermore, by defining an error state for body-fixed frame aerodynamic velocity vector $\delta\mathbf{v}_{AbVDM}$, it is possible to exactly implement invariance of the uncertainty of this error in the update in the covariance model.

Aerodynamic errors are transformed according to

$$\mathbf{T}\mathbf{M}_{sel} \begin{bmatrix} \delta\mathbf{z}_{INS} \\ \delta\mathbf{z}_{VDM} \\ \mathbf{a} \end{bmatrix} = \begin{bmatrix} \delta\Lambda_{VDM} \\ \delta\mathbf{v}_{AbVDM} \\ \boldsymbol{\phi}_{a_lVDM} \\ \delta\mathbf{v}_{Wn} \end{bmatrix}$$

With the psi angle orientation error in level aerodynamic frame coordinates

$$\boldsymbol{\phi}_{a_l} = \mathbf{R}_{a_l n_{VDM}} \boldsymbol{\phi}_n = \begin{bmatrix} \phi_x \\ \phi_y \\ \phi_z \end{bmatrix}$$

The error of aerodynamic velocity vector in body-fixed frame coordinates can be written as

$$\delta\mathbf{v}_{Ab} = \delta \left(\mathbf{R}_{nb}^T (\mathbf{v}_n - \mathbf{v}_{Wn}) \right) = \mathbf{R}_{nb}^T \delta\mathbf{v}_n + \mathbf{R}_{nb}^T (\mathbf{v}_{An} \times \boldsymbol{\phi}_n) - \mathbf{R}_{nb}^T \delta\mathbf{v}_{Wn}$$

With $\mathbf{v}_{AnVDM} = \mathbf{v}_{nVDM} - \mathbf{v}_{Wn}$ the transformation matrix and its inverse are

$$\mathbf{T} = \begin{bmatrix} \mathbf{I} & \mathbf{0} & \mathbf{0} & \mathbf{0} \\ \mathbf{0} & \mathbf{R}_{nbVDM}^T & \mathbf{R}_{nbVDM}^T \text{skew}(\mathbf{v}_{AnVDM}) & -\mathbf{R}_{nbVDM}^T \\ \mathbf{0} & \mathbf{0} & \mathbf{R}_{a_l n_{VDM}} & \mathbf{0} \\ \mathbf{0} & \mathbf{0} & \mathbf{0} & \mathbf{I} \end{bmatrix}$$

$$\mathbf{T}^{-1} = \begin{bmatrix} \mathbf{I} & \mathbf{0} & \mathbf{0} & \mathbf{0} \\ \mathbf{0} & \mathbf{R}_{nbVDM} & -\text{skew}(\mathbf{v}_{AnVDM}) \mathbf{R}_{a_l n_{VDM}}^T & \mathbf{I} \\ \mathbf{0} & \mathbf{0} & \mathbf{R}_{a_l n_{VDM}}^T & \mathbf{0} \\ \mathbf{0} & \mathbf{0} & \mathbf{0} & \mathbf{I} \end{bmatrix}$$

The error correction (3-11) corresponds to the following linearized update of transformed error state

$$\begin{bmatrix} \delta\Lambda_{VDM} \\ \delta\mathbf{v}_{AbVDM} \\ \boldsymbol{\phi}_{a_lVDM} \\ \delta\mathbf{v}_{Wn} \end{bmatrix}^+ = \mathbf{K}_1 \begin{bmatrix} \delta\Lambda_{VDM} \\ \delta\mathbf{v}_{AbVDM} \\ \boldsymbol{\phi}_{a_lVDM} \\ \delta\mathbf{v}_{Wn} \end{bmatrix}^- + \mathbf{K}_2 \mathbf{M}_{ref} \begin{bmatrix} \delta\mathbf{z}_{INS} \\ \delta\mathbf{z}_{VDM} \\ \mathbf{a} \end{bmatrix}^- = \begin{bmatrix} \delta\Lambda_{VDM}^- \\ \delta\mathbf{v}_{AbVDM}^- \\ \mathbf{0} \\ \phi_{yVDM}^- \\ \phi_{zVDM}^- \\ \delta\mathbf{v}_{Wn}^- \end{bmatrix}$$

In the transformed error state space only the first element of VDM orientation error is reset with the corresponding information from the inertial motion model. This consistently models the covariance when the error in VDM aerodynamic bank angle is corrected using inertial motion model reference orientation.

Consequently, \mathbf{K}_1 is the 12×12 identity matrix with exception of a zero in the row corresponding to the first component of $\boldsymbol{\phi}_{a_{lVDM}}$. \mathbf{K}_2 is a zero matrix with exception of the entry

$$[1 \ 0 \ 0] \mathbf{R}_{a_{lnVDM}}$$

in the row corresponding to the first component of $\boldsymbol{\phi}_{a_{lVDM}}$ and the columns corresponding to $\boldsymbol{\phi}_{n_{INS}}$.

The correction of aerodynamic model heading according to equation (3-12) can be written as update of transformed error states

$$\mathbf{T} \mathbf{M}_{sel} \begin{bmatrix} \delta \mathbf{z}_{INS} \\ \delta \mathbf{z}_{VDM} \\ \mathbf{a} \end{bmatrix} = \begin{bmatrix} \delta \Lambda_{VDM} \\ \delta \mathbf{v}_{AbVDM} \\ \boldsymbol{\phi}_{nVDM} \\ \delta \mathbf{v}_{Wn} \end{bmatrix}$$

with the transformation matrix

$$\mathbf{T} = \begin{bmatrix} \mathbf{I} & \mathbf{0} & \mathbf{0} & \mathbf{0} \\ \mathbf{0} & \mathbf{R}_{nbVDM}^T & \mathbf{R}_{nbVDM}^T \text{skew}(\mathbf{v}_{AnVDM}) & -\mathbf{R}_{nbVDM}^T \\ \mathbf{0} & \mathbf{0} & \mathbf{I} & \mathbf{0} \\ \mathbf{0} & \mathbf{0} & \mathbf{0} & \mathbf{I} \end{bmatrix}$$

Again, an error state for body-fixed frame aerodynamic velocity vector $\delta \mathbf{v}_{AbVDM}$ is defined and remains exactly constant in the update

$$\begin{bmatrix} \delta \Lambda_{VDM} \\ \delta \mathbf{v}_{AbVDM} \\ \boldsymbol{\phi}_{nVDM} \\ \delta \mathbf{v}_{Wn} \end{bmatrix}^+ = \mathbf{K}_1 \begin{bmatrix} \delta \Lambda_{VDM} \\ \delta \mathbf{v}_{AbVDM} \\ \boldsymbol{\phi}_{nVDM} \\ \delta \mathbf{v}_{Wn} \end{bmatrix}^- + \mathbf{K}_2 \mathbf{M}_{ref} \begin{bmatrix} \delta \mathbf{z}_{INS} \\ \delta \mathbf{z}_{VDM} \\ \mathbf{a} \end{bmatrix}^- = \begin{bmatrix} \delta \Lambda_{VDM}^- \\ \delta \mathbf{v}_{AbVDM}^- \\ \boldsymbol{\phi}_{nVDM}^- \\ \boldsymbol{\phi}_{EVDM}^- \\ \boldsymbol{\phi}_{D_{INS}}^- \\ \delta \mathbf{v}_{Wn}^- \end{bmatrix}$$

Only the vertical component of aerodynamic model phi orientation error $\boldsymbol{\phi}_{nVDM}$ is updated to be equal to the error of the inertial model used as reference. \mathbf{K}_1 is the 12×12 identity matrix with exception of a zero in the row corresponding to $\boldsymbol{\phi}_{D_{VDM}}$. \mathbf{K}_2 is a zero matrix with exception of a one in the row corresponding to $\boldsymbol{\phi}_{D_{VDM}}$ and the column corresponding to $\boldsymbol{\phi}_{D_{INS}}$.

Finally, for the update of aerodynamic model position, no transformation of error states is required

$$\mathbf{T} = \mathbf{I}$$

With a redefinition of \mathbf{M}_{sel} and \mathbf{M}_{ref} so that

$$\mathbf{M}_{sel} \begin{bmatrix} \delta \mathbf{z}_{INS} \\ \delta \mathbf{z}_{VDM} \\ \mathbf{a} \end{bmatrix} = \delta \Lambda_{VDM}$$

the uncertainty of VDM height or position is reset with the corresponding value for the inertial model providing the reference information.

3.2.4 Wind information, aiding measurements and operational integration

The aerodynamic navigation method allows for integration of any slowly-varying wind vector estimate, e.g. from a weather forecast model. For this, the wind vector data is simply used as input to the aerodynamic model. Furthermore, the auxiliary covariance model can account for uncertainty of aerodynamic model wind input if appropriate statistical information is available. Although this will not influence the computed navigation data of the desensitized method, it can be used to improve the covariance output provided to the navigation data user.

Because the aerodynamic navigation method is designed to be a backup for flight navigation when GNSS is denied, availability of GNSS for aiding of low-cost inertial navigation is assumed as the normal operation condition. In this case, the modified inertial motion model can be set to normal operation by choosing $\omega = \omega_S$ and conventional integrated INS/GNSS navigation is used to provide navigation and covariance user data. To allow for smooth transition to GNSS-denied mode if necessary, the aerodynamic model is already active and updated with the desensitized constraints in 3.2.1 using INS/GNSS as reference. Because accurate absolute position information is available, the aerodynamic model position can be updated continuously to match the INS/GNSS reference position.

For initialization of the aerodynamic motion model, the airplane must be in air. This ensures that the control inputs are valid. An increase in INS/GNSS height of several meters can be used as trigger signal. Thanks to the high robustness of covariance-free aerodynamic navigation with the desensitized constraints in 3.2.1, initialization is not critical. Reference values for velocity, orientation and angular rates from INS/GNSS are sufficient.

Although the previous subsection presented a covariance model for the desensitized aerodynamic navigation method, the primary requirement for this method is that unreliable statistical models never influence navigation data output. Therefore, only the inertial motion model with an accurate uncertainty model may be used to integrate auxiliary aiding measurements and the aerodynamic motion model should never be corrected with state estimation filter updates. This is the case for barometric altitude and 3-D magnetometer, which are used as aiding measurement for the modified inertial model. If additionally an airspeed measurement is available, it can be integrated with INS/GNSS but not with the modified inertial model due to the modified horizontal velocities. Aiding the aerodynamic motion model with airspeed would not only require reliable uncertainty models for aerodynamic flight and dynamic atmosphere, but also require an online calibration of the aerodynamic model to correct trim condition errors resulting in discrepancies of measured and computed airspeed. Because modification of the aerodynamic model coefficients is prohibitive in the operational navigation method, an airspeed measurement can only be used in INS/GNSS mode.

3.3 CONCLUSION

Covariance-free integration for combined inertial and aerodynamic flight navigation was presented in the preceding section of this chapter. Optimal, and some suboptimal, state estimation techniques have been favored in the known literature on navigation with vehicle models. The detailed discussion of the fixed-wing aircraft flight navigation problem without GNSS aiding has revealed that the best way of combining information from low-cost inertial and high-quality airplane aerodynamic models is predefined by their complementary characteristics and can be implemented even without accurate and reliable statistical models of atmosphere processes.

The optimal model fusion techniques presented in the first section compute a best estimate combination of the motion described by inertial model and simulated vehicle motion. This is based on the plausible assumption that the truth processes approximated by the two motion models are identical. As a consequence, the respective uncertainties of the two models to be fused must be known with good statistical significance. Because of the great diversity of possible atmospheric conditions influencing open-air aerodynamic flight, reliable and accurate statistical uncertainty models are nearly impossible to define. For an optimal design of the model fusion filter, the model fusion will likely be biased, with a significant reduction in performance.

A second detrimental effect of inaccurate uncertainty models of dynamic atmosphere effects and aerodynamic flight in rough atmosphere is that aerodynamic motion model states may be estimated inconsistently: If the optimal filter is tuned assuming smooth atmosphere condition, it will resolve observed noisy discrepancies between computed inertial and aerodynamic motion mostly by updating motion model states, not wind states. In turbulence, computed dynamic inertial and aerodynamic motion differ significantly. Assuming a large correlation time coefficient for wind vector, the optimal filter makes large inconsistent corrections to aerodynamic model aerodynamic angles of attack and sideslip. Because of the strong dynamics of aerodynamic flight for fixed-wing aircraft, disturbing aerodynamic angle of attack or aerodynamic angle of sideslip of the simulated motion can cause large errors especially in orientation. Resulting linearization errors in covariance propagation and filter updates may lead to failure of the optimal model fusion filter in rough atmosphere conditions.

These issues with optimal model fusion for airplanes can partly be resolved with a tuned model fusion method which is optimized using a detailed simulation tool, resulting in good performance and robustness in simulation. Although the reliability of this tuned method in a real application is strictly limited by the extent to which the high fidelity simulation environment needed for tuning can be verified, it points to a new solution. The filter tuning does not rely on accurate statistical models of dynamic atmosphere uncertainties but instead implements a prioritized fusion of model information based on complementary characteristics. Still, method robustness is not guaranteed but depends on tuning quantitatively.

The proposed method therefore uses the airplane aerodynamic model for horizontal translational propagation and the modified inertial model aided by barometric altitude and 3-D magnetometer for orientation and vertical motion in a covariance-free integration. Unlike for the tuned model fusion method, this fully exploits complementary motion model

characteristics and eliminates the need for tuning altogether. The best way to implement GNSS-denied airplane flight navigation is an exclusive combination of optimal aerodynamic translational and inertial rotational information offering comparable performance and superior robustness.

Correction of the aerodynamic motion model is implemented using a set of aerodynamically desensitized constraints. These constraints allow to improve the position propagation performance using inertial navigation reference information on vehicle orientation. Furthermore, method robustness is maximized thanks to the isolation of sensitive flight dynamics degrees of freedom.

4 SYSTEM SIMULATION AND REAL DATA POST PROCESSING

Due to its complexity, the behavior of the aerodynamic navigation method can only qualitatively be predicted based on theoretical considerations. For a more thorough assessment, parts of or the complete navigation method must be studied in simulation or in a test with real data.

The simulation approach requires all inputs to the method to be created using corresponding process and measurement models. The generation of simulated input data consists of two separate steps. First, actual vehicle motion is simulated, in this case airplane flight. The simulated motion and all inputs (such as pilot controls and wind) are recorded and constitute the truth reference for the definition of simulated navigation method output errors. The second step of simulated navigation input generation uses the truth data to compute simulated measurement data of the sensors available to the navigation method.

Using simulated input data for the inertial motion model requires a high level of kinematic consistency of accelerations and angular rates with the simulated true motion. Only if the simulated truth motion trajectory satisfies the inertial quality requirement it is possible to strictly relate the output errors observed in simulation to errors in navigation [87]. High fidelity of the simulation environment is required for the evaluation of aerodynamic flight navigation – including models for dynamic atmosphere and flight dynamics.

Method evaluation in simulation allows controlling all input errors affecting the navigation method. This includes the case where all errors are disabled. In this case, the navigation method output should be near perfect in order to verify method implementation. Only after this initial verification of simulation tool and navigation method implementation can input errors be accounted for in order to predict navigation method behavior and accuracy in a real application. This requires that all relevant input errors present in a real application are included in the simulation. Furthermore, in order to attain meaningful results for method behavior and performance, all error models must be sufficiently accurate and represent at least the most influential error effects.

This simulation tool is used in two ways in this work. First, single simulation runs of the navigation method under test using input data generated from a single truth motion trajectory allow for a detailed assessment of method behavior. Monte Carlo evaluation (MCE) is based on a large number of simulation runs and allows for a statistically significant assessment of method performance.

Simulation evaluation is continuously applied to the preliminary navigation methods developed in this work. This not only affirms gradual improvement in performance but also is crucial for identification of method shortcomings. The simulation tool is specifically designed to account for a wide range of operational conditions for the navigation method. In many cases for the preliminary methods, a lack of robustness in special operational conditions is discovered.

The proposed aerodynamic navigation method is thoroughly evaluated with this simulation tool with respect to accuracy and robustness. Due to the high fidelity of the simulation framework and the large number of different missions and operational conditions considered in the extensive Monte Carlo evaluation, a meaningful result is presented. In addition to

Monte Carlo evaluation, the proposed aerodynamic navigation method is directly applied to real flight data, without any modifications to the method. This demonstrates the maturity of the new method.

4.1 SIMULATION FRAMEWORK

For practical judgement of improvement or deterioration of method performance related to changes in its design, Monte Carlo evaluation (MCE) is employed throughout method development. This section first presents the simulated truth flight data used in the assessment of developed aerodynamic navigation methods. The following subsections describe the flight simulation needed to create this data consisting of a flight autopilot for the aerodynamic motion model and models for dynamic atmosphere processes. The last two subsections discuss models for input error generation for sensor measurements and the aerodynamic model coefficients.

4.1.1 Evaluation of preliminary flight navigation methods

For the evaluation of preliminary methods a different set of truth flight data files is used than in the final assessment of performance and robustness in section 4.2. The set consists of 100 flights of 1h along roughly the same trajectory in space shown in Figure 17. Each single simulated flight takes place in a unique dynamic atmosphere. The flight data is generated using the waypoint autopilot presented in the following subsection.

Due to different wind velocity and wind rates time histories, the simulated truth flight path, rotational motion and control inputs vary for every run. Additionally, the length of the flight path or the time when a certain maneuver is flown is not the same for any two Monte Carlo runs. Besides precise evaluation of single simulation runs, only high level performance measures can therefore be studied in ensemble results in Monte Carlo evaluation. Since it is not intended to weight navigation performance requirements for specific instances along the trajectory (e.g. dynamic/stationary), the total variability of the flight process may simply be included when determining worst, typical or some percentile navigation performance (e.g. horizontal position errors) over the flight time of 3600s.

For every simulation run of Monte Carlo evaluation, sensor errors and navigation initial guess errors are generated randomly, including the errors of coefficients of the vehicle dynamics model used for navigation as well as weight and balance errors. The details of how the representative uncertainty model for all vehicle dynamics model information is generated can be found in 4.1.5. It will be assumed that the VDM used for navigation is of good quality achievable with state of the art methods of system identification.

Wind drift from integrating true wind velocity vector \mathbf{v}_{Wn} for the complete flight duration of 3600s is $\sim 12NM/h$ 2drms or better than 5.3NM/h for the best 50% and better than 2.1NM/h for the best 10% for this set of flights. For comparison with the performance of the simulated navigation methods, the statistics of integrated wind velocity error given an exact initial guess at time $t_0 = 900s$ are shown in Figure 19. The initial guess of wind velocity vector is set to decay exponentially with a time constant of 400s.

4.1.2 Trajectory generation

For Monte Carlo evaluation of aerodynamic flight navigation methods, a large number of simulated flights is required, accounting for the variety of atmospheric conditions that affect aerodynamic motion. For this reason a waypoint flight autopilot was developed and presented in [87]. This trajectory generation tool allows to quickly create a large number of simulated flights along a predefined waypoint path, under varying atmospheric conditions.

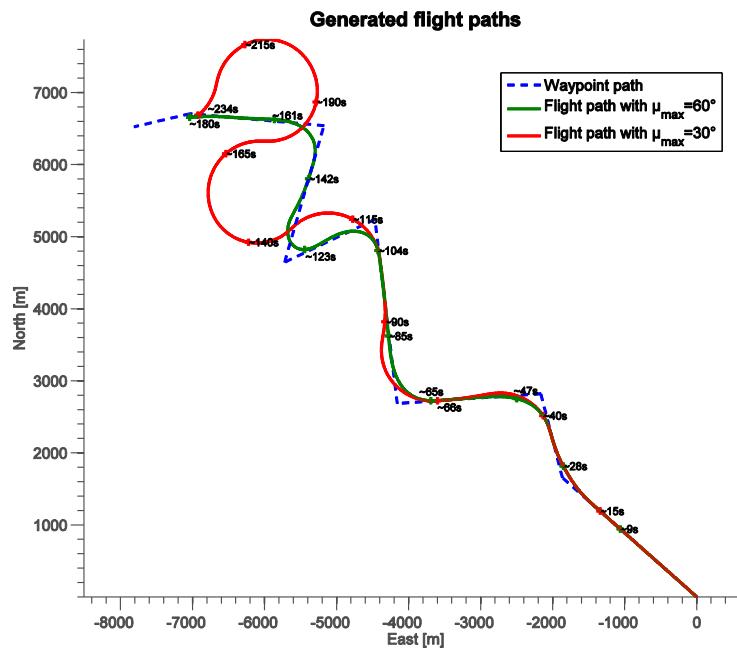


Figure 20: Flight paths generated for kinematic bank angle limits of 60° and 30° (from [87])

The trajectory generation tool creates truth motion data with high kinematic consistency that satisfies the inertial quality requirement [87]. Furthermore, the truth motion can be exactly computed by the aerodynamic navigation method if model coefficient and generated input errors are zero in an ideal simulation. In this work, only one aerodynamic motion model is used as truth model in the trajectory generation process. Uncertainty in the aerodynamic model available for the aerodynamic flight navigation method is accounted for by random model coefficient errors, see section 4.1.5.

The waypoint autopilot tool is used to create the four different sets of flight data used for Monte Carlo evaluation presented in sections 4.1.2, 4.1.5.1, 4.2.1 and 4.2.2. For evaluation of the robustness of the desensitized aerodynamic navigation method in 4.2.2 an additional truth flight trajectory is used created by manually piloted simulated flight.

4.1.3 Dynamic atmosphere models

In this work a statistical model for local (i.e. at aircraft position) wind velocity vector written in NED coordinates \mathbf{v}_{Wn} is used. This model was developed in [88] based on airliner flight measurement data below $10000ft$. It has previously been used for similar purpose in [19] to describe random variations of wind velocity vector during $1h$ of flight using Gauß-Markov statistical models for wind velocity in North and East directions. The implementation is based on the model presented in [19]

$$\dot{v}_{WN} = -\frac{1}{T_W}v_{WN} + n_{WN}$$

$$\dot{v}_{WE} = -\frac{1}{T_W}v_{WE} + n_{WE}$$

The correlation time coefficient is $T_W = 400s$. n_{WN} and n_{WE} are driving white noise processes with zero mean and noise density $5m/s \cdot \sqrt{\frac{2}{T_W}}$.

A reduced value of $1m/s \cdot \sqrt{\frac{2}{T_W}}$ is used in this work for simulated flight in calm atmosphere. Additionally, the following model for the Down component of wind velocity vector is used in this work

$$\dot{v}_{WD} = -\frac{1}{T_W}v_{WD} + n_{WD}$$

With again $T_W = 400s$ and a smaller noise density for the zero mean white noise process n_{WD} of $1m/s \cdot \sqrt{\frac{2}{T_W}}$, or $0.1m/s \cdot \sqrt{\frac{2}{T_W}}$ for simulated flight in calm atmosphere.

The models above are used both for simulation purposes, i.e. to generate dynamic wind velocity vector time histories in the generation process of aerodynamic flight trajectories, and as basis for augmented filter state uncertainty models for use in model fusion (c.f. appendix A.8 for filter augmentation). Additionally, simple trigonometric stochastic gust models are used to generate a number of vertical and horizontal random discrete gusts in aerodynamic flight simulations. Gust velocities are superimposed with dynamic wind velocity vector \mathbf{v}_{Wn} in trajectory generation.

To account for rough atmosphere conditions in the generation of aerodynamic flight trajectories, the Dryden turbulence model is used in this work [89, 90]. The implementation corresponds to MATLAB/Simulink® release 2014b block "Dryden Wind Turbulence Model (+q +r)" [91], according to specifications in standard [90]. Wind speed at $6m$ is $15m/s$ in direction 0° and turbulence scale length for medium and high altitudes is $533.4m$. The Dryden turbulence model outputs both high frequency wind velocity disturbances that will be superimposed with \mathbf{v}_{Wn} and wind angular rates $\boldsymbol{\omega}_{Wb}$. Various levels of intensity and corresponding probabilities of exceedance are defined [90, 91]. See Figure 46 and Figure 47 for examples of wind velocity vector and wind rates in severe turbulence simulated for robustness evaluation of the proposed aerodynamic navigation method.

If not noted otherwise, the level of turbulence intensity in simulations of aerodynamic flight in this work will vary randomly according to the specified statistics (probability of exceedance

of a certain level of turbulence). This random variation is implemented by switching to higher turbulence level when a first order Gauß-Markov process with a time correlation coefficient of $500s$ exceeds a specified threshold value.

This implementation aims at generating short patches of strong turbulence during standard $1h$ simulations. That way, the variability of atmosphere conditions encountered in real airplane flight is realistically accounted for. The continuous change of level of turbulence in the simulations of aerodynamic flight in this work constitutes a challenge to aerodynamic navigation methods. It furthermore avoids that the developed aerodynamic navigation methods are specialized to work in a single atmospheric condition only.

4.1.4 Sensor error models

For all sensor measurements available to the aerodynamic navigation method, error models are implemented. This includes IMU consisting of accelerometer and gyroscope triads, barometric altimeter, airspeed probe, 3-D magnetometer and control deflection and throttle setting sensors.

White and flicker power-law noise [83] is used in all measurement models, see Figure 21 - Figure 23. The influence of barometric altitude and airspeed measurement errors on the desensitized aerodynamic navigation method is very limited. Therefore, approximate and conservative error models were used for these sensor measurements. Although errors in the aerodynamic model control inputs can have significant influence on navigation method performance, this is specifically the case for constant or slowly-varying components of error. Constant control input errors are equivalent to error in the aerodynamic model control derivatives. Because this error is already accounted for by the aerodynamic coefficients uncertainty model presented in 4.1.5., the control inputs measurement error model can be considered insignificant.

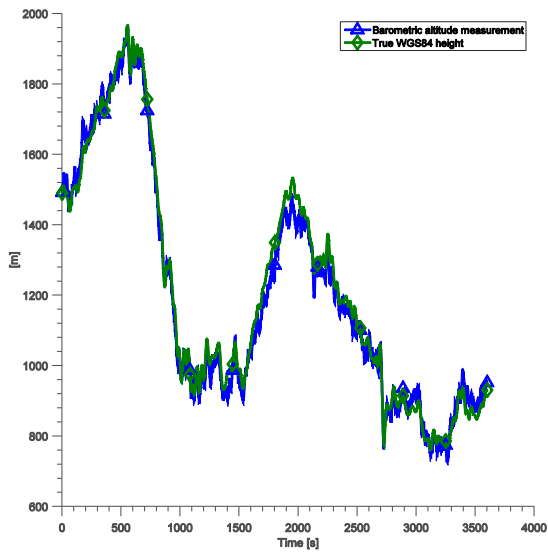
The 3-D magnetometer error model is implemented according to the specifications for a commercially available low-cost sensor, see Figure 23. Although errors in the magnetometer measurement due to distortions in the environmental magnetic field can be significant and threaten the robustness of optimal filter navigation methods, they are not accounted for in simulation. For the desensitized aerodynamic navigation method, only accuracy is affected by large magnetic field measurement errors. Because of the transient character of these disturbances and the first order position error growth for the proposed navigation method, the effect on accuracy is negligible.

The IMU measurement error model corresponds to the model described in [83]. IMU errors are defined in three levels of quality, see Table 4. In simulation, only in-run errors are accounted for by the inertial sensors measurement model. Initial errors (i.e. switch-on) are considered as errors of navigation system initial guess only.

IMU	Low quality	Medium quality	High quality
Gyro bias* and noise	10°/h, 0.3°/sqrt(h)	1°/h, 0.3°/sqrt(h)	0.1°/h, 0.1°/sqrt(h)
SF and misalignment	1500ppm, 1mrad	500ppm, 1mrad	100ppm, 0.1mrad
Accel. bias* and noise	100µg, 29µg/sqrt(Hz)	100µg, 29µg/sqrt(Hz)	10µg, 50µg/sqrt(Hz)
SF and misalignment	1000ppm, 0.5mrad	500ppm, 0.5mrad	500ppm, 0.3mrad

Table 4: IMU qualities. All values except noise are RMS of flicker noise processes. SF processes are low pass filtered at 0.001Hz.

* Total operational in run variability



5

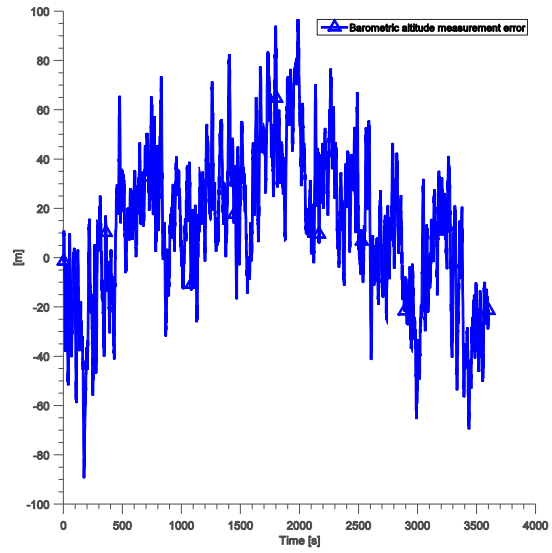


Figure 21: Barometric altitude measurement model

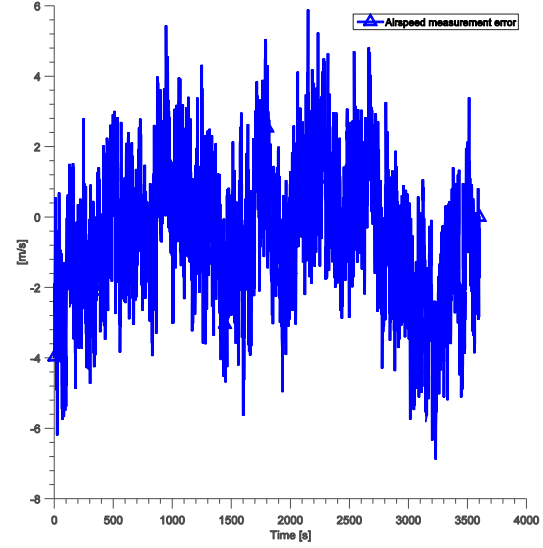
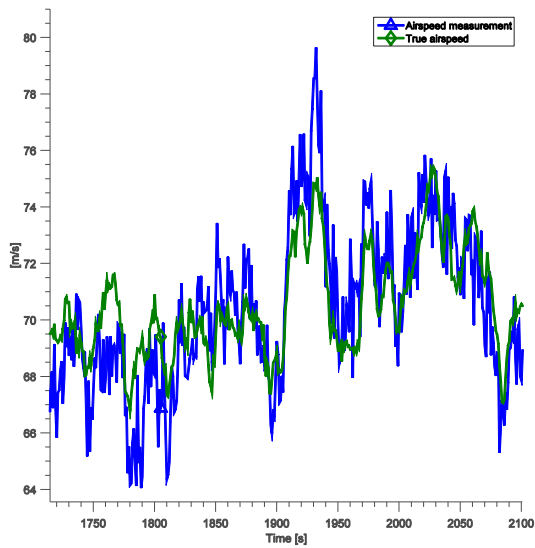


Figure 22: Airspeed measurement model

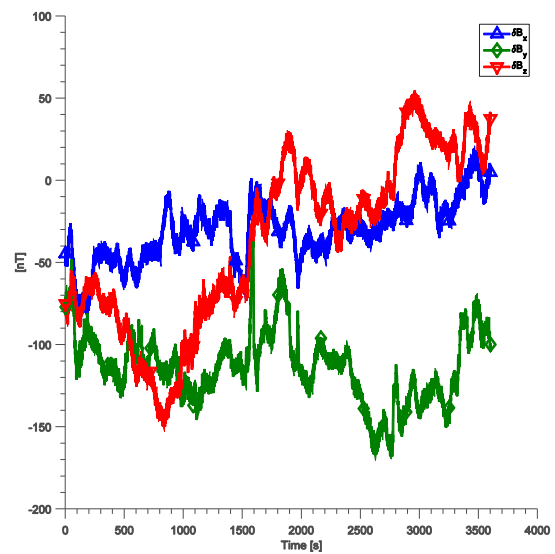
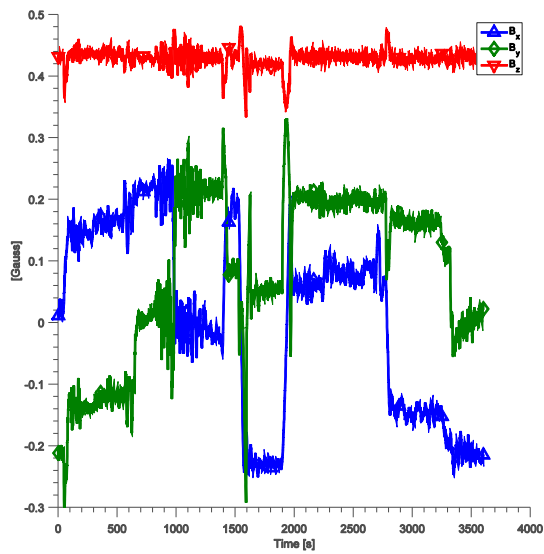


Figure 23: 3-D magnetometer measurement model

4.1.5 Aerodynamic model uncertainty

In previous studies of navigation methods aided by models of fixed wing aircraft [9, 92, 93], very basic means to account for the difference between true flight process and computation model were applied. Uncertainty models are needed for this research in two ways: first in the design of the estimation method, second to generate realistic errors in evaluation of the method using a simulation tool. In the known literature, independent random errors of the model coefficients were assumed for both method design and simulation, with error magnitude taken as some percentage of true model coefficient value.

This work aims to make reliable statements on aerodynamic navigation accuracy and robustness. Due to the infinite number of possible combinations of vehicle state and atmosphere condition, a large number of tests is necessary and simulation for Monte Carlo evaluation (MCE) becomes the only viable option to meaningfully assess method performance. In order to account for the effect of model error on computed aerodynamic and propulsion forces in a realistic way in simulation, two detailed uncertainty models for the aerodynamic motion model, one optimistic and one conservative, are presented in this subsection. In the definition of these uncertainty models, it is assumed that the vehicle dynamics model is created using system identification methods based on flight test data [48].

In case of system identification, where the model is estimated based on time histories of a limited number of in-flight measurements, model coefficients are generally observed in combinations. Consequently, errors in coefficient estimates are correlated, depending on the choice of vehicle model parametrization (i.e. the definition of model coefficients). This correlation of errors reflects that although the estimates of individual coefficients are not accurate, the output of a function of coefficients might be estimated with better accuracy in a certain flight envelope. This is for example the case for the estimate of aerodynamic pitch moment derivative with respect to aerodynamic angle of attack $C_{m\alpha}$, which is strongly correlated with the aerodynamic lift aerodynamic angle of attack derivative $C_{L\alpha}$. In combination, the estimated sum of pitch moments in the center of gravity will very accurately match the equilibrium observed in stationary flight at various aerodynamic angles of attack in the flight test data. But individual coefficient estimation errors are larger because they are never perfectly observed independently. Another example is the correlation of errors of the coefficients of aerodynamic parasitic and induced drag for estimation. Especially when using flight data at a single flight condition and lift coefficient C_L , these coefficients will be estimated inaccurately. Still, in combination they will give a good match to observed aerodynamic drag (which, again, is correlated with thrust model error).

This indicates the importance of an uncertainty model for the aerodynamic motion model describing the coefficient error variance and their correlation: Not the individual model coefficient error but rather the final flight dynamics error influences aerodynamic navigation performance. The intention is to define an uncertainty model that will realistically represent achievable model quality depending on the measurement accuracy of flight test instrumentation used for system identification. Additional modeling error stems from the fact that VDM is a low-order approximation of true flight. This type of error is more challenging to realistically account for in method evaluation in simulation. The optimistic VDM uncertainty model will assume all relevant effects are modeled and error only is caused by inaccurate

coefficient estimates. The conservative VDM uncertainty model will also account for low-order approximation error.

In the following, simulation is used to quantify model errors and covariance of errors for the aerodynamic motion model. Simulating all steps of actual system identification would provide the highest level of realism for VDM errors, but would be too complex. Some challenges of real system identification can be easily bypassed in simulation: Choice of initial guess and model parametrization, flight envelope grid and model parameter interpolation that usually require system identification expertise, can be left out as will be described later.

Other difficulties can readily be avoided in simulation, such as those involved with data recording, sensor calibration, airplane weight and balance, fuel consumption etc.

4.1.5.1 Simulation for uncertainty model generation

For the simulations used to define the aerodynamic motion uncertainty model, the highly dynamic flight trajectory of approximately 1h duration shown in Figure 24 was created. The single simulated flight data serves as basis for the generation of initial guess and measurement data with random errors for 500 runs of system identification simulation.

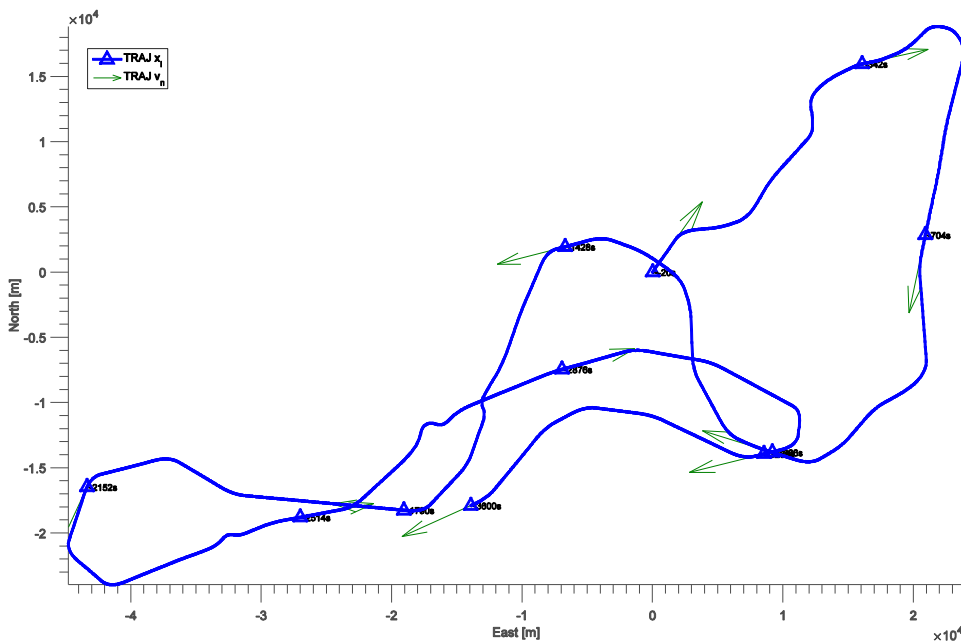


Figure 24: Dynamic flight path for system ID simulations (average kinematic velocity of 70m/s)

A very calm atmosphere was simulated throughout this single flight. The Dryden turbulence model was deactivated, and low intensity dynamic wind velocity vector processes were used (see 4.1.3). Consequently, only very weak atmospheric disturbance due to dynamic wind velocity vector is present, see Figure 25. The dynamic flight covers a large part of the flight envelope of a small general aviation airplane in cruise configuration, see Figure 26 and Figure 27.

To increase vehicle dynamics model coefficient observability, 2 · 3 direct control input maneuvers were included, c.f. Figure 28 and Figure 29. Additionally, at 3 instances time varying angle of sideslip is commanded (c.f. Figure 30).

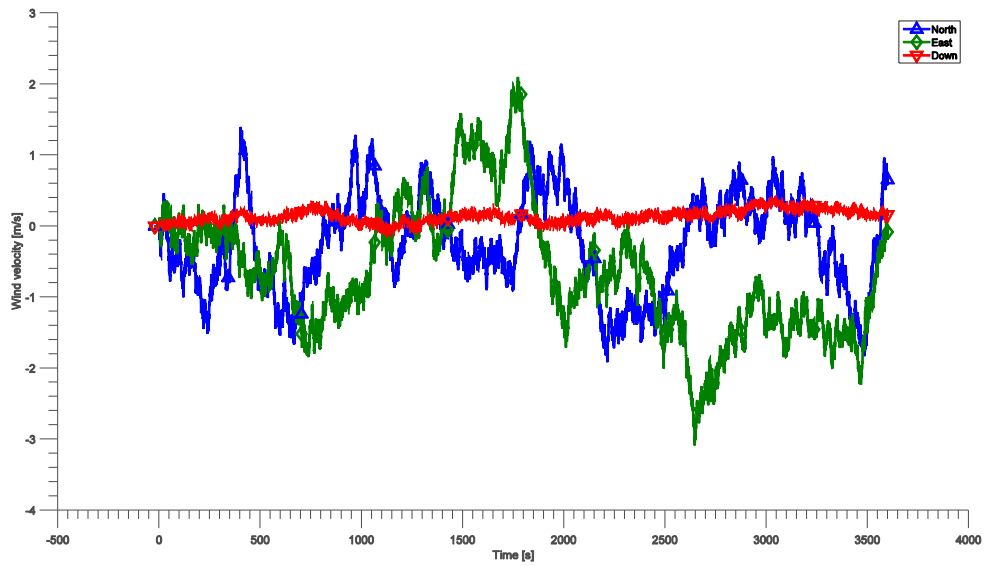


Figure 25: Wind velocity vector

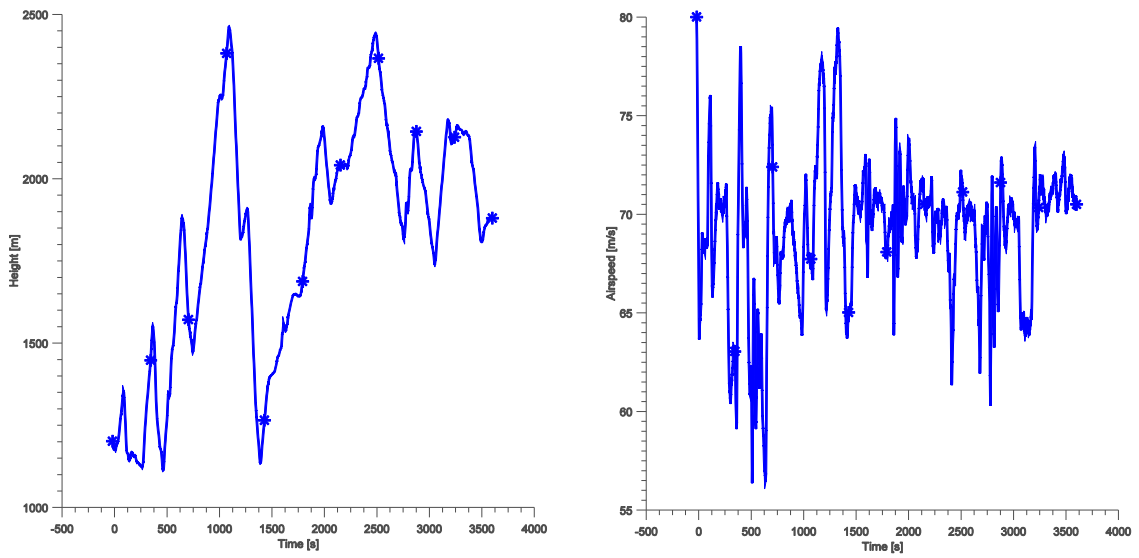


Figure 26: WGS84 height and airspeed

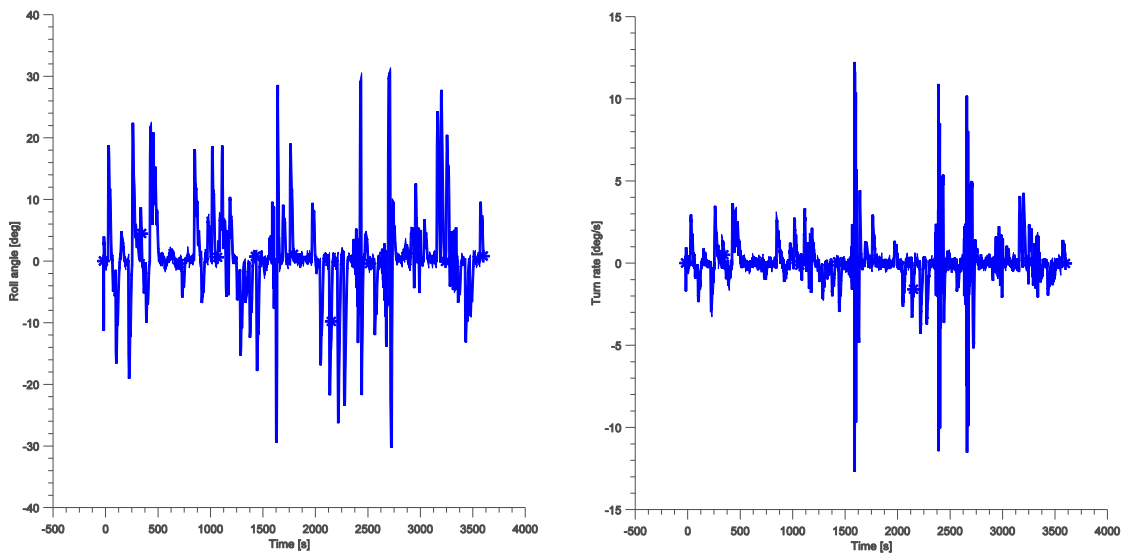


Figure 27: Roll angle and turn rate

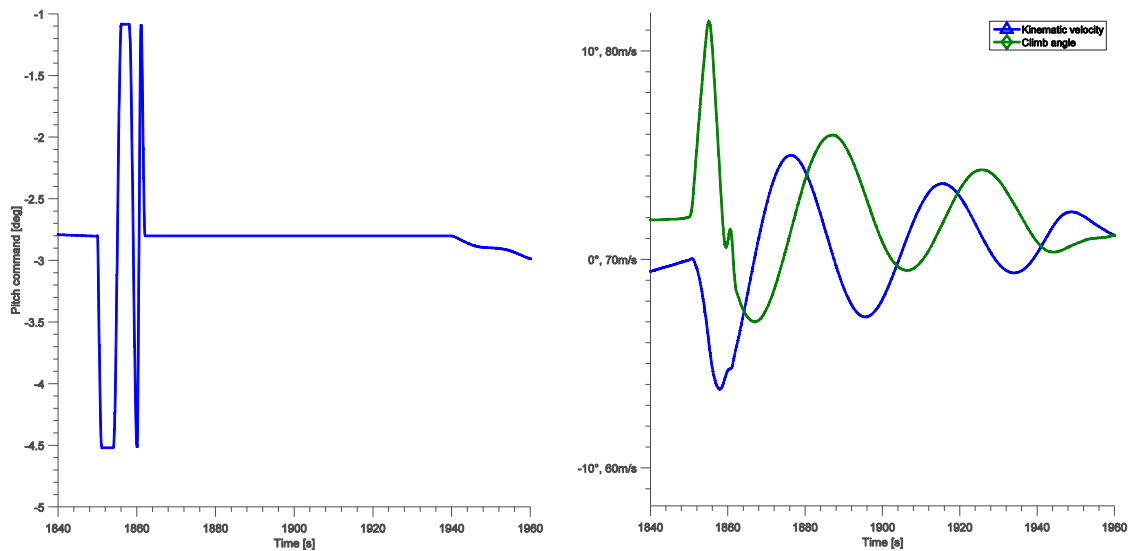


Figure 28: Direct pitch command input and phugoid response (one of three occurrences)

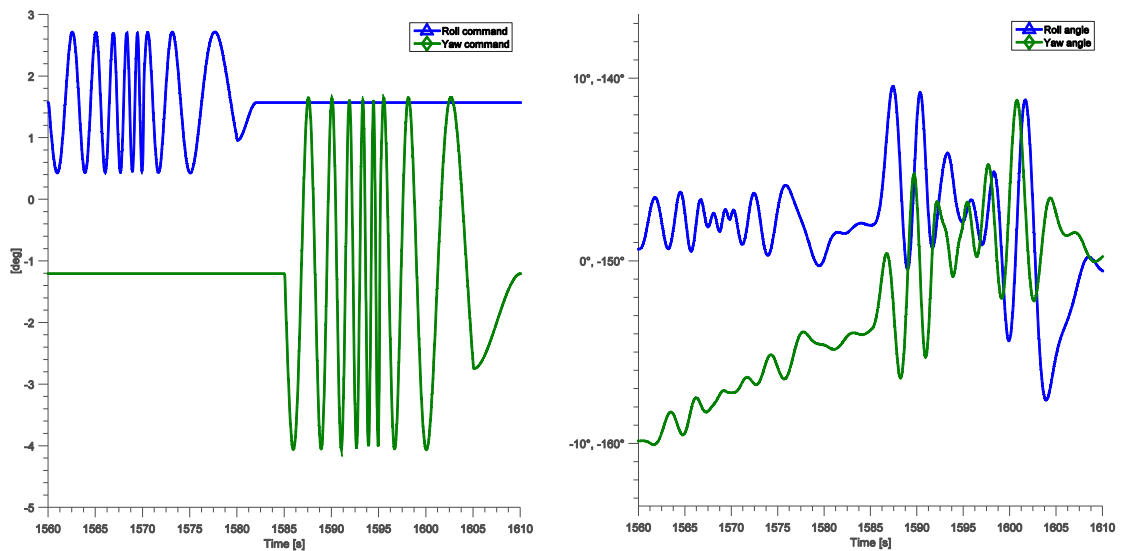


Figure 29: Direct roll and yaw command input and response (one of three occurrences)

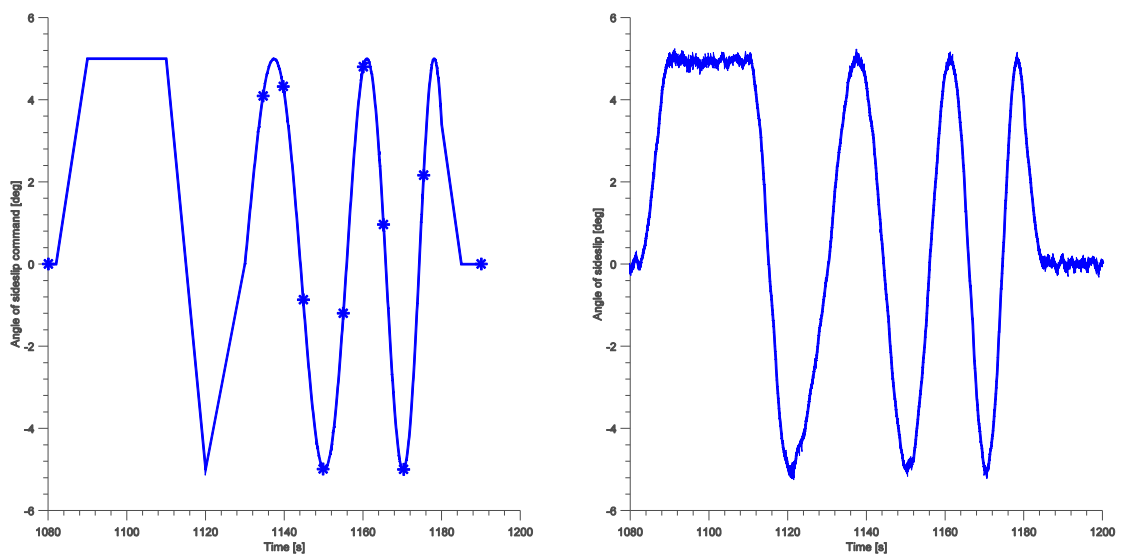


Figure 30: Commanded angle of sideslip and response (one of three occurrences)

4.1.5.2 Weight and balance uncertainty model

In this work, weight and balance is the set of all aircraft properties related to mass and mass distribution. This is total mass m , center of gravity location \mathbf{r}_b^{RG} , moments of inertia I_{xx}, I_{yy}, I_{zz} and products of inertia I_{xy}, I_{xz}, I_{yz} . Due to fuel consumption, all of these quantities change during flight, related to reduction of fuel mass in the (wing) tanks.

To account for the imperfect knowledge of these quantities both in system identification and aerodynamic navigation, a weight and balance uncertainty model is defined. Because an exact fuel consumption model is used in all simulations, this uncertainty model is designed to represent both initial and average uncertainty of weight and balance quantities.

Because variations in mass, center of gravity and inertia generally are not independent, but all related to changes in mass distribution, a simple geometry of uncertain point masses is defined in order to generate consistent errors. Using the standard deviations specified in Table 5, a generic covariance matrix of errors $\delta m, \delta I_{xx}, \delta I_{yy}, \delta I_{zz}, \delta I_{xy}, \delta I_{xz}, \delta I_{yz}, \delta r_x^G, \delta r_y^G, \delta r_z^G$ can be computed.

For a suitable choice of point mass geometry, Cholesky decomposition [94] can be applied to this covariance matrix in order to create consistent random weight and balance errors from a multivariate random distribution.

Point Mass Location	Accurate (System ID)	Normal (Standard flight)
Center	3kg	5kg
Nose luggage	1kg	5kg
Aft luggage	2kg	5kg
Left wing fuel tank	5kg	5kg
Right wing fuel tank	3kg	10kg
Elevator	1kg	1kg
Canopy	1kg	1kg
Left wing tip	1kg	1kg
Left engine	3kg	3kg
Left landing gear	2kg	2kg

Table 5: Point mass uncertainties (standard deviation) for accurate and normal weight and balance uncertainty model

For the simulations of aerodynamics and propulsion model parameter estimation in the remainder of this subsection, an accurate weight and balance uncertainty model given by small point mass uncertainties will be used for estimation filter design and generation of errors.

In all other simulations of aerodynamic flight navigation in this work, the weight and balance uncertainty (and similarly simulated errors) will be assumed to be large, corresponding to the last column in Table 5.

4.1.5.3 Optimistic uncertainty model

This work is not concerned with development or application of actual system identification, which is also not needed for creating an uncertainty model. Only the core part of actual coefficient estimation is simulated, yet in a simplified way using the same extended Kalman filter framework as used for navigation, augmented by model coefficient errors defined below.

Everything else that constitutes the engineering challenges of real system identification is considered in an abstract way only. For the optimistic uncertainty model an accurate model parametrization is assumed that is valid for the complete flight envelope. It is assumed that the resulting nonlinear estimation problem is mastered perfectly, e.g. by linearization, ideal local model identification and ideal interpolation of locally valid linear models.

To create this uncertainty model, model parameter estimation with the augmented navigation filter is conducted in simulation, but only significant linear aerodynamic and propulsion coefficients are chosen to be estimated. All higher order effects present in the truth model used for flight test trajectory generation are perfectly known.

For the computation of vehicle forces and moments the functions $\mathbf{F}_{b\ Aero}^A$, $\mathbf{M}_{b\ Aero}^G$, $\mathbf{F}_{b\ Prop}^P$ and $\mathbf{M}_{b\ Prop}^G$ are used, each implemented in the form

$$\mathbf{F}_{b\ Aero}^A = \mathbf{F}_{b\ Aero,ideal}^A + \Delta\mathbf{F}_{b\ Aero}^A \quad (4-1)$$

where $\mathbf{F}_{b\ Aero,ideal}^A$ is exactly the function used in the generation of the flight trajectory and the “ Δ -model” is implemented as function of the “ Δ -coefficients” to be estimated

$$\mathbf{c}_v = [\Delta C_{D0}, \Delta k, \Delta C_{Y0}, \Delta C_{Y\beta}, \Delta C_{L0}, \Delta C_{L\alpha}, \Delta C_{L0}, \Delta C_{L\beta}, \Delta C_{lp}, \Delta C_{lr}, \Delta C_{l\xi}, \Delta C_{m0}, \Delta C_{m\alpha}, \Delta C_{mq}, \Delta C_{m\eta}, \Delta C_{n0}, \Delta C_{n\beta}, \Delta C_{np}, \Delta C_{nr}, \Delta C_{n\zeta}, \Delta F_{x\ Prop,0}, \Delta F_{x\ Prop,\delta_T}, \Delta M_{x\ Prop,\delta_T}, \Delta M_{z\ Prop,\delta_T}] \quad (4-2)$$

With this compute

$$\Delta C_L = \Delta C_{L0} + \Delta C_{L\alpha}\alpha$$

$$\Delta C_Y = \Delta C_{Y0} + \Delta C_{Y\beta}\beta$$

$$\Delta C_D = \Delta C_{D0} + \Delta k(C_L - C_{L0})^2 + (k + \Delta k)(2(C_L - C_{L0})\Delta C_L + \Delta C_L^2)$$

$$\Delta C_l = \Delta C_{l0} + \Delta C_{l\beta}\beta + \Delta C_{lp}p^* + \Delta C_{lr}r^* + \Delta C_{l\xi}\xi$$

$$\Delta C_m = \Delta C_{m0} + \Delta C_{m\alpha}\alpha + \Delta C_{m\eta}\eta$$

$$\Delta C_n = \Delta C_{n0} + \Delta C_{n\beta}\beta + \Delta C_{np}p^* + \Delta C_{nr}r^* + \Delta C_{n\zeta}\zeta$$

Aerodynamic forces and moments

$$\Delta\mathbf{F}_{b\ Aero}^A = qS_{ref}\mathbf{R}_{ab}^T \begin{bmatrix} -\Delta C_D \\ \Delta C_Y \\ -\Delta C_L \end{bmatrix}$$

and

$$\Delta \mathbf{M}_{b_{Aero}}^G = q S_{ref} \mathbf{R}_{ab}^T \begin{bmatrix} b \Delta C_l \\ \bar{c} \Delta C_m \\ b \Delta C_n \end{bmatrix} + \mathbf{r}_b^{GA} \times \Delta \mathbf{F}_{b_{Aero}}^A - \Delta \mathbf{r}_b^G \times \left(q S_{ref} \mathbf{R}_{ab}^T \begin{bmatrix} -C_D - \Delta C_D \\ C_Y + \Delta C_Y \\ -C_L - \Delta C_L \end{bmatrix} \right)$$

And propulsion forces and moments (for a two-engine airplane)

$$\Delta F_{x_{Prop,Left}} = \Delta F_{x_{Prop,0}} + \Delta F_{x_{Prop,\delta_T}} \delta_{T,Left}$$

$$\Delta F_{x_{Prop,Right}} = \Delta F_{x_{Prop,0}} + \Delta F_{x_{Prop,\delta_T}} \delta_{T,Right}$$

$$\Delta \mathbf{F}_{b_{Prop}}^P = \left(\Delta F_{x_{Prop,Left}} + \Delta F_{x_{Prop,Right}} \right) \mathbf{e}_1$$

$$\begin{aligned} \Delta \mathbf{M}_{b_{Prop}}^G &= \Delta F_{x_{Prop,Left}} \mathbf{r}_b^{G_{PLeft}} \times \mathbf{e}_1 + \Delta F_{x_{Prop,Right}} \mathbf{r}_b^{G_{PRight}} \times \mathbf{e}_1 - \Delta \mathbf{r}_b^G \times \left(\mathbf{F}_{b_{Prop}}^P + \Delta \mathbf{F}_{b_{Prop}}^P \right) \\ &+ \Delta M_{x_{Prop,\delta_T}} (\delta_{T,Left} + \delta_{T,Right}) \mathbf{e}_1 + \Delta M_{z_{Prop,\delta_T}} (\delta_{T,Left} + \delta_{T,Right}) \mathbf{e}_3 \end{aligned}$$

This “ Δ -model” approach corresponds to system identification using ideal flight test data, where perturbations of state and input from selected linearization point are small. Because the estimation problem is significantly facilitated in this case, convergence of estimation errors (4-2) can easily be achieved, see Figure 31. All true values of the “ Δ -coefficients” c_v are zeros.

Again, building a global model from multiple locally valid, linear models can be left to the hypothetical real case of full system ID. The uncertainty model is given by the resulting coefficient estimation errors of this simulation and the filter covariance matrix for seed 1 and can be applied independent of reference state.

This optimistic uncertainty model represents achievable aerodynamic motion model accuracy from system identification considering flight test sensor and measurement errors, wind estimation inaccuracy and limited coefficient observability. It is assumed that masterly system identification would manage to include any relevant higher order effects in the VDM and could identify them from interpolation of local linear models. This optimistic uncertainty model will be used for assessment for best achievable accuracy and robustness of VDM navigation.

Compared to previous ways to account for VDM error, this approach offers a higher level of realism by considering some of the limitations of real system ID that do not depend on engineering skills. The aerodynamic motion model quality is strongly related to flight instrumentation accuracy available for system identification.

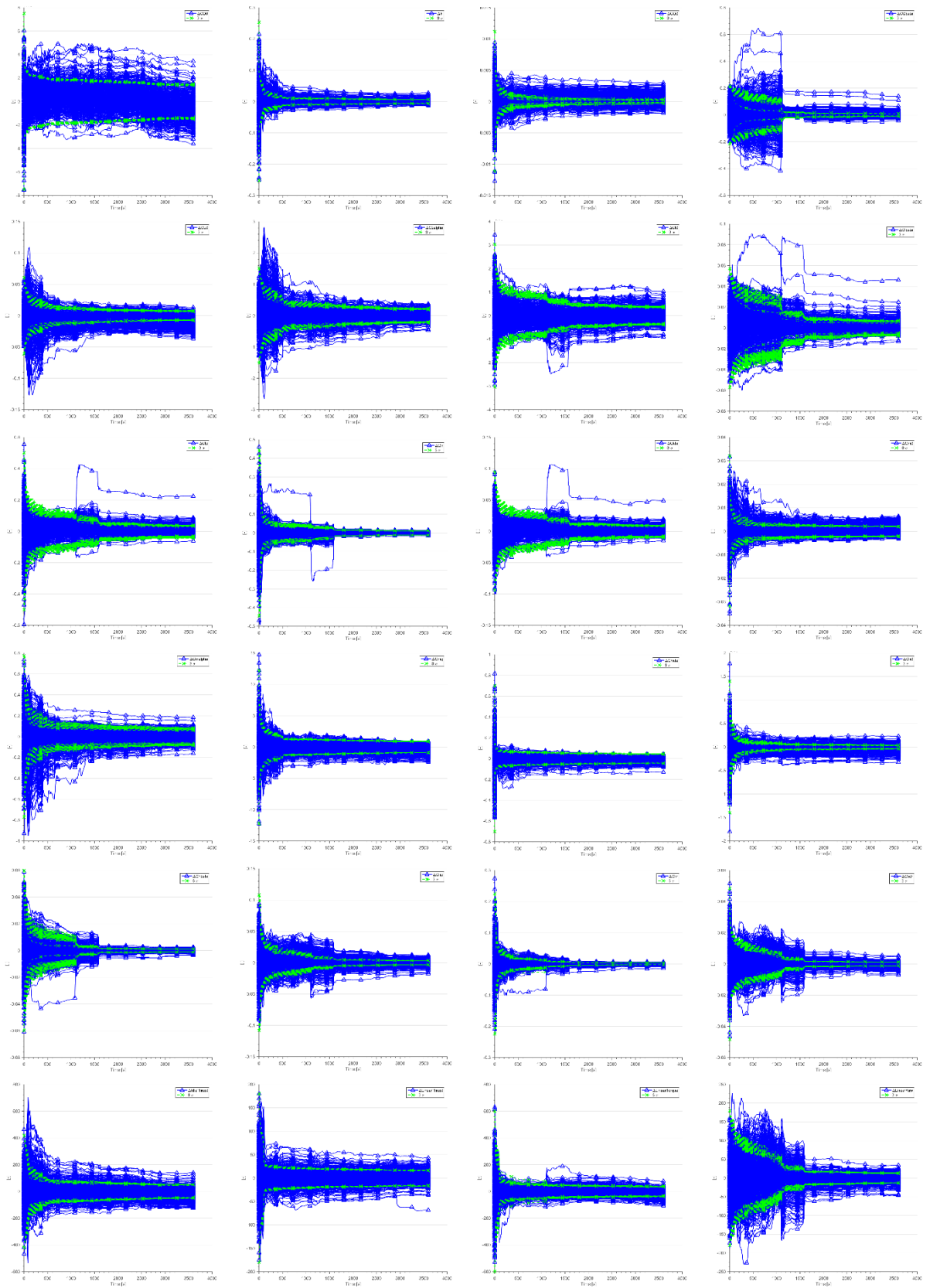


Figure 31: Estimation of "Δ-model" coefficients c_v (500 sample estimates and 3- σ)

4.1.5.4 Conservative uncertainty model

With less optimistic assumptions on how well the system ID is performed to create the aerodynamic motion model used for navigation, a second uncertainty model can be defined, used to evaluate conservative or worst-case performance.

Again, simplified system ID is simulated, but without ideal knowledge of higher order effects present in the truth model used for test flight trajectory simulation. The estimation problem becomes considerably more involved due to large model error.

The exact true model functions in equation (4-1) are replaced by linear approximations

$$\mathbf{F}_{b\ Aero}^A = \mathbf{F}_{b\ Aero,linear}^A + \Delta\mathbf{F}_{b\ Aero}^A$$

with

$$\mathbf{F}_{b\ Aero,linear}^A = qS_{ref}\mathbf{R}_{ab}^T \begin{bmatrix} -(C_{D0} + k(C_L - C_{L0})^2) \\ C_{Y0} + C_{Y\beta}\beta \\ -\underbrace{(C_{L0} + C_{L\alpha}\alpha)}_{C_L} \end{bmatrix}$$

and a similar computation scheme for $\mathbf{M}_{b\ Aero,Linear}^G$ based on the linear aerodynamic coefficients model (2-12). Linear propulsion forces and moments are computed consistent with the corresponding “ Δ -model”

$$F_{xProp,Left} = F_{xProp,0} + F_{xProp,\delta_T}\delta_{T,Left}$$

$$F_{xProp,Right} = F_{xProp,0} + F_{xProp,\delta_T}\delta_{T,Right}$$

$$\mathbf{F}_{b\ Prop}^P = (F_{xProp,Left} + F_{xProp,Right})\mathbf{e}_1$$

$$\begin{aligned} \mathbf{M}_{b\ Prop}^G &= F_{xProp,Left}\mathbf{r}_b^{GPLeft} \times \mathbf{e}_1 + F_{xProp,Right}\mathbf{r}_b^{GPRight} \times \mathbf{e}_1 + M_{xProp,\delta_T}(\delta_{T,Left} + \delta_{T,Right})\mathbf{e}_1 \\ &\quad + M_{zProp,\delta_T}(\delta_{T,Left} + \delta_{T,Right})\mathbf{e}_3 \end{aligned}$$

An approximate guess is used for the constant linear model coefficients. Because the aerodynamic and propulsion models used in the generation of simulated flight paths include significant complex or higher order effects not implemented in the linear model above (or the “ Δ -model” used for corrections), estimation convergence and accuracy are reduced.

This model of VDM uncertainty is less general than the optimistic one, since it depends on the choice of model parametrization. Yet it represents a conservative assumption on VDM quality.

4.2 METHOD EVALUATION IN MONTE CARLO SIMULATION

The proposed aerodynamic navigation method will be assessed in detail in this section. Monte Carlo evaluation (MCE) is the essential tool for testing and verification of complex navigation methods. Although theoretical analysis of inertial navigation has become a powerful tool thanks to the expertise of generations of navigation engineers that could not rely on modern computers (e.g. [51, 53, 54]), it is limited in the effects induced by dynamic vehicle motion it can account for. For low-cost strapdown inertial technology this becomes even more important – for example because of significant scale factor error. For integrated navigation using state estimation techniques, the importance of dynamic vehicle motion for system behavior and performance is further increased due to the dependence of error observability and thus estimation on vehicle motion.

Aerodynamic navigation exhibits several qualities that mandate Monte Carlo evaluation. Aerodynamic motion model error propagation is strongly coupled with vehicle dynamics and analytical approaches are limited to simplified flight conditions (see 2.2.3). The same is true for the modified inertial motion model where horizontal accelerations induce attitude error. Attitude error in turn causes error in the observation of heading error using a 3-D magnetometer measurement.

The advantages of Monte Carlo evaluation make it a perfect completion to the theoretical studies in the previous chapters of this work: The complete navigation method software implementation can be tested, without any simplifications. Realistic vehicle dynamic motion can be simulated in full complexity and in combination with physical realizations of all errors. That way, a large number of combinations of errors and dynamic motion conditions can be evaluated accounting for nonlinearities and possible error rectification. In addition, Monte Carlo evaluation of the navigation method in a realistic simulation framework can be used to assess method robustness. Studying outliers in the results often gives hints to problems and limited robustness of the method implementation under test.

The large number of simulation runs allows for a statistically significant evaluation of navigation method performance. For a GNSS-denied flight navigation method, horizontal position accuracy is decreasing over time and the corresponding statistic should consequently be evaluated as a function of time. Neglecting the weak influence of horizontal position error and initial wind estimate, the changes in the statistics are negligible for a number of other error states, such as aerodynamic velocity vector in body-fixed frame coordinates. Aerodynamic angle of attack and aerodynamic angle of sideslip are of special interest for flight control applications and will be studied in detail with respect to their accuracy.

Finally, the influence of inertial sensors and aerodynamic motion model quality on the proposed aerodynamic navigation method performance will be assessed with Monte Carlo simulations. The new navigation method design is based on a low-cost requirement, and the penalty of using a low-cost IMU instead of more accurate inertial sensor will be evaluated. Similarly, the question whether the requirement for model quality may be relaxed will be addressed.

4.2.1 Position drift

For Monte Carlo evaluation of the final aerodynamic navigation method proposed in this work, a different set of simulated flights is used as truth trajectory than for testing preliminary methods earlier. Figure 32 shows the truth flight path and navigation result for one of a total of 500 simulation runs. The test scenario consists of 15min of initial GNSS-aided navigation followed by a transition and 45min of GNSS-denied aerodynamic navigation.

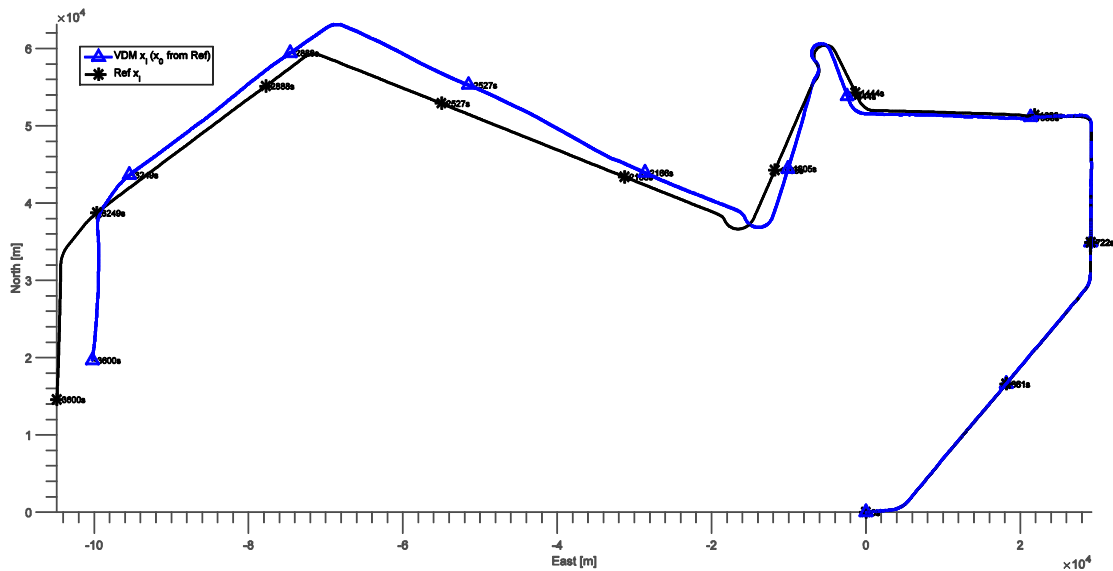


Figure 32: Flight path B for Monte Carlo evaluation and navigation trajectory for run 1

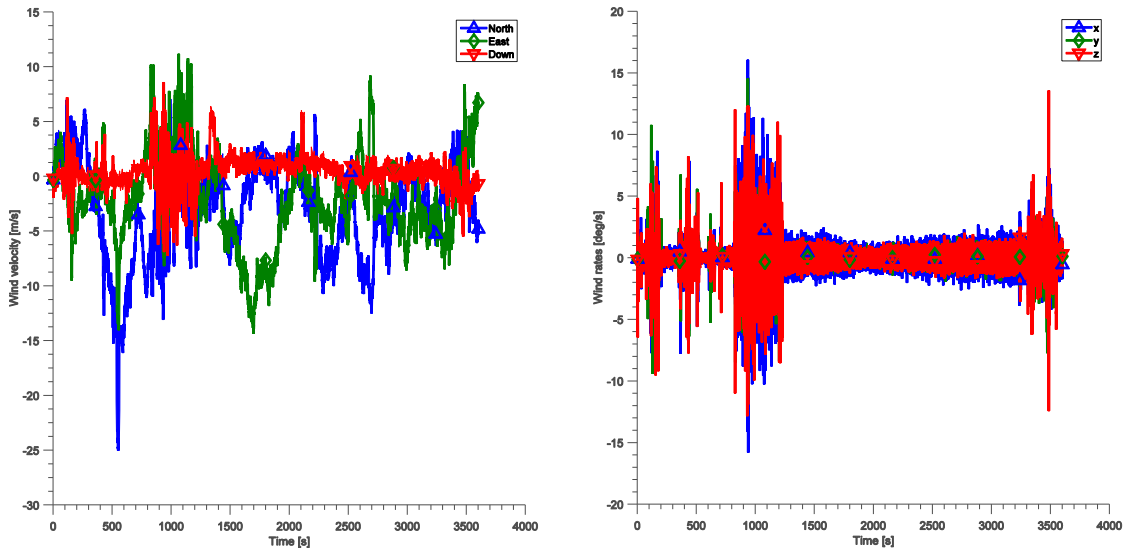


Figure 33: Wind velocity and wind rates vectors (realization for seed 1)

Dynamic atmosphere, including random discrete gusts and turbulence with varying level of intensity (see 4.1.3), is accounted for with a different time history for every simulation run (see Figure 33 for an example). The waypoint autopilot used for fast generation of 500 flight

trajectories along the same predefined waypoint path is intentionally configured to only loosely and slowly counteract perturbations in flight condition and direction. This will introduce a great variability of simulated truth flight process due to random dynamic atmosphere effects. Figure 34 shows the vertical flight path and airplane roll angle time history for the truth trajectory of run 1. In both cases, the effect of strong turbulence (in this simulation run e.g. at $t = 1000s$) and gusts (e.g. approximately at $500s$) is easily discernible.

The results for ideal position drift due to unknown wind velocity only are shown in Figure 35. For evaluation of these statistics, an exact initial guess is set to decay exponentially with a time constant of $400s$ corresponding to the wind model time constant (see 4.1.3).

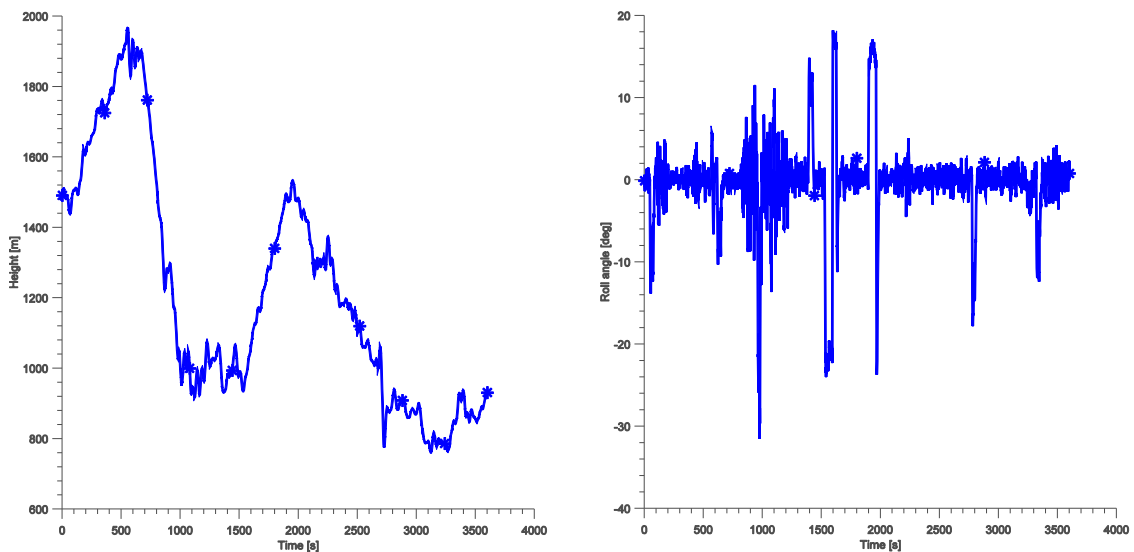


Figure 34: WGS84 height and roll angle (realization for seed 1)

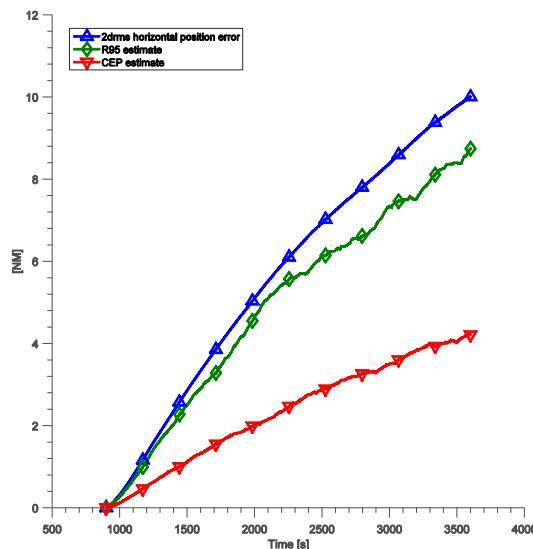


Figure 35: Ideal position error due to wind drift with exact initial guess exponentially decaying with time constant $T = 400s$

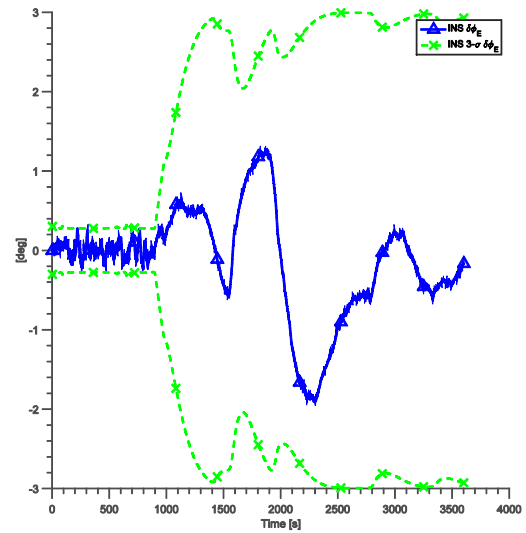
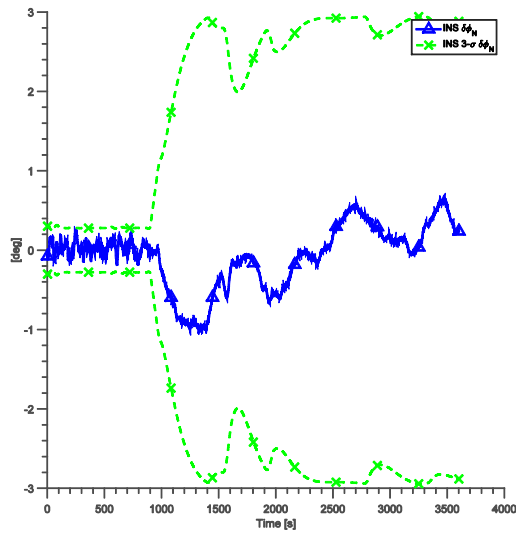


Figure 36: Modified inertial model attitude errors for run 1

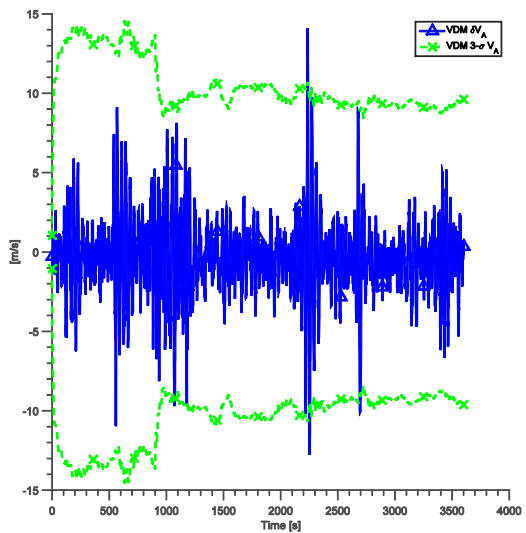
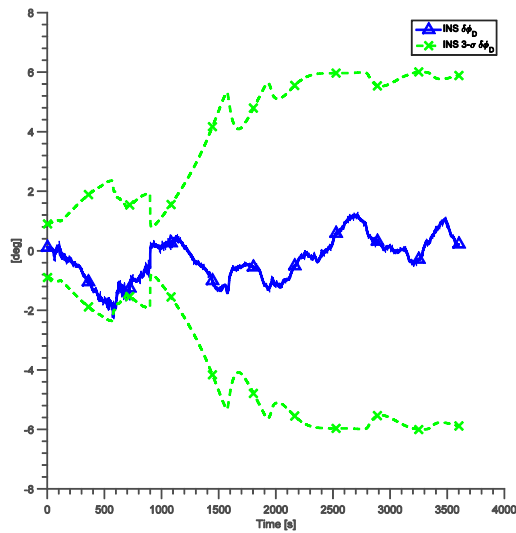


Figure 37: Modified inertial model vertical orientation error for run 1

Figure 38: Aerodynamic model airspeed error for run 1

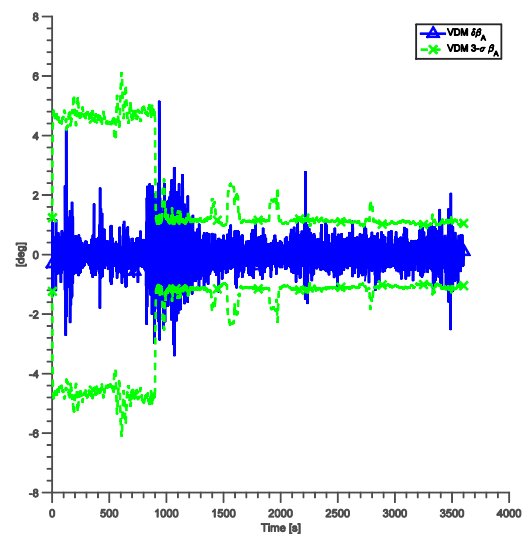
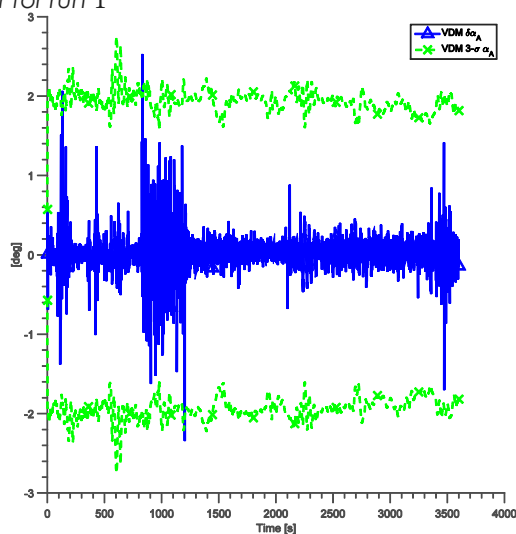


Figure 39: Aerodynamic model aerodynamic angle of attack and angle of sideslip errors for run 1

After selecting a different truth trajectory for every run of Monte Carlo simulation, each perturbed by random atmosphere effects, the navigation state initial guess, sensor measurement and model coefficient errors are accounted for. Model coefficient errors are generated according to the optimistic uncertainty model defined in 4.1.5.3 and 4.1.5.2. Consequently, the randomness of aerodynamic motion model error is accounted for by varying the model used for navigation while the same truth model is used for generation of all trajectories.

Navigation results for a single run of Monte Carlo simulation are shown in Figure 36 - Figure 39. Again, the influence of atmospheric disturbances is visible in the errors of aerodynamic velocity magnitude and aerodynamic angles of attack and sideslip. For the aerodynamic quantities, the change in covariance is due to a change in the wind uncertainty model. Initially, during GNSS-aided navigation, it is optimized for good wind velocity vector estimation. During GNSS-denied aerodynamic navigation in the last 45min of simulation, the wind uncertainty model has no influence on navigation method behavior and is simply set to best represent drift due to slowly-varying wind vector.

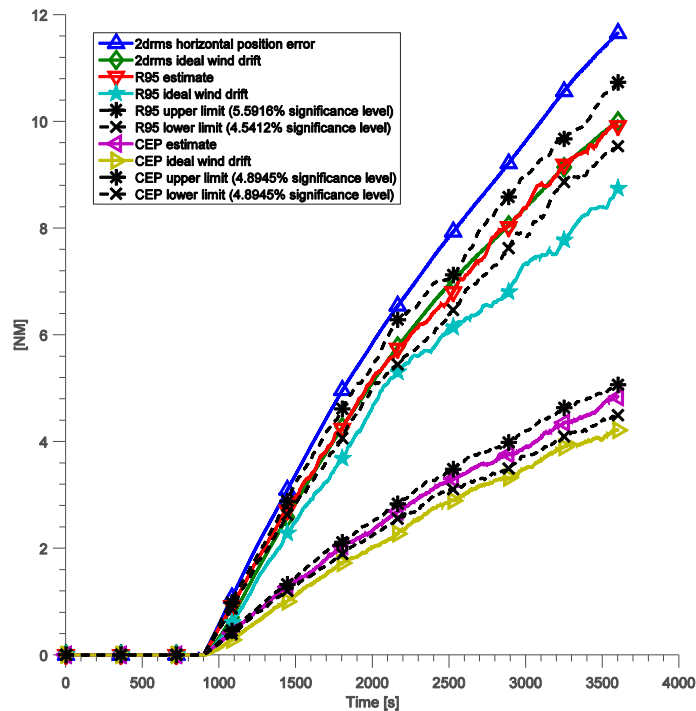


Figure 40: Position drift statistics for 500 runs

Figure 40 shows the statistics of position drift for the desensitized aerodynamic navigation method in 500 Monte Carlo simulation runs. The statistics for ideal wind drift are also included in this figure for comparison, demonstrating the good performance of the aerodynamic position propagation model. Typical position drift performance (CEP) of GNSS-denied aerodynamic flight navigation amounts to $\sim 6.4 \text{ NM/h}$. The 95% radial position accuracy (R95) grows at $\sim 13.21 \text{ NM/h}$ after loss of GNSS aiding.

4.2.2 Velocity and attitude errors

Vertical position and velocity, attitude and heading are computed by the modified inertial navigation model aided by barometric altimeter and 3-D magnetometer. In the covariance-free model integration based on complementary characteristics of inertial and aerodynamic models, the influence of the aerodynamic motion model on modified inertial navigation is very limited. Because the aerodynamic motion model has been found to be indifferent to true vehicle heading, exhibit divergence in lateral motion and only weak stability in vertical motion with possible large trim error, only position and horizontal velocities are used to improve orientation propagation in inertial navigation.

Consequently, the errors in vertical motion and vehicle orientation are mostly determined by errors in inertial, altimeter and magnetometer measurements in combination with errors due to imperfect elimination of horizontal accelerations in the modified inertial model algorithm. Although these are important performance parameters for the proposed aerodynamic navigation method, they are not related to the original research of this work. A detailed evaluation of these errors for a variety of different implementations of modified inertial navigation and measurement errors (e.g. due to environmental disturbances) is therefore omitted. Instead, position drift was evaluated in the previous subsection using the straightforward implementation of modified inertial navigation presented in 2.2.2.3 and sensor errors of a 3-D magnetometer from 4.1.4, therefore giving an impression of achievable performance. This could possibly be improved with more sophisticated elimination of horizontal accelerations in attitude propagation or deteriorated in presence of strong disturbances of the magnetic field measurement.

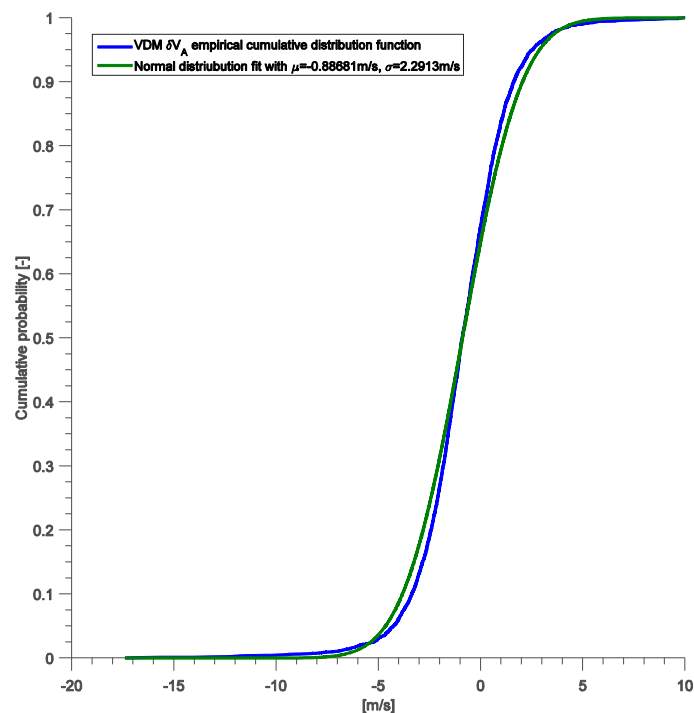


Figure 41: Outlier-prone empirical cumulative distribution (ECDF) of airspeed errors (excess kurtosis of 5.3)

Similarly, the aerodynamic quantities airspeed, angle of attack, angle of sideslip and aerodynamic climb angle are solely determined by the aerodynamic motion model flight dynamics. The aerodynamically desensitized model constraints proposed in 3.2.1 explicitly leave these aerodynamic states unchanged in the complementary covariance-free integration of inertial navigation and aerodynamic model. The aerodynamic errors are determined by the quality of flight dynamics system identification and are very important for the performance of the final aerodynamic navigation method. The optimistic aerodynamic motion uncertainty model proposed in 4.1.5 allows to realistically evaluate the achievable performance if system identification is accomplished very successfully and model quality is only limited by the accuracy of flight test instrumentation and wind estimation. Besides noise-like error, the uncertainty of control input to the aerodynamic motion model is also reflected by model coefficient uncertainties, e.g. of the coefficient determining thrust at zero throttle.

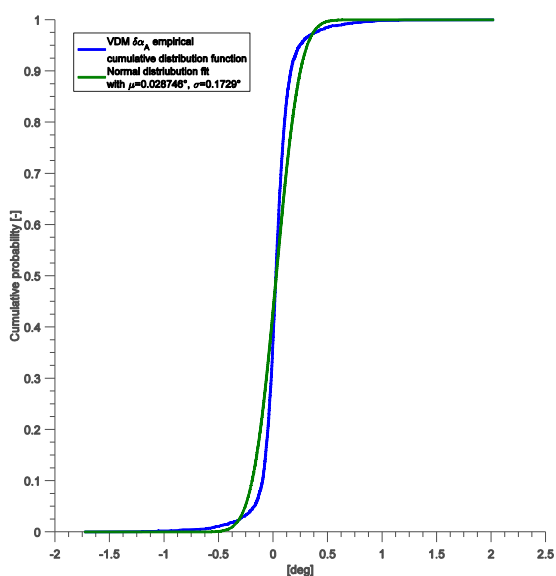


Figure 42: Outlier-prone empirical cumulative distribution (ECDF) of aerodynamic angle of attack errors (excess kurtosis of 18.4)

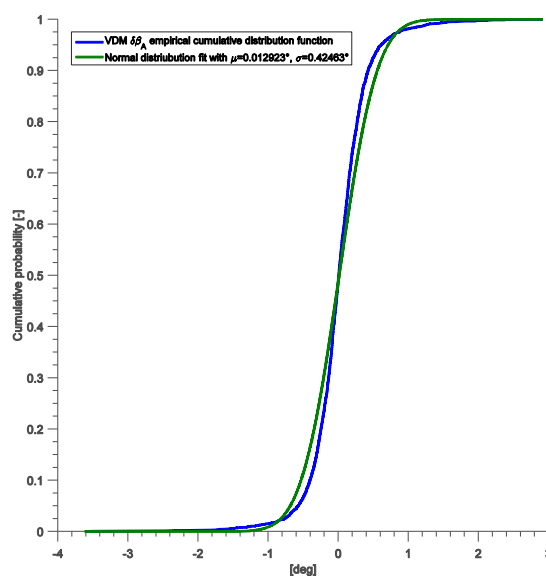


Figure 43: Outlier-prone empirical cumulative distribution (ECDF) of aerodynamic angle of sideslip errors (excess kurtosis of 9.0)

Unlike for position, evaluation of empirical cumulative distribution functions (ECDFs) of errors in airspeed and aerodynamic angles of attack and sideslip is possible assuming stationary statistics. In addition to system errors, statistics shown in Figure 41, Figure 42 and Figure 43 in addition depend on the choice of dynamic atmosphere models used in Monte Carlo simulation, see 4.1.3. High excess values of kurtosis (airspeed 5.3, AOA 18.4 and AOSS 9.0) are proof of the non-Gaussian statistics that are due to the intermittent nature of atmospheric turbulence strongly affecting aerodynamic states.

In the covariance-free integration of inertial navigation and aerodynamic motion model using the aerodynamically desensitized constraints, the aerodynamic states airspeed, angles of attack and sideslip and aerodynamic climb angle are directly determined by model propagation. They are deliberately not corrected or updated otherwise – in contrast to methods based on an optimal filter – which would represent an estimation of aerodynamic states.

4.2.3 Robustness in rough atmosphere

Rough atmosphere conditions have been identified as potential failure causes of aerodynamic navigation methods. Especially state estimation based techniques suffer from low robustness in turbulence depending on the choice of filter tuning parameters. The proposed aerodynamic navigation method is designed to offer a significant improvement in terms of robustness. In the following, the simulations used to assess method robustness and the results for the proposed navigation method will be presented. Four different test cases of 1h duration each are used, one manually piloted flight in sustained moderate turbulence and three realizations of autopiloted flight in severe turbulence for a total of 10% mission time. Similarly to the Monte Carlo evaluation of method accuracy, GNSS-aiding is available for the first 15min of flight, followed by 45min of GNSS-denied navigation.

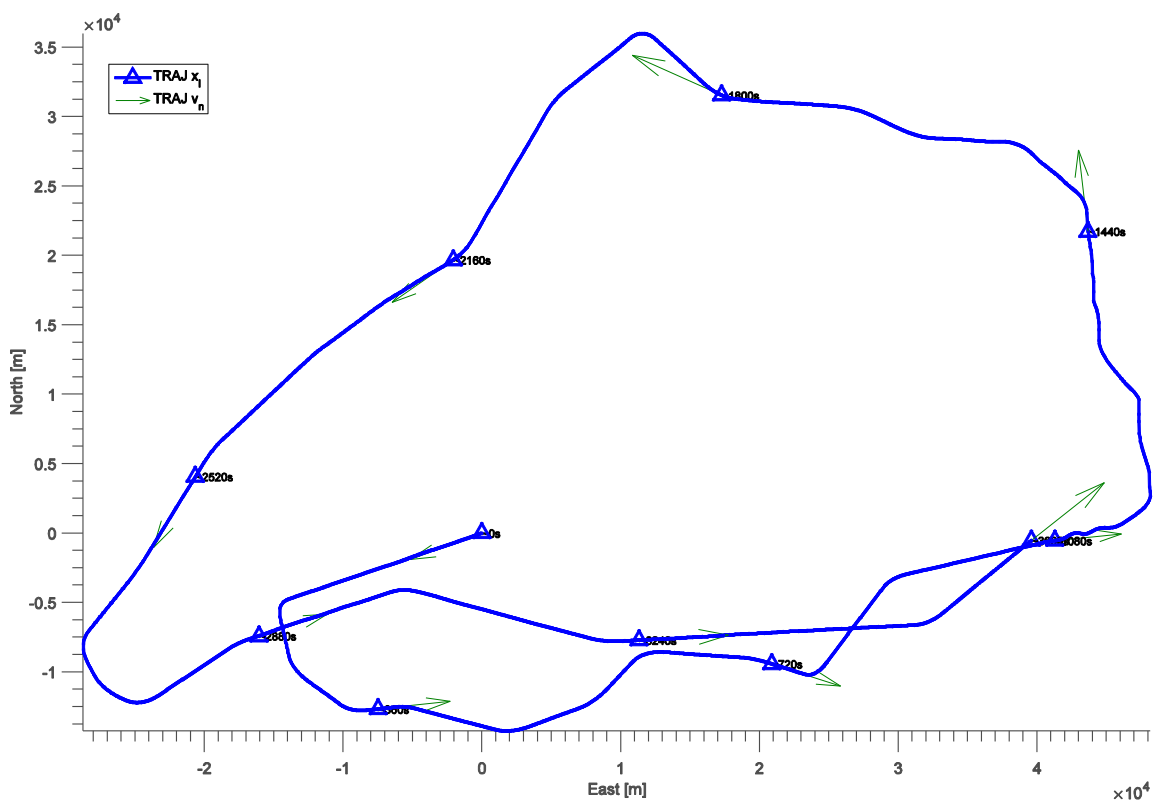


Figure 44: Flight path A for robustness evaluation (one of three realizations)

The three autopiloted flight trajectories are generated using the same list of waypoints as in 4.1.1, see Figure 44. The intensity of atmospheric turbulence smoothly changes according to the implementation described in 4.1.3. Severe turbulence [90] is present for 6min. The probability of exceedance for severe turbulence is specified as 10^{-5} in [90] representing an extreme atmospheric condition. Figure 46 and Figure 47 show the strong fluctuations in wind velocity and rates.

Monte Carlo evaluation is conducted using these three truth trajectories repeatedly in combination with initial and input errors in a total of 100 simulation runs. Figure 48 shows the horizontal navigation position errors for all runs. No single event of navigation failure occurred.

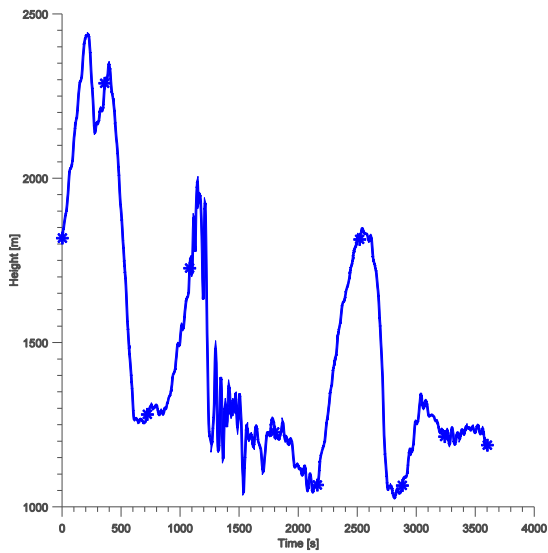


Figure 45: WGS84 height

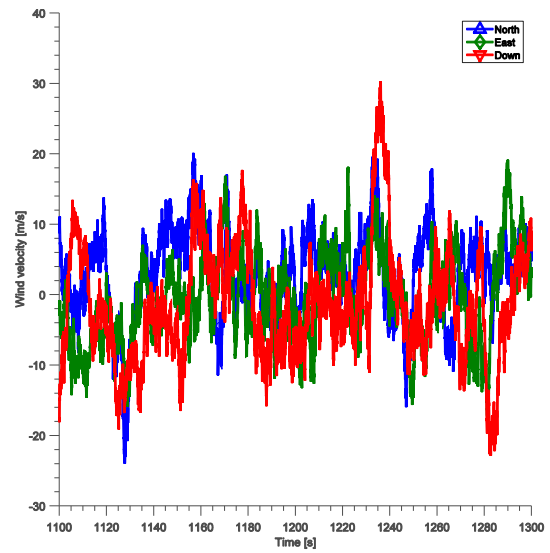


Figure 46: Sample wind velocity vector in severe turbulence

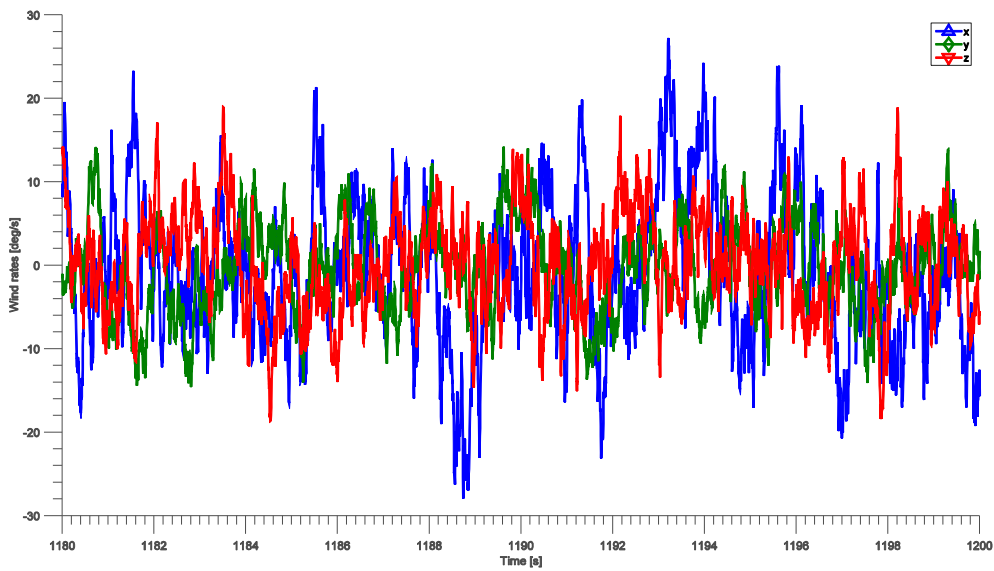


Figure 47: Sample wind rates vector in severe turbulence

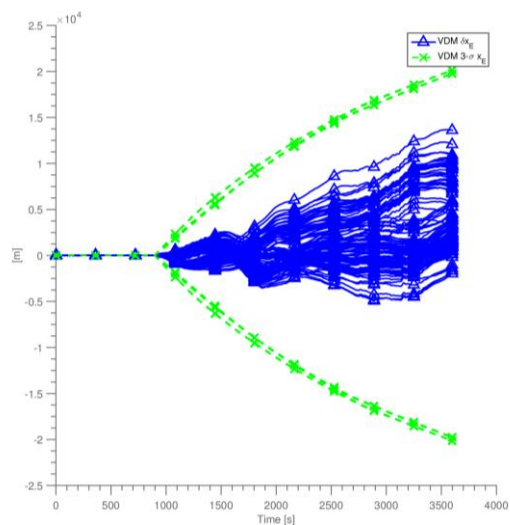
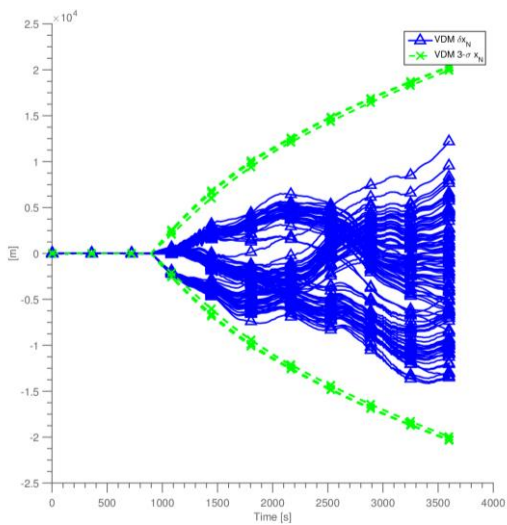


Figure 48: Horizontal position error in flight path A robustness test

In addition to the simulated trajectories created with the waypoint autopilot tool described in 4.1.2, one flight path of 1h duration was created by manually controlling the airplane model, see Figure 49 and Figure 50. For lack of motion cueing, the control inputs do not include any high frequency feedback of atmospheric disturbances. Moderate turbulence (corresponding to a probability of exceedance of 10^{-3} according to [90]) was present throughout. Figure 51 and Figure 52 show samples of the turbulent wind velocity and wind rates vectors.

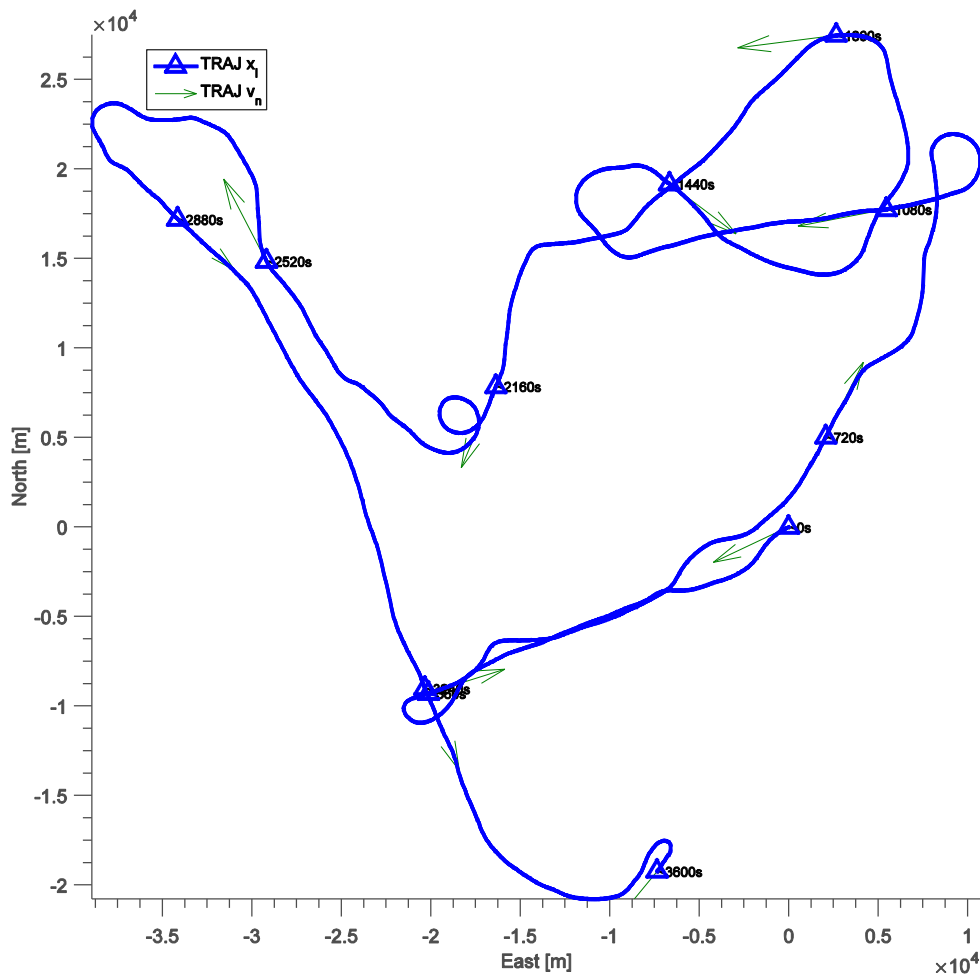


Figure 49: Flight path B for robustness evaluation (manually piloted)

100 Monte Carlo runs are simulated using this truth trajectory in combination with random navigation initial and input errors in order to assess method robustness in sustained moderate turbulence. Figure 53 shows the horizontal position errors for 100 runs. Due to the single dynamic atmosphere truth in this Monte Carlo simulation, the results are clearly biased, which is not an issue in this case. The proposed aerodynamic navigation method showed no restrictions with respect to robustness in this simulation test.

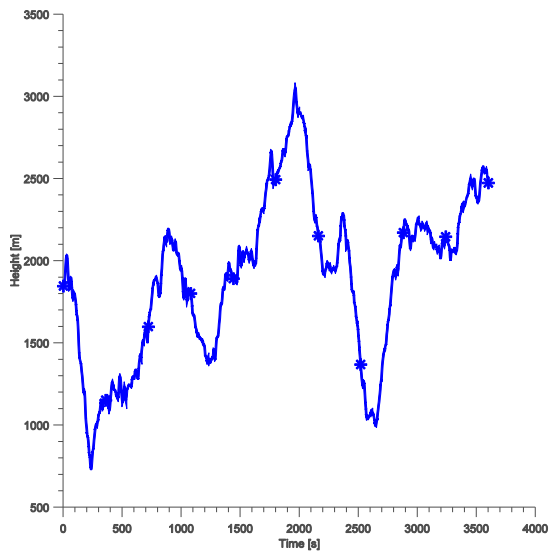


Figure 50: WGS84 height

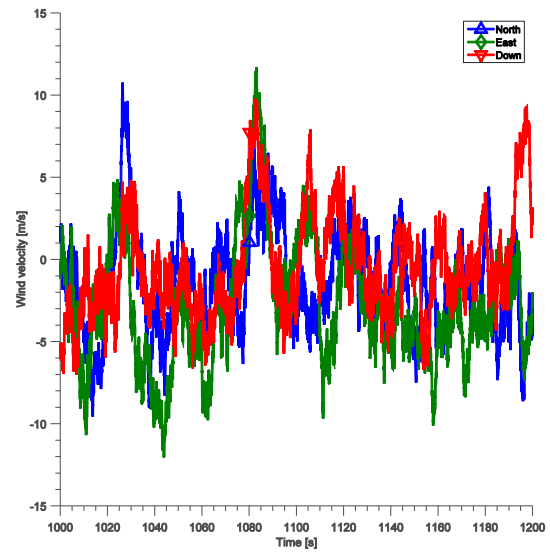


Figure 51: Sample wind velocity vector

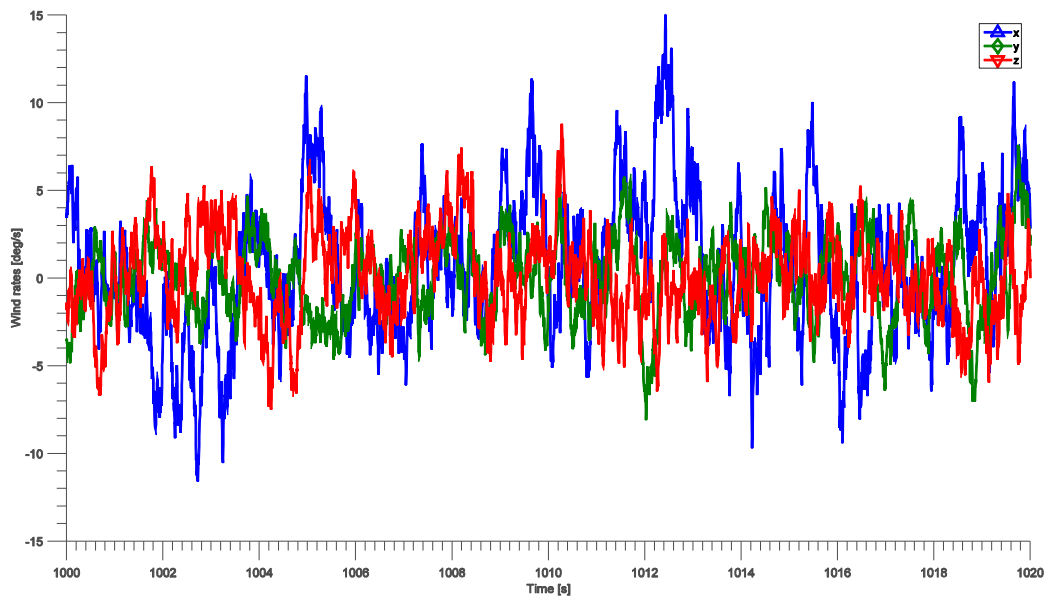


Figure 52: Sample wind rates vector

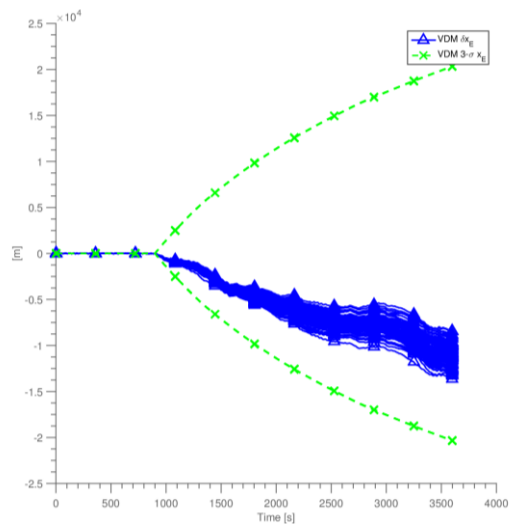
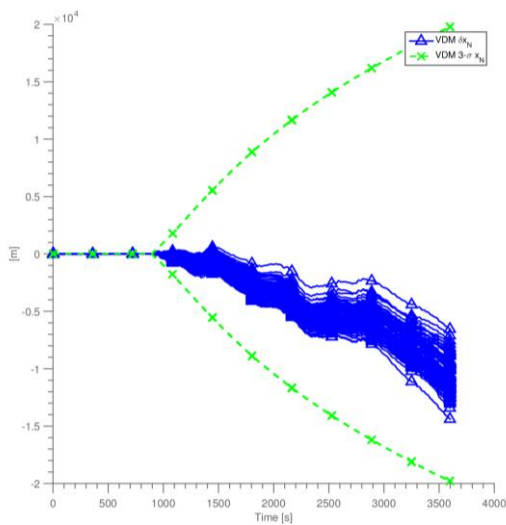


Figure 53: Horizontal position error in manually piloted flight path robustness test

4.2.4 Effect of IMU and aerodynamic model quality on method performance

The aerodynamic navigation method developed in this work is designed to use a combination of low-cost inertial sensors and high-quality aerodynamic motion model. The efficiency of this design will be evaluated in the following by studying the influence of increasing inertial sensor quality or reducing model quality. Although robustness properties of the method are affected by reducing aerodynamic model quality as well, the principal performance measure for this study is position drift.

Figure 54 shows $2drms$ horizontal accuracy for the proposed aerodynamic navigation method in three Monte Carlo simulations (4.1.1) using the different IMU error models in Table 4. Ideal information on wind velocity and rates is available throughout the simulation duration of 3600s. For medium and high quality IMU error models, the horizontal error natural frequency of the modified inertial motion model (3.2.2) can be set to $\omega = \omega_S$ while maintaining damping with aerodynamic model velocities. Attitude errors and, as a consequence of reduced 3-D magnetometer observation error, vertical orientation error are significantly smaller than for the low quality IMU error model.

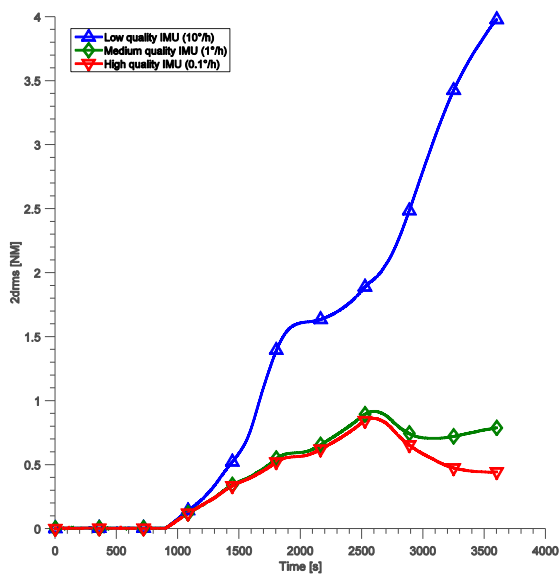


Figure 54: Improvement of position drift with IMU quality, ideal wind information available

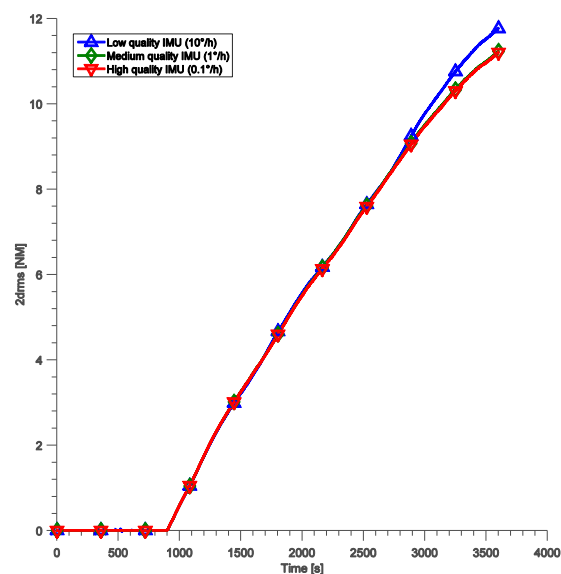


Figure 55: Improvement of position drift with IMU quality, wind initially estimated

Although the aerodynamic motion model is unchanged and the accuracy of initial wind vector estimation during availability of GNSS-aiding not important because of ideal wind information, Figure 54 shows strong improvement of position accuracy with better IMU quality. The improvement is due to the reduction of error in flight direction of the aerodynamic motion model corrected in heading using inertial orientation in equation (3-12).

The strong improvement is only observed in the ideal case with perfect wind information available to the aerodynamic navigation method. Figure 55 shows the results of the same comparison for Monte Carlo simulations with unknown wind velocity and rates using the

models described in 4.1.3. Although accuracy of initial wind estimation depends on IMU quality, the effect on position drift during GNSS-denied navigation is negligible. Consequently, for the expected operation condition with standard unknown wind velocity, the performance of the proposed aerodynamic navigation method is largely independent of IMU quality.

Using the conservative (low quality) aerodynamic motion uncertainty model developed in 4.1.5.4 has only limited effect on method performance. Figure 56 shows $2drms$ horizontal accuracy of aerodynamic navigation in Monte Carlo simulations using the optimistic and conservative model uncertainty variants. Again, ideal wind information is available to the navigation method in this simulation. In Monte Carlo simulations with unknown dynamic atmosphere, no significant difference in performance is observable for different qualities of the aerodynamic model.

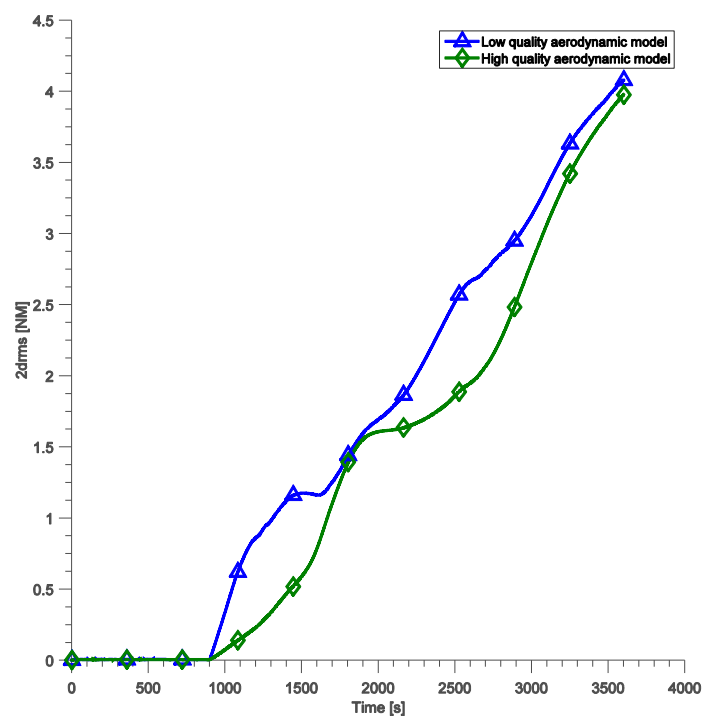


Figure 56: Improvement of position drift with aerodynamic model quality

Consequently, a perfect model is not required for desensitized aerodynamic flight navigation. Simple system identification may be acceptable for the aerodynamic navigation method, if only nominal performance is of interest. It will be sufficient to replicate longitudinal stationary flight for conventional operating flight conditions, which is most important for position drift. But for reliable performance and robustness, a high quality model with large flight envelope and verified accuracy is necessary. The presented aerodynamic navigation method relies on similar benign flight dynamics of the aerodynamic model and the true airplane for safe operation.

4.3 POST PROCESSING OF REAL FLIGHT DATA

Although the simulation tool used in this work was developed specifically to account for limitations of the accuracy of aerodynamic navigation due to model error and input error, not all effects can be modeled adequately. Therefore, a test of the aerodynamic navigation method using real flight data is required to demonstrate that all challenges of a real-world application can be mastered.

Most significantly, the real flight will exhibit a number of complex processes that could not be considered in simulation. This includes airframe deformations and fuel slosh that dynamically influence weight and balance properties. Because the aerodynamic navigation method is applied to a different airplane than the one used for system identification flight testing, scaling and offset of the measured control inputs or surface deflections and throttle setting may differ. While this does not affect stability properties, it will cause error in the aerodynamic model longitudinal trim condition determined by airspeed, climb angle and altitude.

Similarly, the position and orientation of the IMU may differ from the flight test system instrumentation, which will affect the aerodynamic navigation method. Note that the proposed aerodynamic navigation method reduces the influence of IMU and aerodynamic model misalignment, because pitch is not corrected (see 3.2.1).

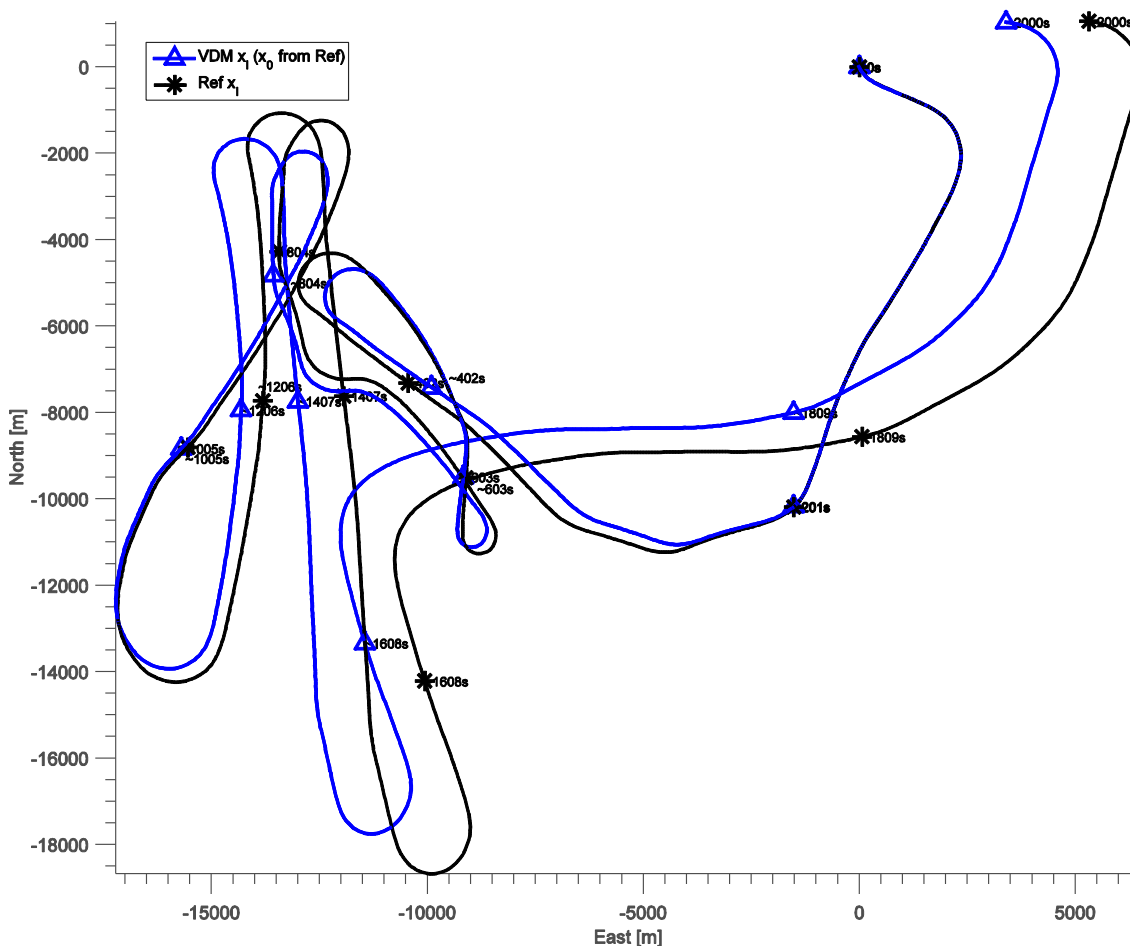


Figure 57: Flight path of navigation method and reference data. GNSS-denied from 200s

The true flight data used for method evaluation and the navigation flight path determined with the proposed aerodynamic navigation method are shown in Figure 57. After 200s of GNSS-aiding, the performance of GNSS-denied aerodynamic flight navigation is demonstrated for 1800s. Barometric altitude, airspeed and control measurements are taken from recorded real measurements directly. 3-D magnetometer measurements are simulated using the recorded reference truth flight trajectory. IMU data is derived from recorded high-quality data by application of the low-quality IMU error model (4.1.4).

In this case, an error in the aerodynamic motion model trim condition is observable: Comparison of true and navigation flight path shown in Figure 57 indicates noticeable along-track velocity error. Because it is independent of flight direction, it is not related to unknown wind velocity vector. Instead, errors in the aerodynamic motion model lead to this navigation error. Figure 61 indicates a bias of kinematic velocity in down direction throughout the test duration corresponding to too small kinematic climb angle. This points to an error in the longitudinal force model determined by thrust and drag. In addition, errors in the pitch moment model can have a similar effect on aerodynamic model trim condition, but Figure 62 gives no indication of bias of angle of attack. Due to the frequent turns in true flight path, the effect of error in longitudinal trim on position error cancels to some extent, as can be seen especially in the north position error Figure 59.

Figure 58 and Figure 60 show typical performance of the modified inertial motion model with low-cost sensors. North and east orientation error are clearly disturbed by the frequent horizontal accelerations in true flight path, resulting in a bias in $\delta\phi_N$. Because this bias is directly related to error in the heading error observation with a 3-D magnetometer (see 2.3.2.4), vertical orientation error $\delta\phi_D$ contains significant bias too.

The effect of unknown wind velocity vector is clearly visible in the aerodynamic angle of sideslip error computed assuming zero wind, see Figure 62. The computed error correlates with changes in direction of flight.

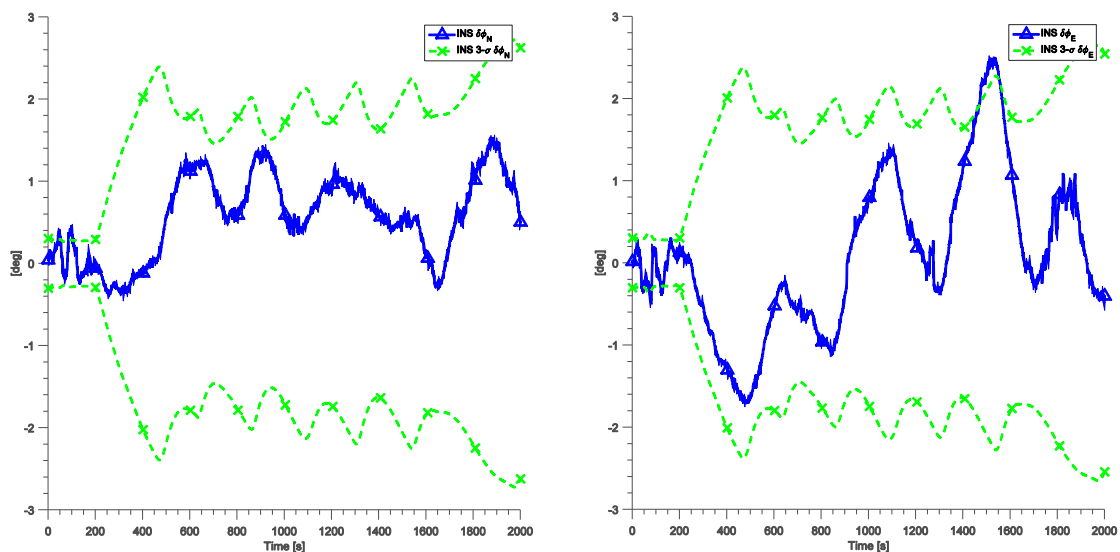


Figure 58: Modified inertial model attitude errors (versus reference)

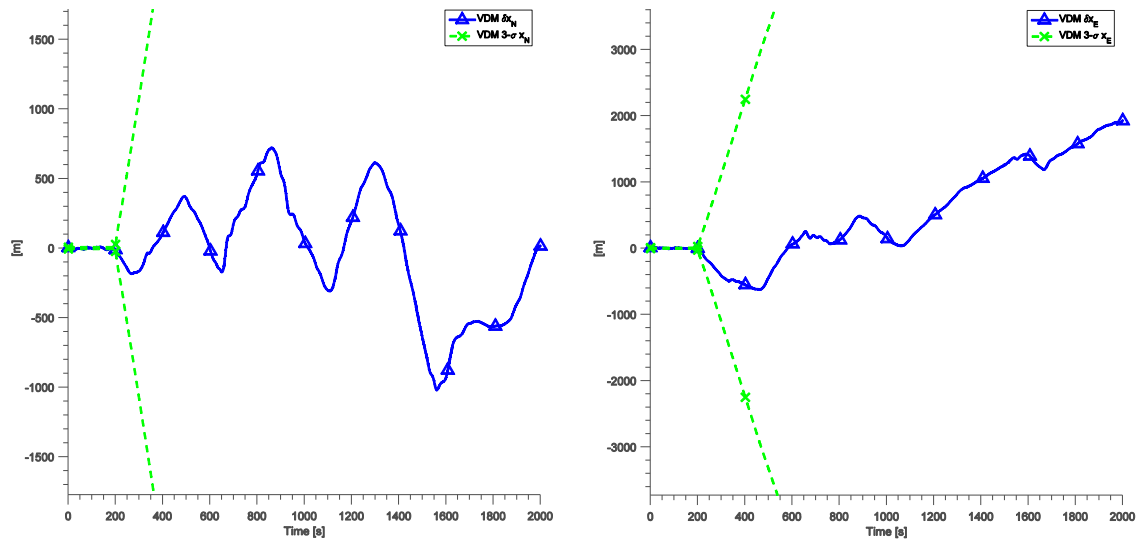


Figure 59: Aerodynamic model horizontal position errors

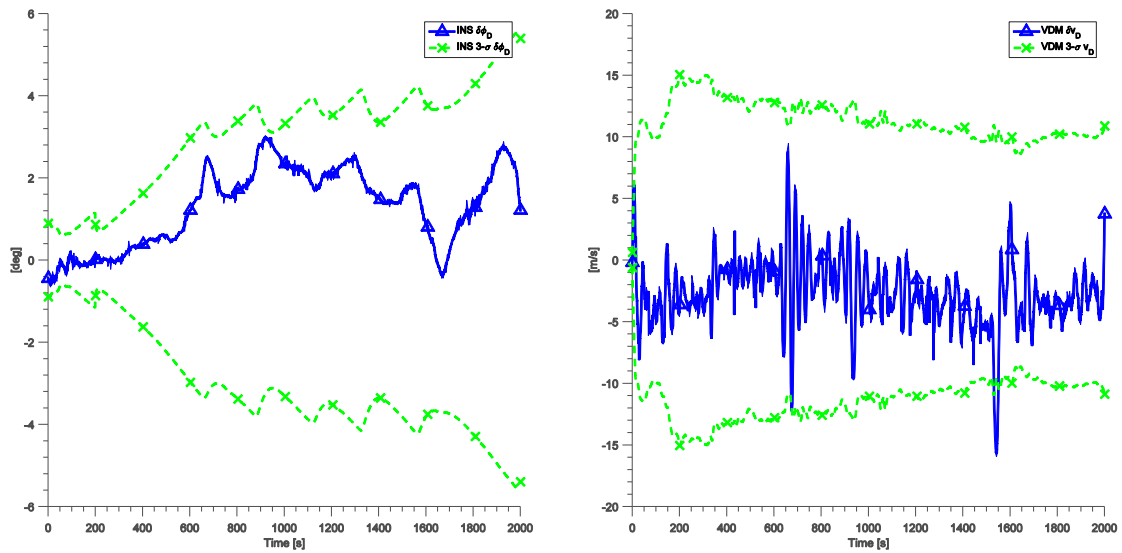


Figure 60: Modified inertial model vertical orientation error (versus reference)

Figure 61: Aerodynamic model vertical velocity error

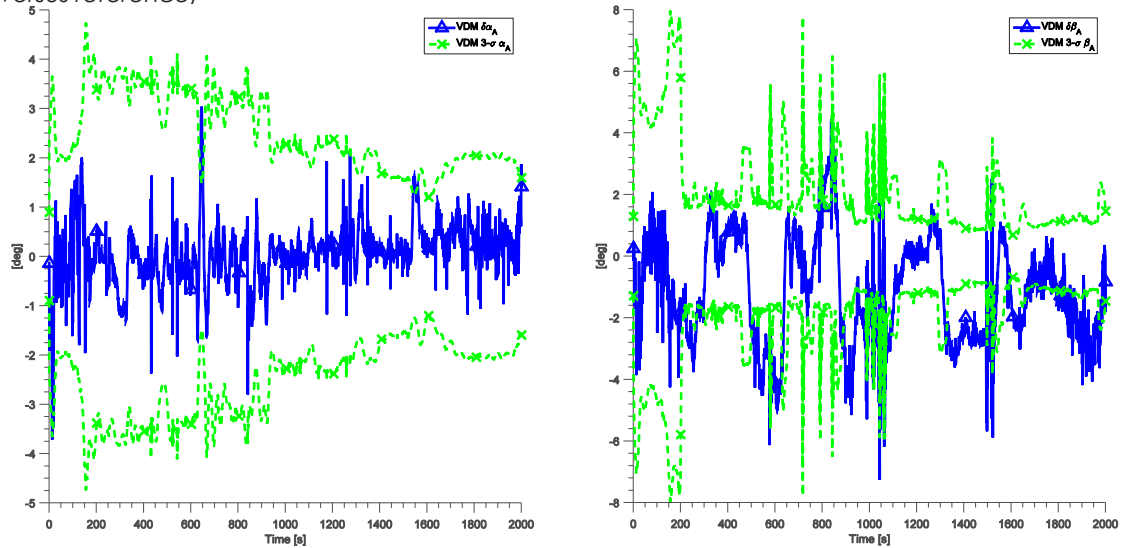


Figure 62: Aerodynamic model angle of attack and angle of sideslip errors (versus kinematic reference)

5 SYSTEM IMPROVEMENTS FOR FUTURE APPLICATIONS REQUIRING CERTIFICATION

The accuracy of the proposed aerodynamic navigation method is primarily limited by drift due to unknown wind velocity vector. Using the dynamic wind model based on airliner flight measurement data published in [88] in Monte Carlo simulations for performance assessment, the positioning performance of aerodynamic navigation is found to be not suitable for continuous flight navigation. Aerodynamic navigation is better suited as a backup function for low precision navigation allowing for safe contingency operation for a limited time, leaving the area where GNSS is denied.

For example, performance specifications similar to RNAV 5 [95, 96] for enroute operations could be addressed. EASA AMC 20-4A [95] specifies basic area navigation (RNAV 5) performance for continental enroute operations in designated European airspace. For RNAV 5, the accuracy requirements might match the performance of the desensitized aerodynamic navigation method for a reasonable duration of backup navigation operation, as will be discussed later.

GNSS standalone operation with single hardware and RAIM can be considered as suitable primary navigation source satisfactory for basic RNAV. Basic RNAV does not require monitoring and alerting functions or redundant hardware, because comparison with other navigation means by the pilots and change to alternate (ground based) navigation is possible [95, 96]. Consequently, the proposed aerodynamic navigation method can be a replacement of ground-based navigation aids (radio navigation) used as backup.

Loss of all navigation function is required improbable by EASA AMC 25-11 [97]. When ground based navigation is not used as alternate to GNSS, simultaneous loss of GNSS standalone and backup navigation function and misleading information should be considered a major failure condition similar to RNAV 1 and RNAV 2 navigation specifications [96] and FAA specifications for RNAV equipment in [98]. This corresponds to a probability of failure of $10^{-4}/h$ or $10^{-5}/h$ for single/multi-engine small airplanes [99].

For the required probability of loss of all navigation function, redundant hardware is mandatory if radio navigation is not used. With single GNSS standalone as primary and aerodynamic navigation as backup function, this requirement could be met. In case of the desensitized aerodynamic backup navigation method, additional hardware redundancy can be implemented low-cost. Redundant computing boards can be used and redundant input data for the aerodynamic motion model is available either from additional measurement of stick and pedal position and engine RPM or from digital control commands if available.

RNAV 5 operation requires a total system error (TSE) – a combination of error in determined aircraft position and all other error sources that cause a deviation of actual from desired flight path (flight technical error, FTE) – to be less than $5NM$ for 95% of flight time [95]. Accounting for a flight technical error of $1NM$ 95%, the required accuracy of computed aircraft position is $4.9NM$ for 95% of flight time.

The applicability of the desensitized aerodynamic navigation method for RNAV 5 operations will be studied in the following subsection. Shortcomings and possible future improvements of the proposed method will be discussed.

5.1 IMPROVEMENT OF SYSTEM PERFORMANCE WITH WIND INFORMATION

The identified position accuracy requirement for RNAV 5 operations of 4.9NM 95% can be met by the aerodynamic navigation method only for a limited time due to position drift. As discussed in 4.2.4, the position drift evaluated in simulations is largely determined by wind drift when using the realistic wind uncertainty model described in 4.1.3. Only if wind uncertainty is reduced, e.g. by providing wind velocity information to the aerodynamic navigation method, other system parameters such as IMU and aerodynamic model quality, will influence position performance noticeably.

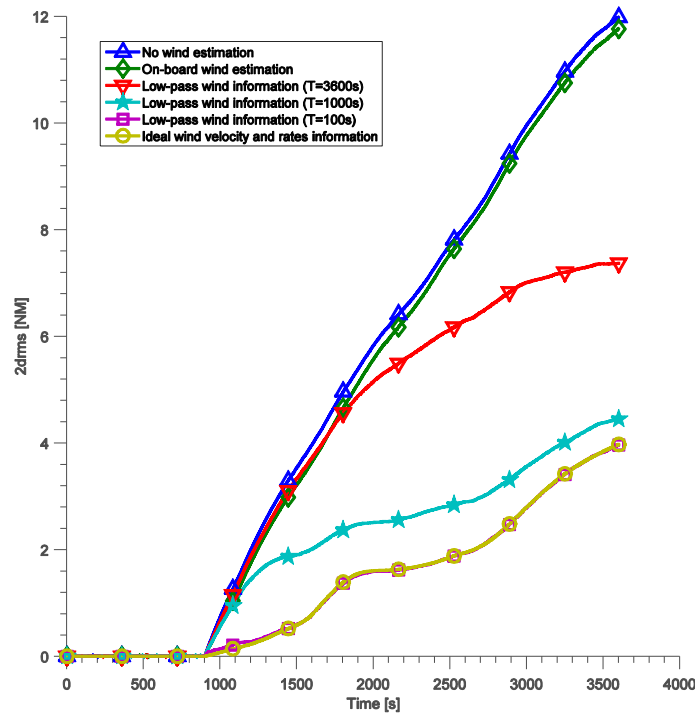


Figure 63: Improvement of position drift with wind information

Figure 63 presents a comparison of position performance in Monte Carlo simulations (4.1.1) using the dynamic wind vector model (4.1.3) and with various levels of wind information available to the aerodynamic navigation method.

With on-board wind vector estimation (active while GNSS is still available), the results of Monte Carlo simulation in this work indicate that GNSS-denied navigation can be continued with RNAV 5 accuracy for approximately 900s. This result is based on the realistic wind uncertainty model used in simulations. The performance would be badly affected by an extreme change in wind vector while GNSS is denied. Consequently, only short-term RNAV 5

operations are possible without external wind vector information, assuming the GNSS-aided wind vector estimate remains valid for short time intervals.

Figure 63 shows that providing only the slowly-varying components of dynamic wind vector to the navigation method already has a significant impact on performance. For the used atmospheric models, a low-frequency information of true wind velocity vector at aircraft position with a time coefficient of less than $1000s$ enables the proposed low-cost desensitized aerodynamic navigation method to sustain operations according to RNAV 5 accuracy specifications for about $45min$.

With accurate external low-pass wind information, aerodynamic navigation performance is independent of the true low-frequency dynamic wind. Note that this is necessary to implement an aerodynamic navigation method with reliable long-term performance, considering the possibility of extreme atmosphere conditions. Otherwise, wind speeds of $26m/s$ with a probability of occurrence 10% at an altitude of $1km$ [86] would prohibit any use of aerodynamic navigation as reliable source.

The results for aerodynamic navigation with external low-pass wind information are independent of model assumptions for slowly-varying wind used in simulation. The effect of high-pass dynamic wind (i.e. not contained in the wind information) on position performance on the other hand is difficult to evaluate and the results are specific to the simulation models used. For high-frequency content, the effect is limited due to aircraft inertia and the low-pass behavior of flight dynamics and becomes negligible for high frequencies compared to other system errors caused by magnetic measurement, IMU and model imperfections. The small contribution of high frequency content to position uncertainty could be approximated with an adaptive model observing increasing noise in accelerometer and gyroscope measurement due to rough atmosphere. Development of reliable adaptive uncertainty models for high-frequency atmospheric disturbances for prediction of position error statistics should be considered for future research.

Note that the notion of low-frequency dynamic wind velocity at aircraft position relates to strong correlation of a corresponding wind velocity vector field in space and time (i.e. with large temporal and spatial correlation coefficients). This results in low-frequency content in the wind velocity vector at aircraft position as the aircraft flies through the vector field at limited speed.

The ideal requirement of a low-pass information of true wind velocity vector at aircraft position can of course only approximately be met. The following subsection present ideas for an extension of the desensitized aerodynamic navigation method with sources of approximate wind information.

5.2 WEATHER PREDICTION AND AIRCRAFT-TO-AIRCRAFT WEATHER INFORMATION

Aerodynamic flight navigation requires reliable information on low-frequency dynamic wind vector in order to achieve a performance improvement for enroute navigation. Furthermore, this wind information source could provide uncertainty statistics for the determination of allowable duration of GNSS-denied navigation.

Two possibilities of implementing this information source with available means can be identified. First, radio weather prediction data may be used, such as the Rapid Refresh (RAP) numerical weather model [100] which is run by the U.S. National Centers for Environmental Prediction (NCEP). Due to the much stronger signal of radio transmission and the absence of a ranging problem, it can be considered a much more reliable signal. For increased reliability, the implementation of on-board weather prediction model fed by broadcast data could be considered, but constant propagation of wind vector in rare interruptions of transmission would be sufficient for limited durations.

A broadcast weather prediction is based on meteorological computations using a large array of weather measurements distributed over the region (or globally). The availability of reference data from measurement stations allows for evaluation of statistics of errors in the spatial extrapolation and temporal prediction of especially low-frequency wind vector.

Secondly, for populated airspaces and routes, other airplanes may have passed the same area shortly beforehand while GNSS-aiding was available to them, either because a local GNSS-denial event has not yet occurred, or because loss of GNSS of the aircraft to be navigated is due to on-board faults. In this case, performance of GNSS-denied aerodynamic flight navigation of the succeeding airplane could be improved by aircraft-to-aircraft communication of wind vector estimate. Due to limited distance in space and time, the error in low-frequency wind velocity vector, which is strongly correlated in space and time, can be expected to be small.

Because the routes and altitudes for the small airplanes under consideration in this work will be mostly populated by similar small generation aircraft (away from airports), the sensor quality on board of nearby aircraft is low. Consequently, the reliability of estimated wind vector is an issue. Alternatively, the aircraft-to-aircraft approach could be implemented via a data hub and centralized estimation. This allows to include data or estimations from airliners with verified accurate on-board sensors in addition to small aircraft sensors and spatial interpolation. Similar to above weather prediction model approach, this relies on the estimation of an atmospheric wind velocity vector field parametrized in space and time and becomes a meteorological problem.

Consequently, a very important task for future research is the assessment of meteorological methods for use for aerodynamic navigation. Both the accurate estimation of low-frequency wind velocity vector and the availability of reliable uncertainty statistics for this component of dynamic wind would be key contributions to a potential future use of the desensitized aerodynamic navigation method as backup in airplane operations.

6 SUMMARY AND CONCLUSIONS

Throughout this work, special consideration is given to the unique qualities of the flight dynamics of small general aviation airplanes and low-cost inertial navigation. The detailed understanding of the complementary characteristics of these two motion models is the basis for the presented solutions and innovations.

The main achievement of the presented work is twofold. First, a new way is found to reliably integrate knowledge of airplane flight dynamics with inertial navigation even if severe deficiencies in modeling of atmosphere processes and uncertainties exist. The innovation overcomes a fundamental limitation of earlier optimal state estimation based techniques affecting robustness of aerodynamic navigation for airplanes in rough atmosphere conditions.

Second, a robust backup navigation function for GNSS-denied phases of flight is proposed, which uses a high-quality model of airplane flight dynamics. This thesis thoroughly elaborates in theory and experiment the capability of integrated navigation propagation models for low-cost applications. The innovative covariance-free integration of inertial and aerodynamic models is applied to small general aviation airplanes and tested rigorously. The study comprises a new approach to realistically account for aerodynamic model errors in simulation and an unadjusted application to real flight data in postprocessing.

New findings in system theory

In more detail, the presented research can be summarized as follows. Heading and airspeed dead reckoning, inertial navigation and the aerodynamic motion model are studied and compared with respect to their qualities for low-cost navigation propagation without GNSS aiding. Unaided position propagation is discussed qualitatively and quantitatively for short and long time intervals. Favorable error propagation characteristics with linear position drift are identified for the dead reckoning method and the aerodynamic motion model under the restriction that a specific lateral error mode must be damped. The advantages of navigation propagation methods with linear position drift behavior for use with low-cost sensors and high risk of temporary disturbances are explained.

Low-cost inertial navigation error propagation and observability with on-board aiding measurements is discussed in detail. It is explained why low-cost inertial navigation is preferable for aided estimation of rotational motion and vertical motion but suffers from unfavorable error propagation for horizontal translational motion in GNSS-denied phases. The basic design of a combination of inertial navigation and aerodynamic motion model is conceived, using inertial orientation computation to restrain aerodynamic motion lateral divergence and improve the accuracy of translational aerodynamic motion. A modified inertial motion model is developed which is optimized for rotational motion accuracy.

This work is the first dealing with the application of an airplane aerodynamic motion model to navigation that identifies an important restriction in aiding the aerodynamic model with auxiliary measurements in a navigation filter. The findings are explained with the specifics of airplane flight dynamics. Changes in the aerodynamic degrees of freedom governing

airplane aerodynamic flight, such as aerodynamic angle of sideslip, stimulate strong dynamic modes especially affecting rotational motion. If corrections are not applied consistently as equilibrium changes to all flight dynamics degrees of freedom and aerodynamic model coefficients simultaneously – which would require very accurate filter covariance models of aerodynamic flight and model uncertainty – the resulting dynamic disturbances can cause large errors affecting filter linearization and potentially lead to filter failure. Due to the intermittency of atmospheric disturbances, large wind estimation errors in turbulence usually are not consistently described by filter covariance models. Consequently, large erroneous corrections to aerodynamic degrees of freedom often occur if an estimation filter with imperfect covariance models of atmosphere and model uncertainties is used to update aerodynamic model kinematic states.

Nevertheless, it is shown that in standard conditions lateral error divergence can effectively be mitigated by aiding attitude or heading errors. This allows using the aerodynamic motion model for propagation of translational motion with linear position drift. How to robustly correct aerodynamic model motion in challenging atmosphere conditions is addressed later in section 2 of chapter 3.

Innovative integration architecture

A considerable part of the research related with this thesis dealt with inertial and aerodynamic model fusion, which is favored in the available literature. In model fusion, optimal state estimation techniques are employed assuming exact equivalence of truth motion for both models. Others have demonstrated good results with model fusion for multicopter applications which clearly proves the capability of model fusion for this type of vehicle.

This thesis deals with small general aviation airplanes and shows that model fusion is not the best choice for this specific application. This is discussed in detail and the problems encountered with model fusion are related to the specifics of airplane aerodynamic flight in an unprotected atmosphere environment. Due to the long flight durations and distances travelled, short but extreme atmospheric disturbances must be expected. The intermittency of these events makes both accurate on-board modeling of underlying processes (prediction) and of related uncertainty statistics impossible. This modeling deficiency is a significant drawback for the application of optimal state estimation techniques. A tuned model fusion filter is developed which overcomes these problems to some extent and provides the inspiration for further research in this work. But the fundamental drawbacks of model fusion for airplanes persist and motivate the development of a new method.

The proposed covariance-free integration comprises three contributions. First, the complementary integration strategy for low-cost inertial navigation and high-quality airplane aerodynamic motion model is defined. This approach allows replacing statistically weighted averaging of information by a predefined selection of only one of the models for any part of vehicle motion, i.e. rotational, vertical and horizontal translational motion. Based on the discussion of system theory, it applies the modified inertial motion model to provide information about vertical motion and rotational motion. Inertial rotational motion is used to restrain aerodynamic model lateral errors. In turn, the aerodynamic model, with damped lateral error, provides accurate information on horizontal translational motion with first order

position drift. With this integration strategy, the limitations of model fusion techniques due to modeling deficiencies are successfully resolved. The covariance-free integration eliminates the need for accurately modeling uncertainties of inertial and aerodynamic motion models for combination of the two models.

The aerodynamically desensitized constraints for airplane aerodynamic motion successfully solve the second problem of model fusion for airplanes, i.e. the restrictions in aiding the aerodynamic model in dynamic atmosphere conditions. Based on the discussion of flight dynamics of small general aviation airplanes, a set of correction schemes for the aerodynamic model is proposed that allows integration with inertial navigation but fully preserves robustness in rough atmosphere. The desensitized constraints are the recommended choice to use airplane flight dynamics for navigation propagation with first order position drift. At the same time, they are suited for robustly controlling the model in phases of flight with GNSS-aiding.

An add-on covariance model is developed for use with the new covariance-free integration method. It is fully consistent with the aerodynamically desensitized constraints and can be used to provide auxiliary covariance information to the navigation data user. Covariance modeling is fully separated from the computation of navigation state, for the reasons elaborated earlier. Still, if models are available that are deemed appropriate for this purpose, they can be used to compute covariance of aerodynamic navigation.

Capability demonstration and proposals for future development

To study the behavior of the new method under realistic conditions encountered in flight and to demonstrate achievable performance for small general aviation airplanes, the thesis comprises an extensive evaluation in simulation and experiment. An automatic trajectory generation tool is used to generate reference data for a large variety of aerodynamic flight scenarios. Special consideration is given to challenging atmosphere conditions, and realistic models for dynamic wind vector and turbulence are implemented.

For system simulation, an innovative way to account for the uncertainties of aerodynamic and propulsion forces and moments in aerodynamic navigation is proposed. Two uncertainty models for aerodynamic motion are developed. One represents best achievable aerodynamic model accuracy given a realistic quality of sensor instrumentation used for system identification flight tests. It is assumed that all challenges related to system identification are accomplished expertly, resulting in a high-quality model. A second, conservative uncertainty model is defined for studying the effect of low aerodynamic model quality on the performance of the proposed method.

The benefit of using Monte Carlo simulation for evaluation of the proposed method lies in the large variety of scenarios of aerodynamic flight that are tested. The automatic trajectory generation tool is used to create a database of more than 600 flights of 1h length, each affected by a different time history of dynamic atmosphere processes. This causes the individual flights to differ significantly, especially in rotational motion and (auto-)pilot control inputs. Furthermore, each flight is representative in a way that it accounts for the intermittency of atmosphere conditions and includes smooth and turbulent phases in random succession. The large number of reference flight data is then used to generate realistic sensor measurement data time histories, again with different realizations for each

simulation run. Consequently, the results of Monte Carlo evaluation presented in this thesis provide a meaningful picture of method behavior in a large number of combinations of true motion dynamics, measurement errors, atmosphere conditions and control inputs.

The work concludes with a comprehensive assessment of the GNSS-denied navigation performance and robustness of the proposed method both using the Monte Carlo simulation framework and a real flight data postprocessing test. The demonstrated robustness is good without any failure in large collection of tests. Position accuracy is close to ideal drift determined by wind estimation error. These results validate the complementary integration strategy for inertial and aerodynamic motion and the development of aerodynamically desensitized constraints. The combination of meaningful Monte Carlo evaluation with good results in a real data test encourages studying the application of the method in navigation systems for small general aviation airplanes.

Nevertheless, the amount of empirical validation of the new navigation method is still low. Therefore, future efforts of aerodynamic navigation development should address the question how a similar level of trust can be achieved as for conventional INS/GNSS integrated navigation. A possible solution is to initially include the aerodynamic navigation function as "payload" only, i.e. without providing output to the pilot. That way, a large dataset of recorded inputs and accurate reference data from INS/GNSS can be generated. Although true wind velocity vector will not be known, the data set can be used to simulate GNSS-denied navigation and determine an empirical model of method accuracy. This model may be considered as more reliable replacement for the covariance information computed with the add-on model based on simple assumptions of dynamic atmosphere uncertainty.

Finally, the demonstrated performance of the method in its current form is compared with the requirements of applicable navigation performance specifications. It is generally suitable as replacement of classical ground based navigation aids for use as backup navigation function for contingency operations with low navigation accuracy when GNSS is denied. Without external wind information, GNSS-denied navigation could be continued with RNAV 5 accuracy for more than $10min$, based on the results of Monte Carlo simulation presented in section 4.2.1. For an airplane travelling at $140kn$, this corresponds to a distance travelled of approximately $43km$. This demonstrates that the requirement to be able to leave the area where GNSS is denied safely by navigating with the backup system can be met.

In order to meet RNAV 5 horizontal position accuracy requirements for a longer time, the rate of position drift must be limited. A possible extension of the new aerodynamic navigation method is proposed that provides low-pass wind velocity vector information for improved aerodynamic motion model position propagation. Possibilities how this wind information can be broadcast or computed are discussed. Because of the crucial influence on accuracy and reliability, the transfer of meteorological knowledge to the field of aerodynamic navigation and especially the integration of available weather information are identified as further important aspects of future research.

REFERENCES

- [1] Trimble Inc, "GNSS Planning Online," URL = <http://www.trimble.com/GNSSPlanningOnline/>.
- [2] J. Safar, P. Williams, and A. Grant, "Analysis, Modeling, and Mitigation of Cross-Rate Interference in eLoran," *J Inst Navig*, vol. 63, no. 3, pp. 295–319, 2016.
- [3] D. A. Divis, "U.S. Nears eLoran Decision with Broad International Implications," *Inside GNSS (March/April 2015)*, URL = <http://www.insidegnss.com/auto/marapr15-WV.pdf>.
- [4] A. Cameron, "eLoran Progresses Toward GPS Back-Up Role in U.S, Europe," *GPS World (June 25, 2015)*, URL = <http://gpsworld.com/eloran-progresses-toward-gps-back-up-role-in-u-s-europe/>.
- [5] W. Pelgrum et al, "eDME On Air: Design, Implementation, and Flight-Test Demonstration," in *Proceedings of the 2015 International Technical Meeting of The Institute of Navigation*, 2015, pp. 40–61.
- [6] T. Ertan and M. L. Psiaki, "Alternative Position and Navigation Based on DME Accumulated Delta Range," *J Inst Navig*, vol. 63, no. 2, pp. 145–159, 2016.
- [7] W. R. Fried and M. Kayton, *Avionics navigation systems*, 2nd ed. New York: Wiley, 1997.
- [8] Anon, *Garmin G1000 Cockpit Reference Guide for the Cessna Citation Mustang: 190-00600-00 Rev. B*, 2006.
- [9] M. Koifman and I. Y. Bar-Itzhack, "Inertial navigation system aided by aircraft dynamics," *IEEE Trans. Contr. Syst. Technol*, vol. 7, no. 4, pp. 487–493, 1999.
- [10] M. Koifman and S. J. Merhav, "Autonomously aided strapdown attitude reference system," *Journal of Guidance, Control, and Dynamics*, vol. 14, no. 6, pp. 1164–1172, 1991.
- [11] S. J. Julier and H. F. Durrant-Whyte, "A Horizontal Model Fusion Paradigm," in *Aerospace/Defense Sensing and Controls: SPIE*, 1996, pp. 37–48.
- [12] J. Vasconcelos, C. Silvestre, and P. Oliveira, "Embedded Vehicle Dynamics and LASER Aiding Techniques for Inertial Navigation Systems," in *AIAA Guidance, Navigation, and Control Conference and Exhibit*, 2006.
- [13] J. Vasconcelos, C. Silvestre, P. Oliveira, and B. Guerreiro, "Embedded UAV model and LASER aiding techniques for inertial navigation systems," *Control Engineering Practice*, vol. 18, no. 3, pp. 262–278, 2010.
- [14] P. Crocoll, L. Görcke, G. F. Trommer, and F. Holzapfel, "Unified Model Technique for Inertial Navigation Aided by Vehicle Dynamics Model," *J Inst Navig*, vol. 60, no. 3, pp. 179–193, 2013.
- [15] P. D. Groves, *Principles of GNSS, inertial, and multisensor integrated navigation systems*. Boston: Artech House, 2013.
- [16] W. Torge, *Geodesy*, 3rd ed. Berlin: Walter de Gruyter, 2001.
- [17] C. Jekeli, *Geometric Reference Systems in Geodesy*. Ohio: Ohio State University, 2006.
- [18] NIMA Technical Report TR8350.2, *Department of Defense World Geodetic System 1984, Its Definition and Relationships With Local Geodetic Systems*. Third Edition, Amendment 1, 3 Jan 2000: National Imagery and Mapping Agency.
- [19] D. Gebre-Egziabher, "Design and performance analysis of a low-cost aided dead reckoning navigator," Dissertation, Stanford University, 2004.
- [20] R. M. Rogers, *Applied mathematics in integrated navigation systems*, 2nd ed. Reston, VA: American Institute of Aeronautics and Astronautics, 2003.

- [21] D. H. Titterton and J. L. Weston, *Strapdown inertial navigation technology*, 2nd ed. Stevenage: Institution of Electrical Engineers, 2004.
- [22] R. F. Stengel, *Flight dynamics*. Princeton, NJ: Princeton University Press, 2004.
- [23] A. B. Chatfield, *Fundamentals of high accuracy inertial navigation*. Reston, Va.: American Institute of Aeronautics and Astronautics, 1997.
- [24] S. Weinberg, *Gravitation and cosmology: principles and applications of the general theory of relativity*. New York: Wiley, 1972.
- [25] V. Petkov, *Inertia and gravitation: From Aristotle's natural motion to geodesic worldlines in curved spacetime*. Montreal: Minkowski Institute Press, 2012.
- [26] Robert DiSalle, "Space and Time: Inertial Frames," *The Stanford Encyclopedia of Philosophy (Winter 2009 Edition)*, Edward N. Zalta (ed.), URL = <http://plato.stanford.edu/archives/win2009/entries/spacetime-iframes/>.
- [27] W. Lowrie, *Fundamentals of geophysics*, 2nd ed. Cambridge: Cambridge University Press, 2007.
- [28] A. Lawrence, *Modern inertial technology: Navigation, guidance, and control*, 2nd ed. New York: Springer, 1998.
- [29] J. L. Farrell, *GNSS aided navigation & tracking: Inertially augmented or autonomous*. Baltimore, Md.: American Literary Press, 2007.
- [30] C. Jekeli, *Inertial navigation systems with geodetic applications*. Berlin, New York: Walter de Gruyter, 2001.
- [31] J. Dambeck, "Diagnose und Therapie geodätischer Trägheitsnavigationssysteme," Dissertation, Universität Stuttgart, 1998.
- [32] A. Dachs, "Rechenzeitoptimierung, Robustifizierung und Tuning eines Kalmanfilters zur Datenfusion für Navigationsanwendungen," Dissertation, Universität der Bundeswehr München, 2010.
- [33] U. M. Ascher and L. R. Petzold, *Computer methods for ordinary differential equations and differential-algebraic equations*. Philadelphia: Society for Industrial and Applied Mathematics, 1998.
- [34] P. G. Savage, "Strapdown Inertial Navigation Integration Algorithm Design Part 1: Attitude Algorithms," *Journal of Guidance, Control, and Dynamics*, vol. 21, no. 1, pp. 19–28, 1998.
- [35] E. Süli and D. F. Mayers, *An introduction to numerical analysis*. Cambridge, New York: Cambridge University Press, 2003.
- [36] P. G. Savage, "Strapdown Inertial Navigation Integration Algorithm Design Part 2: Velocity and Position Algorithms," *Journal of Guidance, Control, and Dynamics*, vol. 21, no. 2, pp. 208–221, 1998.
- [37] W. A. Heiskanen and H. Moritz, *Physical Geodesy*: W. H. Freeman and Company, 1967.
- [38] N. K. Pavlis, S. A. Holmes, S. C. Kenyon, and J. K. Factor, "The development and evaluation of the Earth Gravitational Model 2008 (EGM2008)," *J. Geophys. Res.*, vol. 117, no. B4, 2012.
- [39] L. Görcke, "Integration of Dynamic Models in INS/GNSS Navigation Systems," Diploma Thesis, Institute of Flight System Dynamics, Technical University of Munich, Garching, 2011.
- [40] B. Etkin and L. D. Reid, *Dynamics of flight: Stability and control*, 3rd ed. New York: Wiley, 1996.
- [41] B. L. Stevens and F. L. Lewis, *Aircraft control and simulation*, 3rd ed. Hoboken, N.J.: Wiley, 2016.
- [42] R. v. Mises, *Theory of Flight*. New York: Dover Publications, 1959.

- [43] J. D. Anderson, *Fundamentals of aerodynamics*, 3rd ed. Boston: McGraw-Hill, 2001.
- [44] R. C. Nelson, *Flight stability and automatic control*. New York: McGraw-Hill, 1989.
- [45] International Civil Aviation Organization (ICAO), *Manual of the ICAO standard atmosphere : extended to 80 kilometres (262 500 feet)*, 3rd ed. Montreal, Quebec: International Civil Aviation Organization, 1993.
- [46] J. Roskam and C. E. Lan, *Airplane aerodynamics and performance*. Lawrence, Kan.: DARcorporation, 1997.
- [47] International Civil Aviation Organization (ICAO), *Manual of Criteria for the Qualification of Flight Simulation Training Devices: Volume I — Aeroplanes*. Doc 9625 AN/938, 3rd ed, 2009.
- [48] R. V. Jategaonkar, *Flight vehicle system identification: A time domain methodology*. Reston, VA: American Institute of Aeronautics and Astronautics, 2006.
- [49] R. Jategaonkar and W. Moennich, "Identification of DO-328 aerodynamic database for a Level D flight simulator," in *Modeling and Simulation Technologies Conference*, 1997.
- [50] J. G. Mark and D. A. Tazartes, "Tuning of Coning Algorithms to Gyro Data Frequency Response Characteristics," *Journal of Guidance, Control, and Dynamics*, vol. 24, no. 4, pp. 641–647, 2001.
- [51] K. R. Britting, *Inertial navigation systems analysis*. New York: Wiley-Interscience, 1971.
- [52] D. Benson, "A Comparison of Two Approaches to Pure-Inertial and Doppler-Inertial Error Analysis," *IEEE Trans. Aerosp. Electron. Syst*, vol. AES-11, no. 4, pp. 447–455, 1975.
- [53] G. A. Kachikas, "Error Analysis for Cruise Systems," in *Inertial Guidance*, G. R. Pitman, Ed, New York: Wiley, 1962.
- [54] J. C. Pinson, "Inertial Guidance for Cruise Vehicles," in *Guidance and Control of Aerospace Vehicles*, C. T. Leondes, Ed, New York: McGraw-Hill, 1963.
- [55] B. M. Scherzinger, "Inertial navigator error models for large heading uncertainty," in *Position, Location and Navigation Symposium - PLANS '96*, 1996, pp. 477–484.
- [56] B. M. Scherzinger and D. B. Reid, "Modified strapdown inertial navigator error models," in *1994 IEEE Position, Location and Navigation Symposium - PLANS'94*, 1994, pp. 426–430.
- [57] Myeong-Jong Yu, Jang Gyu Lee, and Heung-Won Park, "Comparison of SDINS in-flight alignment using equivalent error models," *IEEE Trans. Aerosp. Electron. Syst*, vol. 35, no. 3, pp. 1046–1054, 1999.
- [58] B. Friedland, "Analysis Strapdown Navigation Using Quaternions," *IEEE Trans. Aerosp. Electron. Syst*, vol. AES-14, no. 5, pp. 764–768, 1978.
- [59] J. A. Farrell and M. Barth, *The Global Positioning System & Inertial Navigation*. New York: McGraw-Hill Companies, 1999.
- [60] T. Martin, "Zur Integritätsprüfung von Satelliten/Inertial-Navigation für die Luftfahrt," Dissertation, Technische Universität Carolo-Wilhelmina zu Braunschweig, 2011.
- [61] H. Moritz, "Geodetic Reference System 1980," *Bulletin Geodesique*, vol. 66, pp. 187–192, 1992.
- [62] Ausman, J. Stanley, "Baro-Inertial Loop for the USAF Standard RLG INU 1," *J Inst Navig*, vol. 38, no. 2, pp. 205–220, 1991.
- [63] Ausman, J. Stanley, "A Kalman Filter Mechanization for the Baro-Inertial Vertical Channel," in *Proceedings of the 47th Annual Meeting of The Institute of Navigation (1991)*, 1991, pp. 153–159.
- [64] J. Lunze, *Regelungstechnik 1: Systemtheoretische Grundlagen, Analyse und Entwurf einschleifiger Regelungen*, 9th ed. Berlin: Springer, 2013.

- [65] Federal Aviation Administration (FAA), *Federal Aviation Regulations (FAR): Part 23 - Airworthiness Standards: Normal, Utility, Acrobatic, and Commuter Category Airplanes*: U.S. Government Publishing Office.
- [66] European Aviation Safety Agency (EASA), *CS-23: Certification Specifications and Acceptable Means of Compliance for Normal, Utility, Aerobatic, and Commuter Category Aeroplanes*. Amendment 4, 2015.
- [67] Federal Aviation Administration (FAA), *Advisory Circular (AC) 23-8C: Flight Test Guide for Certification of Part 23 Airplanes*, 2011.
- [68] B. P. Gibbs, *Advanced kalman filtering, least-squares and modeling: A practical handbook*. Hoboken, N.J.: Wiley, 2011.
- [69] D. Simon, *Optimal state estimation: Kalman, H [infinity] and nonlinear approaches*. Hoboken, N.J.: Wiley-Interscience, 2006.
- [70] M. S. Grewal and A. P. Andrews, *Kalman filtering: Theory and practice using MATLAB*, 3rd ed. Hoboken, N.J.: Wiley, 2008.
- [71] A. M. Mood, F. A. Graybill, and D. C. Boes, *Introduction to the theory of statistics*, 3rd ed. Auckland: McGraw-Hill, 1974.
- [72] W. Gracey, *Measurement of aircraft speed and altitude*. Hampton, VA: NASA Langley Research Center, 1980.
- [73] J. Dobyne, "The accuracy of barometric altimeters with respect to geometric altitude," in *Proceedings of the International Technical Meeting of the Satellite Division of The Institute of Navigation (ION GPS 1988)*, 1988, pp. 451–459.
- [74] S. Myschik, F. Holzapfel, and G. Sachs, "Low-Cost Sensor Based Integrated Airdata and Navigation System for General Aviation Aircraft," in *AIAA Guidance, Navigation and Control Conference and Exhibit*, 2008.
- [75] K. Wise, "Flight Testing of the X-45A J-UCAS Computational Alpha-Beta System," in *AIAA Guidance, Navigation, and Control Conference and Exhibit*, 2006.
- [76] Chulliat, A. S. Macmillan, P. Alken, C. Beggan, M. Nair, B. Hamilton, A. Woods, V. Ridley, S. Maus and A. Thomson, *The US/UK World Magnetic Model for 2015-2020: Technical Report*. Boulder, CO: NOAA National Geophysical Data Center, 2015.
- [77] A. Sendobry, "A Model Based Navigation Architecture for Small Unmanned Aerial Vehicles," in *Proceedings of the European Navigation Conference 2011*: Royal Institute of Navigation (RIN), 2011.
- [78] P. Crocoll, "Modellbasierte Quadropter-Navigation mit Laserstützung," Dissertation, Karlsruher Institut für Technologie (KIT), 2015.
- [79] L. Görcke, J. Dambeck, and F. Holzapfel, "Results of Model-Aided Navigation with Real Flight Data," in *Proceedings of the 2014 International Technical Meeting of The Institute of Navigation*, 2014, pp. 407–412.
- [80] M. Morgado, P. Oliveira, C. Silvestre, and J. F. Vasconcelos, "Embedded Vehicle Dynamics Aiding for USBL/INS Underwater Navigation System," *IEEE Trans. Contr. Syst. Technol.*, vol. 22, no. 1, pp. 322–330, 2014.
- [81] M. Bryson and S. Sukkarieh, "Vehicle Model Aided Inertial Navigation for a UAV using Low-cost Sensors," in *Australasian Conference on Robotics and Automation (ACRA '04)*, 2004.
- [82] M. Khaghani and J. Skaloud, "Autonomous Vehicle Dynamic Model-Based Navigation for Small UAVs," *J Inst Navig*, vol. 63, no. 3, pp. 345–358, 2016.
- [83] B. Braun, "High Performance Kalman Filter Tuning for Integrated Navigation Systems," Dissertation, Technical University of Munich, 2016.

- [84] D. Simon, "Kalman filtering with state constraints: A survey of linear and nonlinear algorithms," *IET Control Theory & Applications*, vol. 4, no. 8, pp. 1303–1318, 2010.
- [85] P. Crocoll, J. Seibold, G. Scholz, and G. F. Trommer, "Model-Aided Navigation for a Quadrotor Helicopter: A Novel Navigation System and First Experimental Results," *J Inst Navig*, vol. 61, no. 4, pp. 253–271, 2014.
- [86] U.S. Department of Defense, *MIL-HDBK-310: Global Climatic Data for Developing Military Products*, 1997.
- [87] L. Görcke, F. Holzappel, and J. Dambeck, "Aerodynamic flight simulation in inertial quality," in *Proceedings of the 2013 International Technical Meeting of The Institute of Navigation*, 2013, pp. 415–425.
- [88] Z. Berman and J. D. Powell, "The role of dead reckoning and inertial sensors in future general aviation navigation," in *IEEE 1998 Position Location and Navigation Symposium*, 1998, pp. 510–517.
- [89] T. R. Beal, "Digital simulation of atmospheric turbulence for Dryden and von Karman models," *Journal of Guidance, Control, and Dynamics*, vol. 16, no. 1, pp. 132–138, 1993.
- [90] *Military Standard, Flying Qualities of Piloted Airplanes*, MIL-STD-1797A, 2004.
- [91] The MathWorks, Inc, *Documentation. Dryden Wind Turbulence Model (Continuous)*: <http://de.mathworks.com/help/aeroblks/drydenwindturbulencemodelcontinuous.html>.
- [92] T. S. Bruggemann, "Investigation of MEMS Inertial Sensors and Aircraft Dynamic Models in Global Positioning System Integrity Monitoring for Approaches with Vertical Guidance," Dissertation, Queensland University of Technology, 2009.
- [93] L. R. Cork, "Aircraft dynamic navigation for unmanned aerial vehicles," Dissertation, Queensland University of Technology, 2014.
- [94] E. W. Weisstein, *CRC concise encyclopedia of mathematics*. Boca Raton, Fla.: CRC Press, 1999.
- [95] European Aviation Safety Agency (EASA), *AMC 20-4A: Airworthiness Approval and Operational Criteria For the Use of Navigation Systems in European Airspace Designated For Basic RNAV Operations*. Annex V to ED Decision 2013/026/R of 12/09/2013, 2013.
- [96] International Civil Aviation Organization (ICAO), *ICAO EUR PBN Approvals Guidance Material (EUR Doc 029)*, 1st ed, 2013.
- [97] European Aviation Safety Agency (EASA), *AMC 25-11: Electronic Display Systems*. Annex to ED Decision 2007/010/R, 2007.
- [98] Federal Aviation Administration (FAA), *Advisory Circular (AC) 20-138C: Airworthiness Approval of Positioning and Navigation Systems*, 2012.
- [99] Federal Aviation Administration (FAA), *Advisory Circular (AC) 23.1309-1E: System Safety Analysis and Assessment for Part 23 Airplanes*.
- [100] S. G. Benjamin *et al*, "A North American Hourly Assimilation and Model Forecast Cycle: The Rapid Refresh," *Mon. Wea. Rev.*, vol. 144, no. 4, pp. 1669–1694, 2016.
- [101] R. A. McKern, "A Study of Transformation Algorithms for Use in a Digital Computer," M.S. Thesis, Massachusetts Institute of Technology, Cambridge, 1968.
- [102] P. S. Maybeck, *Stochastic Models, Estimation and Control. Volume 1*. New York: Academic Press, 1979.
- [103] K. Meyberg and P. Vachenauer, *Höhere Mathematik 2*, 4th ed. Berlin: Springer, 2006.
- [104] G. Bierman, "Measurement updating using the U-D factorization," in *1975 IEEE Conference on Decision and Control including the 14th Symposium on Adaptive Processes*, pp. 337–346.

Appendix A

A.1 MATH

This appendix is based on the author's Diploma thesis [39] and the references cited therein.

Basic functions

The function *skew* applied to a 3-D vector $\mathbf{v} = [v_1 \ v_2 \ v_3]^T$

$$\mathit{skew}(\mathbf{v}) = [\mathbf{v} \times] = \begin{bmatrix} 0 & -v_3 & v_2 \\ v_3 & 0 & -v_1 \\ -v_2 & v_1 & 0 \end{bmatrix} \quad (\text{A-1})$$

computes the skew-symmetric matrix equivalent so that for another 3-D vector \mathbf{l}

$$\mathbf{v} \times \mathbf{l} = \mathit{skew}(\mathbf{v})\mathbf{l} \quad (\text{A-2})$$

Inversely, the function *veck* computes the vector equivalent of a skew-symmetric 3-D matrix. Consequently,

$$\mathit{veck}(\mathit{skew}(\mathbf{v})) = \mathbf{v} \quad (\text{A-3})$$

Coordinate transformations of 3-D vectors

The direction cosine matrix (DCM) or rotation matrix $\mathbf{R}_{ab} \in SO(3)$ (i.e. a 3-D orthogonal matrix with determinant +1) is defined to transform the coordinates of a 3-D vector \mathbf{v} from cartesian frame b to cartesian frame a

$$\mathbf{v}_a = \mathbf{R}_{ab}\mathbf{v}_b \quad (\text{A-4})$$

The rotation matrix \mathbf{R}_{ab} is related to other parameters of relative orientation of frame b with respect to frame a as follows:

If frame b can be constructed by rotation of frame a about a single axis (1,2,3) with an angle α_{ab} , the two frames are aligned in this specific axis and \mathbf{R}_{ab} is

$$\text{1st axis: } \mathbf{R}_{ab} = \mathbf{R}_1(\alpha_{ab}) = \begin{bmatrix} 1 & 0 & 0 \\ 0 & \cos(\alpha_{ab}) & -\sin(\alpha_{ab}) \\ 0 & \sin(\alpha_{ab}) & \cos(\alpha_{ab}) \end{bmatrix} \quad (\text{A-5})$$

$$\text{2nd axis: } \mathbf{R}_{ab} = \mathbf{R}_2(\alpha_{ab}) = \begin{bmatrix} \cos(\alpha_{ab}) & 0 & \sin(\alpha_{ab}) \\ 0 & 1 & 0 \\ -\sin(\alpha_{ab}) & 0 & \cos(\alpha_{ab}) \end{bmatrix} \quad (\text{A-6})$$

$$\text{3rd axis: } \mathbf{R}_{ab} = \mathbf{R}_3(\alpha_{ab}) = \begin{bmatrix} \cos(\alpha_{ab}) & -\sin(\alpha_{ab}) & 0 \\ \sin(\alpha_{ab}) & \cos(\alpha_{ab}) & 0 \\ 0 & 0 & 1 \end{bmatrix} \quad (\text{A-7})$$

For general relative orientation of frame b with respect to frame a , a maximum of three consecutive rotations about different axes is sufficient to construct frame b from frame a . Obviously, a number of possibilities exists for selection and order of rotation axes. In this work, the Euler angle definition is adopted. Frame a is first rotated about its 3rd axis with angle $\alpha_{ab,3}$, then rotated about the 2nd axis of the frame constructed by the first single-axis rotation with angle $\alpha_{ab,2}$ and finally about the 1st axis of the frame constructed by the previous two single-axis rotations with angle $\alpha_{ab,1}$. Consequently, the rotation matrix \mathbf{R}_{ab} defined by these Euler angles $\alpha_{ab,1}$, $\alpha_{ab,2}$ and $\alpha_{ab,3}$ is

$$\begin{aligned} \mathbf{R}_{ab} &= \mathbf{R}([\alpha_{ab,1} \ \alpha_{ab,2} \ \alpha_{ab,3}]^T) := \mathbf{R}_3(\alpha_{ab,3})\mathbf{R}_2(\alpha_{ab,2})\mathbf{R}_1(\alpha_{ab,1}) \quad (\text{A-8}) \\ &= \begin{bmatrix} \cos(\alpha_{ab,3})\cos(\alpha_{ab,2}) & \cos(\alpha_{ab,3})\sin(\alpha_{ab,1})\sin(\alpha_{ab,2}) - \cos(\alpha_{ab,1})\sin(\alpha_{ab,3}) & \sin(\alpha_{ab,1})\sin(\alpha_{ab,3}) + \cos(\alpha_{ab,1})\cos(\alpha_{ab,3})\sin(\alpha_{ab,2}) \\ \cos(\alpha_{ab,2})\sin(\alpha_{ab,3}) & \cos(\alpha_{ab,1})\cos(\alpha_{ab,3}) + \sin(\alpha_{ab,1})\sin(\alpha_{ab,3})\sin(\alpha_{ab,2}) & \cos(\alpha_{ab,1})\sin(\alpha_{ab,3})\sin(\alpha_{ab,2}) - \cos(\alpha_{ab,3})\sin(\alpha_{ab,1}) \\ -\sin(\alpha_{ab,2}) & \cos(\alpha_{ab,2})\sin(\alpha_{ab,1}) & \cos(\alpha_{ab,1})\cos(\alpha_{ab,2}) \end{bmatrix} \end{aligned}$$

Specifically for a transformation from body-fixed frame b to NED frame n , the Euler angles are (in this order) roll angle Φ_{nb} , pitch angle Θ_{nb} and yaw angle (or Azimuth) Ψ_{nb} . With this

$$\mathbf{R}_{nb} = \mathbf{R}([\Phi_{nb} \ \Theta_{nb} \ \Psi_{nb}]^T) \quad (\text{A-9})$$

As a generalization of the single-axis rotation matrices (A-5) through (A-7), frame b can be constructed by rotation of frame a about an unit vector \mathbf{n}_a , $\|\mathbf{n}_a\| = 1$ with an angle α_{ab} . The corresponding rotation matrix \mathbf{R}_{ab} will be derived in the following.

First, define a coordinate frame r with the first axis aligned with the vector of rotation direction \mathbf{n}_a . I.e., the first basis vector of frame r written in coordinates of frame a is

$$\mathbf{R}_{ra}^T \mathbf{e}_1 = \mathbf{n}_a \quad (\text{A-10})$$

The second basis vector of frame r is chosen arbitrarily but orthogonal to the first, i.e.

$$\mathbf{R}_{ra}^T \mathbf{e}_2 = \mathbf{u}_a, \text{ with } \|\mathbf{u}_a\| = 1, \mathbf{n}_a^T \mathbf{u}_a = 0 \quad (\text{A-11})$$

The third basis vector completes the orthonormal basis of frame r and therefore the transformation matrix can be written as

$$\mathbf{R}_{ra}^T = [\mathbf{n}_a \quad \mathbf{u}_a \quad \mathbf{n}_a \times \mathbf{u}_a] \quad (\text{A-12})$$

With $(\mathbf{n}_a^T \mathbf{n}_a)(\mathbf{u}_a^T \mathbf{u}_a) = 1$ and $(\mathbf{n}_a^T \mathbf{u}_a) = 0$ it is straightforward to verify that

$$\det(\mathbf{R}_{ra}) = \det(\mathbf{R}_{ra}^T) = 1 \quad (\text{A-13})$$

Furthermore

$$\mathbf{R}_{ra}^T \mathbf{R}_{ra} = \mathbf{n}_a \mathbf{n}_a^T + \mathbf{u}_a \mathbf{u}_a^T + (\mathbf{n}_a \times \mathbf{u}_a)(\mathbf{n}_a \times \mathbf{u}_a)^T = \mathbf{I} \quad (\text{A-14})$$

Which is evident by the fact that multiplication of $\mathbf{R}_{ra}^T \mathbf{R}_{ra}$ with each of the three linear independent vectors \mathbf{n}_a , \mathbf{u}_a and $\mathbf{n}_a \times \mathbf{u}_a$ results in the identical vector. This verifies that above equation (A-12) defines a rotation matrix $\mathbf{R}_{ra} \in SO(3)$.

With equation (A-5), the rotation matrix \mathbf{R}_{ab} given by rotation axis unit vector \mathbf{n}_a and angle α_{ab} becomes

$$\begin{aligned} \mathbf{R}_{ab} = \mathbf{R}(\mathbf{n}_a, \alpha_{ab}) &= \mathbf{R}_{ra}^T \mathbf{R}_1(\alpha_{ab}) \mathbf{R}_{ra} \\ &= \mathbf{n}_a \mathbf{n}_a^T + \cos(\alpha_{ab}) \mathbf{u}_a \mathbf{u}_a^T + \sin(\alpha_{ab}) (\mathbf{n}_a \times \mathbf{u}_a) \mathbf{u}_a^T \\ &\quad - \sin(\alpha_{ab}) \mathbf{u}_a (\mathbf{n}_a \times \mathbf{u}_a)^T + \cos(\alpha_{ab}) (\mathbf{n}_a \times \mathbf{u}_a) (\mathbf{n}_a \times \mathbf{u}_a)^T \end{aligned} \quad (\text{A-15})$$

Note that unit vector \mathbf{u}_a is chosen arbitrarily with $\mathbf{n}_a^T \mathbf{u}_a = 0$.

Equation (A-15) reveals the expected properties of \mathbf{R}_{ab} , e.g. $\mathbf{R}_{ab} \mathbf{n}_a = \mathbf{n}_a$. More interestingly, on inspection of for the skew-symmetric part of \mathbf{R}_{ab}

$$\frac{1}{2}(\mathbf{R}_{ab} - \mathbf{R}_{ab}^T) = \sin(\alpha_{ab}) (\mathbf{n}_a \times \mathbf{u}_a) \mathbf{u}_a^T - \sin(\alpha_{ab}) \mathbf{u}_a (\mathbf{n}_a \times \mathbf{u}_a)^T \quad (\text{A-16})$$

the following holds for every 3-D vector $\mathbf{v}_a = \mathbf{R}_{ra}^T [v_1 \quad v_2 \quad v_3]^T$ with $v_1, v_2, v_3 \in \Re$

$$\frac{1}{2}(\mathbf{R}_{ab} - \mathbf{R}_{ab}^T) \mathbf{v}_a = \sin(\alpha_{ab}) \mathbf{n}_a \times \mathbf{v}_a \quad (\text{A-17})$$

From the generality of vector \mathbf{v}_a it follows that equivalently the skew-symmetric part of rotation matrix \mathbf{R}_{ab} is

$$\frac{1}{2}(\mathbf{R}_{ab} - \mathbf{R}_{ab}^T) = \sin(\alpha_{ab}) \text{skew}(\mathbf{n}_a) \quad (\text{A-18})$$

With this, equation (A-15) becomes

$$\mathbf{R}_{ab} = \mathbf{n}_a \mathbf{n}_a^T + \cos(\alpha_{ab}) (\mathbf{u}_a \mathbf{u}_a^T + (\mathbf{n}_a \times \mathbf{u}_a) (\mathbf{n}_a \times \mathbf{u}_a)^T) + \sin(\alpha_{ab}) \text{skew}(\mathbf{n}_a) \quad (\text{A-19})$$

For the unit vector \mathbf{n}_a the identity $\mathbf{I} - \mathbf{n}_a \mathbf{n}_a^T + \text{skew}(\mathbf{n}_a)^2 = \mathbf{0}$ holds and can be used together with equation (A-14) to further simplify equation (A-19)

$$\mathbf{R}_{ab} = \mathbf{I} + \sin(\alpha_{ab}) \text{skew}(\mathbf{n}_a) + (1 - \cos(\alpha_{ab})) \text{skew}(\mathbf{n}_a)^2 \quad (\text{A-20})$$

This is the analytical expression of a rotation matrix corresponding to a rotation vector that was derived in [101].

Rotation matrix ordinary differential equation

In the following, the differential equation for a general rotation matrix \mathbf{R}_{cb} will be derived. Assume a frame a with constant orientation relative to frame c , $\mathbf{R}_{ca} = \text{const.}$, so that

$$\dot{\mathbf{R}}_{cb} = \underbrace{\dot{\mathbf{R}}_{ca}}_{=0} \mathbf{R}_{ab} + \mathbf{R}_{ca} \dot{\mathbf{R}}_{ab} \quad (\text{A-21})$$

With equation (A-20)

$$\dot{\mathbf{R}}_{cb} = \mathbf{R}_{ca} \frac{d}{dt} (\mathbf{I} + \sin(\alpha_{ab}) \text{skew}(\mathbf{n}_a) + (1 - \cos(\alpha_{ab})) \text{skew}(\mathbf{n}_a)^2) \quad (\text{A-22})$$

Without loss of generality chose $\alpha_{ab} = 0$ so that $\mathbf{R}_{ca} = \mathbf{R}_{cb}$ and with equation (A-14)

$$\dot{\mathbf{R}}_{cb} = \mathbf{R}_{cb} \dot{\alpha}_{ab} \text{skew}(\mathbf{n}_a) \quad (\text{A-23})$$

Note that no assumption was made on how the rotation vector direction \mathbf{n}_a evolves in time.

Define the angular rates vector

$$\boldsymbol{\omega}_{cb} := \dot{\alpha}_{ab} \mathbf{n}_a \quad (\text{A-24})$$

and the skew-symmetric matrix equivalent of $\boldsymbol{\omega}_{cb}$

$$\boldsymbol{\Omega}_{cb} = \text{skew}(\boldsymbol{\omega}_{cb}) = [\boldsymbol{\omega}_{cb} \times] \quad (\text{A-25})$$

With this, (A-23) gives the differential equation of the rotation matrix \mathbf{R}_{cb} for arbitrary coordinate frames c and a

$$\dot{\mathbf{R}}_{cb} = \mathbf{R}_{cb} \boldsymbol{\Omega}_{cb} \quad (\text{A-26})$$

Quaternion orientation parametrization

In the following the basic concept of quaternion orientation parametrization is presented.

Define the hypercomplex space

$$\mathbb{H} = \{q_0 + iq_1 + jq_2 + kq_3 \mid q_0, q_1, q_2, q_3 \in \mathbb{R}\} \quad (\text{A-27})$$

i, j and k are imaginary units with $ij = ji = -k, ik = ki = -j, jk = kj = -i$.

Multiplying two quaternions $\tilde{q}, \tilde{p} \in \mathbb{H}$ gives

$$\begin{aligned} \tilde{q} \cdot \tilde{p} &= (q_0 + iq_1 + jq_2 + kq_3) \cdot (p_0 + ip_1 + jp_2 + kp_3) \\ &= q_0p_0 - (q_1p_1 + q_2p_2 + q_3p_3) \\ &\quad + i(q_0p_1 + q_1p_0 + q_2p_3 - q_3p_2) \\ &\quad + j(q_0p_2 + q_2p_0 + q_3p_1 - q_1p_3) \\ &\quad + k(q_0p_3 + q_3p_0 + q_1p_2 - q_2p_1) \end{aligned} \quad (\text{A-28})$$

The quaternion inverse with $\tilde{q} \cdot \tilde{q}^{-1} = 1 \in \mathbb{H}$ is defined for $\tilde{q} \neq 0$ by

$$\tilde{q}^{-1} = \frac{1}{q_0^2 + q_1^2 + q_2^2 + q_3^2} (q_0 - iq_1 - jq_2 - kq_3) \quad (\text{A-29})$$

Define a function that transforms a 3-D vector to a quaternion

$$\begin{aligned} \tilde{\mathbf{x}} : \mathbb{R}^{3 \times 1} &\rightarrow \mathbb{H}, \mathbf{x} \mapsto \tilde{\mathbf{x}} \\ \tilde{\mathbf{x}}([x_1, x_2, x_3]^T) &= ix_1 + jx_2 + kx_3 \end{aligned} \quad (\text{A-30})$$

For a unit quaternion $\tilde{q} \in \mathbb{H}_1$ with $\mathbb{H}_1 = \{q_0 + iq_1 + jq_2 + kq_3 \in \mathbb{H} \mid q_0^2 + q_1^2 + q_2^2 + q_3^2 = 1\} \subset \mathbb{H}$ and with above definitions the following transformations are equivalent

$$\begin{aligned} \tilde{\mathbf{y}} &= \tilde{q} \cdot \tilde{\mathbf{x}} \cdot \tilde{q}^{-1} \\ &\Leftrightarrow \\ \mathbf{y} &= \mathbf{R}(\tilde{q})\mathbf{x} \end{aligned} \quad (\text{A-31})$$

where $\tilde{\mathbf{x}}$ and $\tilde{\mathbf{y}}$ are the quaternion counterparts of 3-D vectors \mathbf{x} and \mathbf{y} and

$$\mathbf{R}(\tilde{q}) = \begin{bmatrix} q_0^2 + q_1^2 - q_2^2 - q_3^2 & 2(q_1q_2 - q_0q_3) & 2(q_1q_3 + q_0q_2) \\ 2(q_1q_2 + q_0q_3) & q_0^2 - q_1^2 + q_2^2 - q_3^2 & 2(q_2q_3 - q_0q_1) \\ 2(q_1q_3 - q_0q_2) & 2(q_2q_3 + q_0q_1) & q_0^2 - q_1^2 - q_2^2 + q_3^2 \end{bmatrix} \quad (\text{A-32})$$

$\mathbf{R}(\tilde{q})$ will be shown to be a rotation matrix $\mathbf{R}(\tilde{q}) \in SO(3)$ in the following subsection.

With this, a quaternion $\tilde{q}_{ab} \in \mathbb{H}_1$ can be used to describe the orientation of frame b with respect to frame a , e.g.

$$\begin{aligned} \tilde{\mathbf{v}}_a &= \tilde{q}_{ab} \cdot \tilde{\mathbf{v}}_b \cdot \tilde{q}_{ab}^{-1} \\ &\Leftrightarrow \\ \mathbf{v}_a &= \mathbf{R}(\tilde{q}_{ab})\mathbf{v}_b \end{aligned} \quad (\text{A-33})$$

With the rotation matrix

$$\mathbf{R}_{ab} = \mathbf{R}(\tilde{q}_{ab}) \quad (\text{A-34})$$

Rotation vector and orientation quaternion

By comparing the rotation matrix \mathbf{R}_{ab} given by a rotation axis unit vector \mathbf{n}_a and an angle α_{ab} from equation (A-20)

$$\mathbf{R}_{ab} = \mathbf{I} + \sin(\alpha_{ab})\text{skew}(\mathbf{n}_a) + (1 - \cos(\alpha_{ab}))\text{skew}(\mathbf{n}_a)^2 \quad (\text{A-35})$$

and the equivalent transformation matrix described by a unit quaternion $\tilde{\mathbf{q}}_{ab} = q_0 + iq_1 + jq_2 + kq_3 \in \mathbb{H}_1$ from equation (A-32)

$$\begin{aligned} \mathbf{R}(\tilde{\mathbf{q}}_{ab}) &= \begin{bmatrix} q_0^2 - q_1^2 - q_2^2 - q_3^2 & 0 & 0 \\ 0 & q_0^2 - q_1^2 - q_2^2 - q_3^2 & 0 \\ 0 & 0 & q_0^2 - q_1^2 - q_2^2 - q_3^2 \end{bmatrix} \\ &+ 2 \begin{bmatrix} q_1^2 & q_1q_2 & q_1q_3 \\ q_1q_2 & q_2^2 & q_2q_3 \\ q_1q_3 & q_2q_3 & q_3^2 \end{bmatrix} + 2q_0 \begin{bmatrix} 0 & -q_3 & q_2 \\ q_3 & 0 & -q_1 \\ -q_2 & q_1 & 0 \end{bmatrix} \\ &= (q_0^2 - q_1^2 - q_2^2 - q_3^2)\mathbf{I} + 2 \begin{bmatrix} q_1 \\ q_2 \\ q_3 \end{bmatrix} [q_1 \quad q_2 \quad q_3] \\ &+ 2q_0\text{skew}([q_1 \quad q_2 \quad q_3]^T) \end{aligned} \quad (\text{A-36})$$

we find for the skew-symmetric parts

$$\begin{aligned} \sin(\alpha_{ab})\text{skew}(\mathbf{n}_a) &= 2q_0\text{skew}([q_1 \quad q_2 \quad q_3]^T) \\ \Leftrightarrow \sin(\alpha_{ab})\mathbf{n}_a &= 2q_0 \begin{bmatrix} q_1 \\ q_2 \\ q_3 \end{bmatrix} \end{aligned} \quad (\text{A-37})$$

With $\|\mathbf{n}_a\| = 1$ it follows that

$$\sin^2(\alpha_{ab}) = 4q_0^2(q_1^2 + q_2^2 + q_3^2) \quad (\text{A-38})$$

With $\tilde{\mathbf{q}}_{ab} \in \mathbb{H}_1$ this gives

$$\sin^2(\alpha_{ab}) = 4q_0^2(1 - q_0^2) \quad (\text{A-39})$$

With the solutions

$$q_0 \in \left\{ \cos\left(\frac{\alpha_{ab}}{2}\right), -\cos\left(\frac{\alpha_{ab}}{2}\right), \sin\left(\frac{\alpha_{ab}}{2}\right), -\sin\left(\frac{\alpha_{ab}}{2}\right) \right\} \quad (\text{A-40})$$

Requiring that $\mathbf{R}(\tilde{\mathbf{q}}_{ab}) = \mathbf{I}$ for $\alpha_{ab} = 0$ reduces the solutions to $q_0 = \pm \cos(\alpha_{ab}/2)$. Both are valid: from the quadratic form of equation (A-32) follows that $\mathbf{R}(-\tilde{\mathbf{q}}_{ab}) = \mathbf{R}(\tilde{\mathbf{q}}_{ab})$.

Choosing the solution $q_0 = \cos(\alpha_{ab}/2)$ and with equation (A-37) and the sum identity $\sin(\alpha_{ab}) = 2\sin(\alpha_{ab}/2)\cos(\alpha_{ab}/2)$ we get

$$\tilde{\mathbf{q}}_{ab} = \cos(\alpha_{ab}/2) + \sin(\alpha_{ab}/2)\tilde{\mathbf{n}}_a \quad (\text{A-41})$$

where $\tilde{\mathbf{n}}_a$ is the quaternion counterpart of rotation axis unit vector \mathbf{n}_a .

With the sum identity $\cos(\alpha_{ab}) = \cos^2(\alpha_{ab}/2) - \sin^2(\alpha_{ab}/2)$ and the half-angle formula $2\sin^2(\alpha_{ab}/2) = 1 - \cos(\alpha_{ab})$ we find for the symmetric parts of equation (A-36)

$$(q_0^2 - q_1^2 - q_2^2 - q_3^2)\mathbf{I} + 2 \begin{bmatrix} q_1 \\ q_2 \\ q_3 \end{bmatrix} [q_1 \quad q_2 \quad q_3] = \cos(\alpha_{ab})\mathbf{I} + (1 - \cos(\alpha_{ab}))\mathbf{n}_a\mathbf{n}_a^T \quad (\text{A-42})$$

For the unit vector \mathbf{n}_a the identity $\mathbf{I} - \mathbf{n}_a \mathbf{n}_a^T + skew(\mathbf{n}_a)^2 = \mathbf{0}$ holds and equation (A-42) can be further simplified

$$(q_0^2 - q_1^2 - q_2^2 - q_3^2)\mathbf{I} + 2 \begin{bmatrix} q_1 \\ q_2 \\ q_3 \end{bmatrix} [q_1 \quad q_2 \quad q_3] = \mathbf{I} + (1 - \cos(\alpha_{ab})) skew(\mathbf{n}_a)^2 \quad (\text{A-43})$$

This proves the equivalence of the symmetric parts of equations (A-35) and (A-36).

Consequently, the transformation matrix equivalent $\mathbf{R}(\check{\mathbf{q}}_{ab})$ of a unit quaternion $\check{\mathbf{q}}_{ab}$ given by equation (A-32) and repeated in (A-36) is a rotation matrix $\mathbf{R}_{ab} \in SO(3)$. The rotation is defined by the rotation angle α_{ab} and the rotation unit vector \mathbf{n}_a that can be extracted from equations (A-41) and (A-35) (repeated from (A-20)).

Orientation quaternion ordinary differential equation

In the following, the differential equation for a general orientation quaternion \check{q}_{cb} will be derived. Assume a frame a with constant orientation relative to frame c , $\check{q}_{ca} = \text{const.}$, so that from equation (A-23)

$$\check{q}_{cb} = \check{q}_{ca}\check{q}_{ab} \quad (\text{A-44})$$

And the time derivative becomes

$$\dot{\check{q}}_{cb} = \underbrace{\dot{\check{q}}_{ca}}_{=0}\check{q}_{ab} + \check{q}_{ca}\dot{\check{q}}_{ab} \quad (\text{A-45})$$

With equation (A-41)

$$\dot{\check{q}}_{cb} = \check{q}_{ca} \frac{d}{dt} (\cos(\alpha_{ab}/2) + \sin(\alpha_{ab}/2)\check{n}_a) \quad (\text{A-46})$$

Without loss of generality chose $\alpha_{ab} = 0$ so that $\check{q}_{ca} = \check{q}_{cb}$ and consequently

$$\dot{\check{q}}_{cb} = \frac{1}{2}\check{q}_{cb}\dot{\alpha}_{ab}\check{n}_a \quad (\text{A-47})$$

With the quaternion equivalent of the angular rates vector defined in equation (A-24) $\check{\omega}_{cb} = i\omega_{cb,x} + j\omega_{cb,y} + k\omega_{cb,z}$ the differential equation for orientation quaternion \check{q}_{cb} becomes

$$\dot{\check{q}}_{cb} = \frac{1}{2}\check{q}_{cb} \cdot \check{\omega}_{cb} \quad (\text{A-48})$$

A.2 TRANSLATIONAL MOTION OF A POINT MASS

This appendix is based on chapter 2 of the author's Diploma thesis [39] and the references cited therein.

Translational motion of a point mass

The classical mechanics of Newton conceptually understand the influence of gravitation as a force comparable to conventional forces such as aerodynamic forces. The force acting on a point mass m in P is

$$\mathbf{F}_i(P) = \mathbf{F}_{i,external}(P) + \mathbf{F}_{i,gravitation}(P) \quad (\text{A-49})$$

$\mathbf{F}_{i,gravitation}(P) = m \cdot \mathbf{g}_{i,universe}(P)$ is the gravitational force resulting from all other masses in the universe. $\mathbf{F}_{i,external}(P)$ is the sum of all other forces acting on the point mass. This force can be 'felt' by an observer and is proportional to the specific force \mathbf{f}_b measured by an ideal accelerometer aligned with the axes of frame b and located in point P :

$$\mathbf{F}_{i,external}(P) = m\mathbf{R}_{ib}\mathbf{f}_b(P) \quad (\text{A-50})$$

Furthermore, Newton's physics state the existence of an inertial reference frame i where the translational motion of the point mass m in P is given by

$$\mathbf{a}_i = \ddot{\mathbf{x}}_i = \frac{1}{m}\mathbf{F}_i(P) \quad (\text{A-51})$$

If no other point is given as argument, \mathbf{x}_i is the vector from the center of frame i to P .

Although superseded by the theory of relativity, the errors from using classical mechanics with equations (A-49) and (A-51) are extremely small for velocities much smaller than the speed of light and relatively small masses. Consequently, effects of relativity can be neglected for applications in general aviation.

The gravitational force resulting from all other masses in the universe cannot be modeled. Assuming Galilei-invariance, we can circumvent this problem by describing the motion of point P in an earth centered and earth fixed (ECEF) frame with index e :

$$\mathbf{a}_i = \mathbf{a}_i(P_e) + \frac{d^2}{dt^2}(\mathbf{R}_{ie}\mathbf{x}_e) \quad (\text{A-52})$$

When describing motion with respect to the earth's center P_e , only the difference of gravitational acceleration due to masses in the universe in P_e and P remains. This is referred to as tidal acceleration. These differences are relatively small and can be neglected for most aviation applications:

$$\frac{d^2}{dt^2}(\mathbf{R}_{ie}\mathbf{x}_e) = \mathbf{a}_i - \mathbf{a}_i(P_e) \approx \mathbf{R}_{ib}\mathbf{f}_b(P) + \mathbf{g}_{i,earth}(P) + \underbrace{\mathbf{g}_{i,tidal}(P, t)}_{\approx \mathbf{0}} \quad (\text{A-53})$$

Note that it has been assumed here that the point mass is negligible compared to earth's mass. The earth is in free fall: $\mathbf{f}_b(P_e) = \mathbf{0}$.

With the differential equation for direction cosine matrices (DCM) $\dot{\mathbf{R}}_{ab} = \mathbf{R}_{ab}[\boldsymbol{\omega}_{ab} \times]$ (A-26) the relative acceleration can be written as

$$\frac{d^2}{dt^2}(\mathbf{R}_{ie}\mathbf{x}_e) = \mathbf{R}_{ie} \left(\dot{\mathbf{v}}_e + 2\boldsymbol{\omega}_{ie} \times \mathbf{v}_e + \underbrace{\dot{\boldsymbol{\omega}}_{ie} \times \mathbf{x}_e}_{\approx \mathbf{0}} + \boldsymbol{\omega}_{ie} \times (\boldsymbol{\omega}_{ie} \times \mathbf{x}_e) \right) \quad (\text{A-54})$$

Where Euler acceleration due to earth angular acceleration can be neglected ($\boldsymbol{\omega}_{ie} \approx \text{const.}$ is a very good approximation).

Equating (A-53) and (A-54), translational motion in ECEF reference frame of a point mass m in P can be calculated from inertial measurements in P as

$$\dot{\mathbf{v}}_e \approx \mathbf{R}_{eb}\mathbf{f}_b(P) + \boldsymbol{\gamma}_e(P) - 2\boldsymbol{\omega}_{ie} \times \mathbf{v}_e \quad (\text{A-55})$$

A model for the gravity vector

$$\boldsymbol{\gamma}_e(P) = \mathbf{g}_{e,earth}(P) - \boldsymbol{\omega}_{ie} \times (\boldsymbol{\omega}_{ie} \times \mathbf{x}_e) \quad (\text{A-56})$$

and the rate of earth rotation $\omega_{ie} = \|\boldsymbol{\omega}_{ie}\|_2 = 7292115 \cdot 10^{-11} \text{rad/s}$ must be provided (e.g. by the WGS84 model, see [18] and following subsections of this appendix). By definition $\mathbf{e}_{z,i} \parallel \mathbf{e}_{z,e}$, therefore

$$\boldsymbol{\omega}_{ie} = \omega_{ie} \cdot \begin{bmatrix} 0 \\ 0 \\ 1 \end{bmatrix} \quad (\text{A-57})$$

Inertial navigation equations in ECEF frame

For a rigid body, the translational equation takes its simplest form if the location of the accelerometer and the reference point of motion are identical: $P_{IMU} = P$. In that case, the translational equation is identical to the equation for a point mass (A-55):

$$\dot{\mathbf{v}}_e = \mathbf{R}_{eb}\mathbf{f}_b(P) + \boldsymbol{\gamma}_e(P) - 2\boldsymbol{\omega}_{ie} \times \mathbf{v}_e \quad (\text{A-58})$$

In the context of rigid body motion, frame b is referred to as body-fixed frame. In the body-fixed frame b , the rigid body constraints can be written as

$$\dot{\mathbf{x}}_b(P) = \mathbf{0} \quad \text{for any point } P \text{ on the body} \quad (\text{A-59})$$

The most general way to describe the body's orientation is with the direction cosine matrix (DCM) for transformation from b to ECEF frame \mathbf{R}_{eb} .

With $\mathbf{R}_{eb} = \mathbf{R}_{ie}^T \cdot \mathbf{R}_{ib}$ a different form of the differential equation for the DCM (A-26) can be derived where the gyroscope measurement $\boldsymbol{\omega}_{ib}$ appears directly as input:

$$\dot{\mathbf{R}}_{eb} = \mathbf{R}_{ie}^T \cdot \dot{\mathbf{R}}_{ib} + \dot{\mathbf{R}}_{ie}^T \cdot \mathbf{R}_{ib} = \mathbf{R}_{eb}\boldsymbol{\Omega}_{ib} - \boldsymbol{\Omega}_{ie}\mathbf{R}_{eb} \quad (\text{A-60})$$

Finally, the differential equation for the position in ECEF frame $\mathbf{r}_e = \mathbf{r}_e(P)$ completes the set of equations. The inertial navigation system equations in ECEF frame and with DCM orientation parametrization are

$$\dot{\mathbf{x}}_e = \mathbf{v}_e \quad (\text{A-61})$$

$$\dot{\mathbf{v}}_e = \mathbf{R}_{eb}\mathbf{f}_b + \boldsymbol{\gamma}_e(\mathbf{x}_e) - 2\boldsymbol{\omega}_{ie} \times \mathbf{v}_e \quad (\text{A-62})$$

$$\dot{\mathbf{R}}_{eb} = \mathbf{R}_{eb}\boldsymbol{\Omega}_{ib} - \boldsymbol{\Omega}_{ie}\mathbf{R}_{eb} \quad (\text{A-63})$$

With the IMU measurements

$$\mathbf{u}_{IMU} = \begin{bmatrix} \mathbf{f}_b \\ \boldsymbol{\omega}_{ib} \end{bmatrix} \quad (\text{A-64})$$

Inertial navigation equations in n-frame

In this section the inertial navigation equations are derived for position in WGS84 geodetic coordinates, velocities in north-east-down directions (NED frame, index n) and orientation parametrization with quaternions.

The NED frame is defined as north-indicating and locally tangential to the WGS84 ellipsoid [18]. In this text the origin of the NED frame will always be located in the origin of the body-fixed frame P_b . Therefore it serves as rotational reference frame only. It is necessary to explicitly define the velocity in n -frame as

$$\mathbf{v}_n = \mathbf{R}_{en}^T \mathbf{v}_e \quad (\text{A-65})$$

The transformation from n to e frame is

$$\begin{aligned} \mathbf{R}_{en} &= \begin{bmatrix} \cos(\lambda) & -\sin(\lambda) & 0 \\ \sin(\lambda) & \cos(\lambda) & 0 \\ 0 & 0 & 1 \end{bmatrix} \cdot \begin{bmatrix} -\sin(\phi) & 0 & -\cos(\phi) \\ 0 & 1 & 0 \\ \cos(\phi) & 0 & -\sin(\phi) \end{bmatrix} \\ &= \begin{bmatrix} -\sin(\phi) \cos(\lambda) & -\sin(\lambda) & -\cos(\phi) \cos(\lambda) \\ -\sin(\phi) \sin(\lambda) & \cos(\lambda) & -\cos(\phi) \sin(\lambda) \\ \cos(\phi) & 0 & -\sin(\phi) \end{bmatrix} \end{aligned} \quad (\text{A-66})$$

With the geodetic latitude ϕ and the geodetic longitude λ of point P_b . The WGS84 position of P_b is defined by the triple (ϕ, λ, h)

$$\boldsymbol{\lambda} = [\phi, \lambda, h]^T \quad (\text{A-67})$$

With the height above WGS84 reference ellipsoid h .

The position of P_b in ECEF frame \mathbf{x}_e can be calculated from WGS84 coordinates with [16]

$$\mathbf{x}_e = -\mathbf{R}_{en} \begin{bmatrix} 0 \\ 0 \\ N(\phi) + h \end{bmatrix} - \begin{bmatrix} 0 \\ 0 \\ e^2 N(\phi) \sin(\phi) \end{bmatrix} = \begin{bmatrix} (N(\phi) + h) \cos(\phi) \cos(\lambda) \\ (N(\phi) + h) \cos(\phi) \sin(\lambda) \\ ((1 - e^2)N(\phi) + h) \sin(\phi) \end{bmatrix} \quad (\text{A-68})$$

With the normal curvature radius $N(\phi) = \frac{a}{\sqrt{1 - e^2 \sin^2 \phi}}$ and the first eccentricity $e = \sqrt{\frac{a^2 - b^2}{a^2}}$ [16]. a and b are the semi-major and semi-minor axis of the WGS84 ellipsoid respectively [18].

The differential equation for WGS84 position with NED velocities as input can be derived from

$$\mathbf{v}_n = \begin{bmatrix} v_N \\ v_E \\ v_D \end{bmatrix} = \mathbf{R}_{en}^T \mathbf{v}_e \quad (\text{A-69})$$

by inserting

$$\begin{aligned} \mathbf{v}_e = \dot{\mathbf{x}}_e &= -\dot{\mathbf{R}}_{en} \begin{bmatrix} 0 \\ 0 \\ N(\phi) + h \end{bmatrix} - \mathbf{R}_{en} \begin{bmatrix} 0 \\ 0 \\ N'(\phi) \dot{\phi} + \dot{h} \end{bmatrix} - \begin{bmatrix} 0 \\ 0 \\ e^2 N'(\phi) \dot{\phi} \sin(\phi) \end{bmatrix} \\ &\quad - \begin{bmatrix} 0 \\ 0 \\ e^2 N(\phi) \cos(\phi) \dot{\phi} \end{bmatrix} \end{aligned} \quad (\text{A-70})$$

This gives

$$\begin{aligned}
\mathbf{v}_n &= -[\boldsymbol{\omega}_{en} \times] \begin{bmatrix} 0 \\ 0 \\ N(\phi) + h \end{bmatrix} - \begin{bmatrix} 0 \\ 0 \\ N'(\phi)\dot{\phi} + \dot{h} \end{bmatrix} \\
&\quad - e^2 \begin{bmatrix} \cos(\phi) \\ 0 \\ -\sin(\phi) \end{bmatrix} (N'(\phi) \sin(\phi) + N(\phi) \cos(\phi))\dot{\phi} \\
&= \begin{bmatrix} 0 \\ 0 \\ N(\phi) + h \end{bmatrix} \times \boldsymbol{\omega}_{en} - \begin{bmatrix} M(\phi) \cot(\phi) \dot{\phi} \\ 0 \\ \dot{h} \end{bmatrix}
\end{aligned} \tag{A-71}$$

With the meridian curvature radius $M(\phi) = \frac{a(1-e^2)}{(1-e^2 \sin^2 \phi)^{\frac{3}{2}}}$ [16].

The angular rate between NED and ECEF frame is defined by the differential equation for \mathbf{R}_{en} as

$$\boldsymbol{\omega}_{en} = \text{veck}(\mathbf{R}_{en}^T \dot{\mathbf{R}}_{en}) = \text{veck} \begin{bmatrix} 0 & \sin(\phi) \dot{\lambda} & -\dot{\phi} \\ -\sin(\phi) \dot{\lambda} & 0 & -\cos(\phi) \dot{\lambda} \\ \dot{\phi} & \cos(\phi) \dot{\lambda} & 0 \end{bmatrix} = \begin{bmatrix} \cos(\phi) \dot{\lambda} \\ -\dot{\phi} \\ -\sin(\phi) \dot{\lambda} \end{bmatrix} \tag{A-72}$$

$\boldsymbol{\omega}_{en}$ is referred to as transport rate. Rotating with $\boldsymbol{\omega}_{en}$ the NED frame remains north indicating and locally tangential to the WGS84 ellipsoid.

Inserting equation (A-72) in (A-71) and after some simplification of the terms including normal and meridian curvature radii

$$\mathbf{v}_n = \begin{bmatrix} (N(\phi) + h)\dot{\phi} - M(\phi) \cot(\phi) \dot{\phi} \\ (N(\phi) + h) \cos(\phi) \dot{\lambda} \\ -\dot{h} \end{bmatrix} = \begin{bmatrix} (M(\phi) + h)\dot{\phi} \\ (N(\phi) + h) \cos(\phi) \dot{\lambda} \\ -\dot{h} \end{bmatrix} \tag{A-73}$$

Equation (A-73) can be inverted to find the WGS84 position differential equations with velocities in n -frame:

$$\begin{aligned}
\dot{\phi} &= \frac{v_N}{M(\phi) + h} \\
\dot{\lambda} &= \frac{v_E}{(N(\phi) + h) \cos(\phi)} \\
\dot{h} &= -v_D
\end{aligned} \tag{A-74}$$

With equation (A-74) the transport rate $\boldsymbol{\omega}_{en}$ becomes

$$\boldsymbol{\omega}_{en}(\phi, h, v_N, v_E) = \begin{bmatrix} \frac{v_E}{N(\phi) + h} \\ \frac{v_N}{M(\phi) + h} \\ \frac{\tan(\phi) v_E}{N(\phi) + h} \end{bmatrix} \tag{A-75}$$

Deriving the differential equation for velocities in n -frame from the ECEF inertial navigation equation (A-62) is straightforward:

$$\begin{aligned}
\dot{\mathbf{v}}_n &= \frac{d}{dt} (\mathbf{R}_{en}^T \mathbf{v}_e) = \dot{\mathbf{R}}_{en}^T \mathbf{v}_e + \mathbf{R}_{en}^T \dot{\mathbf{v}}_e \\
&= -\boldsymbol{\omega}_{en} \times \mathbf{v}_n - 2(\mathbf{R}_{en}^T \boldsymbol{\omega}_{ie}) \times \mathbf{v}_n + \mathbf{R}_{nb} \mathbf{f}_b + \boldsymbol{\gamma}_n(\mathbf{x}_e)
\end{aligned} \tag{A-76}$$

The differential equation for the NED to body-fixed frame orientation quaternion is (A-48)

$$\dot{\check{\mathbf{q}}}_{nb} = \frac{1}{2} \check{\mathbf{q}}_{nb} \cdot \check{\boldsymbol{\omega}}_{nb} \quad (\text{A-77})$$

Alternatively with $\check{\boldsymbol{\omega}}_{nb} = \check{\boldsymbol{\omega}}_{ib} - \check{\mathbf{q}}_{nb}^{-1} \cdot \check{\boldsymbol{\omega}}_{in} \cdot \check{\mathbf{q}}_{nb}$ and preferable because IMU rate measurements $\boldsymbol{\omega}_{ib}$ explicitly appear as input:

$$\dot{\check{\mathbf{q}}}_{nb} = \frac{1}{2} (\check{\mathbf{q}}_{nb} \cdot \check{\boldsymbol{\omega}}_{ib} - \check{\boldsymbol{\omega}}_{in} \cdot \check{\mathbf{q}}_{nb}) \quad (\text{A-78})$$

Finally the full set of inertial navigation equations for WGS84 positions, NED-velocities and orientation parametrization with quaternions is

$$\begin{aligned} \dot{\phi} &= \frac{v_N}{M(\phi) + h} \\ \dot{\lambda} &= \frac{v_E}{(N(\phi) + h) \cos(\phi)} \end{aligned} \quad (\text{A-79})$$

$$\begin{aligned} \dot{h} &= -v_D \\ \dot{\mathbf{v}}_n &= \mathbf{R}_{nb}(\check{\mathbf{q}}_{nb}) \cdot \mathbf{f}_b + \boldsymbol{\gamma}_n(\phi, h) - (2\mathbf{R}_{en}^T(\phi, \lambda) \cdot \boldsymbol{\omega}_{ie} + \boldsymbol{\omega}_{en}(\phi, h, v_n, v_e)) \times \mathbf{v}_n \end{aligned} \quad (\text{A-80})$$

$$\dot{\check{\mathbf{q}}}_{nb} = \frac{1}{2} (\check{\mathbf{q}}_{nb} \cdot \check{\boldsymbol{\omega}}_{ib} - \check{\boldsymbol{\omega}}_{in}(\phi, \lambda, h, v_n, v_e) \cdot \check{\mathbf{q}}_{nb}) \quad (\text{A-81})$$

Like equations (A-61) through (A-63) these equations take the measurements of a body-fixed IMU sensor as input. Because of this they are referred to as strapdown equations. If not mentioned otherwise, the function \mathbf{s} will refer to the strapdown equations (A-79) through (A-81) in this text with

$$\dot{\mathbf{z}}_n(t) = \mathbf{s}(\mathbf{z}_n(t), \mathbf{f}_b(t), \boldsymbol{\omega}_{ib}(t)) \quad (\text{A-82})$$

$$\mathbf{z}_n(t) = \begin{bmatrix} \phi(t) \\ \lambda(t) \\ h(t) \\ \mathbf{v}_n(t) \\ \check{\mathbf{q}}_{nb}(t) \end{bmatrix} \text{ and } \mathbf{u}_{IMU}(t) = \begin{bmatrix} \mathbf{f}_b \\ \boldsymbol{\omega}_{ib} \end{bmatrix} \quad (\text{A-83})$$

Note that for $\phi \rightarrow +\frac{\pi}{2}$ and $\phi \rightarrow -\frac{\pi}{2}$ the derivative of geodetic longitude $\dot{\lambda}$ and the transport rate $\boldsymbol{\omega}_{en}$ (see equation (A-75)) go to ∞ . Because the transport rate appears in the differential equations for \mathbf{v}_n and \mathbf{q}_{nb} as well, the complete set of inertial navigation system equations in the form of equations (A-79) through (A-81) is invalid at the geographic poles. This shortcoming can be accepted in most cases (for $\phi \leq 84^\circ$: $\frac{1}{\cos(\phi)} \leq 10$). If all-world applicability is required, $\dot{\phi}$ and $\dot{\lambda}$ differential equations can be substituted by a quaternion position differential equation. Furthermore, north-indicating azimuth navigation must be given up in vicinity of the geographic poles (c.f. polar navigation and world-wide capability in [20, 21]).

The definition of the WGS84 ellipsoid as a geocentric equipotential ellipsoid [18] reduces the effort of gravity modeling for small heights h to a 1D model

$$\boldsymbol{\gamma}_n = \begin{bmatrix} 0 \\ 0 \\ \gamma_D \end{bmatrix} \quad (\text{A-84})$$

where only the gravity component normal to the WGS84 ellipsoid is nonzero.

On the ellipsoid surface this is in accordance with the exact closed form solution for the gravity field of an equipotential ellipsoid provided by the formula of Somigliana

$$\gamma_D(\phi, h)|_{h=0} = \gamma_e \frac{1 + k \sin^2(\phi)}{\sqrt{1 - e^2 \sin^2(\phi)}} \quad (\text{A-85})$$

with $k = \frac{b\gamma_p}{a\gamma_e} - 1$, see [18].

The equipotential ellipsoid is defined by semi-major axis a , ellipsoidal flattening f , angular rate ω_{ie} and the earth's gravitational constant GM . See [18] for the values of these parameters and formulas for derived parameters used in Somigliana's formula, such as semi-minor axis b , first eccentricity e and gravity at equator and poles γ_e and γ_p .

For heights below $30km$ a 2nd order approximation yields acceptable results

$$\gamma_D(\phi, h) \approx \gamma_D(\phi, h)|_{h=0} \cdot \left(1 - \frac{2}{a} (1 + f + m - 2f \sin^2(\phi))h + \frac{3}{a^2} h^2 \right) \quad (\text{A-86})$$

with $m = \frac{\|\omega_{ie}\|^2 a^2 b}{GM}$, see [18].

A.3 SPECIFIC FORCE LEVER ARM

This appendix is an more detailed version of the derivation found in section 2.6 of the author's Diploma thesis [39].

Starting with the relationship of kinematic velocity of navigation reference point R and center of gravity G

$$\mathbf{v}_e^R = \mathbf{v}_e^G + \dot{\mathbf{r}}_e^{GR} \quad (\text{A-87})$$

With the definition of NED kinematic velocity $\mathbf{v}_n := \mathbf{R}_{en}^T \mathbf{v}_e$ and the rigid body assumption $\dot{\mathbf{r}}_b^{GR} = \mathbf{0}$ this becomes

$$\mathbf{v}_n^R = \mathbf{R}_{en}^T \mathbf{v}_e^G + \mathbf{R}_{nb} (\boldsymbol{\omega}_{eb} \times \mathbf{r}_b^{GR}) \quad (\text{A-88})$$

Taking the time derivative of above equation yields the desired differential equation of NED velocity in navigation reference point R (again with $\dot{\mathbf{r}}_b^{GR} = \mathbf{0}$)

$$\dot{\mathbf{v}}_n^R = \mathbf{R}_{en}^T (\boldsymbol{\omega}_{ne} \times \mathbf{v}_e^G) + \mathbf{R}_{en}^T \dot{\mathbf{v}}_e^G + \mathbf{R}_{nb} (\boldsymbol{\omega}_{nb} \times (\boldsymbol{\omega}_{eb} \times \mathbf{r}_b^{GR})) + \mathbf{R}_{nb} (\dot{\boldsymbol{\omega}}_{eb} \times \mathbf{r}_b^{GR}) \quad (\text{A-89})$$

The equations of motion of a point mass are valid in the center of gravity. Consequently, they can be inserted for the time derivative of kinematic velocity of the center of gravity $\dot{\mathbf{v}}_e^G$. The first two terms on the right hand side become

$$\mathbf{R}_{en}^T (\boldsymbol{\omega}_{ne} \times \mathbf{v}_e^G) + \mathbf{R}_{en}^T \dot{\mathbf{v}}_e^G = \mathbf{R}_{en}^T (\boldsymbol{\omega}_{ne} \times \mathbf{v}_e^G) + \mathbf{R}_{nb} \mathbf{f}_b^G + \mathbf{R}_{en}^T \boldsymbol{\gamma}_e^G - 2\mathbf{R}_{en}^T (\boldsymbol{\omega}_{ie} \times \mathbf{v}_e^G) = \dot{\mathbf{v}}_n^G \quad (\text{A-90})$$

This gives

$$\dot{\mathbf{v}}_n^R = \dot{\mathbf{v}}_n^G + \underbrace{\mathbf{R}_{nb} (\boldsymbol{\omega}_{nb} \times (\boldsymbol{\omega}_{eb} \times \mathbf{r}_b^{GR})) + \mathbf{R}_{nb} (\dot{\boldsymbol{\omega}}_{eb} \times \mathbf{r}_b^{GR})}_{\Delta \mathbf{a}_{n,1}^{GR}} \quad (\text{A-91})$$

The two last terms on the right hand side are caused by the lever arm between center of gravity and navigation reference point \mathbf{r}_b^{GR} . Additionally, when writing center of gravity NED velocity time derivative $\dot{\mathbf{v}}_n^G$ as function of navigation reference point velocity and computing gravity vector in point R

$$\begin{aligned} \dot{\mathbf{v}}_n^G &= \mathbf{R}_{nb} \mathbf{f}_b^G + \mathbf{g}_n^R \underbrace{- \Delta \mathbf{g}_n^{GR}}_{\approx 0} - \mathbf{R}_{en}^T (\boldsymbol{\omega}_{ie} \times (\boldsymbol{\omega}_{ie} \times \mathbf{r}_e^G)) - \mathbf{R}_{en}^T ((2\boldsymbol{\omega}_{ie} + \mathbf{R}_{en} \boldsymbol{\omega}_{en}) \times (\mathbf{R}_{en} \mathbf{v}_n^R - \dot{\mathbf{r}}_e^{GR})) \\ &= \mathbf{R}_{nb} \mathbf{f}_b^G + \mathbf{g}_n^R - (2\mathbf{R}_{en}^T \boldsymbol{\omega}_{ie} + \boldsymbol{\omega}_{en}) \times \mathbf{v}_n^R \\ &\quad + \underbrace{\mathbf{R}_{en}^T (\boldsymbol{\omega}_{ie} \times (\boldsymbol{\omega}_{ie} \times (\mathbf{R}_{eb} \mathbf{r}_b^{GR})) + (2\mathbf{R}_{en}^T \boldsymbol{\omega}_{ie} + \boldsymbol{\omega}_{en}) \times (\mathbf{R}_{nb} (\boldsymbol{\omega}_{eb} \times \mathbf{r}_b^{GR})))}_{\Delta \mathbf{a}_{n,2}^{GR}} \end{aligned} \quad (\text{A-92})$$

With the lever arm corrections $\Delta \mathbf{a}_b^{GR} := \mathbf{R}_{nb}^T (\Delta \mathbf{a}_{n,1}^{GR} + \Delta \mathbf{a}_{n,2}^{GR})$ an equivalent specific force in navigation reference point R can be defined that may consistently be used as input to the strapdown equations to determine $\dot{\mathbf{v}}_n^R$ (i.e. corresponds to what an ideal accelerometer triad would measure at this point)

$$\mathbf{f}_b^R := \mathbf{f}_b^G + \Delta \mathbf{a}_b^{GR} \quad (\text{A-93})$$

Writing

$$\begin{aligned} \Delta \mathbf{a}_{n,2}^{GR} = & \mathbf{R}_{nb} \left((2\mathbf{R}_{eb}^T \boldsymbol{\omega}_{ie}) \times (\boldsymbol{\omega}_{eb} \times \mathbf{r}_b^{GR}) + (\mathbf{R}_{nb}^T \boldsymbol{\omega}_{en}) \times (\boldsymbol{\omega}_{eb} \times \mathbf{r}_b^{GR}) \right) \\ & + \mathbf{R}_{en}^T \left(\boldsymbol{\omega}_{ie} \times (\boldsymbol{\omega}_{ie} \times (\mathbf{R}_{eb} \mathbf{r}_b^{GR})) \right) \end{aligned} \quad (\text{A-94})$$

And inserting $\Delta \mathbf{a}_{n,1}^{GR}$ and $\Delta \mathbf{a}_{n,2}^{GR}$ in $\Delta \mathbf{a}_b^{GR}$

$$\begin{aligned} \Delta \mathbf{a}_b^{GR} = & \boldsymbol{\omega}_{ib} \times (\boldsymbol{\omega}_{eb} \times \mathbf{r}_b^{GR}) + (\mathbf{R}_{eb}^T \boldsymbol{\omega}_{ie}) \times (\boldsymbol{\omega}_{eb} \times \mathbf{r}_b^{GR}) + \dot{\boldsymbol{\omega}}_{eb} \times \mathbf{r}_b^{GR} \\ & + \mathbf{R}_{eb}^T \left(\boldsymbol{\omega}_{ie} \times (\boldsymbol{\omega}_{ie} \times (\mathbf{R}_{eb} \mathbf{r}_b^{GR})) \right) \end{aligned} \quad (\text{A-95})$$

Using the identity

$$\boldsymbol{\omega}_{ib} \times (\boldsymbol{\omega}_{eb} \times \mathbf{r}_b^{GR}) = -\mathbf{r}_b^{GR} \times (\boldsymbol{\omega}_{ib} \times \boldsymbol{\omega}_{eb}) - \boldsymbol{\omega}_{eb} \times (\mathbf{r}_b^{GR} \times \boldsymbol{\omega}_{ib}) \quad (\text{A-96})$$

This becomes

$$\begin{aligned} \Delta \mathbf{a}_b^{GR} = & (\mathbf{R}_{eb}^T \boldsymbol{\omega}_{ie}) \times (\boldsymbol{\omega}_{eb} \times \mathbf{r}_b^{GR}) + \boldsymbol{\omega}_{eb} \times (\boldsymbol{\omega}_{ib} \times \mathbf{r}_b^{GR}) + (\boldsymbol{\omega}_{ib} \times \boldsymbol{\omega}_{eb}) \times \mathbf{r}_b^{GR} + \dot{\boldsymbol{\omega}}_{eb} \times \mathbf{r}_b^{GR} \\ & + \mathbf{R}_{eb}^T \left(\boldsymbol{\omega}_{ie} \times (\boldsymbol{\omega}_{ie} \times (\mathbf{R}_{eb} \mathbf{r}_b^{GR})) \right) \end{aligned} \quad (\text{A-97})$$

With

$$\begin{aligned} & (\mathbf{R}_{eb}^T \boldsymbol{\omega}_{ie}) \times (\boldsymbol{\omega}_{eb} \times \mathbf{r}_b^{GR}) + \boldsymbol{\omega}_{eb} \times (\boldsymbol{\omega}_{ib} \times \mathbf{r}_b^{GR}) \\ & = (\mathbf{R}_{eb}^T \boldsymbol{\omega}_{ie}) \times (\boldsymbol{\omega}_{eb} \times \mathbf{r}_b^{GR}) + \boldsymbol{\omega}_{eb} \times \left((\mathbf{R}_{eb}^T \boldsymbol{\omega}_{ie}) \times \mathbf{r}_b^{GR} + \boldsymbol{\omega}_{eb} \times \mathbf{r}_b^{GR} \right) \\ & = \boldsymbol{\omega}_{ib} \times (\boldsymbol{\omega}_{eb} \times \mathbf{r}_b^{GR}) + (\boldsymbol{\omega}_{ib} - \mathbf{R}_{eb}^T \boldsymbol{\omega}_{ie}) \times \left((\mathbf{R}_{eb}^T \boldsymbol{\omega}_{ie}) \times \mathbf{r}_b^{GR} \right) \\ & = \boldsymbol{\omega}_{ib} \times (\boldsymbol{\omega}_{ib} \times \mathbf{r}_b^{GR}) - (\mathbf{R}_{eb}^T \boldsymbol{\omega}_{ie}) \times \left((\mathbf{R}_{eb}^T \boldsymbol{\omega}_{ie}) \times \mathbf{r}_b^{GR} \right) \end{aligned} \quad (\text{A-98})$$

This simplifies to

$$\Delta \mathbf{a}_b^{GR} = \boldsymbol{\omega}_{ib} \times (\boldsymbol{\omega}_{ib} \times \mathbf{r}_b^{GR}) + (\boldsymbol{\omega}_{ib} \times \boldsymbol{\omega}_{eb}) \times \mathbf{r}_b^{GR} + \dot{\boldsymbol{\omega}}_{eb} \times \mathbf{r}_b^{GR} \quad (\text{A-99})$$

With $\dot{\boldsymbol{\omega}}_{ib} = \frac{d}{dt} (\mathbf{R}_{eb}^T \boldsymbol{\omega}_{ie} + \boldsymbol{\omega}_{eb}) = \mathbf{R}_{eb}^T (\boldsymbol{\omega}_{be} \times \boldsymbol{\omega}_{ie}) + \dot{\boldsymbol{\omega}}_{eb} = \boldsymbol{\omega}_{ib} \times \boldsymbol{\omega}_{eb} + \dot{\boldsymbol{\omega}}_{eb}$ finally

$$\Delta \mathbf{a}_b^{GR} = \boldsymbol{\omega}_{ib} \times (\boldsymbol{\omega}_{ib} \times \mathbf{r}_b^{GR}) + \dot{\boldsymbol{\omega}}_{ib} \times \mathbf{r}_b^{GR} \quad (\text{A-100})$$

Note that only the change in gravitation was neglected $\Delta \mathbf{g}_n^{GR} \approx \mathbf{0}$.

A.4 RIGID BODY EQUATIONS OF ROTATIONAL MOTION

This appendix is based on chapter 4 of the author's Diploma thesis [39].

With equations (A-49) and (A-51) for an infinitesimal mass dm located in P_{dm}

$$dF_{i,external}(P_{dm}) = dm \cdot \mathbf{a}_i(P_{dm}) - dF_{i,gravitation}(P_{dm}) \quad (A-101)$$

With the vector from center of gravity G to P_{dm} $\Delta \mathbf{x}_i(P_{dm})$

$$\mathbf{x}_i(P_{dm}) = \Delta \mathbf{x}_i(P_{dm}) + \mathbf{x}_i(G) \quad (A-102)$$

and

$$\mathbf{a}_i(P_{dm}) = \Delta \ddot{\mathbf{x}}_i(P_{dm}) + \mathbf{a}_i(G) \quad (A-103)$$

the integral of infinitesimal moments in G due to infinitesimal external forces is

$$\begin{aligned} \mathbf{M}_{i,sum} &:= \int_m \Delta \mathbf{x}_i(P_{dm}) \times dF_{i,external}(P_{dm}) \\ &= \int_m \Delta \mathbf{x}_i(P_{dm}) \times \Delta \ddot{\mathbf{x}}_i(P_{dm}) dm - \int_m \Delta \mathbf{x}_i(P_{dm}) dm \times (\mathbf{a}_i(G) + \mathbf{g}_i(G)) \end{aligned} \quad (A-104)$$

where variations of gravitational acceleration over the body have been neglected, i.e. $\mathbf{g}_i(P_{dm}) \approx \mathbf{g}_i(G)$. From the definition of the center of gravity G and with equation (A-102) it follows that

$$\int_m \Delta \mathbf{x}_i(P_{dm}) dm = \int_m \mathbf{x}_i(P_{dm}) dm - m \mathbf{x}_i(G) \equiv \mathbf{0} \quad (A-105)$$

Furthermore with the direction cosine matrix differential equation (A-26) and for a constant mass distribution and with rigid body constraints (A-59)

$$\Delta \ddot{\mathbf{x}}_i(P_{dm}) = \frac{d^2}{dt^2}(\Delta \mathbf{x}_b(P_{dm})) = \frac{d^2 \mathbf{R}_{ib}}{dt^2} \Delta \mathbf{x}_b(P_{dm}) = (\mathbf{R}_{ib} \boldsymbol{\Omega}_{ib} \boldsymbol{\Omega}_{ib} + \mathbf{R}_{ib} \dot{\boldsymbol{\Omega}}_{ib}) \Delta \mathbf{x}_b(P_{dm}) \quad (A-106)$$

This gives

$$\begin{aligned} \mathbf{M}_{b,sum} &:= \mathbf{R}_{ib}^T \int_m \Delta \mathbf{x}_i(P_{dm}) \times \Delta \ddot{\mathbf{x}}_i(P_{dm}) dm \\ &= \int_m \text{skew}(\Delta \mathbf{x}_b(P_{dm})) (\boldsymbol{\Omega}_{ib} \boldsymbol{\Omega}_{ib} + \dot{\boldsymbol{\Omega}}_{ib}) \Delta \mathbf{x}_b(P_{dm}) dm \end{aligned} \quad (A-107)$$

This result can be simplified using the Jacobi identity $\mathbf{v}_1 \times (\mathbf{v}_2 \times \mathbf{v}_3) + \mathbf{v}_2 \times (\mathbf{v}_3 \times \mathbf{v}_1) + \mathbf{v}_3 \times (\mathbf{v}_1 \times \mathbf{v}_2) = \mathbf{0}$. For two skew symmetric matrices $\boldsymbol{\Omega}_1 = \text{skew}(\mathbf{v}_1)$ and $\boldsymbol{\Omega}_2 = \text{skew}(\mathbf{v}_2)$ this cross product identity gives

$$\boldsymbol{\Omega}_1 \boldsymbol{\Omega}_2 = \boldsymbol{\Omega}_2 \boldsymbol{\Omega}_1 + \text{skew}(\boldsymbol{\Omega}_1 \mathbf{v}_2) = \boldsymbol{\Omega}_2 \boldsymbol{\Omega}_1 - \text{skew}(\boldsymbol{\Omega}_2 \mathbf{v}_1) \quad (A-108)$$

Using this identity

$$\begin{aligned}
& skew(\Delta \mathbf{x}_b(P_{dm})) \boldsymbol{\Omega}_{ib} \boldsymbol{\Omega}_{ib} \Delta \mathbf{x}_b(P_{dm}) \\
&= \left(\boldsymbol{\Omega}_{ib} skew(\Delta \mathbf{x}_b(P_{dm})) - skew(\boldsymbol{\Omega}_{ib} \Delta \mathbf{x}_b(P_{dm})) \right) \boldsymbol{\Omega}_{ib} \Delta \mathbf{x}_b(P_{dm}) \quad (\text{A-109}) \\
&= \boldsymbol{\Omega}_{ib} skew(\Delta \mathbf{x}_b(P_{dm})) \boldsymbol{\Omega}_{ib} \Delta \mathbf{x}_b(P_{dm})
\end{aligned}$$

Now with $\boldsymbol{\Omega}_{ib} \Delta \mathbf{x}_b(P_{dm}) = -skew(\Delta \mathbf{x}_b(P_{dm})) \boldsymbol{\omega}_{ib}$ and $\dot{\boldsymbol{\Omega}}_{ib} \Delta \mathbf{x}_b(P_{dm}) = -skew(\Delta \mathbf{x}_b(P_{dm})) \dot{\boldsymbol{\omega}}_{ib}$

$$\begin{aligned}
\mathbf{M}_{b,sum} &= - \int_m skew(\Delta \mathbf{x}_b(P_{dm})) skew(\Delta \mathbf{x}_b(P_{dm})) dm \dot{\boldsymbol{\omega}}_{ib} \\
&- \boldsymbol{\Omega}_{ib} \int_m skew(\Delta \mathbf{x}_b(P_{dm})) skew(\Delta \mathbf{x}_b(P_{dm})) dm \boldsymbol{\omega}_{ib}
\end{aligned} \quad (\text{A-110})$$

Define the inertia matrix

$$\mathbf{I}_{bb} := - \int_m skew(\Delta \mathbf{x}_b(P_{dm})) skew(\Delta \mathbf{x}_b(P_{dm})) dm \quad (\text{A-111})$$

For $\Delta \mathbf{x}_b(P_{dm}) = [\Delta x \ \Delta y \ \Delta z]^T$ this is

$$\mathbf{I}_{bb} = \int_m \begin{bmatrix} \Delta y^2 + \Delta z^2 & -\Delta x \Delta y & -\Delta x \Delta z \\ -\Delta x \Delta y & \Delta x^2 + \Delta z^2 & -\Delta y \Delta z \\ -\Delta x \Delta z & -\Delta y \Delta z & \Delta x^2 + \Delta y^2 \end{bmatrix} dm \quad (\text{A-112})$$

Inserting (A-111) in (A-110) gives the equation of rotational motion in body-fixed frame

$$\mathbf{M}_{b,sum} = \mathbf{I}_{bb} \dot{\boldsymbol{\omega}}_{ib} + \boldsymbol{\Omega}_{ib} \mathbf{I}_{bb} \boldsymbol{\omega}_{ib} \quad (\text{A-113})$$

Note that with $\mathbf{I}_{bb} = const.$ this is equivalent to

$$\mathbf{M}_{i,sum} = \mathbf{R}_{ib} \mathbf{M}_{b,sum} = \frac{d}{dt} (\mathbf{R}_{ib} \mathbf{I}_{bb} \boldsymbol{\omega}_{ib}) \quad (\text{A-114})$$

A.5 ERROR STATE PROPAGATION MODEL FOR HEADING AND AIRSPEED DEAD RECKONING

In the perturbation analysis of equation (2-2)

$$\dot{\mathbf{\Lambda}}_H = \begin{bmatrix} \frac{1}{M(\phi_{WGS84,0}^R) + h_{WGS84}^R} & 0 \\ 0 & \frac{1}{(N(\phi_{WGS84,0}^R) + h_{WGS84}^R) \cos(\phi_{WGS84}^R)} \end{bmatrix} \mathbf{v}_{Hn} \quad (\text{A-115})$$

errors in the computation of normal and meridian radii can be neglected because they correspond to scale factor errors on the order of $1ppm$ for distances travelled in north direction of $\sim 100km$ (and radii computed at initial position). Similarly, errors in height of up to $5500m$ (approximately $18000ft$) will cause a scale factor error in position propagation of less than $1000ppm$ which is still negligibly small.

Notice that integration of longitude becomes very sensitive to latitude errors at high latitudes. $10km$ north position error introduce a scale factor error in longitude propagation of $15000ppm$ at 85° latitude and $2600ppm$ at 60° latitude respectively. For the applications considered here, this effect may be dismissed from analysis as well.

Consequently, horizontal position error approximately evolves in time according to

$$\delta \dot{\mathbf{\Lambda}}_H \approx \begin{bmatrix} \frac{1}{M(\phi_{WGS84,0}^R) + h_{WGS84}^R} & 0 \\ 0 & \frac{1}{(N(\phi_{WGS84,0}^R) + h_{WGS84}^R) \cos(\phi_{WGS84}^R)} \end{bmatrix} \delta \mathbf{v}_{Hn} \quad (\text{A-116})$$

with the error in horizontal kinematic velocity vector due to errors in wind and aerodynamic horizontal velocity vectors

$$\delta \mathbf{v}_{Hn} = \delta \mathbf{v}_{HWn} + \delta \mathbf{v}_{HAN} \quad (\text{A-117})$$

The error in aerodynamic velocity vector is due to errors in computed body-frame orientation, errors in computed aerodynamic angles of attack and sideslip and due to error in measured airspeed:

$$\begin{aligned} \delta \mathbf{v}_{An} &= \delta (\mathbf{R}_{nb} \mathbf{R}_{ab}^T [V_A \ 0 \ 0]^T) \\ &= (\mathbf{I} - \hat{\mathbf{R}}_{nb} \mathbf{R}_{nb}^T) \mathbf{R}_{na_i} [V_A \ 0 \ 0]^T \\ &\quad + \mathbf{R}_{nb} (\mathbf{R}_{ab}^T \hat{\mathbf{R}}_{ab} - \mathbf{I}) \hat{\mathbf{R}}_{ab}^T [V_A \ 0 \ 0]^T + \mathbf{R}_{na_i} [\delta V_A \ 0 \ 0]^T \end{aligned} \quad (\text{A-118})$$

With the linearization of orientation error $\mathbf{I} - \hat{\mathbf{R}}_{nb} \mathbf{R}_{nb}^T \approx [\boldsymbol{\Psi} \times]$ (see section 2.2.2.1) accounting for small heading error only $\boldsymbol{\Psi} \approx [0 \ 0 \ \delta \Psi_{nb}]^T$ and with

$$\mathbf{R}_{na_i} = \begin{bmatrix} \cos(\chi_A) & -\sin(\chi_A) & 0 \\ \sin(\chi_A) & \cos(\chi_A) & 0 \\ 0 & 0 & 1 \end{bmatrix} \begin{bmatrix} \cos(\gamma_A) & 0 & \sin(\gamma_A) \\ 0 & 1 & 0 \\ -\sin(\gamma_A) & 0 & \cos(\gamma_A) \end{bmatrix} \quad (\text{A-119})$$

the first term in equation (A-118) can be approximated with $\Psi_{nb} \approx \chi_A$ and $\cos(\gamma_A) \approx 1$ as

$$(\mathbf{I} - \hat{\mathbf{R}}_{nb} \mathbf{R}_{nb}^T) \mathbf{R}_{na_i} \begin{bmatrix} V_A \\ 0 \\ 0 \end{bmatrix} \approx \begin{bmatrix} -\sin(\Psi_{nb}) \\ \cos(\Psi_{nb}) \\ 0 \end{bmatrix} \delta \Psi_{nb} V_A \quad (\text{A-120})$$

Note that in this simplification horizontal orientation error (i.e. error in computed roll and pitch) is assumed negligible.

Because no information is available on aerodynamic angles of attack and sideslip, the values of computed aerodynamic angles of attack and sideslip are zero and $\hat{\mathbf{R}}_{ab} = \mathbf{I}$. This gives approximately for small true aerodynamic angles of attack and sideslip

$$(\mathbf{R}_{ab}^T \hat{\mathbf{R}}_{ab} - \mathbf{I}) \hat{\mathbf{R}}_{ab}^T [V_A \ 0 \ 0]^T \approx \begin{bmatrix} V_A \\ 0 \\ 0 \end{bmatrix} \times \begin{bmatrix} 0 \\ \alpha_A \\ -\beta_A \end{bmatrix}$$

With

$$\mathbf{R}_{nb} = \begin{bmatrix} \cos(\Psi_{nb}) & -\sin(\Psi_{nb}) & 0 \\ \sin(\Psi_{nb}) & \cos(\Psi_{nb}) & 0 \\ 0 & 0 & 1 \end{bmatrix} \begin{bmatrix} \cos(\theta_{nb}) & 0 & \sin(\theta_{nb}) \\ 0 & 1 & 0 \\ -\sin(\theta_{nb}) & 0 & \cos(\theta_{nb}) \end{bmatrix} \begin{bmatrix} 1 & 0 & 0 \\ 0 & \cos(\Phi_{nb}) & -\sin(\Phi_{nb}) \\ 0 & \sin(\Phi_{nb}) & \cos(\Phi_{nb}) \end{bmatrix}$$

this gives for the second term in equation (A-118)

$$\begin{aligned} \mathbf{R}_{nb} (\mathbf{R}_{ab}^T \hat{\mathbf{R}}_{ab} - \mathbf{I}) \hat{\mathbf{R}}_{ab}^T [V_A \ 0 \ 0]^T \\ \approx \begin{bmatrix} -\sin(\Psi_{nb}) \\ \cos(\Psi_{nb}) \\ 0 \end{bmatrix} (\cos(\Phi_{nb}) \beta_A - \sin(\Phi_{nb}) \alpha_A) V_A + \left(\begin{bmatrix} \cos(\Psi_{nb}) \\ \sin(\Psi_{nb}) \\ 0 \end{bmatrix} \sin(\theta_{nb}) + \begin{bmatrix} 0 \\ 0 \\ 1 \end{bmatrix} \cos(\theta_{nb}) \right) \\ + (\sin(\Phi_{nb}) \beta_A + \cos(\Phi_{nb}) \alpha_A) V_A \end{aligned}$$

In the following, elevation angle is assumed small and $\sin(\theta_{nb}) \approx 0$.

Finally, the last term becomes with $\Psi_{nb} \approx \chi_A$ and $\cos(\gamma_A) \approx 1$ and equation (A-119)

$$\mathbf{R}_{na_l} [\delta V_A \ 0 \ 0]^T \approx \begin{bmatrix} \cos(\Psi_{nb}) \\ \sin(\Psi_{nb}) \\ 0 \end{bmatrix} \delta V_A - \begin{bmatrix} 0 \\ 0 \\ \sin(\gamma_A) \end{bmatrix} \delta V_A$$

The horizontal aerodynamic velocity error becomes approximately

$$\delta \mathbf{v}_{HAN} \approx \begin{bmatrix} \cos(\Psi_{nb}) \\ \sin(\Psi_{nb}) \end{bmatrix} \delta V_A + \begin{bmatrix} -\sin(\Psi_{nb}) \\ \cos(\Psi_{nb}) \end{bmatrix} (\delta \Psi_{nb} + \cos(\Phi_{nb}) \beta_A - \sin(\Phi_{nb}) \alpha_A) V_A \quad (\text{A-121})$$

Inserting equations (A-121) and (A-117) in (A-116) gives equation (2-16).

Elevation angle θ_{nb} , aerodynamic angles of attack and sideslip and errors error in computed roll and pitch are assumed small. Furthermore, $\Psi_{nb} \approx \chi_A$ and $\cos(\gamma_A) \approx 1$ is assumed.

A.6 PERTURBATION ERROR DIFFERENTIAL EQUATIONS

This appendix is based on section 3.2 of the author's Diploma thesis [39] and the references cited therein.

The navigation state error vector is defined in this work as

$$\delta \mathbf{z} := \begin{bmatrix} \delta \phi \\ \delta \lambda \\ \delta h \\ \delta \mathbf{v}_n \\ \boldsymbol{\phi} \end{bmatrix} \quad (\text{A-122})$$

with the equivalence of Euler angle parametrization of orientation error $\boldsymbol{\Phi}$ and the phi angle orientation error $\boldsymbol{\phi}_n$ in linear approximation

$$\boldsymbol{\phi}_n \doteq \boldsymbol{\Phi}$$

the linear differential equations for phi angle orientation error $\boldsymbol{\phi}_n$ can be derived by linearizing the nonlinear differential equations for the orientation error Euler angles $\boldsymbol{\Phi}$.

The starting point is the following system of nonlinear navigation error differential equations

$$\begin{bmatrix} \delta \dot{\phi} \\ \delta \dot{\lambda} \\ \delta \dot{h} \\ \delta \dot{\mathbf{v}}_n \\ \dot{\boldsymbol{\phi}} \end{bmatrix} = \begin{bmatrix} \phi - \hat{\phi} \\ \lambda - \hat{\lambda} \\ h - \hat{h} \\ \mathbf{v}_n - \hat{\mathbf{v}}_n \\ [\delta \dot{\phi}_1, \delta \dot{\phi}_2, \delta \dot{\phi}_3]^T \end{bmatrix} \quad (\text{A-123})$$

The derivatives of computed values are calculated from known equations and using known parameters and input values only.

For the translation states with equation (A-82) accounting for accelerometer measurement error $\delta \mathbf{f}_b$ and gravity model error $\delta \boldsymbol{\gamma}_n$:

$$\begin{bmatrix} \delta \dot{\phi} \\ \delta \dot{\lambda} \\ \delta \dot{h} \end{bmatrix} = \begin{bmatrix} \frac{\hat{v}_N + \delta v_N}{M(\hat{\phi} + \delta \phi) + \hat{h} + \delta h} \\ \frac{\hat{v}_E + \delta v_E}{(N(\hat{\phi} + \delta \phi) + \hat{h} + \delta h) \cdot \cos(\hat{\phi} + \delta \phi)} \\ -\hat{v}_D - \delta v_D \end{bmatrix} - \begin{bmatrix} \frac{\hat{v}_N}{M(\hat{\phi}) + \hat{h}} \\ \frac{\hat{v}_E}{(N(\hat{\phi}) + \hat{h}) \cdot \cos \hat{\phi}} \\ -\hat{v}_D \end{bmatrix} \quad (\text{A-124})$$

and

$$\begin{aligned} \delta \dot{\mathbf{v}}_n &= \mathbf{R}_{nb}(\tilde{\mathbf{f}}_b + \delta \mathbf{f}_b) - \hat{\mathbf{R}}_{nb} \tilde{\mathbf{f}}_b + \hat{\boldsymbol{\gamma}}_n(\hat{\phi} + \delta \phi, \hat{h} + \delta h) + \delta \boldsymbol{\gamma}_n - \hat{\boldsymbol{\gamma}}_n(\hat{\phi}, \hat{h}) \\ &\quad - (2\mathbf{R}_{en}^T(\hat{\phi} + \delta \phi, \hat{\lambda} + \delta \lambda) \boldsymbol{\omega}_{ie} \\ &\quad + \boldsymbol{\omega}_{en}(\hat{\phi} + \delta \phi, \hat{h} + \delta h, \hat{v}_N + \delta v_N, \hat{v}_E + \delta v_E)) \times (\hat{\mathbf{v}}_n + \delta \mathbf{v}_n) \\ &\quad + (2\mathbf{R}_{en}^T(\hat{\phi}, \hat{\lambda}) \boldsymbol{\omega}_{ie} + \boldsymbol{\omega}_{en}(\hat{\phi}, \hat{h}, \hat{v}_N, \hat{v}_E)) \times \hat{\mathbf{v}}_n \end{aligned} \quad (\text{A-125})$$

Errors in the approximation of Earth's angular rate are negligible and not considered here, i.e. $\hat{\boldsymbol{\omega}}_{ie} = \boldsymbol{\omega}_{ie}$.

The differential equation for the error in the NED to body-fixed rotation matrix $\mathbf{R}_{nb}\hat{\mathbf{R}}_{nb}^T$ can be derived by accounting for gyroscope measurement error $\delta\boldsymbol{\omega}_{ib} = \boldsymbol{\omega}_{ib}^b - \tilde{\boldsymbol{\omega}}_{ib}$ and equations (A-25)-(A-26)

$$\begin{aligned} \frac{d}{dt}(\mathbf{R}_{nb}\hat{\mathbf{R}}_{nb}^T) &= \dot{\mathbf{R}}_{nb}\hat{\mathbf{R}}_{nb}^T + \mathbf{R}_{nb}\dot{\hat{\mathbf{R}}}_{nb}^T = \dot{\mathbf{R}}_{nb}\hat{\mathbf{R}}_{nb}^T + \mathbf{R}_{nb} \underbrace{\dot{\hat{\mathbf{R}}}_{nb}^T \hat{\mathbf{R}}_{nb}}_{\text{skew-symmetric}} \hat{\mathbf{R}}_{nb}^T \\ &= \dot{\mathbf{R}}_{nb}\hat{\mathbf{R}}_{nb}^T - \mathbf{R}_{nb}\hat{\mathbf{R}}_{nb}^T \dot{\hat{\mathbf{R}}}_{nb} \hat{\mathbf{R}}_{nb}^T \\ &= (\mathbf{R}_{nb}\boldsymbol{\Omega}_{ib} - \boldsymbol{\Omega}_{in}\mathbf{R}_{nb})\hat{\mathbf{R}}_{nb}^T - \mathbf{R}_{nb}\hat{\mathbf{R}}_{nb}^T(\hat{\mathbf{R}}_{nb}\hat{\boldsymbol{\Omega}}_{ib} - \hat{\boldsymbol{\Omega}}_{in}\hat{\mathbf{R}}_{nb})\hat{\mathbf{R}}_{nb}^T \\ &= \mathbf{R}_{nb}\hat{\mathbf{R}}_{nb}^T(\hat{\mathbf{R}}_{nb}\delta\boldsymbol{\Omega}_{ib}\hat{\mathbf{R}}_{nb}^T + \hat{\boldsymbol{\Omega}}_{in}) - \boldsymbol{\Omega}_{in}\mathbf{R}_{nb}\hat{\mathbf{R}}_{nb}^T \end{aligned} \quad (\text{A-126})$$

The differential equation for the orientation error Euler angles $\boldsymbol{\Phi}$ is obtained by differentiation of equation (2-21)

$$\begin{aligned} \delta\phi_1 &= \text{atan}\left(\frac{R_{32}}{R_{33}}\right) \\ \delta\phi_2 &= \text{asin}(-R_{31}) \\ \delta\phi_3 &= \text{atan}\left(\frac{R_{21}}{R_{11}}\right) \end{aligned} \quad (\text{A-127})$$

with the elements R_{ij} of $\mathbf{R} = \mathbf{R}_{nb}\hat{\mathbf{R}}_{nb}^T$. This gives

$$\begin{aligned} \delta\dot{\phi}_N &= \frac{\cos(\delta\varphi)}{\cos(\delta\vartheta)}\dot{R}_{32} - \frac{\sin(\delta\varphi)}{\cos(\delta\vartheta)}\dot{R}_{33} \\ \delta\dot{\phi}_E &= -\frac{1}{\cos(\delta\vartheta)}\dot{R}_{31} \\ \delta\dot{\phi}_D &= \frac{\cos(\delta\psi)}{\cos(\delta\vartheta)}\dot{R}_{21} - \frac{\sin(\delta\psi)}{\cos(\delta\vartheta)}\dot{R}_{11} \end{aligned} \quad (\text{A-128})$$

To simplify derivation write $\dot{\mathbf{R}} = \mathbf{R}\text{skew}(\boldsymbol{\omega}_1) - \text{skew}(\boldsymbol{\omega}_2)\mathbf{R}$. This gives

$$\begin{aligned} \dot{R}_{11} &= R_{12}\omega_{1,z} - R_{13}\omega_{1,y} + R_{21}\omega_{2,z} - R_{31}\omega_{2,y} \\ \dot{R}_{21} &= R_{22}\omega_{1,z} - R_{23}\omega_{1,y} - R_{11}\omega_{2,z} + R_{31}\omega_{2,x} \\ \dot{R}_{31} &= R_{32}\omega_{1,z} - R_{33}\omega_{1,y} + R_{11}\omega_{2,y} - R_{21}\omega_{2,x} \\ \dot{R}_{32} &= -R_{31}\omega_{1,z} + R_{33}\omega_{1,x} + R_{12}\omega_{2,y} - R_{22}\omega_{2,x} \\ \dot{R}_{33} &= R_{31}\omega_{1,y} - R_{32}\omega_{1,x} + R_{13}\omega_{2,y} - R_{23}\omega_{2,x} \end{aligned} \quad (\text{A-129})$$

The elements of $\mathbf{R} = \mathbf{R}_{nb}\hat{\mathbf{R}}_{nb}^T$ can be determined with equation (A-8) by setting $\mathbf{R} = \mathbf{R}_3(\delta\phi_D)\mathbf{R}_2(\delta\phi_E)\mathbf{R}_1(\delta\phi_N)$.

Finally, with equations (A-128) and (A-129), the nonlinear differential equation of orientation error Euler angles $\boldsymbol{\Phi}$ is

$$\begin{aligned}
\delta\dot{\phi}_1 &= \omega_{1,x} + \sin(\delta\phi_1) \tan(\delta\phi_2) \omega_{1,y} + \cos(\delta\phi_1) \tan(\delta\phi_2) \omega_{1,z} \\
&\quad - \frac{\cos(\delta\phi_3)}{\cos(\delta\phi_2)} \omega_{2,x} - \frac{\sin(\delta\phi_3)}{\cos(\delta\phi_2)} \omega_{2,y} \\
\delta\dot{\phi}_2 &= \cos(\delta\phi_1) \omega_{1,y} - \sin(\delta\phi_1) \omega_{1,z} + \sin(\delta\phi_3) \omega_{2,x} - \cos(\delta\phi_3) \omega_{2,y} \\
\delta\dot{\phi}_3 &= \frac{\sin(\delta\phi_1)}{\cos(\delta\phi_2)} \omega_{1,y} + \frac{\cos(\delta\phi_1)}{\cos(\delta\phi_2)} \omega_{1,z} - \tan(\delta\phi_2) \cos(\delta\phi_3) \omega_{2,x} \\
&\quad - \tan(\delta\phi_2) \sin(\delta\phi_3) \omega_{2,y} - \omega_{2,z}
\end{aligned} \tag{A-130}$$

with

$$\begin{aligned}
\boldsymbol{\omega}_1 &= \hat{\mathbf{R}}_{nb} \delta \boldsymbol{\omega}_{ib} + \boldsymbol{\omega}_{in}(\hat{\phi}, \hat{\lambda}, \hat{h}, \hat{v}_N, \hat{v}_E) \\
\boldsymbol{\omega}_2 &= \boldsymbol{\omega}_{in}(\hat{\phi} + \delta\phi, \hat{\lambda} + \delta\lambda, \hat{h} + \delta h, \hat{v}_N + \delta v_n, \hat{v}_E + \delta v_e)
\end{aligned} \tag{A-131}$$

The nonlinear error differential equations (A-124), (A-125) and (A-130) are linearized with respect to navigation state errors $\delta \mathbf{z}$ and sensor and model errors $\delta \mathbf{s} = [\delta \mathbf{f}_b^T, \delta \boldsymbol{\omega}_{ib}^T, \delta \boldsymbol{\gamma}_n^T]^T$ in the stationary point $\delta \mathbf{z} = \mathbf{0}, \delta \mathbf{s} = \mathbf{0}$.

The linearized differential equation of WGS84 position errors is

$$\begin{aligned}
\begin{bmatrix} \delta\dot{\phi} \\ \delta\dot{\lambda} \\ \delta\dot{h} \end{bmatrix} &= \begin{bmatrix} -\frac{\hat{v}_N}{(M(\hat{\phi}) + \hat{h})^2} \frac{dM}{d\phi} \Big|_{\hat{\phi}} & 0 & -\frac{\hat{v}_N}{(M(\hat{\phi}) + \hat{h})^2} \\ \frac{(M(\hat{\phi}) + \hat{h}) \tan(\hat{\phi}) \hat{v}_E}{(N(\hat{\phi}) + \hat{h})^2 \cos(\hat{\phi})} & 0 & -\frac{\hat{v}_E}{(N(\hat{\phi}) + \hat{h})^2 \cdot \cos(\hat{\phi})} \\ 0 & 0 & 0 \end{bmatrix} \begin{bmatrix} \delta\phi \\ \delta\lambda \\ \delta h \end{bmatrix} \\
&+ \begin{bmatrix} 1 & 0 & 0 \\ M(\hat{\phi}) + \hat{h} & 0 & 0 \\ 0 & \frac{1}{(N(\hat{\phi}) + \hat{h}) \cdot \cos(\hat{\phi})} & 0 \\ 0 & 0 & -1 \end{bmatrix} \delta \mathbf{v}_n
\end{aligned} \tag{A-132}$$

where $M(\phi) = \frac{a(1-e^2)}{(1-e^2 \sin^2 \phi)^{3/2}}$ and $N(\phi) = \frac{a}{\sqrt{1-e^2 \sin^2 \phi}}$ (see [16] and appendix A.2). Because a position error in north direction of $1m$ translates to an error in meridian curvature radius of $\sim 1cm$ or less, $\frac{dM}{d\phi} \Big|_{\hat{\phi}}$ can generally be neglected. Furthermore $\frac{M+h}{N+h} = \frac{M}{N+h} + \frac{h}{N+h} = \frac{M}{N} + \left(1 - \frac{M}{N}\right) \frac{h}{N} + o\left(\frac{h^2}{N^2}\right) \approx \frac{M}{N}$ equals 1 for low altitudes compared to Earth's radius with a maximum error of the order of $e^2 \approx 0.00669438$. Therefore it is valid to simplify the linearization as

$$\begin{aligned}
\begin{bmatrix} \delta\dot{\phi} \\ \delta\dot{\lambda} \\ \delta\dot{h} \end{bmatrix} &\approx \begin{bmatrix} 0 & 0 & -\frac{\hat{v}_N}{(M(\hat{\phi}) + \hat{h})^2} \\ \frac{\tan(\hat{\phi}) \hat{v}_E}{(N(\hat{\phi}) + \hat{h}) \cos(\hat{\phi})} & 0 & -\frac{\hat{v}_E}{(N(\hat{\phi}) + \hat{h})^2 \cdot \cos(\hat{\phi})} \\ 0 & 0 & 0 \end{bmatrix} \begin{bmatrix} \delta\phi \\ \delta\lambda \\ \delta h \end{bmatrix} \\
&+ \begin{bmatrix} 1 & 0 & 0 \\ M(\hat{\phi}) + \hat{h} & 0 & 0 \\ 0 & \frac{1}{(N(\hat{\phi}) + \hat{h}) \cdot \cos(\hat{\phi})} & 0 \\ 0 & 0 & -1 \end{bmatrix} \delta \mathbf{v}_n
\end{aligned} \tag{A-133}$$

The linearized differential equation for NED-velocity errors is with

$$(\mathbf{R}_{nb} - \widehat{\mathbf{R}}_{nb})\tilde{\mathbf{f}}_b = (\mathbf{R}_{nb}\widehat{\mathbf{R}}_{nb}^T - \mathbf{I})\widehat{\mathbf{R}}_{nb}\tilde{\mathbf{f}}_b$$

and equation (2-19)

$$\begin{aligned} \delta\dot{\mathbf{v}}_n \doteq & skew(\boldsymbol{\phi}_n)\widehat{\mathbf{R}}_{nb}\mathbf{f}'_b + \widehat{\mathbf{R}}_{nb}\delta\mathbf{f}_b + \begin{bmatrix} 0 \\ 0 \\ \left.\frac{d\gamma_D}{d\phi}\right|_{\hat{\phi},\hat{h}} \end{bmatrix} \delta\phi + \begin{bmatrix} 0 \\ 0 \\ \left.\frac{d\gamma_D}{dh}\right|_{\hat{\phi},\hat{h}} \end{bmatrix} \delta h + \delta\boldsymbol{\gamma}_n \\ & - \left(2skew(\delta\phi\mathbf{e}_2)\mathbf{R}_{en}^T(\hat{\phi},\hat{\lambda}) \cdot \boldsymbol{\omega}_{ie} + \left.\frac{d\boldsymbol{\omega}_{en}}{dz^T}\right|_{(\hat{\phi},\hat{h},\hat{v}_N,\hat{v}_E)} \delta\mathbf{z} \right) \times \hat{\mathbf{v}}_n \\ & - skew\left(2\mathbf{R}_{en}^T(\hat{\phi},\hat{\lambda})\boldsymbol{\omega}_{ie} + \boldsymbol{\omega}_{en}(\hat{\phi},\hat{h},\hat{v}_N,\hat{v}_E)\right)\delta\mathbf{v}_n \end{aligned} \quad (\text{A-134})$$

The gradients of normal gravity γ_D in height and geodetic latitude can be derived from equations (A-85) and (A-86).

The approximation of Earth's angular rate in NED frame is

$$\mathbf{R}_{en}^T(\hat{\phi},\hat{\lambda})\boldsymbol{\omega}_{ie} = \begin{bmatrix} \omega_{ie} \cos(\hat{\phi}) \\ 0 \\ -\omega_{ie} \sin(\hat{\phi}) \end{bmatrix} \quad (\text{A-135})$$

The approximated transport rate is

$$\boldsymbol{\omega}_{en}(\hat{\phi},\hat{h},\hat{v}_N,\hat{v}_E) = \begin{bmatrix} \frac{\hat{v}_E}{N(\hat{\phi}) + \hat{h}} \\ -\frac{\hat{v}_N}{M(\hat{\phi}) + \hat{h}} \\ -\frac{\tan(\hat{\phi})v'_E}{N(\hat{\phi}) + \hat{h}} \end{bmatrix} \quad (\text{A-136})$$

It follows that

$$\begin{aligned}
& \frac{d\omega_{en}}{dz^T} \Big|_{(\hat{\phi}, \hat{h}, \hat{v}_N, \hat{v}_E)} \delta \mathbf{z} \\
&= \begin{bmatrix} -\frac{\hat{v}_E}{(N(\hat{\phi}) + \hat{h})^2} \frac{dN}{d\hat{\phi}} \Big|_{\hat{\phi}} & 0 & -\frac{\hat{v}_E}{(N(\hat{\phi}) + \hat{h})^2} \\ \frac{\hat{v}_N}{(M(\hat{\phi}) + \hat{h})^2} \frac{dM}{d\hat{\phi}} \Big|_{\hat{\phi}} & 0 & \frac{\hat{v}_N}{(M(\hat{\phi}) + \hat{h})^2} \\ \frac{\tan(\hat{\phi}) \hat{v}_E}{(N(\hat{\phi}) + \hat{h})^2} \frac{dN}{d\hat{\phi}} \Big|_{\hat{\phi}} - \frac{\hat{v}_E}{(N(\hat{\phi}) + \hat{h}) \cos^2(\hat{\phi})} & 0 & \frac{\tan(\hat{\phi}) \hat{v}_E}{(N(\hat{\phi}) + \hat{h})^2} \end{bmatrix} \begin{bmatrix} \delta\phi \\ \delta\lambda \\ \delta h \end{bmatrix} \\
&+ \begin{bmatrix} 0 & \frac{1}{N(\hat{\phi}) + \hat{h}} & 0 \\ -\frac{1}{M(\hat{\phi}) + \hat{h}} & 0 & 0 \\ 0 & -\frac{\tan(\hat{\phi})}{N(\hat{\phi}) + \hat{h}} & 0 \end{bmatrix} \delta \mathbf{v}_n \\
&\approx \begin{bmatrix} -\frac{\hat{v}_E}{(N(\hat{\phi}) + \hat{h})^2} \delta h \\ \frac{\hat{v}_N}{(M(\hat{\phi}) + \hat{h})^2} \delta h \\ -\frac{\hat{v}_E}{(N(\hat{\phi}) + \hat{h}) \cos^2(\hat{\phi})} \delta\phi + \frac{\tan(\hat{\phi}) \hat{v}_E}{(N(\hat{\phi}) + \hat{h})^2} \delta h \end{bmatrix} + \begin{bmatrix} \frac{\delta v_E}{N(\hat{\phi}) + \hat{h}} \\ -\frac{\delta v_N}{M(\hat{\phi}) + \hat{h}} \\ -\frac{\tan(\hat{\phi}) \delta v_E}{N(\hat{\phi}) + \hat{h}} \end{bmatrix}
\end{aligned} \tag{A-137}$$

Again the derivatives of normal and meridian curvature radii have been neglected. As mentioned above, errors in the curvature radii due to position error are very small.

The linearization can then be rewritten as

$$\begin{aligned}
& \delta \dot{\mathbf{v}}_n \approx [\hat{\mathbf{R}}_{nb}, \mathbf{0}_3, \mathbf{I}_3] \delta \mathbf{s} \\
&+ \begin{bmatrix} -2\omega_{ie} \cos(\hat{\phi}) \hat{v}_E - \frac{\hat{v}_E^2}{(N(\hat{\phi}) + \hat{h}) \cos^2(\hat{\phi})} & 0 & \frac{\tan(\hat{\phi}) \hat{v}_E^2}{(N(\hat{\phi}) + \hat{h})^2} - \frac{\hat{v}_N \hat{v}_D}{(M(\hat{\phi}) + \hat{h})^2} \\ 2\omega_{ie} (\cos(\hat{\phi}) \hat{v}_N - \sin(\hat{\phi}) \hat{v}_D) + \frac{\hat{v}_N \hat{v}_E}{(N(\hat{\phi}) + \hat{h}) \cos^2(\hat{\phi})} & 0 & -\frac{\tan(\hat{\phi}) \hat{v}_N \hat{v}_E + \hat{v}_E \hat{v}_D}{(N(\hat{\phi}) + \hat{h})^2} \\ \frac{d\gamma_D}{d\hat{\phi}} \Big|_{\hat{\phi}, \hat{h}} + 2\omega_{ie} \sin(\hat{\phi}) \hat{v}_E & 0 & \frac{d\gamma_D}{dh} \Big|_{\hat{\phi}, \hat{h}} + \frac{\hat{v}_E^2}{(N(\hat{\phi}) + \hat{h})^2} + \frac{\hat{v}_N^2}{(M(\hat{\phi}) + \hat{h})^2} \end{bmatrix} \begin{bmatrix} \delta\phi \\ \delta\lambda \\ \delta h \end{bmatrix} \\
&+ \begin{bmatrix} \frac{\hat{v}_D}{M(\hat{\phi}) + \hat{h}} & -2\omega_{ie} \sin(\hat{\phi}) - \frac{2 \tan(\hat{\phi}) \hat{v}_E}{N(\hat{\phi}) + \hat{h}} & \frac{\hat{v}_N}{M(\hat{\phi}) + \hat{h}} \\ 2\omega_{ie} \sin(\hat{\phi}) + \frac{\tan(\hat{\phi}) \hat{v}_E}{N(\hat{\phi}) + \hat{h}} & \frac{\tan(\hat{\phi}) \hat{v}_N + \hat{v}_D}{N(\hat{\phi}) + \hat{h}} & 2\omega_{ie} \cos(\hat{\phi}) + \frac{\hat{v}_E}{N(\hat{\phi}) + \hat{h}} \\ -\frac{2 \hat{v}_N}{M(\hat{\phi}) + \hat{h}} & -2\omega_{ie} \cos(\hat{\phi}) - \frac{2 \hat{v}_E}{N(\hat{\phi}) + \hat{h}} & 0 \end{bmatrix} \delta \mathbf{v}_n \\
&+ \begin{bmatrix} 0 & \hat{f}_D & -\hat{f}_E \\ -\hat{f}_D & 0 & \hat{f}_N \\ \hat{f}_E & -\hat{f}_N & 0 \end{bmatrix} \boldsymbol{\phi}_n
\end{aligned} \tag{A-138}$$

Finally, the orientation error Euler angles $\boldsymbol{\phi}$ differential equations are linearized:

$$\dot{\boldsymbol{\phi}} \doteq \hat{\mathbf{R}}_{nb} \delta \boldsymbol{\omega}_{ib} + \begin{bmatrix} 0 & \hat{\omega}_{in,D} & -\hat{\omega}_{in,E} \\ -\hat{\omega}_{in,D} & 0 & \hat{\omega}_{in,N} \\ \hat{\omega}_{in,E} & -\hat{\omega}_{in,N} & 0 \end{bmatrix} \begin{bmatrix} \delta\phi_1 \\ \delta\phi_2 \\ \delta\phi_3 \end{bmatrix} - \frac{d\omega_{in}}{dz^T} \Big|_{(\hat{\phi}, \hat{h}, \hat{v}_N, \hat{v}_E)} \delta \mathbf{z} \tag{A-139}$$

with

$$\boldsymbol{\omega}_{in}(\hat{\phi}, \hat{h}, \hat{v}_N, \hat{v}_E) = \hat{\mathbf{R}}_{en}^T \boldsymbol{\omega}_{ie} + \hat{\boldsymbol{\omega}}_{en} = \begin{bmatrix} \omega_{ie} \cos(\hat{\phi}) + \frac{\hat{v}_E}{N(\hat{\phi}) + \hat{h}} \\ -\frac{\hat{v}_N}{M(\hat{\phi}) + \hat{h}} \\ -\omega_{ie} \sin(\hat{\phi}) - \frac{\tan(\hat{\phi}) \hat{v}_E}{N(\hat{\phi}) + \hat{h}} \end{bmatrix} \quad (\text{A-140})$$

and

$$\begin{aligned} \frac{d\boldsymbol{\omega}_{in}}{d\mathbf{z}^T} \Big|_{(\hat{\phi}, \hat{h}, \hat{v}_N, \hat{v}_E)} \delta\mathbf{z} &= \frac{d(\mathbf{R}_{en}^T \boldsymbol{\omega}_{ie})}{d\mathbf{z}^T} \Big|_{\hat{\phi}} \delta\mathbf{z} + \frac{d\boldsymbol{\omega}_{en}}{d\mathbf{z}^T} \Big|_{(\hat{\phi}, \hat{h}, \hat{v}_N, \hat{v}_E)} \delta\mathbf{z} \\ &\approx \begin{bmatrix} -\omega_{ie} \sin(\hat{\phi}) \delta\phi \\ 0 \\ -\omega_{ie} \cos(\hat{\phi}) \delta\phi \end{bmatrix} + \begin{bmatrix} -\frac{\hat{v}_E}{(N(\hat{\phi}) + \hat{h})^2} \delta h \\ \frac{\hat{v}_N}{(M(\hat{\phi}) + \hat{h})^2} \delta h \\ -\frac{\hat{v}_E}{(N(\hat{\phi}) + \hat{h}) \cos^2(\hat{\phi})} \delta\phi + \frac{\tan(\hat{\phi}) \hat{v}_E}{(N(\hat{\phi}) + \hat{h})^2} \delta h \end{bmatrix} + \begin{bmatrix} \frac{\delta v_E}{N(\hat{\phi}) + \hat{h}} \\ \frac{\delta v_N}{M(\hat{\phi}) + \hat{h}} \\ -\frac{\tan(\hat{\phi}) \delta v_E}{N(\hat{\phi}) + \hat{h}} \end{bmatrix} \end{aligned} \quad (\text{A-141})$$

The linearized differential equation can be rewritten as

$$\dot{\boldsymbol{\phi}} \approx [\mathbf{0}_3, \hat{\mathbf{R}}_{nb}, \mathbf{0}_3] \delta\mathbf{s}$$

$$\begin{aligned} &+ \begin{bmatrix} \omega_{ie} \sin(\hat{\phi}) & 0 & \frac{\hat{v}_E}{(N(\hat{\phi}) + \hat{h})^2} \\ 0 & 0 & -\frac{\hat{v}_N}{(M(\hat{\phi}) + \hat{h})^2} \\ \omega_{ie} \cos(\hat{\phi}) + \frac{\hat{v}_E}{(N(\hat{\phi}) + \hat{h}) \cos^2(\hat{\phi})} & 0 & -\frac{\tan(\hat{\phi}) \hat{v}_E}{(N(\hat{\phi}) + \hat{h})^2} \end{bmatrix} \begin{bmatrix} \delta\phi \\ \delta\lambda \\ \delta h \end{bmatrix} \\ &+ \begin{bmatrix} 0 & -\frac{1}{N(\hat{\phi}) + \hat{h}} & 0 \\ \frac{1}{M(\hat{\phi}) + \hat{h}} & 0 & 0 \\ 0 & \frac{\tan(\hat{\phi})}{N(\hat{\phi}) + \hat{h}} & 0 \end{bmatrix} \delta\mathbf{v}_n \\ &+ \begin{bmatrix} 0 & -\omega_{ie} \sin(\hat{\phi}) - \frac{\tan(\hat{\phi}) \hat{v}_E}{N(\hat{\phi}) + \hat{h}} & \frac{\hat{v}_N}{M(\hat{\phi}) + \hat{h}} \\ \omega_{ie} \sin(\hat{\phi}) + \frac{\tan(\hat{\phi}) \hat{v}_E}{N(\hat{\phi}) + \hat{h}} & 0 & \omega_{ie} \cos(\hat{\phi}) + \frac{\hat{v}_E}{N(\hat{\phi}) + \hat{h}} \\ -\frac{\hat{v}_N}{M(\hat{\phi}) + \hat{h}} & -\omega_{ie} \cos(\hat{\phi}) - \frac{\hat{v}_E}{N(\hat{\phi}) + \hat{h}} & 0 \end{bmatrix} \boldsymbol{\phi} \end{aligned} \quad (\text{A-142})$$

A.7 INTEGRATED INS/GNSS NAVIGATION

This appendix is based on section 3.2 of the author's Diploma thesis [39] and the references cited therein.

Equations of a conventional Kalman filter for uncorrelated measurements

A Kalman-Filter has the property of an optimal state estimator for systems described by the following non-deterministic state-space equation (see also [68–70, 102])

$$\dot{\mathbf{z}}(t) = \mathbf{A}_k \mathbf{z}(t) + \mathbf{B}_k \mathbf{s}_k \quad (\text{A-143})$$

with the systems state vector \mathbf{z} and the vector of noisy inputs \mathbf{s}_k

$$\mathbf{s}_k = \mathbf{u}(t_k) + \mathbf{w}_k \quad (\text{A-144})$$

$\mathbf{u}(t)$ is the vector-valued function of deterministic system inputs that is sampled at discrete time points t_k . \mathbf{w}_k is the vector of unbiased and white Gaussian system- or process-noise averaged over time interval $[t_k, t_{k+1}]$. The covariance matrix of the system noise \mathbf{w}_k is defined by

$$\mathbf{Q}_k = E[\mathbf{s}_k \mathbf{s}_k^T] = E[\mathbf{w}_k \mathbf{w}_k^T] \quad (\text{A-145})$$

The system and input matrices $\mathbf{A}_k = \mathbf{A}(t_k)$ and $\mathbf{B}_k = \mathbf{B}(t_k)$ and the input vector \mathbf{s}_k are constant for $t_k \leq t \leq t_{k+1}$. In that interval, both the fundamental solution of the homogenous system and a particular solution from variation of constants can be found for the state-space equation (A-143)

$$\mathbf{z}_{k+1} = \underbrace{e^{\mathbf{A}_k(t_{k+1}-t_k)}}_{=: \boldsymbol{\Phi}_k} \mathbf{z}_k + \underbrace{\int_{t_k}^{t_{k+1}} e^{\mathbf{A}_k(t_{k+1}-\tau)} d\tau \mathbf{B}_k \mathbf{s}_k}_{=: \boldsymbol{\Gamma}_k} \quad (\text{A-146})$$

See [103] and other textbooks.

In equation (A-146), we define the time-discrete propagation matrix $\boldsymbol{\Phi}_k$ and the time-discrete control matrix $\boldsymbol{\Gamma}_k$. For many applications it is admissible to truncate 3rd order and higher order terms in the matrix exponential series expansion:

$$\boldsymbol{\Phi}_k \doteq \mathbf{I} + \mathbf{A}_k(t_{k+1} - t_k) + \mathbf{A}_k^2 \frac{(t_{k+1} - t_k)^2}{2} \quad (\text{A-147})$$

$$\boldsymbol{\Gamma}_k \doteq \left(\mathbf{I}(t_{k+1} - t_k) + \mathbf{A}_k \frac{(t_{k+1} - t_k)^2}{2} \right) \mathbf{B}_k \quad (\text{A-148})$$

The Filter state vector of a time-discrete Kalman-Filter corresponds to the sampled state vector of the linear system (A-143)

$$\mathbf{x}_k = \mathbf{z}_k \quad (\text{A-149})$$

The motivation for data fusion is to find from an a priori estimate of the filter state \mathbf{x}_k^- and a related measurement $\tilde{\mathbf{y}}_x$ at time t_k a new (a posteriori) estimate \mathbf{x}_k^+ that – if all filter inputs are unbiased – is unbiased, i.e. $E[\mathbf{x}_k^+] = \mathbf{x}_k$ and is optimal in the sense of smallest (co-)variance.

In general, the filter state estimate (a priori or a posteriori) $\hat{\mathbf{x}}_k$ is a vector. The corresponding covariance matrix is defined for a priori and a posteriori estimates of \mathbf{x}_k as

$$\mathbf{P}_k = E[(\hat{\mathbf{x}}_k - E[\hat{\mathbf{x}}_k])(\hat{\mathbf{x}}_k - E[\hat{\mathbf{x}}_k])^T] \quad (\text{A-150})$$

Note that since $E[\mathbf{x}_k^-] = E[\mathbf{x}_k^+] = \mathbf{x}_k$, \mathbf{P}_k can also be interpreted as covariance of the estimation error $\delta\mathbf{x} = \hat{\mathbf{x}} - \mathbf{x}$ with $E[\delta\mathbf{x}] = \mathbf{0}$. Also note that the Kalman-Filter only provides a modeled approximation of the true filter state covariance given in equation (A-150). For better readability this will not be indicated by notation in the following.

For vector-valued filter state estimates, smallest covariance is not an unambiguous requirement. One possible mathematical definition of this optimality that results in a rather easy derivation of the filter equations is

$$\text{trace}(\mathbf{P}_k) \rightarrow \min! \quad (\text{A-151})$$

Measurement vector $\tilde{\mathbf{y}}_x$ and filter state vector \mathbf{x} are not necessarily identical in size or meaning. With a transformation matrix \mathbf{H}_k from filter state space to measurement space the linear combination of a priori estimate and measurement is

$$\mathbf{x}_k^+ = \mathbf{x}_k^- + \mathbf{K}_k \cdot (\tilde{\mathbf{y}}_x - \mathbf{H}_k \mathbf{x}_k^-) \quad (\text{A-152})$$

The term in brackets is termed innovation. It vanishes for ideal (error-free) measurements and estimates. The Kalman-Gain matrix \mathbf{K}_k corresponds to the relative weight of the measurement $\tilde{\mathbf{y}}_x$ in the update, i.e. equation (A-152) is identical to

$$\mathbf{x}_k^+ = (\mathbf{I} - \mathbf{K}_k \mathbf{H}_k) \mathbf{x}_k^- + \mathbf{K}_k \tilde{\mathbf{y}}_x \quad (\text{A-153})$$

The Kalman-Gain is chosen such that the optimality requirement (A-151) is satisfied. Assuming measurement and a priori filter state estimate are independent and with equation (A-153), the a posteriori filter estimate covariance matrix becomes

$$\mathbf{P}_k^+ = (\mathbf{I} - \mathbf{K}_k \mathbf{H}_k) \mathbf{P}_k^- (\mathbf{I} - \mathbf{K}_k \mathbf{H}_k)^T + \mathbf{K}_k \mathbf{R} \mathbf{K}_k^T \quad (\text{A-154})$$

Equation (A-154) is a combination of a priori filter estimate covariance $\mathbf{P}_k^- = E[(\mathbf{x}_k^- - E[\mathbf{x}_k^-])(\mathbf{x}_k^- - E[\mathbf{x}_k^-])^T]$ and measurement covariance

$$\mathbf{R} = E[(\tilde{\mathbf{y}}_x - E[\tilde{\mathbf{y}}_x])(\tilde{\mathbf{y}}_x - E[\tilde{\mathbf{y}}_x])^T] \quad (\text{A-155})$$

It can be shown (see any of the references given in the beginning of this subsection) that the trace of \mathbf{P}_k is minimal for

$$\mathbf{K}_k = \mathbf{P}_k^- \mathbf{H}_k^T (\mathbf{H}_k \mathbf{P}_k^- \mathbf{H}_k^T + \mathbf{R})^{-1} \quad (\text{A-156})$$

For this optimal Kalman-Gain, the covariance update equation (A-154) can be simplified

$$\begin{aligned} \mathbf{P}_k^+ &= (\mathbf{I} - \mathbf{K}_k \mathbf{H}_k) \mathbf{P}_k^- (\mathbf{I} - \mathbf{K}_k \mathbf{H}_k)^T + \mathbf{K}_k \mathbf{R} \mathbf{K}_k^T && \dots \text{"Josephs Form"} \\ &= (\mathbf{I} - \mathbf{K}_k \mathbf{H}_k) \mathbf{P}_k^- && \dots \text{not recommended} \end{aligned} \quad (\text{A-157})$$

Although the shorter expression reduces computational effort, it is less suitable to preserve the symmetry and positive semi-definiteness properties of \mathbf{P}_k compared to the Josephs form. Various other mathematically equivalent forms exist in literature (e.g. U-D factorization [104]) which are based on factorization of \mathbf{P}_k in order to ensure symmetry of the computed covariance.

The Kalman-Filter update equations are rewritten here for better readability:

$$\begin{aligned}
\mathbf{x}_k^+ &= \mathbf{x}_k^- + \mathbf{K}_k \cdot (\widetilde{\mathbf{y}}_x - \mathbf{H}_k \mathbf{x}_k^-) && \dots \text{filter state estimate update} \\
\mathbf{P}_k^+ &= (\mathbf{I} - \mathbf{K}_k \mathbf{H}_k) \mathbf{P}_k^- (\mathbf{I} - \mathbf{K}_k \mathbf{H}_k)^T + \mathbf{K}_k \mathbf{R} \mathbf{K}_k^T && \dots \text{"Josephs Form" covariance update}
\end{aligned} \tag{A-158}$$

To allow for data fusion when an measurement $\widetilde{\mathbf{y}}_x$ is available, the Filter has to provide for a current a priori filter state estimate \mathbf{x}_k^- and the corresponding a priori state estimate covariance \mathbf{P}_k^- . To that end the Kalman-Filter propagates state estimate and covariance in time, based on equation (A-146):

$$\begin{aligned}
\mathbf{x}_k^- &= \Phi_{k-1} \widehat{\mathbf{x}}_{k-1} + \Gamma_{k-1} \mathbf{u}(t_{k-1}) && \dots \text{filter state estimate propagation} \\
\mathbf{P}_k^- &= \Phi_{k-1} \mathbf{P}_{k-1} \Phi_{k-1}^T + \Gamma_{k-1} \mathbf{Q}_{k-1} \Gamma_{k-1}^T && \dots \text{covariance propagation}
\end{aligned} \tag{A-159}$$

For the derivation of the covariance propagation equation filter state estimate $\widehat{\mathbf{x}}_{k-1}$ and system noise \mathbf{w}_{k-1} were assumed to be uncorrelated.

Equations (A-158) and (A-159) implement the conventional Kalman-Filter for independent measurements and uncorrelated system noise. Note that they allow for multi-sensor and multi-frequency data fusion, i.e. neither must \mathbf{H}_k be the same in every update step nor must updates be computed in equidistant steps. For example, two measurements available at the same time t_k can be used for sequential updates of $\widehat{\mathbf{x}}_k$.

INS/GNSS integration with error state space Kalman-filter

The conventional Kalman-Filter introduced previously in this appendix can be used to estimate errors in an inertial navigation system if sensor measurements or other information related to the navigation state is available (e.g. GPS and barometer measurements). This will be exemplified with loosely-coupled INS/GNSS integration in the following.

For the INS/GNSS integration derived in this section, the filter state lies in the error state space

$$\mathbf{x} = \delta \mathbf{z} \quad (\text{A-160})$$

The corresponding total state space is the linear span of the 10-DOF navigation state vector

$$\mathbf{z} = \mathbf{z}_n = \begin{bmatrix} \phi \\ \lambda \\ h \\ \mathbf{v}_n \\ \tilde{\mathbf{q}}_{nb} \end{bmatrix} \quad (\text{A-161})$$

The linearized perturbation error equations (A-133), (A-138) and (A-142) can be cast into the form of a linear system of ordinary differential equations

$$\delta \dot{\mathbf{z}}(t) = \mathbf{A}_k \cdot \delta \mathbf{z}(t) + \mathbf{B}_k \cdot \delta \mathbf{s}_k \quad (\text{A-162})$$

With this linear approximation of the system of navigation state error differential equations, application of a conventional Kalman-Filter as presented previously in this appendix is possible. The considerations necessary for adaptation of the Kalman-Filter update step are presented in the following.

The filter measurement $\tilde{\mathbf{y}}_x$ can be defined as

$$\tilde{\mathbf{y}}_x := \tilde{\mathbf{y}} - \mathbf{g}'(\mathbf{z}') \quad (\text{A-163})$$

With the real measurement $\tilde{\mathbf{y}}$ that is an observation of the true system state \mathbf{z} disturbed by measurement noise assumed to be unbiased. The nonlinear transformation from system state space to measurement space – referred to as observation equation - is

$$\mathbf{y} = \mathbf{g}(\mathbf{z}) \quad (\text{A-164})$$

This relation between true system state and error-free measurement is only approximately known and modeled as $\mathbf{g}'(\mathbf{z})$. It is assumed that errors in the measurement model are noise-like and unbiased. \mathbf{z}' is the erroneous approximation of the system state

$$\mathbf{z}' = \mathbf{z} - \delta \mathbf{z} \quad (\text{A-165})$$

$\mathbf{z}'(t)$ is a realization of the time integration of noisy IMU measurements by the INS. The stochasticity of this process is not relevant here. Therefore the covariance of the filter measurement is equal to the measurement covariance

$$\mathbf{R} = E[(\tilde{\mathbf{y}}_x - E[\tilde{\mathbf{y}}_x])(\tilde{\mathbf{y}}_x - E[\tilde{\mathbf{y}}_x])^T] = E[(\tilde{\mathbf{y}} - E[\tilde{\mathbf{y}}])(\tilde{\mathbf{y}} - E[\tilde{\mathbf{y}}])^T] \quad (\text{A-166})$$

A linear transformation from filter state space (i.e. system error state space) to filter measurement space can be derived from equation (A-164):

$$\tilde{\mathbf{y}} + \delta \mathbf{y} = \mathbf{g}'(\mathbf{z}' + \delta \mathbf{z}) + \delta \mathbf{g} \quad (\text{A-167})$$

This leads to the following linearization in \mathbf{z}'

$$\tilde{\mathbf{y}} + \delta\mathbf{y} \doteq \mathbf{g}'(\mathbf{z}') + \left. \frac{\partial \mathbf{g}'(\mathbf{z}' + \delta\mathbf{z})}{\partial(\delta\mathbf{z})} \right|_{\mathbf{z}'} \delta\mathbf{z} + \delta\mathbf{g} \quad (\text{A-168})$$

Equation (A-168) can be reordered to give a linear relationship for $\tilde{\mathbf{y}}_x$ and $\delta\mathbf{z}$

$$\tilde{\mathbf{y}} - \mathbf{g}'(\mathbf{z}') \doteq \left. \frac{\partial \mathbf{g}'(\mathbf{z}' + \delta\mathbf{z})}{\partial(\delta\mathbf{z})} \right|_{\mathbf{z}'} \delta\mathbf{z} + \underbrace{\delta\mathbf{g} - \delta\mathbf{y}}_{\text{unbiased noise}} \quad (\text{A-169})$$

For open-loop error estimation the transformation matrix from filter state space to filter measurement space is the measurement model Jacobian matrix evaluated at \mathbf{z}'

$$\mathbf{H} = \left. \frac{\partial \mathbf{g}'(\mathbf{z}' + \delta\mathbf{z})}{\partial(\delta\mathbf{z})} \right|_{\mathbf{z}'} \quad (\text{A-170})$$

For example, if a GPS position measurement in WGS84 geodetic coordinates is available, the measurement matrix is

$$\mathbf{H}_{GPSpos} = [\mathbf{I}_3 \ \mathbf{0}_{3 \times 9}] \quad (\text{A-171})$$

With these definitions the filter state update of the conventional Kalman-Filter becomes

$$\delta\mathbf{z}_k^+ = \delta\mathbf{z}_k^- + \mathbf{K}_k \cdot (\tilde{\mathbf{y}} - \mathbf{g}'(\mathbf{z}'_k) - \mathbf{H}_k \delta\mathbf{z}_k^-) \quad (\text{A-172})$$

The linearization of the error differential equations only is valid if the assumptions made when linearizing are correct: The true system state \mathbf{z} must lie in close proximity of the linearization point. Consequently, for significant nonlinearities in system equation \mathbf{s} or large errors $\delta\mathbf{z}$ the best available estimate of system state $\hat{\mathbf{z}}$ should be used as linearization point.

The best estimate of system state $\hat{\mathbf{z}}$ is obtained by correcting the computed INS system state using an estimate of system state error $\widehat{\delta\mathbf{z}}$:

$$\hat{\mathbf{z}} = \mathbf{z}' + \widehat{\delta\mathbf{z}} \quad (\text{A-173})$$

If the internal INS state is reset to this best estimate this is referred to as full-scale closed-loop error estimation. In this case the linear system (A-162) is derived using

$$\begin{aligned} \delta\dot{\mathbf{z}} &= \mathbf{s}(\mathbf{z}' + \delta\mathbf{z}, \mathbf{u}' + \delta\mathbf{u}) - \underbrace{\mathbf{s}(\mathbf{z}' + \widehat{\delta\mathbf{z}}, \mathbf{u}')}_{\text{closed-loop INS integration}} \\ &\doteq \left. \frac{\partial \mathbf{s}}{\partial \mathbf{z}^T} \right|_{\hat{\mathbf{z}}, \mathbf{u}'} \cdot (\delta\mathbf{z} - \widehat{\delta\mathbf{z}}) + \left. \frac{\partial \mathbf{s}}{\partial \mathbf{u}^T} \right|_{\hat{\mathbf{z}}, \mathbf{u}'} \cdot [\delta \mathbf{f}_b^T \quad \delta \boldsymbol{\omega}_{ib}^T]^T \end{aligned} \quad (\text{A-174})$$

Because the deterministic propagation of estimated errors takes place in the INS time integration following the full-scale closed-loop correction, filter state estimate propagation according to equation (A-159) can be omitted. When a measurement is available, the a posteriori filter estimate will be used immediately to correct the a priori estimate of system state with equation (A-175).

With $\mathbf{g}'(\mathbf{z}'_k) \doteq \mathbf{g}'(\mathbf{z}'_k + \delta\mathbf{z}_k^-) - \mathbf{H}_k \delta\mathbf{z}_k^-$ the closed-loop correction of INS state best estimate is

$$\mathbf{z}_k^+ = \mathbf{z}_k^- + \mathbf{K}_k \cdot (\tilde{\mathbf{y}} - \mathbf{g}'(\mathbf{z}'_k)) \quad (\text{A-175})$$

The transformation matrix of the measurement model is evaluated at $\hat{\mathbf{z}}$

$$\mathbf{H} = \left. \frac{\partial \mathbf{g}'(\mathbf{z}' + \delta\mathbf{z})}{\partial(\delta\mathbf{z})} \right|_{\hat{\mathbf{z}}} \quad (\text{A-176})$$

The error state covariance matrix is updated and propagated linearly according to the equations of the conventional Kalman-Filter (A-158) and (A-159). Note that with equation (A-173) and neglecting the stochasticity of the unaided INS process that computes $\mathbf{z}'(t)$ the covariance of the system state estimate $\hat{\mathbf{z}}$ is equal to the error state estimate covariance \mathbf{P} .

A.8 EXTENDED KALMAN FILTER WITH AUGMENTED AND CONSIDERED STATES

For details on the extended Kalman filter method used in this work, many textbooks are available [68–70, 102]. This subsection will briefly explain the definition of augmented, observed and considered filter states as used in this work and how modifications to the Kalman filter implementation can improve performance for problems where only approximate statistical models are available.

Generally, the extended Kalman filter is employed in this work to estimate the errors $\delta\mathbf{z}$ of motion states computed with one or a combination of the model presented before. In addition, auxiliary (augmented) states \mathbf{a} may be included in the augmented Kalman filter state vector \mathbf{x}

$$\mathbf{x} = \begin{bmatrix} \delta\mathbf{z} \\ \mathbf{a} \end{bmatrix}$$

Because the main goal of filter design in this work is the accurate estimation of motion model errors $\delta\mathbf{z}$, the augmented states are related to either motion model inputs or aiding measurements used to update the extended Kalman filter. Examples are IMU measurement error or the offset in the barometric altitude measurement. Kalman filter state augmentation is discussed in all of the textbooks referenced above.

Different strategies for improving filter performance in presence of real errors in model inputs and measurements are possible. High frequency variations in these errors that cannot be predicted accurately with some process model can simply be considered as down-sampled white noise and accounted for by adapting filter process or measurement noise of the conventional Kalman filter algorithm accordingly. Especially for error in aiding measurements, this yields good results if update rate is low so that the time interval between measurements is much larger than the correlation time of high frequency error.

For components of error with slower variation in time but limited observability, the effect on motion model or measurement uncertainty must be modeled in the filter accounting for process time correlation. This is accomplished by defining a corresponding augmented state with a stochastic process model reflecting time correlation and uncertainty of this error. Because no deterministic propagation model is available for this augmented state, but it changes significantly in medium-term, convergence of the estimate cannot be expected due to a lack of continuous observability. In this case, the estimate for this augmented state is kept constant and only the corresponding uncertainty affecting motion model errors is considered. This is called a consider filter state.

For augmented states with either accurate propagation models, long-term stability or good continuous observability, simultaneous estimation together with the motion model error states is possible and can improve filter performance. In some cases discussed in chapter 3 of this work, augmented states will be estimated although no accurate prediction is possible and observability is bad (in case of wind vector error for optimal model fusion methods). The design decision whether an augmented filter state should be estimated or considered depends on the details of the problem.

For a specific aiding measurement, it may not be desired to update certain motion model errors (c.f. magnetometer aiding). In this case, these motion model errors would also only be

considered in terms of their effect on observation uncertainty, but their estimates would be kept constant in the filter update.

Depending on the considerations above, the decision which filter states are estimated and which are considered can be different for each measurement update. The filter state vector can be partitioned as follows

$$\begin{bmatrix} \mathbf{x}_e \\ \mathbf{x}_h \\ \mathbf{x}_c \end{bmatrix} = \mathbf{M}\mathbf{x}$$

\mathbf{M} is a permutation matrix with $\mathbf{M}\mathbf{M}^T = \mathbf{I}$. The observation equation becomes

$$\tilde{\mathbf{y}}_x = \mathbf{H}_e\mathbf{x}_e + \mathbf{H}_h\mathbf{x}_h = [\mathbf{H}_e \quad \mathbf{H}_h \quad \mathbf{0}] \mathbf{M}\mathbf{x} = \mathbf{H}\mathbf{x}$$

Only filter state elements with subscripts e or h appear in the observation. \mathbf{x}_e are the filter states that are updated as in the conventional Kalman filter. The states \mathbf{x}_h are only considered for their uncertainty in above observation equation, but not updated. Note that the matrix \mathbf{H}_e may include zero columns.

Because not all information theoretically available is used to correct the filter estimate, the consider-state Kalman filter update is suboptimal

$$\mathbf{x}_e^+ = \mathbf{x}_e^- + \mathbf{K}_e(\tilde{\mathbf{y}}_x - \mathbf{H}\mathbf{x})$$

The suboptimal gain matrix \mathbf{K}_e can be derived from the Kalman gain \mathbf{K} by deleting all rows that do not correspond to estimated states \mathbf{x}_e .

$$\mathbf{K}_e = [\mathbf{P}_{ee} \quad \mathbf{P}_{eh}] \begin{bmatrix} \mathbf{H}_e \\ \mathbf{H}_h \end{bmatrix} \left([\mathbf{H}_e \quad \mathbf{H}_h] \begin{bmatrix} \mathbf{P}_{ee} & \mathbf{P}_{eh} \\ \mathbf{P}_{eh}^T & \mathbf{P}_{hh} \end{bmatrix} \begin{bmatrix} \mathbf{H}_e \\ \mathbf{H}_h \end{bmatrix} + \mathbf{R} \right)^{-1}$$

The filter covariance matrix is partitioned as follows

$$\mathbf{M}\mathbf{P}_x\mathbf{M}^T = \begin{bmatrix} \mathbf{P}_{ee} & \mathbf{P}_{eh} & \mathbf{P}_{ec} \\ & \mathbf{P}_{hh} & \mathbf{P}_{hc} \\ sym. & & \mathbf{P}_{cc} \end{bmatrix}$$

A.9 SPECIFIC FORCE LINEARIZATION

$$\frac{\partial \mathbf{f}_b^R}{\partial \delta \mathbf{z}_n^T} = \frac{1}{m} \frac{\partial \Sigma \mathbf{F}_{bi}^G}{\partial \delta \mathbf{z}_n^T} + \text{skew}(\mathbf{r}_b^{RG}) \mathbf{I}_{bb}^G{}^{-1} \frac{\partial \Sigma \mathbf{M}_{bi}^G}{\partial \delta \mathbf{z}_n^T}$$

$$\frac{\partial \mathbf{f}_b^R}{\partial \boldsymbol{\omega}_{ib}^T} = \frac{1}{m} \frac{\partial \Sigma \mathbf{F}_{bi}^G}{\partial \delta \boldsymbol{\omega}_{ib}^T} + \text{skew}(\mathbf{r}_b^{RG}) \mathbf{I}_{bb}^G{}^{-1} \left(\frac{\partial \Sigma \mathbf{M}_{bi}^G}{\partial \delta \boldsymbol{\omega}_{ib}^T} - \text{skew}(\boldsymbol{\omega}_{ib}) \mathbf{I}_{bb}^G + \text{skew}(\mathbf{I}_{bb}^G \boldsymbol{\omega}_{ib}) \right) + \text{skew}(\boldsymbol{\omega}_{ib} \times \mathbf{r}_b^{RG})$$

$$+ \text{skew}(\boldsymbol{\omega}_{ib}) \text{skew}(\mathbf{r}_b^{RG})$$

$$\frac{\partial \mathbf{f}_b^R}{\partial \mathbf{v}_{Wn}^T} = - \frac{\partial \mathbf{f}_b^R}{\partial \mathbf{v}_n^T}$$

$$\frac{\partial \mathbf{f}_b^R}{\partial \boldsymbol{\omega}_{Wb}^T} = - \frac{1}{m} \frac{\partial \Sigma \mathbf{F}_{bi}^G}{\partial \delta \boldsymbol{\omega}_{ib}^T} - \text{skew}(\mathbf{r}_b^{RG}) \mathbf{I}_{bb}^G{}^{-1} \frac{\partial \Sigma \mathbf{M}_{bi}^G}{\partial \delta \boldsymbol{\omega}_{ib}^T}$$

$$\frac{\partial \mathbf{f}_b^R}{\partial \mathbf{u}_p^T} = \frac{1}{m} \frac{\partial \Sigma \mathbf{F}_{bi}^G}{\partial \mathbf{u}_p^T} + \text{skew}(\mathbf{r}_b^{RG}) \mathbf{I}_{bb}^G{}^{-1} \frac{\partial \Sigma \mathbf{M}_{bi}^G}{\partial \mathbf{u}_p^T}$$

$$\frac{\partial \mathbf{f}_b^R}{\partial \mathbf{c}_v^T} = \frac{1}{m} \frac{\partial \Sigma \mathbf{F}_{bi}^G}{\partial \mathbf{c}_v^T} + \text{skew}(\mathbf{r}_b^{RG}) \mathbf{I}_{bb}^G{}^{-1} \frac{\partial \Sigma \mathbf{M}_{bi}^G}{\partial \mathbf{c}_v^T}$$

$$\frac{\partial \mathbf{f}_b^R}{\partial m} = - \frac{\Sigma \mathbf{F}_{bi}^G}{m^2}$$

$$\frac{\partial \mathbf{f}_b^R}{\partial \delta \mathbf{I}_{bb}^G{}^T} = \text{skew}(\mathbf{r}_b^{RG}) \frac{\partial \mathbf{I}_{bb}^G{}^{-1} \dot{\boldsymbol{\omega}}_{ib}}{\partial \delta \mathbf{I}_{bb}^G{}^T} - \text{skew}(\mathbf{r}_b^{RG}) \mathbf{I}_{bb}^G{}^{-1} \text{skew}(\boldsymbol{\omega}_{ib}) \frac{\partial \mathbf{I}_{bb}^G \boldsymbol{\omega}_{ib}}{\partial \delta \mathbf{I}_{bb}^G{}^T}$$

with $\dot{\boldsymbol{\omega}}_{ib} = \mathbf{I}_{bb}^G{}^{-1} (\Sigma \mathbf{M}_{bi}^G - \boldsymbol{\omega}_{ib} \times (\mathbf{I}_{bb}^G \boldsymbol{\omega}_{ib}))$. While $\frac{\partial \mathbf{I}_{bb}^G \mathbf{a}}{\partial \delta \mathbf{I}_{bb}^G{}^T}$ with any vector $\mathbf{a} \in \mathfrak{R}^{3 \times 1}$ is a simple operator

$$\frac{\partial \mathbf{I}_{bb}^G \mathbf{a}}{\partial \delta \mathbf{I}_{bb}^G{}^T} = \begin{bmatrix} a_1 & 0 & 0 & -a_2 & -a_3 & 0 \\ 0 & a_2 & 0 & -a_1 & 0 & -a_3 \\ 0 & 0 & a_3 & 0 & -a_1 & -a_2 \end{bmatrix}$$

The nonlinear operator $\frac{\partial \mathbf{I}_{bb}^G{}^{-1} \mathbf{a}}{\partial \delta \mathbf{I}_{bb}^G{}^T}$ is more complex and should be derived and implemented using a symbolic math software package.

$$\frac{\partial \mathbf{f}_b^R}{\partial \mathbf{r}_b^{RG}{}^T} = \text{skew}(\mathbf{r}_b^{RG}) \mathbf{I}_{bb}^G{}^{-1} \frac{\partial \Sigma \mathbf{M}_{bi}^G}{\partial \mathbf{r}_b^{RG}{}^T} - \text{skew} \left(\mathbf{I}_{bb}^G{}^{-1} (\Sigma \mathbf{M}_{bi}^G - \boldsymbol{\omega}_{ib} \times (\mathbf{I}_{bb}^G \boldsymbol{\omega}_{ib})) \right) - \text{skew}(\boldsymbol{\omega}_{ib}) \text{skew}(\boldsymbol{\omega}_{ib})$$